University of Alberta

Towards a Structural Model of the Plasma Membrane Cl^-/HCO_3^- Exchanger, AE1

by

Pamela Therese Bonar

A thesis submitted to the Faculty of Graduate Studies and Research
in partial fulfillment of the requirements for the degree of

Doctor of Philosophy

Department of Biochemistry

Fall 2013
Edmonton, Alberta

Abstract

AE1 is an electroneutral Cl^-/HCO_3^- exchanger expressed in erythrocytes and the renal collecting duct. There is no high-resolution structure of the membrane domain, which alone is required for the transport activity of AE1. Here, a *Saccharomyces cerevisiae* expression and immuno-affinity purification system was developed for the AE1 membrane domain. The human AE1 membrane domain (residues 388-911), followed by a rhodopsin antibody epitope (AE1MD-Rho), was expressed at 0.3 mg/l of culture, and milligram quantities were purified to 93% homogeneity. AE1MD-Rho transport activity was indistinguishable from erythrocyte AE1, as assessed by radioactive $[^{35}S]SO_4^{2-}$ efflux assays in reconstituted proteoliposomes. More recently, an electron microscopy structure of the AE1 membrane domain was proposed to have a similar protein fold to ClC chloride channels. A three-dimensional homology model of the AE1 membrane domain was created, using the *Escherichia coli* ClC channel structure as a template. This model agrees well with AE1 cysteine scanning mutagenesis data and blood group antigen sites. To investigate the transport mechanism of AE1, point mutations were introduced in regions of the AE1 homology model corresponding to sites involved in the ClC transport mechanism. The transport activity of these mutants was assessed by Cl^-/HCO_3^- exchange assays in HEK293 cells and *Xenopus laevis* oocytes. Several AE1 mutations, at sites corresponding to ClC transport mechanism residues, resulted in significant changes in transport

activity compared to wild-type AE1, without changes in electrogenicity or transport stoichiometry. A study of the *E. coli* ClC dimer interface identified tryptophan mutations, which disrupted the dimer interface of ClC. In a similar fashion, AE1 tryptophan mutations were made in an AE1 membrane domain background, using the AE1 homology model as a guide. The majority of AE1 tryptophan mutations decreased AE1 protein expression; however, no disruptions of the dimer interface were observed using chemical crosslinking. Chemical crosslinking may not have the sensitivity to monitor slight disruptions in the AE1 dimer interface, and thus alternate strategies to monitor the oligomeric state of AE1 tryptophan mutants must be investigated. Together, these studies have provided valuable insights into the structure and transport mechanism of AE1.

Acknowledgements

First, I would like to thank my supervisor Dr. Joseph Casey. His guidance throughout my Ph.D. program has allowed me to flourish as a scientist. He also provided me with several opportunities to travel the world and share my research, which has been one of the most rewarding aspects of my degree.

I would also like to thank all of my committee members, Dr. Marek Michalak, Dr. Mark Glover, and Dr. Joanne Lemieux, for their support. In particular, the wonderful supervision of Dr. Marek Michalak, during my undergraduate research project and summer studentship, helped to solidify my decision to pursue my Ph.D.

During the final year of my degree, I had the pleasure of working at the Technical University of Kaiserslautern in Germany with Dr. Joachim Dietmeir and Dr. Holger Becker, who guided me through the field of electrophysiology. I would like to thank them and their lab members for their generosity during my stay in Germany.

Throughout my Ph.D. program, I worked with a long list of talented lab members. I would like to thank Hans-Peter Schneider, at the Technical University of Kaiserslautern, as his superior expertise in *Xenopus laevis* oocytes and electrophysiology helped to make my stay in Germany productive and enjoyable. I will forever be thankful to Anita Quon for her passionate organization of the Casey lab. Dr. Gonzalo Vilas was an invaluable

source of knowledge and gave me excellent advice during my degree. Fellow graduate students Dr. Danielle Johnson, Sampath Loganathan, Brittany Brown, and Haley Shandro were all great friends and made some of the long and hard days in the lab seem a little shorter and brighter. Post-docs Dr. Arghya Basu, Dr. Patricio Morgan, and Dr. Shirley Mazor were great mentors during my time in the lab. I would also like to thank Sam Post in the Casey lab for always making sure the glassware was clean and tip boxes were filled.

Members from the Department of Biochemistry, Department of Physiology, and Membrane Protein and Disease Research Group have greatly enriched my experience at the University of Alberta. Specifically, Dr. Kate Witkowska has been a great friend, who was always available to discuss the trials of graduate school or to celebrate a success.

I would also like to thank all of my friends and extended family. They constantly reminded me of exactly why I pursued a Ph.D. and what contributions I was making to society, while encouraging me to enjoy the finer things in life like dodgeball and beer. My parents (Dave and Kathy Bonar) and brothers (David and Michael Bonar) are my biggest supporters, who never fail to encourage me to keep chasing my dreams.

Table of Contents

List of Figures

List of Tables

List of Abbreviations

3D; three-dimensional

AE; Cl^-/HCO_3^- anion exchanger

AE1-Ct; GST fused to residues 872-911 of human AE1

AE1-Rho; human AE1 with the nine C-terminal amino acids of rhodopsin

AE1(Q434C).AE1(Q434C)-C$^-$; Q434C mutations in each monomer of a cysteineless AE1 concatamer

AE1MD; AE1 membrane domain

AE1MD-Rho; human AE1 membrane domain residues 388-911 with the nine C-terminal amino acids of rhodopsin

AE1MD346; human AE1 membrane domain residues 346-911

Band 3 HT; a high transport human AE1 mutant

BCA; bicinchoninic acid

BCECF-AM; 2′,7′-Bis(2-carboxyethyl)-5(6)-carboxyfluorescein acetoxymethyl ester

$C_{12}E_8$; octaethylene glycol mono-n-dodecyl ether

CAII; carbonic anhydrase isoform II

CBS; cystathionine beta-synthase

cdAE1; N-terminal cytoplasmic domain of AE1

cDNA; complementary deoxyribonucleic acid

CMC; critical micelle concentration

cmClC; *C. merolae* ClC

cRNA; complementary ribonucleic acid

DADS; 4,4'-diaminostilbene-2,2'-disulfonate

DDM; n-dodecyl-β-D-maltopyranoside

DEPC; diethyl pyrocarbonate

DIC; differential interference contrast microscopy

DIDS; 4,4'-diisothiocyanostilbene-2,2'-disulfonate

DMEM; Dulbecco's modified Eagle media

DMMA; dimethylmaleic anhydride

DMSO; dimethyl sulfoxide

DNA; deoxyribonucleic acid

dRTA; distal renal tubular acidosis

DSP; dithiobis(succinimidylpropionate)

DTT; dithiothreitol

eAE1; erythrocyte AE1

ecClC; *E. coli* ClC

EDTA; ethylenediaminetetraacetic acid

ER; endoplasmic reticulum

EYPC; egg yolk phosphatidylcholine

FC; Fos-choline 14

FRET; fluorescence resonance energy transfer

GAPDH; glyceraldehyde 3-phosphate dehydrogenase

GFP; green fluorescent protein

GPA; glycophorin A

GST; glutathione S-transferase

H_2DIDS; 4,4'-diisothiocyanodihydrostilbene-2,2'-disulfonate

HA; hemagglutinin tag

HEK293 cells; human embryonic kidney 293 cells

HEPES; 4-(2-hydroxyethyl)-1-piperazineethanesulfonic acid

HRP; horseradish peroxidase

HS; hereditary spherocytosis

HUGO; Human Genome Organization

I/V; current/voltage

IMAC; immobilized metal affinity chromatography

IPTG; isopropyl β-D-1-thiogalactopyranoside

kAE1; kidney AE1

LCP; lipid cubic phase

LPC; lysophosphatidyl choline

MFS; major facilitator superfamily

NAP-taurine; N-(4-azido-2-nitrophenyl)-2-aminoethylsulfonate

NMR; nuclear magnetic resonance

OG; n-octyl-β-D-glycopyranoside

PcAEP; *P. chrysosporium* anion exchanger protein

PCR; polymerase chain reaction

PDB; Protein Data Bank

PDB ID; Protein Data Bank identifier

PEG; polyethylene glycol

PMA1; *S. cerevisiae* plasma membrane marker (H^+-ATPase)

pPB1; AE1MD-Rho yeast expression construct

RBC; red blood cell

Rho; rhodopsin epitope tag (the nine C-terminal amino acids)

RNA; ribonucleic acid

SAO; southeast Asian ovalocytosis

SDS; sodium dodecyl sulfate

SDS-PAGE; sodium dodecyl sulfate polyacrylamide gel electrophoresis

SE; standard error

Sec61; *S. cerevisiae* ER marker (ER membrane protein translocon)

SITS; 4-acetamido-4'-isothiocyanostilbene-2-2'-disulfonate

SLC; solute carrier

smFRET; single molecule FRET

T; total

TEV; tobacco etch virus protease

U; unbound

UV; ultraviolet

WT; wild-type

YEpM; yeast expression vector

Chapter 1: General Introduction

Portions of this chapter are published in P.T. Bonar, J.R. Casey, Plasma membrane Cl^-/HCO_3^- exchangers: Structure, mechanism and physiology. *Channels (Austin)* **2**, 337-345 (2008). (Reproduced with permission)

1.1 Thesis Overview

The objective of this thesis is to examine AE1 membrane domain structure through various methods, to provide insights into AE1 structural features and transport mechanism. A dual approach to investigate AE1 structure implemented a novel expression and purification strategy and homology modeling of the AE1 membrane domain. Human AE1 purification from erythrocytes is well documented and resulted in numerous low-resolution AE1 electron microscopy (EM) structures. Here, an alternate approach to AE1 purification from protein overexpressed in *Saccharomyces cerevisiae* was developed to produce protein suitable for crystallization trials. In addition, a three-dimensional homology model of AE1 was created on the basis of the *Escherichia coli* ClC chloride channel structure, as previous low-resolution structures have revealed similar structural features between the proteins.

AE1 is a bicarbonate transport protein, and the introduction begins with a discussion about the importance of bicarbonate transporters. The specific function of AE1 in physiology and disease is discussed to highlight the importance of understanding AE1 mechanistic features. As the focus of the thesis is to investigate the structure of AE1 a large section of the introduction discusses the numerous studies of AE1 topology, dimerization, helical packing, purification, and crystallization. In addition, a discussion on membrane proteins of known structure is included to highlight the special difficulties of working with integral membrane proteins. This section of the

introduction will also compare membrane protein folds from known structures. As the AE1 homology model, discussed in the thesis, was created using *E. coli* ClC as a template structure, a portion of the introduction also discusses ClC chloride channels.

1.2 Bicarbonate Transport

1.2.1 Bicarbonate Physiology

The by-product of mitochondrial respiration is the acid, CO_2, which must be removed from the body to maintain pH homeostasis. Our bodies have developed mechanisms to deal with metabolic acid build-up including: CO_2 exhalation through the lungs, H^+ secretion and HCO_3^- reabsorption in the kidney, and an extensive buffering system to neutralize acid. CO_2 is in equilibrium with bicarbonate through the reaction $CO_2 + H_2O \leftrightarrow HCO_3^- + H^+$. This reaction has a pKa of 6.2, which is close to the physiological pH of 7.2. Thus, the CO_2/HCO_3^- equilibrium forms the main pH buffering system in our bodies, reflecting the high physiological abundance of CO_2 and HCO_3^-. Since CO_2 is a gas, it freely moves across the plasma membrane; however, HCO_3^- is a membrane impermeant anion. In order to transport HCO_3^- across the plasma membrane, bicarbonate transporter proteins are required (*1*). One of the major classes of bicarbonate transporters are the electroneutral Cl^-/HCO_3^- exchangers, also known as anion exchangers (Fig. 1.1). The other functional classes of bicarbonate transporters are the sodium coupled HCO_3^- transporters (comprised of Na^+/HCO_3^- co-transporters and Na^+ dependent Cl^-

/HCO_3^- exchangers), and the SLC26 exchangers (electrogenic and electroneutral) and anion channels (Fig. 1.1).

1.2.2 Bicarbonate Transporters

Electroneutral and electrogenic Cl^-/HCO_3^- exchangers move bicarbonate either into or out of the cell in exchange for chloride, thereby either alkalinizing or acidifying the cell, respectively. Na^+/HCO_3^- co-transporters alkalinize or acidify the cell by move bicarbonate along with sodium into or out of the cell, respectively. Bicarbonate transporters not only contribute to the maintenance of physiological pH, but are also involved in volume regulation and acid/base secretion (*1*). There are a wide range of differences between the different bicarbonate transporters, including differences in tissue distribution, apical or basolateral epithelial expression, electrogenicity, regulation, and physiological roles (*1*). Due to the importance of these proteins, it is not surprising that they are involved in many diseases including cardiac hypertrophy (*2-4*), hereditary spherocytosis of the erythrocyte (*5-9*), proximal and distal renal tubular acidosis (*7, 10-18*), goiter (*19*), epilepsy (*20, 21*), Pendred syndrome (*22-24*), and cystic fibrosis (*25-30*). Most of the mutations that cause this wide range of diseases are the result of endoplasmic reticulum (ER)-retained phenotypes (*1, 17, 31-33*). In some cases this causes a dominant pattern of inheritance, because heterodimers of wild-type (WT) and mutant proteins may become ER-retained (*1, 17, 31-33*).

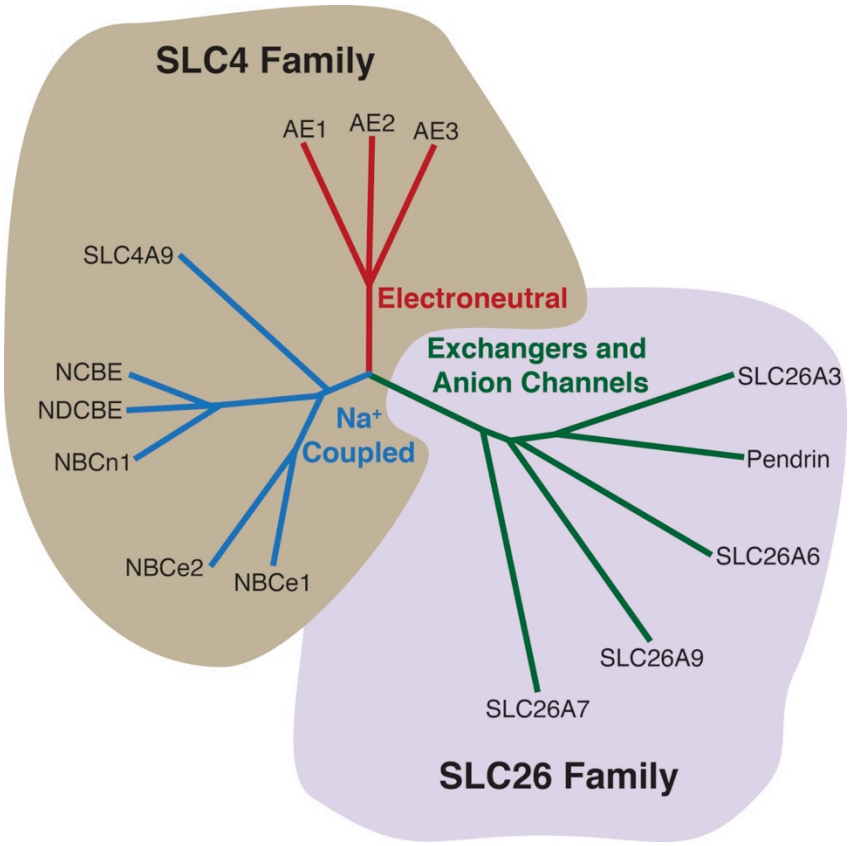

Figure 1.1 Phylogenetic Dendrogram of Human Bicarbonate Transporters.

Amino acid sequences corresponding to human bicarbonate transporters were aligned using Clustal W software (http://align.genome.jp/). On the basis of the alignment Clustal W plotted phylogenetic relationships, where the length of each line denotes the relative evolutionary distance between transporters. Bicarbonate transporters cluster into two families, SLC4 (beige) and SLC26 (lilac). The SLC26 family is comprised of exchangers and anion channels (green) and the SLC4 family is comprised of two sub-families, the Na^+ coupled bicarbonate transporters (blue) and the electroneutral Cl^-/HCO_3^- exchangers (red).

Anion exchanger proteins are found in two genetically distinct lineages, SLC4 (*34*) and SLC26 (*35*) (Fig. 1.1). The Human Genome Organization (HUGO) has termed these proteins solute carrier transport proteins and given them the nomenclature "SLC" (*36*). The SLC4 family contains sodium bicarbonate co-transporters (SLC4A9, NBCn1, NBCe2, and NBCe1), sodium dependent chloride bicarbonate exchangers (NDCBE and NCBE), and sodium independent chloride bicarbonate exchangers (AE1, AE2, and AE3). The SLC26 family supports chloride bicarbonate exchange, in some cases with an electrogenic mechanism, and anion conductance (Table 1.1). There are five different members in this family (SLC26A3, Pendrin, SLC26A6, SLC26A7 and SLC26A9).

The confusing nomenclature of the SLC4 and SLC26 families stems from the discovery of these proteins over a 20 year span (*37, 38*). In many cases the same protein was discovered by independent researchers and thus given different names. Table 1.1 lists all of the anion exchanger proteins by their accepted names, as well as other names given to these proteins. In addition, Table 1.1 provides a summary of the tissue distribution, substrate specificity and electrogenicity of the Cl^-/HCO_3^- exchangers.

Table 1.1 The Expression Profile and Transport Mechanisms of HCO_3^- Transport Proteins.

Expression data compiled from the literature and DNA micro-array data of transcript abundance in human and mouse tissues (http://symatlas.gnf.org/SymAtlas/).

Transport protein (alternate names)	Tissue distribution (epithelial localization)	Mechanism (electrogenicity)	Citations
AE1 (SLC4A1, Band 3, kAE1, eAE1)	RBC, kidney, heart (kAE1 basolateral)	Cl^-/HCO_3^- exchange (electroneutral)	(*38*)
AE2 (SLC4A2)	Widespread (basolateral, and apical in hepatobiliary epithelia)	Cl^-/HCO_3^- exchange (electroneutral)	(*39*)
AE3 (SLC4A3 AE3c, AE3fl)	Brain, heart, retina, pituitary, adrenal gland (non-epithelial)	Cl^-/HCO_3^- exchange (electroneutral)	(*40*)
SLC4A9 (AE4)	Widespread, kidney, testis, pancreas (apical)	Na^+/HCO_3^- co-transport (electroneutral)	(*41-44*)
NCBE (SLC4A10, NBCn2)	Cardiac myocytes, neurons, kidney, uterus, adrenal cortex, choroid plexus (basolateral)	Na^+/HCO_3^- co-transport or Na^+-dependent Cl^-/HCO_3^- exchange (electroneutral)	(*45-47*)
NDCBE (SLC4A8, NDAE1)	Prefrontal cortex of brain, testis, cardiac myocytes, oocytes	Na^+-dependent Cl^-/HCO_3^- exchange (electroneutral)	(*48-50*)
NBCn1 (SLC4A7)	Heart, kidney, skeletal muscle, smooth muscle, submandibular gland, pancreas, stomach (basolateral)	Na^+/HCO_3^- co-transport (electroneutral)	(*51-53*)

NBCe1 (SLC4A4)	Pancreas, kidney, heart, cornea, prostate, colon, stomach, thyroid, brain (basolateral)	Na^+/HCO_3^- co-transport (electrogenic)	(*54-59*)
NBCe2 (SLC4A5)	Brain, epididymis, cardiac muscle, smooth muscle, kidney, choroid plexus (apical)	Na^+/HCO_3^- co-transport (electrogenic)	(*60-63*)
SLC26A3 (DRA, CLD)	Colon, ileum, cardiac myocytes, eccrine sweat gland (apical)	Cl^-/HCO_3^- exchange (electroneutral/ electrogenic)	(*64-66*)
Pendrin (SLC26A4, PDS)	Thyroid, inner ear, thyroid, kidney, prostate (apical)	Cl^-/HCO_3^- exchange, also I^- (electroneutral)	(*67-69*)
SLC26A6 (PAT-1, CFEX)	Kidney, heart, bronchial epithelium, pancreas, prostate, thymus, intestine (apical)	Cl^-/HCO_3^- exchange, also oxalate and formate (electroneutral/ electrogenic)	(*70-72*)
SLC26A7	Thyroid, kidney, stomach, retina, olfactory epithelium (basolateral)	Cl^-/HCO_3^- exchange (electrogenic)/ anion channel	(*37, 73-75*)
SLC26A9	Salivary gland, heart, brain, stomach, trachea, kidney, lung bronchiolar and alveolar epithelial (apical)	Cl^-/HCO_3^- exchange (electrogenic)/ anion channel	(*37, 76-78*)
SLC26A11	Kidney, brain, placenta, and pancreatic duct (apical)	Cl^-/HCO_3^- exchange (electrogenic)/ anion channel	(*79, 80*)

1.3 AE1 Function

AE1 is a bidirectional 1:1 electroneutral chloride/bicarbonate anion exchanger. It has a turnover rate of 5 X 10^4 anions/s, which is much faster than classical transport proteins and only an order of magnitude slower than ion channels (*81*). AE1 mediated anion transport occurs between pH 5-11, unlike AE2 mediated anion transport, which is inhibited by acidic pH (*82*). In addition to chloride and bicarbonate, AE1 is capable of transporting a variety of other anions. Both Br^- and F^- are transported at rates similar to Cl^- and HCO_3^-, but the anion affinity of AE1 differs between these anions (HCO_3^->Cl^- >Br^->F^-), as determined by Cl^-/HCO_3^- exchange inhibition assays (*83*). I^-, HPO_3^{2-} and SO_4^{2-} are transported at slower rates compared to Cl^- and HCO_3^- (*84-86*). In addition, organic phosphates and N-(4-azido-2-nitrophenyl)-2-aminoethylsulfonate (NAP-taurine) are transported by AE1 at very slow rates (*84-86*). AE1 mediated transport of divalent anions occurs by co-transport of proton to maintain electroneutral anion transport (*84-86*). Even though AE1 is capable of transporting numerous anions, its main physiological role is to maintain pH homeostasis by transporting HCO_3^-.

1.3.1 AE1 Physiology

AE1 is expressed as two different isoforms, eAE1 (911 residues) expressed in erythrocytes, and kAE1 (846 residues) expressed on the basolateral side of the α-intercalated cell of the renal collecting duct (*87, 88*). The two isoforms differ because eAE1 has an additional 65 N-terminal amino

acids that are required to form protein-protein interactions with the cytoskeleton of the erythrocyte (*89*).

1.3.1.1 Erythrocyte AE1

There are approximately 10^6 copies of AE1 in every erythrocyte and it comprises 50% of the integral membrane protein of these cells (*90*). With the high abundance of AE1 found in red blood cells (RBCs), it is not surprising that AE1 fulfills a number of important roles (*86*). Firstly, AE1 is a key player in the CO_2/HCO_3^- buffering system of the blood, and is thus involved in CO_2 exhalation (Fig. 1.2 A). When metabolically active tissues produce CO_2 during mitochondrial respiration, the CO_2 diffuses out of these cells into the capillaries. Once CO_2 is in the blood stream it diffuses into erythrocytes where it is converted into HCO_3^- and H^+ ("Bohr H^+") by carbonic anhydrase II (CAII). The "Bohr H^+" is buffered by deoxyhemoglobin, which in turn decreases the O_2 affinity of hemoglobin (*86*). To avoid accumulation of bicarbonate in the red blood cell, AE1 transports the bicarbonate out of the red blood cell into the plasma, in exchange for chloride. Once the blood reaches the lungs this process is reversed. In exchange for chloride, bicarbonate is transported back into the red blood cell by AE1, where it is converted back into CO_2 by CAII. Finally, CO_2 is exhaled through the lungs.

The exchange activity of AE1 is vitally important because it maximizes the blood's CO_2/HCO_3^- carrying capacity, which may be the rate limiting step to cardiovascular performance (*91*). To ensure maximum transport of bicarbonate through AE1, the protein physically interacts with CAII (Fig. 1.2)

(*92, 93*). This forms the bicarbonate transport metabolon, which increases the flux of bicarbonate through the transporter by approximately 40% (*94*). Maximizing bicarbonate transport is of special importance in the bloodstream since erythrocytes pass through a capillary in only 0.3 to 1.0 s (*95*).

The second major function of AE1 in red blood cells is to act as an anchor for the cytoskeleton (Fig. 1.2 B) (*89*). Cytoskeletal interactions with AE1 give erythrocytes the flexibility needed to pass through the capillaries. AE1 exists as dimers and tetramers in the RBC, and in the tetrameric form the cytosolic N-terminal domain of AE1 interacts with ankyrin (*96, 97*). Through ankyrin, AE1 is linked to the cytoskeletal proteins α and β-spectrin (*89*).

Other interactions with glycolytic enzymes, hemoglobin and protein 4.1 and 4.2 are mediated through the N-terminal domain of AE1, and these interactions are dependent on the phosphorylation state of the N-terminal domain (*9, 89*). Interestingly, glycolytic enzymes bound to AE1 were inhibited, indicating a role of AE1 in erythrocyte glycolysis regulation (*98*).

AE1 clustering into microscopic aggregates is also involved in the erythrocyte senescent cell recognition pathway (*99*). Biochemical stresses, such as oxidative crosslinking and hemoglobin denaturation, lead to AE1 clustering, which is recognized by antibodies that signal erythrocyte removal (*99*).

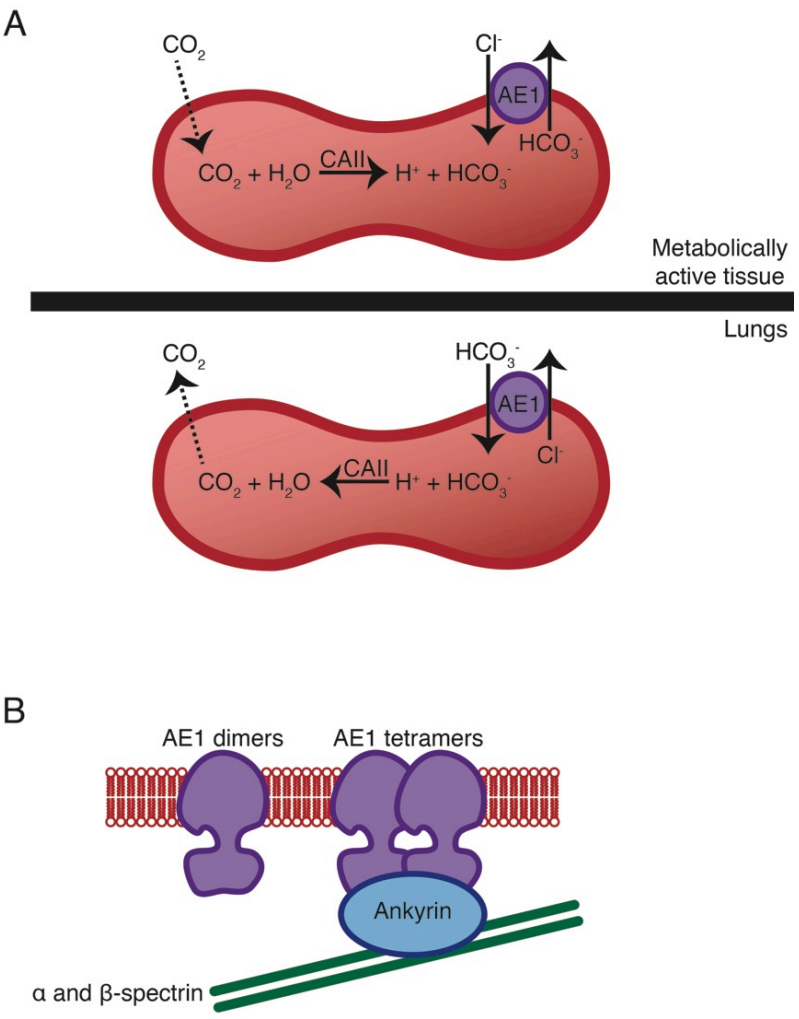

Figure 1.2 Human Erythrocyte AE1 Physiology.

(A) CO_2, produced by metabolically active tissue, diffuses into the erythrocyte and is converted to H^+ and HCO_3^- by the enzyme, CAII (top panel). HCO_3^- is transported out of the cell in exchange for Cl^- by AE1 (top panel). In the lungs HCO_3^- is transported into the cell in exchange for Cl^- by AE1 (bottom panel). HCO_3^- is converted to CO_2 by CAII and CO_2 is exhaled (bottom panel). (B) AE1 exists as dimers and tetramers in the erythrocyte plasma membrane. Ankyrin interacts with AE1 tetramers and α/β-spectrin to anchor the cytoskeleton to the plasma membrane, and this collaboration between the plasma membrane and cytoskeleton maintains the biconcave shape of erythrocytes.

1.3.1.2 Kidney AE1

In the kidneys the main function of AE1 is to contribute to acid-base homeostasis, as well as fluid and electrolyte balance (*100*). kAE1 functions in the kidneys to acidify the urine by reabsorption of bicarbonate (Fig. 1.3). Most bicarbonate reabsorption in the kidney is, however, accomplished by sodium bicarbonate co-transporters in the proximal tubule (*1*). Cl^-/HCO_3^- exchangers in the α and β-intercalated cells of the distal tubule and collecting duct are involved in the fine tuning of bicarbonate reabsorption (*1*). The β-intercalated cells of the distal tubule secrete HCO_3^- under alkalotic conditions, while the α-intercalated cells of the distal tubule secrete H^+ under acidic conditions (*1*).

In the α-intercalated cells CAII coverts CO_2, which diffuses from the blood into the cell, into H^+ and HCO_3^- (Fig 1.3) (*1, 101*). On the apical side of α-intercalated cells H^+ and H^+/K^+ ATPase proteins pump protons into the urine (Fig. 1.3). On the basolateral side of the α-intercalated cells kAE1 operates to move bicarbonate from the cell into the blood in exchange for chloride (Fig. 1.3). Together the apical ATPase proteins and basolateral kAE1 acidify the urine and prevent systemic acidosis (*1, 101*). To maintain ion homeostasis in α-intercalated cells ClC chloride channels and KCC Cl^-/K^+ co-transporters, expressed basolaterally, transport Cl^- and K^+ from the cell into the blood (Fig. 1.3) (*101*).

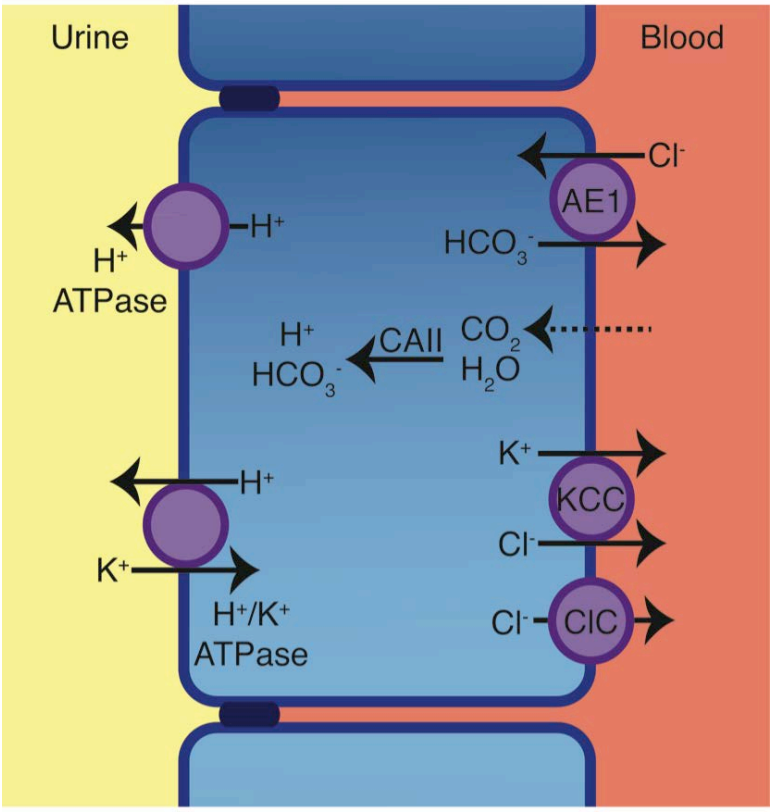

Figure 1.3 Human Kidney AE1 Physiology.

An α-intercalated cell, in the renal collecting duct epithelium, is shown in blue, with tight junctions shown in navy blue. CAII converts CO_2 into H^+ and HCO_3^-. Apical H^+ and H^+/K^+ ATPases (purple) excrete H^+ into the urine (yellow), while HCO_3^- is transported into the blood (red) in exchange for Cl^-, by basolateral kAE1 (purple). To maintain Cl^- and K^+ homeostasis basolateral Cl^- channels and Cl^-/K^+ co-transporters (purple colored ClC and KCC proteins, respectively) transport Cl^- and K^+ into the blood (red).

The N-terminal cytoplasmic domain of kAE1 forms several important protein-protein interactions. More recently, low levels of kAE1 expression in the kidney glomerulus podocytes and interactions with nephrin and integrin-linked kinase were reported (*102, 103*). This led to speculation that kAE1 has a role in maintaining the structure of podocyte foot processes and the slit diaphragm of the glomerulus (*104*).

1.3.2 Diseases Associated with AE1

1.3.2.1 Erythrocyte AE1

Many mutations in AE1, which alter expression and/or function, cause a variety of hereditary erythrocyte and kidney diseases (*1*). Hereditary spherocytosis (HS), which is the most common inherited erythrocyte membrane disorder, occurs when mutations in AE1, spectrin or ankyrin create defective interactions between the cytoskeleton and erythrocyte plasma membrane. Erythrocytes from HS patients are spheroid with a reduced cell surface and are osmotically fragile (*105*). The common features of HS are hyperhaemolysis and anemia, icterus (yellow coloration of skin and mucus membranes) and splenomegaly. Interestingly, the majority of HS AE1 mutations have no associated renal pathology (*1*). The majority of mutations in AE1 that cause HS are dominant, and result in mis-folded protein, which does not accumulate in the plasma membrane (*106*). Interestingly, these mutations localize to both the N-terminal cytoplasmic and membrane domains of AE1 (*106*).

Point mutations within the transmembrane segments of AE1 that confer cation channel activity result in hereditary stomatocytosis (*107*). Stomatocytosis is defined as the expansion of the inner membrane leading to membrane invagination and cup-shaped erythrocytes. Affected RBCs have an increased temperature-dependent Na^+ and K^+ leakage, with no reduction of deformability (*108*).

Southeast Asian Ovalocytosis (SAO) arises from deletion of AE1 residues 400-408 at the beginning of the first transmembrane segment (*109*). Interestingly, the heterozygous SAO mutation has no adverse symptoms, while the homozygous SAO mutation is lethal *in utero*. The SAO mutation abolishes AE1 transport function (*110*), however, the mutation does not alter the transport activity of the WT monomer in heterodimers (*32, 111-113*). WT AE1 in erythrocytes of SAO individuals none the less displays structural differences from WT AE1 in erythrocytes of WT individuals (*113*). Erythrocytes from SAO patients have an increased rigidity, due to stronger interactions between AE1 and the cytoskeleton, which provides protection from the cerebral effects of malaria (*114*). In fact, one of the major contributors to the malarial parasite (*Plasmodium falciparum*) invasion of erythrocytes is the pfalhesin site, which may partially be formed by AE1 (*115, 116*).

In addition, the membrane domain of AE1 is known to form several different blood antigen groups, which include the Diego groups (*117*).

Although it is infrequent, the Diego blood groups can cause transfusion reactions and hemolytic disease in newborns (*117*).

1.3.2.2 Kidney AE1

In the kidney, mutations in AE1 can cause distal renal tubular acidosis (dRTA), which results in metabolic acidosis and impaired urine acidification (*1*). The disease is also characterized by growth retardation, hypercalciuria, hypokalemia, nephrocalcinosis, kidney stones, and eventual renal failure (*118*). Patients can present with complete dRTA, which results in spontaneous metabolic acidosis, or with incomplete dRTA, which generally results in symptoms appearing only after an acid challenge (*16*). A combination of dominant and recessive dRTA-causing mutations result in homozygous, heterozygous and compound heterozygous (two alleles with different dRTA mutations) patients. Often dRTA-causing mutations alter the trafficking of AE1 to the basolateral surface of α-intercalated cells (*119*). Interestingly, four dRTA mutations (R589H, G609R, S613F, and G701D) have been reported to have an AE1 mediated cation leak, while maintaining anion exchange function (*120*).

1.3.2.3 Mouse Models

A homozygous loss of AE1 is presumed to be lethal *in utero*. Only one example of a homozygous Coimbra (V488M) patient has suggested a loss of AE1 expression in erythrocytes and presumably the α-intercalated cells (*7*). The fetus stopped moving at week 34 and was delivered by emergency

cesarean section at week 36 (*7*). This patient had to be resuscitated and kept alive by respiratory assistance and intensive blood transfusions (*7*).

Multiple AE1 knock-out mouse models exist. One mouse model eliminated eAE1 expression, while apparently maintaining kAE1 expression (*121*). Another mouse model eliminated expression of eAE1 and kAE1 (*122*). In both models, the majority of homozygous mice (80-90%) died within two weeks. These mice also had anemia and retarded growth. Erythrocytes from AE1 knock-out mice spontaneously shed membrane vesicles and tubules, leading to severe spherocytosis and hemolysis (*121, 122*). More recently, an AE1 knock-out mouse model demonstrated symptoms consistent with complete dRTA, including nephrocalcinosis, hypercalciuria, hyperphosphaturia, and hypocitraturia (*123*).

1.3.3 Inhibitors of AE1 Transport Activity

AE1 studies have identified several residues involved in Cl^-/HCO_3^- exchange and inhibitor binding. The most studied class of AE1 inhibitors are the stilbene disulfonate compounds, which are widely used as anion exchange inhibitors for a large number of bicarbonate transporters and chloride channels. The K_i of stilbene disulfonate inhibitors on AE1 anion exchange ranges from 0.08 μM for 4,4'-diisothiocyanostilbene-2,2'-disulfonate (DIDS) to >300 μM for 4,4'-diaminostilbene-2,2'-disulfonate (DADS) (*84*). Binding of stilbene disulfonates to AE1 locks the protein in its outward facing conformation (*124*), and is associated with an increase of AE1 thermal stability (*125*). The stilbene disulfonate, 4,4'-

diisothiocyanodihydrostilbene-2,2'-disulfonate (H_2DIDS), covalently cross-links AE1 K539 and K851 (*126*). The stilbene disulfonate binding site is also somewhat buried in the AE1 structure as anti-H_2DIDS antibodies are only effective upon AE1 denaturation (*127*). As well, several regions of AE1 (G565, S643-M663, and S731-S742) become less aqueous accessible upon the addition stilbene disulfonate inhibitors, which indicates that these regions are involved in the inhibitor binding site or undergo conformational changes upon inhibitor binding (*128*).

Other AE1 inhibitors include oxonol dyes, flufenamic acid, and squalamines (*84, 129*). In addition, chemical modification of several AE1 residues (including reductive methylation, dinitrophenylation, and treatment with pyridoxal 5-phosphate or Woodward's reagent K) inhibits transport activity (*84, 130*).

1.3.4 Transport Mechanism

AE1 anion exchange is proposed to occur through a "ping-pong" mechanism, in which there are outward and inward facing conformations of AE1 and a single anion-binding site (*84, 85*). Reorientation of AE1 from the outward to inward facing conformation (or vice-versa) occurs upon binding of a single anion to transport the substrate across the lipid bilayer (*84, 85*). Several AE1 mutations, however, convert the protein into a non-selective cation channel (*107, 120, 131-133*). This suggests that AE1 may be a modified ion channel, with a transmembrane pore comprised of residues that confer

anion exchange activity, which only requires small conformational changes during anion exchange (*134*).

Regions of AE1 vital to Cl^-/HCO_3^- exchange function were investigated by chemical modification or mutational analysis of AE1. Human erythrocyte AE1 E681, and the corresponding mouse AE1 E699, play an essential role in both Cl^- transport and SO_4^{2-}/H^+ co-transport (*130, 135*). Modification of AE1 E681 with Woodward's reagent K, which converts the carboxylate group into a hydroxyl group, abolishes chloride transport and changes SO_4^{2-} transport into a H^+ independent process (*130*). Mutational analysis of human and mouse AE1 confirms these results (*135, 136*). In addition, modification of A666C, S667C, L669C, L673C, L677C, L680C, I684C, and L688C-AE1, with small hydrophilic sulfhydryl compounds, blocked Cl^-/HCO_3^- exchange (*136*). These residues map to the same helical face as AE1 E681, and thus, were identified as pore lining residues (*136*). A similar cysteine-scanning mutagenic study of the C-terminal portion of AE1 identified additional pore lining residues in the region V849-L863 and a substrate charge filter in the S852-L857 region (*137*). AE1 H834 is also important to AE1 mediated anion transport, as assessed by mutagenesis and chemical modification with diethyl pyrocarbonate (DEPC) (*138, 139*). Interestingly, mutation of human AE1 K539, which covalently reacts with H_2DIDS, can restore the activity of AE1 H834 mutants (*140*). Compiling AE1 biochemical data has allowed for the proposal of an "inverted basket" model for AE1 transport, which involves

AE1 K826, R730 and E681 forming a permeation barrier (*141*). There is no structural evidence, however, to support this model.

1.4 AE1 Structure

AE1 is composed of three domains: a cytosolic N-terminal domain, a transmembrane domain and a cytosolic C-terminal domain. The C-terminal domain of AE1 contains an acidic motif (DADD), which interacts with CAII to form the bicarbonate transport metabolon (*92, 94*). The N-terminal cytoplasmic domain of AE1 is approximately 400 residues and forms a large globular structure. The approximately 500 residue long transmembrane domain of AE1 contains 12-14 transmembrane segments (Fig. 1.4). The membrane domain of AE1 is alone responsible for the Cl^-/HCO_3^- exchange function of the protein (*142, 143*). Other electroneutral anion exchangers (AE2 and AE3) share 80% sequence similarity with the AE1 membrane domain, and likely share the same membrane protein fold in this domain.

1.4.1 N-terminal Cytoplasmic Domain

The crystal structure of the N-terminal cytoplasmic domain of erythrocyte AE1 (residues 1-379) has been solved to a resolution of 2.6 Å (*145*). The cytoplasmic domain of AE1 (cdAE1) forms a dimer (75 X 55 X 45 Å) and each monomer of the dimer, containing 11 β strands and 10 α helices, is composed of three sub-domains: the large globular sub-domain (residues 55-290), the helix loop region (residues 291-303), and the dimerization arm (residues 304-357) (Fig. 1.5). The first 54 residues of AE1 are not resolved in the structure. This flexible region is very acidic and known to form multiple

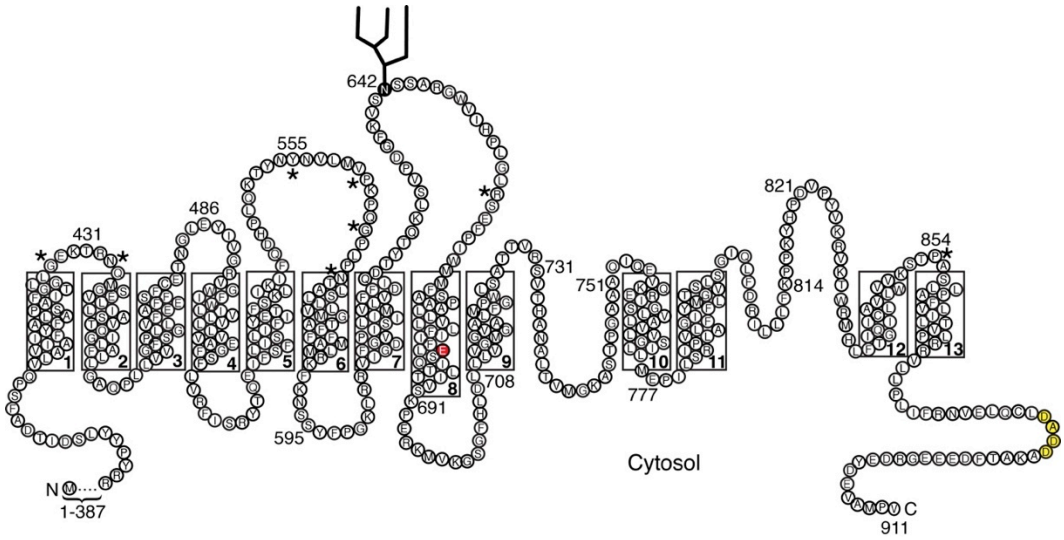

Figure 1.4 Topology Model of Human AE1.

Numbers indicate residue numbers in eAE1, and bold numbers indicate transmembrane segments (boxed regions). Residue E681, involved in the permeability barrier and anion translocation pathway, is shown in red. The DADD CAII binding motif is highlighted in yellow. AE1 has a single N-linked glycosylation site, N642, which is marked by a large branched structure. Blood group antigens are marked by asterisks. N and C indicate N and C-termini, respectively. The extended structure shown in the 806-835 region is not meant to imply folding of the protein in the model (*144*).

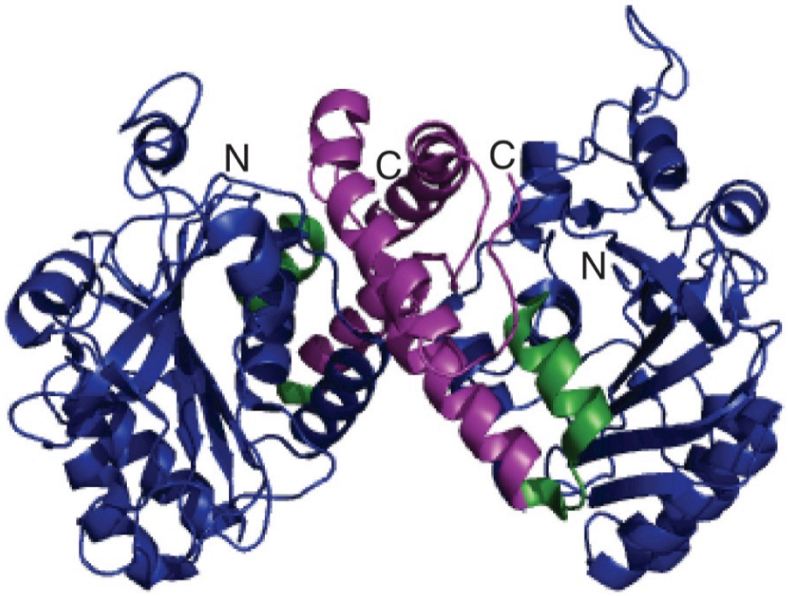

Figure 1.5 AE1 N-terminal Cytoplasmic Domain Structure.

The AE1 N-terminal domain structure is shown as a dimer, with the N and C-termini of each monomer indicated (N and C, respectively). In each monomer the large globular sub-domain (residues 55-290) is colored blue, the helix loop region (residues 291-303) is colored green, and the dimerization arm (residues 304-357) is colored purple (*145*).

protein interactions. Crystallization of cdAE1 was achieved at a pH of 4.8. It is well established that cdAE1 undergoes a reversible pH dependent conformational change, with the protein being more stable and compact at a lower pH (*89*).

Mutational analysis of the AE1 N-terminal cytoplasmic domain has identified regions of AE1 (175-185 and 63-73) important in the formation of AE1 and ankyrin protein-protein contacts (*146*). Molecular docking software identified hydrophobic interactions and salt bridges between AE1 residues in these regions and ankyrin residues (*146*).

1.4.2 Membrane Domain

Substantial structural information is known about the AE1 membrane domain, because of the abundance of AE1 in erythrocytes and the ease of its purification by ion exchange chromatography (*147*). Still, there is no high-resolution structure of the membrane domain of AE1. Extensive work has assessed the topology of AE1, and possible residues involved in the dimer interface or translocation pore of the protein. While these studies have provided a large body of biochemical data, many questions about the structure and transport mechanism of the AE1 membrane domain still remain.

1.4.2.1 Topology

Hydropathy plots of AE1 predict regions of hydrophobicity in the N-terminal half of the AE1 membrane domain, which are consistent with transmembrane spanning helices (*148*). The topology of the C-terminal half

of the AE1 membrane domain is much more controversial, as hydropathy plot analysis in this region is much more difficult to interpret (*148*). Thus, several studies have investigated the topology of AE1 through epitope mapping, N-linked glycosylation insertion, proteolytic cleavage, and cysteine-scanning mutagenesis (*126, 139, 144, 149-157*).

AE1 has a single extracellular glycosylation site at N642, which is not required for transport activity (Fig. 1.4) (*158*). Mutations at several AE1 residues form blood group antigens, thus, these residues must be extracellularly accessible (Fig. 1.4) (*152, 157*). As well, numerous aqueous accessible AE1 proteolytic cleavage sites were identified (*126, 151*). Several of these proteolytic cleavage sites were determined under alkaline conditions, however, and may represent areas of AE1 affected by alkaline induced denaturation.

Several studies investigated AE1 topology using N-glycosylation mutagenesis (*155, 156, 159, 160*). N642D-AE1 was utilized in all N-glycosylation mutagenesis studies, to eliminate the endogenous AE1 glycosylation site. Mutations introduced into N642D-AE1 included N-glycosylation acceptor site insertions (N-X-S/T, where X can be any amino acid) and AE1 extracellular loop 4 insertions. AE1 N-glycosylation insertion mutants were expressed in HEK293 or COS-7 cells by transient transfection, or translated *in vitro* using rabbit reticulocyte lysate or microsomal membranes. The amount of AE1 mutant N-glycosylation was determined by enzymatic deglycosylation, concanavalin A lectin binding, and SDS-PAGE gel

shifts monitored by densitometry. Using this method, the location of several extracellular loops was confirmed and the ends of transmembrane helices were mapped. The data from these experiments is difficult to interpret and implement in topology predictions (*161*).

Fortunately, cysteine-scanning mutagenesis in regions of AE1 has provided additional insights into AE1 topology (*144, 149, 150*). Endogenous AE1 cysteine residues are not required for AE1 transport activity or dimerization (*162*), which permits the utilization of a cysteine-less AE1 mutant in these topological investigations. Y555C-AE1 was used as an extracellularly accessible control, as it is located between two chymotryptic sites in extracellular loop 3. The intracellular control, K892C-AE1, was chosen because it is located in the hydrophilic region corresponding to the intracellular C-terminal domain. AE1 cysteine mutants were expressed in HEK293 cells to determine whether residues were aqueous accessible on the basis of biotin maleimide reactivity. In addition, aqueous accessible AE1 cysteine mutants were further investigated to determine extracellular or intracellular localization. Decreased biotin maleimide reactivity of AE1 aqueous accessible mutants, which were pre-treated with membrane impermeant sulfhydryl compounds, indicated an extracellular localization. Cysteine-scanning mutagenesis of AE1 S643-S690 defined the boundaries of a transmembrane spanning helix (M664-Q683), and placed S643-M663 and I684-S690 on the extracellular and intracellular surfaces, respectively (*149*). Another study examined the C-terminal region of AE1, F806-C885, by

cysteine-scanning mutagenesis (*144*). Regions localized to the plane of the lipid bilayer included F836-K851 and S856-R871. Extracellular regions included P815-K829 and S852-A855, and intracellular regions included I872-C885.

The combination of AE1 biochemical data and hydropathy plot analysis described above has generated an improved AE1 topology model (Fig. 1.4) (*144*). Unique features in this AE1 topology model include a re-entrant loop between helices 9 and 10, and an extended structure in the plane of the lipid bilayer between helices 11 and 12 (Fig. 1.4). More recently, two additional AE1 topology models were proposed in one study (*163*). The first AE1 topology model was generated by assuming AE1 contained an internal repeat, and the second model was generated by assuming AE1 shared structural similarities with *E. coli* ClC (*163*). These AE1 topology models were created because the majority of membrane transport protein structures contain an inverted repeat, and a recent structure of the AE1 membrane domain suggested it shares a common protein fold with ClC proteins (*164*). Both novel AE1 topology models agree to varying degrees with AE1 biochemical data (*161*). Until more structural data can be collected for AE1, an improved topology model remains elusive.

1.4.2.2 Oligomerization and Helical Packing

AE1 dimeric oligomerization was first observed by cross-linking of endogenous AE1 cysteine residues (*165*). Size exclusion chromatography of full-length erythrocyte AE1, in octyloxyethylene dodecylether ($C_{12}E_8$)

detergent micelles, revealed a heterogeneous oligomeric composition composed of 70% dimer and 30% tetramer and high oligomeric forms, which included protein aggregate that eluted at the column's void volume (*97*). Full-length erythrocyte AE1 could only be dissociated into monomers upon protein denaturation with sodium dodecyl sulfate (SDS) or 2,3-dimethylmaleic anhydride (DMMA), indicating strong interactions between monomers and likely a large surface area at the dimeric interface (*97*). AE1 erythrocyte membrane domain was exclusively dimeric, and did not form higher oligomers (*97*). Thus, the N-terminal cytoplasmic domain stabilizes higher oligomeric forms (tetramers) of AE1.

AE1 cross-linking (*166*), and fluorescence resonance energy transfer (FRET) distance measurements (*167*) have attempted to develop a helical packing model of AE1. AE1 FRET distance measurements were made in an AE1 concatamer, where two AE1 monomers were joined to form a single polypeptide AE1 dimer (*167*). In this manner different AE1 cysteine point mutations could be introduced into each AE1 monomer of a cysteine-less AE1 concatamer background. Distance measurements were made with FRET acceptor and donor probes conjugated to sulfhydryl reactive groups, which would react with cysteine residues introduced in the AE1 concatamer, or with FRET probes conjugated to a hydrophobic moiety, which would partition into the lipid bilayer. Using this strategy, AE1 Q434 was found to be located 49 Å from the corresponding Q434 on the second monomer of the AE1 concatamer, and <33 Å from the lipid bilayer (*167*). AE1 cross-linking

measurement were made across the dimer interface of AE1 cysteine point mutants expressed in HEK293 cells, using sulfhydryl reactive cross-linkers of varying lengths (6, 10 and 16 Å) (*166*). On the basis of data gathered by AE1 cross-linking, transmembrane helix two was predicted to be at the dimer interface, transmembrane helices three and six were maximally one helix away from the dimer interface, and transmembrane helices one and four were maximally two helices away from the dimer interface (Fig. 1.4) (*166*). In both studies, AE1 measurements were dependent on correct AE1 topological interpretations and minimal flexibility during AE1 transport of regions examined for consistent distance measurements (*166, 167*). Thus, data from these studies must be viewed critically and likely only represent distance approximations.

Alternatively, co-expression of AE1 fragments was examined by monitoring co-immunoprecipitation and stilbene disulfonate sensitive chloride transport, using *in vitro* cell free translation and *X. laevis* oocytes expression systems (*168-171*). Co-expression of several complementary and overlapping AE1 fragments, which were truncated in AE1 loop regions, integrated in the membrane to allow AE1 mediated chloride transport. Interestingly, co-expression of non-complementary AE1 fragments, which eliminated AE1 N554-K639, generated significant AE1 mediated chloride transport (*169*). Supporting this finding, an AE1 mutant, which replaces residues N554-K639 with a G-S-S-G linker, had stilbene disulfonate sensitive AE1 mediated chloride transport activity when expressed in *X. laevis* oocytes

(*172*). Together, these studies on co-expression of AE1 fragments also generated hypotheses on AE1 helical packing (*168*). Still, a detailed AE1 helical packing model, which confidently assigns locations of all transmembrane spanning segments, cannot be created.

1.4.2.3 Expression and Purification Strategies

Human AE1 is highly expressed and easily purified from erythrocytes (*147*). Erythrocytes are separated from blood plasma, white cells and platelets by centrifugation. If required, old and young erythrocytes may be separated by Percoll density-gradient centrifugation (*173*), to provide a more homogeneous AE1 population. Once erythrocytes are isolated, red blood cell ghosts are prepared by hypotonic lysis and multiple centrifugations to remove cytosolic proteins (*147*). AE1 is fully solubilized from red blood cell ghosts by the detergent $C_{12}E_8$ and purified by ion-exchange chromatography (*147*). Further purification of AE1 or detergent exchange (*174*) is accomplished by size-exclusion chromatography. Alternate non-ionic detergents, such as dodecylmaltoside (DDM), have also been used in AE1 purification (*174, 175*).

The AE1 membrane domain can also be isolated and purified from erythrocytes (*147, 175*). The membrane domain is isolated by treatment of red blood cell ghosts with trypsin and membrane stripping using EDTA and alkaline pH conditions (*147, 175*). This removes the AE1 cytosolic N-terminal domain and all peripheral membrane proteins. Purification of the AE1

membrane domain from erythrocytes produces mg quantities of AE1 with >95% purity, which is suitable for crystallization trials (*175*).

While large amounts of AE1 can be highly purified from erythrocytes and crystallized, there is still no high-resolution structure (*164, 175-179*). This is mainly due to microheterogeneity of erythrocyte AE1 arising from proteolysis, methylation and fatty acylation, which prevent high quality crystal formation (*175*). Thus, attempts at over-expression and purification of human erythrocyte AE1 membrane domain in yeast have been made to produce protein suitable for crystallization trials (*180, 181*). Constitutive expression of AE1 in *S. cerevisiae*, under the yeast phosphoglycerate kinase gene promoter, resulted in expression of 0.7 mg AE1/l of culture (*180*). AE1 was successfully solubilized from yeast membranes with lysophosphatidyl choline (LPC); however, purification of this N-terminally His-tagged AE1 resulted in low yields with only 35% purity (*180*). Also AE1 was not targeted to the plasma membrane, and was likely retained in the ER (*180*). Even though this expression and purification scheme was not entirely successful, it was encouraging as purified AE1 was monodisperse and functionally similar to erythrocyte AE1 (*180*). Another study expressed the AE1 membrane domain in *S. cerevisiae* under the inducible GAL10-CYC1 hybrid promoter (*181*). In contrast to the previous study, there was accumulation of AE1 at the plasma membrane in this study, but no attempts at AE1 purification were made (*181*).

Other groups have attempted over-express fungal AE1 homologues in yeast (*182*, *183*). A *S. cerevisiae* anion transporter homologue, YNL275w, was His-tagged, expressed in *S. cerevisiae*, and purified by metal affinity chromatography. The purified protein was non-glycosylated and bound to stilbene disulfonates. Low expression of the YNL275w construct (~100 μg/l) prevented crystallization trials of this anion transporter homologue. Another fungal AE1 homologue, *Phanerochaete chrysosporium* anion exchanger protein (PcAEP), was overexpressed in *Pichia pastoris* (*183*). PcAEP was His-tagged and purified by metal affinity and size exclusion chromatography. From 1 l of culture 1.5 mg of PcAEP was obtained at >95% purity, and the purified protein bound to stilbene disulfonates. Thus far, PcAEP is the most suitable candidate for future AE1 crystallization trials, with the exception of erythrocyte AE1.

1.4.2.4 Structures

Low-resolution EM structures of the human erythrocyte AE1 membrane domain provide little detail on AE1 structure, but rather provide a surface representation of AE1. The first human erythrocyte AE1 membrane domain structure described was from protein reconstituted with lipids to form two-dimensional tube or sheet crystals (*176*). These crystals were negatively stained, imaged by electron microscopy, and yielded two-dimensional projection maps at 20 Å resolution. The maps revealed two different AE1 dimer structures, with dimensions of 110 X 40 Å for sheet crystals and 120 X 35 Å for tube crystals. Both crystal forms had a

depression in the center of the dimer possibly indicating the anion translocation pore. AE1 monomers were described as having three subdomains, with two subdomains creating a rectangular core (40 X 50 Å) and one subdomain (15 X 25 Å) connected to the core by a flexible linker.

Improvements on the initial two-dimensional AE1 EM structure were made by a subsequent study, which created a three-dimensional projection map by electron microscopy of negatively stained two-dimensional sheet crystals (*177*). Here, AE1 was described as a U-shaped dimer of 60 X 110 Å with a thickness of 80 Å. The base of the U-shaped canyon is 40 Å, sufficient to span the lipid bilayer, and was proposed to be the opening of the translocation pore. The two protrusions of the U-shaped AE1 dimer were hypothesized to be loops connecting transmembrane fragments.

More recently, tubular crystals of human erythrocyte AE1 resulted in an 18 Å resolution three-dimensional structure, obtained by cryo-electron microscopy of unstained protein (*178*). The overall dimensions of this structure (60 X 110 Å with a thickness of 70 Å) were similar to the previous three-dimensional projection map described (*176*), however, differences in protrusions from the structure were observed. These differences were attributed to alterations in crystallization conditions, including the presence of the AE1 inhibitor H_2DIDS and absence of negative stain in the more recently obtained structure (*178*).

Another erythrocyte AE1 EM structure, using previously described AE1 crystallization techniques (*178*), improved upon the resolution (7.5 Å in

X-Y plane and 16 Å along Z-axis) of the three dimensional structure (*164*). This AE1 EM structure was described as a rhombus of 50 X 120 Å, which had a similar appearance as ClC chloride channels. This structure also allowed the visualization of several AE1 transmembrane helices, but lacked sufficient densities to assign positions for all AE1 transmembrane helices. Several long and tilted helices were observed in the AE1 EM structure. When compared to the ClC chloride channel structure, it was found that helices 1+2 and 8+9 of AE1 shared a similar structure as ClC helices B+C and J+K (*164*). Thus, the authors of this study proposed that AE1 and ClC chloride channels share the same protein fold in their respective membrane domains.

Three-dimensional crystals from human AE1 erythrocyte membrane domain have diffracted X-ray to 14 Å (*184*). While a structure was not determined from these crystals, several factors important in AE1 crystallization were described. One of the major issues discussed was protein micro-heterogeneity due to variations in post-translational modifications, such as glycosylation and acylation. Crystals were only obtained upon AE1 deglycosylation and removal of the N-terminal cytoplasmic domain by trypsinolysis. Unfortunately trypsin treatment of AE1 introduces micro-heterogeneity itself, as several tryptic sites are present in the flexible region connecting the AE1 N-terminal cytoplasmic domain to the membrane domain. AE1 crystallization was also highly dependent on the detergent used and amount of lipid molecules co-purified. Together these

factors explain the difficulties faced during erythrocyte AE1 crystallization trails.

Attempts have been made to obtain a structure for full-length erythrocyte AE1 (*179, 185*). A recent 24 Å resolution structure of bovine erythrocyte AE1 was obtained by negative staining electron microscopy and single particle analysis (*179*). There is little detail observed in this AE1 EM structure, but it does reveal two domains of the AE1 dimer (the N-terminal cytoplasmic domain and membrane domain) connected by a flexible linker region.

1.5 Membrane Protein Structures

Relative to soluble proteins, there are very few structures of membrane proteins in the Protein Data Bank (PDB), even though they represent approximately 30% of all proteins. The first membrane protein structure of the photosynthetic reaction center was not determined until 1985 (*186*), and the first structure of a heterologously expressed membrane protein, the KcsA potassium channel, was determined in 1998 (*187*). According to the most recent update of the Membrane Proteins of Known 3D Structure database (*188*), 792 membrane protein structures exist of 281 unique proteins. While advancements in technology and techniques, used to express, purify and crystallize membrane proteins, have steadily increased the frequency of membrane protein structural determinations, several bottlenecks still exist. These include problems with membrane protein expression, denaturation, aggregation, and crystallization conditions. In

particular, eukaryotic membrane proteins are especially difficult to work with, as these proteins are often expressed at low levels and less stable in detergent solutions. Thus, the majority of membrane protein structures are from bacterial homologues.

1.5.1 Expression

Only a limited number of membrane proteins are highly expressed in their native environment (*189*). Thus, heterologous expression is required for many membrane protein crystallization targets. *E. coli* is typically used as a host for soluble protein heterologous expression. While *E. coli* is a suitable expression system for prokaryotic membrane proteins, it lacks an endoplasmic reticulum, Golgi apparatus, and chaperone proteins required to express functionally active eukaryotic membrane proteins (*190*). Quantities of eukaryotic membrane protein suitable for crystallization trials have been expressed in yeast (*P. pastoris* and *S. cerevisiae*) and insect cells (*191, 192*). The yeast expression systems have several advantages compared to insect cells, including low cost, easy culture conditions, and straightforward genetic manipulation. Other eukaryotic membrane protein expression systems, such as mammalian cell lines and cell free extracts, have not been as successful or well characterized (*191, 192*).

In addition to expression system selection, optimization of the expression conditions is important in membrane protein expression (*191, 192*). For soluble proteins the goal is often to express the maximal quantity of protein in the shortest amount of time. For membrane proteins, this

approach often generates mis-folded proteins, which is toxic to the expression system as it overwhelms the membrane protein expression and quality control machinery. As a result this often leads to lower expression levels of both mis-folded and properly folded membrane protein. Modification of the promoter, induction time, and culture temperature are all techniques used to optimize membrane protein expression. The co-expression of protein chaperones or addition of small-molecule chemical chaperones is also an effective strategy for the expression some membrane proteins. As well, special consideration must be made for the addition of purification tags to membrane proteins, as this often affects expression.

In recent years, green fluorescent protein (GFP) has become a useful tool in high-throughput fluorescence based optimization of membrane protein overexpression (*193-195*). When GFP is fused C-terminally to a membrane protein, proper folding of the membrane protein is required for proper folding of fluorescent GFP. Using this technique membrane protein expression can be monitored directly in liquid culture by GFP fluorescence, which allows for rapid screening of expression conditions. GFP fusion is also useful in assessing membrane protein stability and monodispersity in different detergent solubilization conditions prior to purification, by monitoring GFP fluorescence during size exclusion chromatography.

1.5.2 Detergents and Purification

Membrane protein purification is inherently more difficult than soluble protein purification, because membrane proteins must be solubilized

from the lipid bilayer using detergent prior to purification (*196, 197*). The stability of membrane proteins in detergent solution (to avoid protein aggregation or denaturation) is vital for successful protein purification and crystallization. Non-ionic or zwitterionic detergents are used for membrane protein purification, which are much less denaturing than ionic detergents. The detergent alkyl chains are usually seven to twelve carbons long, which form micelles with a hydrophobic core similar in thickness to a lipid bilayer. Detergents with shorter alkyl chains are often used during purification, however, since these detergents have a high critical micelle concentration (CMC), which permits detergent exchange by dialysis that can be useful in optimizing crystallization conditions. The most common classes of detergents used in membrane protein crystal structures thus far are maltosides, glucosides, dimethyl *N*-amine oxides and poly-oxyethylenes (*189, 196*). The detergent concentration, used during membrane protein purification to maintain monodispersity, must be above the CMC for the detergent, which is influenced by temperature and salt concentrations (*196*).

Beyond detergent considerations, purification of membrane proteins utilizes many of the same strategies as soluble proteins (*196, 197*). Affinity tags (antibody epitopes, six-histidine residues, glutathione-S transferase, and maltose binding protein) are typically added to membrane proteins as a purification strategy (*189, 196*). Special considerations, however, need to be made when using affinity tags, as detergent present during membrane protein purification may prevent access to affinity tag protease cleavage sites

or inhibit certain proteases altogether (*197*). The most common membrane protein affinity purification method is immobilized metal-affinity chromatography, since it is a relatively inexpensive technique and the small six-histidine affinity tag does not need to be removed prior to crystallization. Further protein purification is often accomplished by size exclusion or ion exchange chromatography.

1.5.3 Crystallization

Membrane proteins are typically crystallized using techniques also implemented for soluble proteins. Challenges unique to membrane protein crystallization include instability of membrane proteins in detergent micelles, detergent phase separation, and lack of hydrophilic regions capable of forming crystal contacts (*189, 196, 198*). Alterations of the membrane protein being crystallized can increase protein stability. These strategies include the use of homologues from thermophillic organisms and mutant variants, which remove flexible regions or lock the protein in a single conformation. Removal of flexible regions can also be accomplished by proteolysis.

Changes in the crystallization conditions also greatly affect the success of obtaining membrane protein crystals (*189, 196*). Detergent selection plays a prominent role in crystallization success. Using detergents with short alkyl chains that form smaller micelles has advantages, since these detergents expose larger hydrophilic regions capable of forming crystal contacts (*189, 196, 199*). The disadvantage, however, is that these detergents are usually

more denaturing (*174, 189, 196, 200*). While much success has been observed using dodecyl-β-D-maltoside and β-octylglucoside, many membrane proteins are unstable in these detergents (*189, 196*). Thus, synthesis of novel detergents, which provide both protein stability and exposure of protein regions for crystal contact formation, continues to be a priority (*189, 196*). In addition, small amphiphiles, heavy-atom additives, phospholipids and high affinity ligands stabilize membrane proteins, reduce heterogeneity and improve crystal contacts (*189, 196*). Alternatively, co-crystallization of membrane proteins with monoclonal antibody Fab or Fv fragments has also been quite successful, since the antibody fragments provide large surfaces for crystal contacts (*189, 196, 201-204*).

Advances in crystallization techniques aimed at improving membrane protein stability, such as crystallization in lipid cubic phase (LCP) and bicelles, are becoming more widely used for successful membrane protein crystallization trials (*198, 205*). Bicelles are lipid discs composed of long chain phospholipids and amphiphiles in an aqueous environment into which membrane proteins can be reconstituted. The LCP technique uses a synthetic lipid bilayer that forms a three-dimensional matrix. Membrane proteins are reconstituted into the lipid and addition of crystallization cocktail induces lateral membrane protein movement resulting in crystal formation in the LCP. Also, advances in crystallization robot technologies and microfocus beam-lines (to create smaller X-ray beams) will continue to promote determination of membrane protein structures (*189*).

1.5.4 Membrane Transporter Protein Folds

Membrane protein structures have been determined for ion channels, receptors, membrane proteases, ATPases, electron transport chain complexes, transporters, and several other classes of membrane proteins (*188*). The focus here is membrane transporter proteins, and as more crystal structures are published unique trends of membrane transporters are being observed. Firstly, many membrane transport protein structures have described the presence of an internal inverted repeat, where the N and C-terminal halves of the protein have a similar fold. Secondly, it is becoming apparent that many membrane transporters have the same overall protein fold, while having little sequence homology and different functional roles.

One example of this is the major facilitator superfamily (MFS) of integral membrane transporters, which is the largest family of secondary active transporters (*206, 207*). The MFS transporters are not only divergent in sequence, but also include uniporters, symporters, and antiporters that transport a wide range of substrates (amino acids, nucleosides, sugars, ions and drugs among many other things) (*206, 207*). Even with such divergence amongst members of the MFS transporters, all published structures, including LacY (*208, 209*), GlpT (*210*), EmrD (*211*) and OxlT (*212, 213*) share a common fold. The structure of the MFS transporters contains an inverted repeat structure composed of 12 transmembrane spanning helices (*206, 207*).

Similarly, several structures of Na^+ symporters from different gene families all have been described as sharing a common core LeuT fold (*214*). The structures of LeuT (*215*), BetP (*216*), vSGLT (*217*), Mhp1 (*218*), and AdiC (*219*) are all composed of a ten transmembrane helical core, containing two related five helix bundles (*214*).

The only structure available for a member of the cation/proton antiporter family is of *E. coli* NhaA, which was described as a unique fold that contains an inverted topology repeat consisting of transmembrane helices 3-5 and 10-12 (*220*). Homology models of human NHE1 (*221*) and NHA2 (*222*) were successfully created, on the basis of the *E. coli* NhaA crystal structure. Human NHE1 and NHA2 share low sequence identity with *E. coli* NhaA (10% and <15%, respectively), which is normally below the threshold for successful homology modeling. Recent analysis by NMR of the individual transmembrane segments of NHE1 provides experimental support for transmembrane structures predicted by the NHE1 homology model (*223, 224*).

The structure of ClC proteins is also comprised of an internal inverted repeat (*225*). AE1 as well as other bicarbonate transporters (SLC26A3 and SLC26A6), which are not included in the ClC gene family, have been proposed to share a common fold with ClC proteins (*164, 226*). A homology model of murine SLC26A6, was created using *E. coli* ClC as a template structure (*226*). Sequence identity between *E. coli* ClC and SLC26 proteins (11%) is quite low, similar to NHE1 and NHA2 with *E. coli* NhaA. Interestingly, the SLC26A6

homology model revealed a conserved glutamate residue (E357) corresponding to the extracellular glutamate gate of *E. coli* ClC, and drastic changes in SLC26A6 transport activity were observed in E357A and E357K-SLC26A6 (*226*).

1.6 ClC Chloride Channels

Nine human isoforms of ClC chloride channels divide into three homology branches (*227*). One homology branch is comprised of the plasma membrane channel-like ClCs, and the other two homology branches are comprised of intracellular $2Cl^-/H^+$ exchanger ClCs (Fig 1.6). Plasma membrane ClC proteins are involved in transepithelial transport, maintaining cell volume and stabilization of membrane potential. Intracellular ClC proteins are involved in endosomal/lysosomal acidification. Human ClC proteins are widely expressed in the body and associated with diseases such as idiopathic epilepsy, Dent's disease, Bartter's disease, myotonia, and osteopetrosis (*227, 228*).

In addition to eukaryotic ClC proteins, which are expressed in almost every organism, there are several prokaryotic ClC proteins. Numerous structural and functional studies have been conducted on the prokaryotic *E. coli* ClC protein, which functions as a $2Cl^-/H^+$ exchanger (*229*). *E. coli* ClC has a fast turnover rate of 2100 anions/s (*230*) and is capable of transporting not only Cl^-, but also Br^-, NO_3^-, and SCN^- with varying degrees of H^+ coupling (*231*). Mutational analysis of *E. coli* ClC has highlighted the importance of an extracellular glutamate (E148) in chloride transport, as well as residues

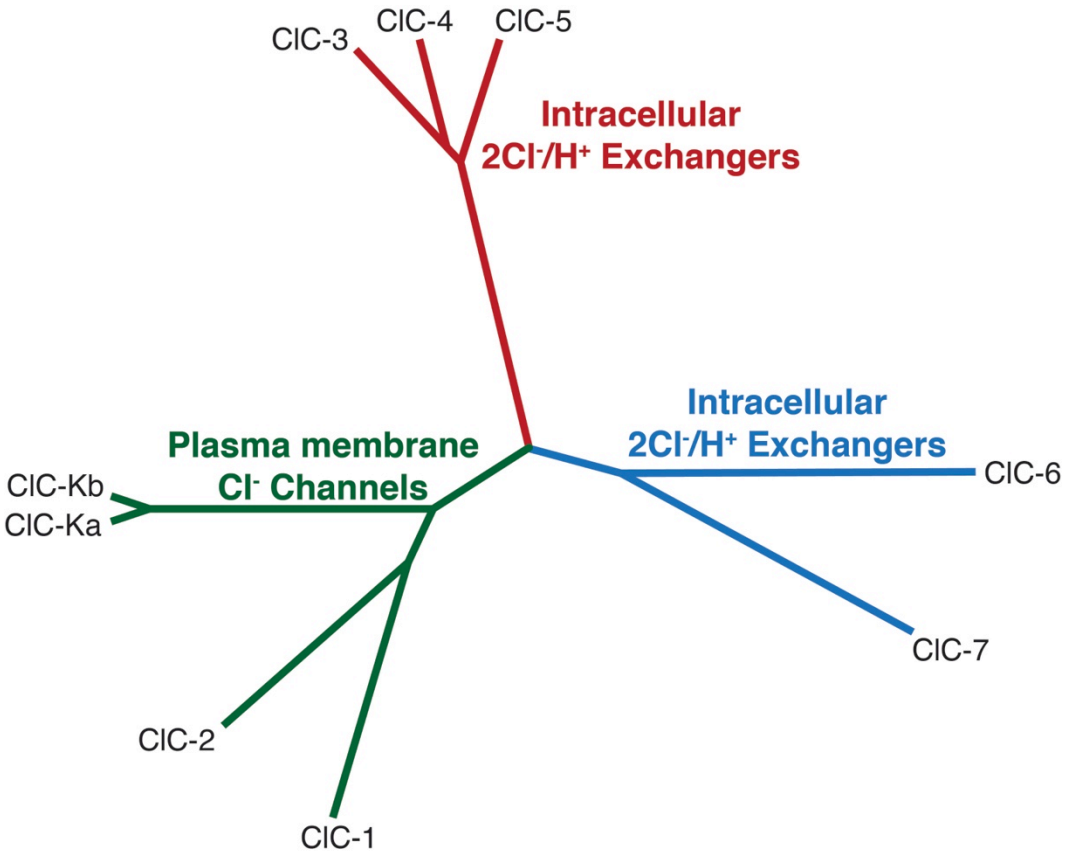

Figure 1.6 Phylogenetic Dendrogram of Human ClC Proteins.

Amino acid sequences corresponding to human ClC proteins were aligned using Clustal W software (http://align.genome.jp/). On the basis of the alignment Clustal W plotted phylogenetic relationships, where the length of each line denotes the relative evolutionary distance between ClC proteins. The ClC protein family clusters into three homology branches, plasma membrane Cl^- channels (green) and intracellular $2Cl^-/H^+$ exchangers (red and blue).

involved in chloride coordination during transport (S107 and Y445) (*230, 232, 233*). Sequence alignments between transporter and channel-like ClC proteins and mutational analysis in *E. coli* ClC also revealed the presence of an intracellular glutamate gate (E203), which is important in H^+ coupled transport (*225, 234*). Taken together, studies of ClC proteins have been successful in determining structural and mechanistic features of anion transport.

1.6.1 Structure

Several high-resolution X-ray crystal structures have been determined for prokaryotic and eukaryotic ClC proteins (*202, 225, 235-238*). The first structures solved from *S. typhimurium* and *E. coli* (3.0 and 3.5 Å, respectively) were essentially the same (*225*). These structures revealed a rhombus shaped ClC dimer approximately 100 X 55 Å and 65 Å thick (Fig. 1.7). Each ClC monomer contained 18 helices and had a pseudo two-fold axis of symmetry, with helices B-I being similar to helices J-Q (Fig. 1.8). In the center of each ClC monomer is a bound chloride ion, which is coordinated by amino acid backbone amide groups from I356 and F357 and side chain hydroxyls from S107 and Y445 in *E. coli* ClC (Fig. 1.7). Large water filled vestibules are located extracellular and intracellular to the central chloride-binding site, and selectivity filters, containing several positively charge residues, are observed closer to the central chloride-binding site. In addition, a glutamate (E148) was found to block the pore on the extracellular side, and movement

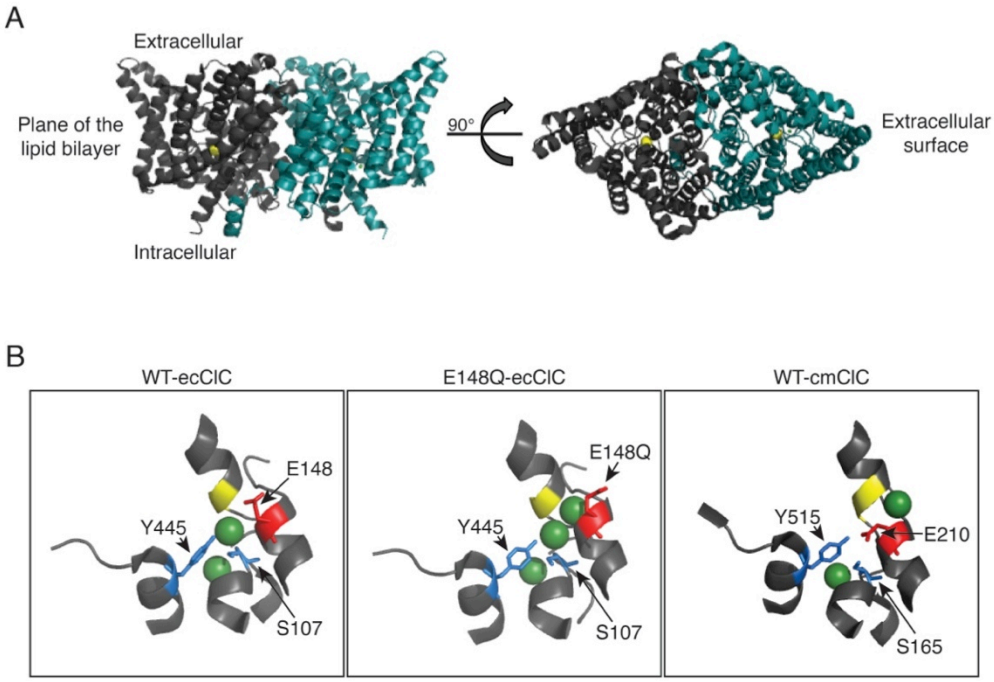

Figure 1.7 Three-Dimensional ClC Structures.

(A) The structure of an *E. coli* ClC dimer is shown, with one monomer in grey and the second monomer in teal (*225*). Yellow spheres represent a Cl^- ion in the central chloride-binding site. Two views of the structure are shown, looking parallel to the lipid bilayer and to the extracellular side. (B) Three-dimensional structures of the chloride-binding sites in wild-type *E. coli* ClC (WT-ecClC) (*225*), E148Q *E. coli* ClC (E148Q-ecClC) (*202*), and wild-type *C. merolae* ClC (WT-cmClC) (*238*). Green spheres represent Cl^- ions in the external, central, and internal chloride binding sites (top to bottom, respectively). The site of the extracellular glutamate gate is labeled and colored red. Tyrosine and serine residues involved in coordination of the central chloride-binding site are labeled and colored blue. Backbone amide groups involved in coordination of the central chloride-binding site are colored yellow.

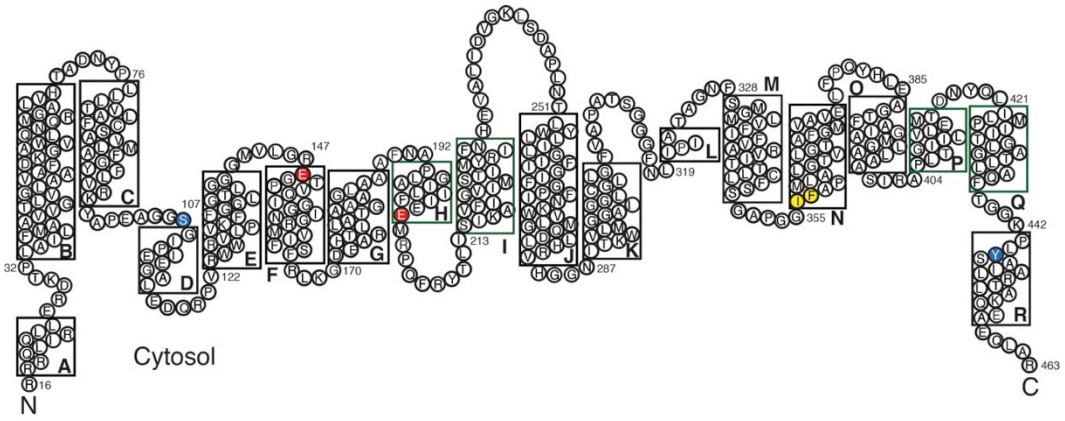

Figure 1.8 *E. coli* ClC Topology Model.

Numbers indicate residue numbers in *E. coli* ClC, and A-R indicates transmembrane helices (boxed regions) as determined by the crystal structure (*225*). The extracellular and intracellular glutamate gates (E148 and E203, respectively) are colored red. Residues involved in coordination of the central chloride-binding site through side chain hydroxyls (S107 and Y445) and backbone amide groups (I356 and F357) are colored blue and yellow, respectively. Transmembrane helices in green boxes (H, I, P, and Q) form the ClC dimer interface. N and C indicate N and C-termini, respectively.

of this glutamate gate would be required to allow chloride movement through the channel (Fig. 1.7).

Additional structures of the *E. coli* ClC protein were solved for WT-ClC, E148A-ClC, and E148Q-ClC bound to Fab fragments (2.5 Å, 3.0 Å and 3.3 Å, respectively) (*202*). These structures are similar to the previous structures determined for ClC. Here, the internal chloride-binding site was described for WT-ClC, which is located at the edge of the intracellular selectivity filter (Fig. 1.7). E148A and E148Q-ClC structures allowed the identification of a third external chloride-binding site (Fig 1.7). E148A-ClC was described as an open channel since the path of bound anions is uninterrupted and links extracellular and intracellular solutions. E148Q-ClC was described as similar to the open conformation of WT-ClC, since the glutamine moiety extends into the extracellular solution rather than blocking the pore (Fig. 1.7).

A structure of E203Q-ClC indicates that there is no difference in the chloride-binding sites compared to WT-ClC, even though there are drastic changes in transport activity of this protein (*235*). Also discussed is the salt bridge formed between E203 and R28 of the other ClC monomer in WT-ClC, which was found not to be functionally relevant during transport.

The eukaryotic ClC X-ray crystal structure (3.5 Å) is from a thermophillic red alga *Cyanidioschyzon merolae* (*238*). Eukaryotic ClC proteins have a C-terminal cytoplasmic cystathionine beta-synthase (CBS) domain, whereas *E. coli* ClC only has a membrane domain. In the structure of *C. merolae* ClC the membrane domain resembles the *E. coli* ClC structure and

the CBS domain resembles other previously described CBS structures (*239*). The CBS domain of *C. merolae* ClC forms several contacts with the transmembrane domain, and aids in maintaining the structure of the central chloride-binding site. Also, the *C. merolae* ClC structure revealed a new conformation of the external glutamate gate (*E. coli* ClC E148), where the glutamate occupies the central chloride-binding site and anions occupy the internal and external chloride-binding sites (Fig. 1.7).

1.6.2 Transport Mechanism

Structures of ClC proteins and site-directed mutagenesis studies guided by these structures led to a proposed $2Cl^-/H^+$ transport mechanism (*238*). When the non-protonated extracellular glutamate gate occupies the central chloride-binding site, a H^+ from the intracellular solution is transferred to the glutamate residue. The protonated extracellular glutamate gate flips into the extracellular solution and two extracellular Cl^- ions move into the extracellular and central chloride-binding sites. The deprotonation of the extracellular glutamate gate causes it to move from extracellular solution to the extracellular chloride-binding site and finally back to the central chloride-binding site, which in turn causes two Cl^- ions to move into the intracellular solution. While this transport mechanism explains the movement of Cl^- through ClC and how H^+ movement is coupled to Cl^- movement, it does not explain how H^+ ions are translocated from the intracellular solution to the intracellular glutamate gate and to the extracellular glutamate gate.

1.6.3 Dimer Interface

The ClC dimer interface is formed by transmembrane helices H, I, P, and Q (Fig. 1.8). These four helices form a large flat hydrophobic surface, which provides the driving force for ClC dimerization. Introduction of tryptophan residues into the dimer interface transmembrane helices of *E. coli* ClC disrupted dimerization (*237*). Mutations to tryptophan residues introduced unfavorable steric interactions in the dimer interface, and promoted interaction of the dimer interface with the lipid bilayer (*240*).

A double tryptophan *E. coli* ClC mutant (I201W/I422W) is exclusively monomeric in both detergent micelles and reconstituted proteoliposomes (*237*). This mutant has a transport activity similar to WT-ClC and a 3.1 Å resolution X-ray crystal structure revealed the same overall protein fold (*237*). The only notable difference between the structure of WT-ClC and the double tryptophan mutant was the location of the cytoplasmic N-terminal helix A (Fig. 1.8) (*237*). Taken together, with other ClC crosslinking studies (*241, 242*), ClC proteins form stable dimers, whose monomers function independently.

1.7 Thesis Objective

The objective of this thesis is to investigate the structure of the AE1 membrane domain in order to further understand unique features of the protein. The initial goal of the thesis was to obtain a high-resolution structure of the AE1 membrane domain. While this goal did not come to

fruition, a homology model of AE1 was successful in providing information on the structural and functional features of AE1.

Chapter 2 of the thesis lists all of the experimental materials and methods. Chapter 3 describes the *S. cerevisiae* expression and antibody affinity purification scheme developed to obtain quantities of AE1 membrane domain protein suitable for future crystallization trails. In Chapter 4, a homology model of AE1, created using *E. coli* ClC as a structural template, is introduced. The validity of the AE1 homology model was investigated through comparison with previous biochemical studies of AE1. In addition, the AE1 homology model successfully guided site-directed mutagenesis studies to identify several transport mechanism residues in AE1. Chapter 5 uses the AE1 homology model to guide mutagenic studies to investigate the dimer interface of AE1. The ability of AE1 mutations to disrupt the dimer interface and form AE1 monomers was assessed by chemical crosslinking. Finally, the thesis summarizes the current understanding of the AE1 structure and transport mechanism, and presents future directions to investigate the structural features of AE1.

1.8 References

1. E. Cordat, J. R. Casey, Bicarbonate transport in cell physiology and disease. *Biochem J* **417**, 423-439 (2009).
2. N. G. Perez, B. V. Alvarez, M. C. Camilion de Hurtado, H. E. Cingolani, pHi regulation in myocardium of the spontaneously hypertensive rat. Compensated enhanced activity of the Na^+-H^+ exchanger. *Circ Res* **77**, 1192-1200 (1995).
3. B. V. Alvarez, J. Fujinaga, J. R. Casey, Molecular Basis for angiotensin II-induced increase of chloride/bicarbonate exchange in the myocardium. *Circ. Res* **89**, 1246-1253 (2001).
4. B. V. Alvarez, Y. Xia, D. Sowah, D. Soliman, P. Light, M. Karmazyn, J. R. Casey, A Carbonic Anhydrase Inhibitor Prevents and Reverts Cardiomyocyte Hypertrophy. *J. Physiol.* **579**, 127-145 (2007).
5. S. a. L. Eber, S. E., Hereditary spherocytosis--defects in proteins that connect the membrane skeleton to the lipid bilayer. *Semin Hematol* **41**, 118-141 (2004).
6. N. Alloisio, P. Texier, A. Vallier, M. L. Ribeiro, L. Morle, M. Bozon, E. Bursaux, P. Maillet, P. Goncalves, M. J. Tanner, G. Tamagnini, J. Delaunay, Modulation of clinical expression and band 3 deficiency in hereditary spherocytosis. *Blood* **90**, 414-420 (1997).
7. M. L. Ribeiro, N. Alloisio, H. Almeida, C. Gomes, P. Texier, C. Lemos, G. Mimoso, L. Morle, F. Bey-Cabet, R. C. Rudigoz, J. Delaunay, G. Tamagnini, Severe hereditary spherocytosis and distal renal tubular acidosis associated with the total absence of band 3. *Blood* **96**, 1602-1604 (2000).
8. A. M. Toye, R. C. Williamson, M. Khanfar, B. Bader-Meunier, T. Cynober, M. Thibault, G. Tchernia, M. Dechaux, J. Delaunay, L. J. Bruce, Band 3 Courcouronnes (Ser667Phe): a trafficking mutant differentially rescued by wild type band 3 and glycophorin A. *Blood*, (2008).
9. S. Perrotta, A. Borriello, A. Scaloni, L. De Franceschi, A. M. Brunati, F. Turrini, V. Nigro, E. M. del Giudice, B. Nobili, M. L. Conte, F. Rossi, A. Iolascon, A. Donella-Deana, V. Zappia, V. Poggi, W. Anong, P. Low, N. Mohandas, F. Della Ragione, The N-terminal 11 amino acids of human erythrocyte band 3 are critical for aldolase binding and protein phosphorylation: implications for band 3 function. *Blood* **106**, 4359-4366 (2005).
10. D. Dinour, M. H. Chang, J. Satoh, B. L. Smith, N. Angle, A. Knecht, I. Serban, E. J. Holtzman, M. F. Romero, A novel missense mutation in the sodium bicarbonate cotransporter (NBCe1/SLC4A4) causes proximal tubular acidosis and glaucoma through ion transport defects. *J Biol Chem* **279**, 52238-52246. (2004).
11. T. Igarashi, J. Inatomi, T. Sekine, G. Seki, M. Shimadzu, F. Tozawa, Y. Takeshima, T. Takumi, T. Takahashi, N. Yoshikawa, H. Nakamura, H. Endou, Novel nonsense mutation in the Na^+/HCO_3^- cotransporter gene

(SLC4A4) in a patient with permanent isolated proximal renal tubular acidosis and bilateral glaucoma. *J Am Soc Nephrol* **12**, 713-718 (2001).
12. T. Igarashi, J. Inatomi, T. Sekine, S. H. Cha, Y. Kanai, M. Kunimi, K. Tsukamoto, H. Satoh, M. Shimadzu, F. Tozawa, T. Mori, M. Shiobara, G. Seki, H. Endou, Mutations in SLC4A4 cause permanent isolated proximal renal tubular acidosis with ocular abnormalities. *Nat. Genet.* **23**, 264-266 (1999).
13. J. Inatomi, S. Horita, N. Braverman, T. Sekine, H. Yamada, Y. Suzuki, K. Kawahara, N. Moriyama, A. Kudo, H. Kawakami, M. Shimadzu, H. Endou, T. Fujita, G. Seki, T. Igarashi, Mutational and functional analysis of SLC4A4 in a patient with proximal renal tubular acidosis. *Pflugers Arch* **448**, 438-444 (2004).
14. S. Horita, H. Yamada, J. Inatomi, N. Moriyama, T. Sekine, T. Igarashi, Y. Endo, M. Dasouki, M. Ekim, L. Al-Gazali, M. Shimadzu, G. Seki, T. Fujita, Functional analysis of NBC1 mutants associated with proximal renal tubular acidosis and ocular abnormalities. *J Am Soc Nephrol* **16**, 2270-2278. (2005).
15. F. Y. Demirci, M. H. Chang, T. S. Mah, M. F. Romero, M. B. Gorin, Proximal renal tubular acidosis and ocular pathology: a novel missense mutation in the gene (SLC4A4) for sodium bicarbonate cotransporter protein (NBCe1). *Mol Vis* **12**, 324-330. (2006).
16. C. Shayakul, S. L. Alper, Inherited renal tubular acidosis. *Curr Opin Nephrol Hypertens* **9**, 541-546 (2000).
17. E. Cordat, Unraveling trafficking of the kidney anion exchanger 1 in polarized MDCK epithelial cells. *Biochem Cell Biol* **84**, 949-959. (2006).
18. P. A. Stehberger, B. E. Shmukler, A. K. Stuart-Tilley, L. L. Peters, S. L. Alper, C. A. Wagner, Distal Renal Tubular Acidosis in Mice Lacking the AE1 (Band3) Cl-/HCO3- Exchanger (slc4a1). *J Am Soc Nephrol*, (2007).
19. I. E. Royaux, K. Suzuki, A. Mori, R. Katoh, L. A. Everett, L. D. Kohn, E. D. Green, Pendrin, the protein encoded by the Pendred syndrome gene (PDS), is an apical porter of iodide in the thyroid and is regulated by thyroglobulin in FRTL-5 cells. *Endocrinology* **141**, 839-845 (2000).
20. G. L. Vilas, D. E. Johnson, P. Freund, J. R. Casey, Characterization of an epilepsy-associated variant of the human Cl^-/HCO_3^- exchanger AE3. *Am J Physiol Cell Physiol* **297**, C526-536 (2009).
21. T. Sander, M. R. Toliat, A. Heils, G. Leschik, C. Becker, F. Ruschendorf, K. Rohde, S. Mundlos, P. Nurnberg, Association of the 867Asp variant of the human anion exchanger 3 gene with common subtypes of idiopathic generalized epilepsy. *Epilepsy Res* **51**, 249-255 (2002).
22. L. A. Everett, I. A. Belyantseva, K. Noben-Trauth, R. Cantos, A. Chen, S. I. Thakkar, S. L. Hoogstraten-Miller, B. Kachar, D. K. Wu, E. D. Green, Targeted disruption of mouse Pds provides insight about the inner-ear defects encountered in Pendred syndrome. *Hum Mol Genet* **10**, 153-161 (2001).
23. K. Nakaya, D. G. Harbidge, P. Wangemann, B. D. Schultz, E. D. Green, S. M. Wall, D. C. Marcus, Lack of pendrin HCO_3^- transport elevates

vestibular endolymphatic [Ca^{2+}] by inhibition of acid-sensitive TRPV5 and TRPV6 channels. *Am J Physiol Renal Physiol* **292**, F1314-1321 (2007).
24. P. Wangemann, K. Nakaya, T. Wu, R. J. Maganti, E. M. Itza, J. D. Sanneman, D. G. Harbidge, S. Billings, D. C. Marcus, Loss of cochlear HCO_3^- secretion causes deafness via endolymphatic acidification and inhibition of Ca^{2+} reabsorption in a Pendred syndrome mouse model. *Am. J. Physiol.* **292**, F1345-1353 (2007).
25. J. J. Wine, Cystic fibrosis: The 'bicarbonate before chloride' hypothesis. *Curr Biol* **11**, R463-466. (2001).
26. Y. Song, D. Salinas, D. W. Nielson, A. S. Verkman, Hyperacidity of secreted fluid from submucosal glands in early cystic fibrosis. *Am J Physiol Cell Physiol* **290**, C741-749 (2006).
27. M. Park, S. B. Ko, J. Y. Choi, G. Muallem, P. J. Thomas, A. Pushkin, M. S. Lee, J. Y. Kim, M. G. Lee, S. Muallem, I. Kurtz, The cystic fibrosis transmembrane conductance regulator interacts with and regulates the activity of the HCO_3^- salvage transporter human Na^+-HCO_3^- cotransport isoform 3. *J Biol Chem* **277**, 50503-50509 (2002).
28. Y. Wang, A. A. Soyombo, N. Shcheynikov, W. Zeng, M. Dorwart, C. R. Marino, P. J. Thomas, S. Muallem, Slc26a6 regulates CFTR activity in vivo to determine pancreatic duct HCO_3^- secretion: relevance to cystic fibrosis. *EMBO J.* **25**, 5049-5057 (2006).
29. S. B. Ko, N. Shcheynikov, J. Y. Choi, X. Luo, K. Ishibashi, P. J. Thomas, J. Y. Kim, K. H. Kim, M. G. Lee, S. Naruse, S. Muallem, A molecular mechanism for aberrant CFTR-dependent HCO_3^- transport in cystic fibrosis. *Embo J* **21**, 5662-5672 (2002).
30. S. B. Ko, W. Zeng, M. R. Dorwart, X. Luo, K. H. Kim, L. Millen, H. Goto, S. Naruse, A. Soyombo, P. J. Thomas, S. Muallem, Gating of CFTR by the STAS domain of SLC26 transporters. *Nat Cell Biol* **6**, 343-350 (2004).
31. L. J. Bruce, D. L. Cope, G. K. Jones, A. E. Schofield, M. Burley, S. Povey, R. J. Unwin, O. Wrong, M. J. Tanner, Familial distal renal tubular acidosis is associated with mutations in the red cell anion exchanger (Band 3, AE1) gene. *J Clin Invest* **100**, 1693-1707 (1997).
32. J. C. Cheung, E. Cordat, R. A. Reithmeier, Trafficking defects of the Southeast Asian ovalocytosis deletion mutant of anion exchanger 1 membrane proteins. *Biochem J* **392**, 425-434. (2005).
33. T. Okiyoneda, H. Barriere, M. Bagdany, W. M. Rabeh, K. Du, J. Hohfeld, J. C. Young, G. L. Lukacs, Peripheral protein quality control removes unfolded CFTR from the plasma membrane. *Science* **329**, 805-810 (2010).
34. M. F. Romero, A. P. Chen, M. D. Parker, W. F. Boron, The SLC4 family of bicarbonate HCO_3^- transporters. *Mol Aspects Med* **34**, 159-182 (2013).
35. S. L. Alper, A. K. Sharma, The SLC26 gene family of anion transporters and channels. *Mol Aspects Med* **34**, 494-515 (2013).

36. H. M. Wain, M. J. Lush, F. Ducluzeau, V. K. Khodiyar, S. Povey, Genew: The Human Gene Nomenclature Database, 2004 updates. *Nucleic Acids Res* **32**, D255-257 (2004).
37. H. Lohi, M. Kujala, S. Makela, E. Lehtonen, M. Kestila, U. Saarialho-Kere, D. Markovich, J. Kere, Functional characterization of three novel tissue-specific anion exchangers: SLC26A7, A8 and A9. *J Biol Chem* **277**, 14246-14254 (2002).
38. R. R. Kopito, H. F. Lodish, Primary structure and transmembrane orientation of the murine anion exchange protein. *Nature* **316**, 234-238 (1985).
39. S. L. Alper, R. R. Kopito, S. M. Libresco, H. F. Lodish, Cloning and characterization of a murine Band 3-related cDNA from kidney and a lymphoid cell line. *J. Biol. Chem.* **263**, 17092-17099 (1988).
40. K. E. Kudrycki, P. R. Newman, G. E. Shull, cDNA cloning and tissue distribution of mRNAs for two proteins that are related to the Band 3 Cl^-/HCO_3^- exchanger. *J. Biol. Chem.* **265**, 462-471 (1990).
41. M. D. Parker, W. F. Boron, M. J. Tanner, Characterization of human "AE4" as an electroneutral sodium bicarbonate cotransporter. *FASEB J* **16**, A796 (2002).
42. M. F. Romero, C. M. Fulton, W. F. Boron, The SLC4 family of HCO_3^- transporters. *Pflugers Arch* **447**, 496-509 (2004).
43. M. D. Parker, E. P. Ourmozdi, M. J. Tanner, Human BTR1, a New Bicarbonate Transporter Superfamily Member and Human AE4 from Kidney. *Biochem Biophys Res Commun* **282**, 1103-1109. (2001).
44. H. Tsuganezawa, K. Kobayashi, M. Iyori, T. Araki, A. Koizumi, S. I. Watanabe, A. Kaneko, T. Fukao, T. Monkawa, T. Yoshida, D. K. Kim, Y. Kanai, H. Endou, M. Hayashi, T. Saruta, A new member of the HCO_3^- transporter superfamily is an apical anion exchanger of beta-intercalated cells in the kidney. *J Biol Chem* **276**, 8180-8189 (2001).
45. C. Z. Wang, H. Yano, K. Nagashima, S. Seino, The Na^+-driven Cl^-/HCO_3^- exchanger: Cloning, tissue distribution, and functional characterization. *J Biol Chem* **275**, 35486-35490 (2000).
46. M. D. Parker, R. Musa-Aziz, J. D. Rojas, I. Choi, C. M. Daly, W. F. Boron, Characterization of human SLC4A10 as an electroneutral Na/HCO3 cotransporter (NBCn2) with Cl^- self-exchange activity. *J Biol Chem* **283**, 12777-12788 (2008).
47. J. Praetorius, L. N. Nejsum, S. Nielsen, A SCL4A10 gene product maps selectively to the basolateral plasma membrane of choroid plexus epithelial cells. *Am J Physiol Cell Physiol* **286**, C601-610 (2004).
48. Grichtchenko, II, I. Choi, X. Zhong, P. Bray-Ward, J. M. Russell, W. F. Boron, Cloning, characterization, and chromosomal mapping of a human electroneutral Na^+-driven Cl^-/HCO_3^- exchanger. *J Biol Chem* **276**, 8358-8363 (2001).
49. M. F. Romero, D. Henry, S. Nelson, P. J. Harte, A. K. Dillon, C. M. Sciortino, Cloning and characterization of a Na^+ driven anion

exchanger (NDAE1): a new bicarbonate transporter. *J. Biol. Chem.* **275**, 24552-24559 (2000).
50. Z. Wang, L. Conforti, S. Petrovic, H. Amlal, C. E. Burnham, M. Soleimani, Mouse Na^+: HCO_3^- cotransporter isoform NBC-3 (kNBC-3): cloning, expression, and renal distribution. *Kidney Int* **59**, 1405-1414 (2001).
51. K. Ishibashi, S. Sasaki, F. Marumo, Molecular cloning of a new sodium bicarbonate cotransporter cDNA from human retina. *Biochem. Biophys. Res. Commun.* **246**, 535-538 (1998).
52. A. Pushkin, N. Abuladze, I. Lee, D. Newman, J. Hwang, I. Kurtz, Cloning, tissue distribution, genomic organization, and functional characterization of NBC3, a new member of the sodium bicarbonate cotransporter family. *J. Biol. Chem.* **274**, 16569-16575 (1999).
53. I. Choi, C. Aalkjaer, E. L. Boulpaep, W. F. Boron, An electroneutral sodium/bicarbonate cotransporter NBCn1 and associated sodium channel. *Nature* **405**, 571-575 (2000).
54. C. E. Burnham, H. Amlal, Z. Wang, G. E. Shull, M. Soleimani, Cloning and functional expression of a human kidney Na^+:HCO_3^- cotransporter. *J. Biol. Chem.* **272**, 19111-19114 (1997).
55. M. F. Romero, M. A. Hediger, E. L. Boulpaep, W. F. Boron, Expression cloning and characterization of a renal electrogenic Na^+/HCO_3^- cotransporter. *Nature* **387**, 409-413 (1997).
56. N. Abuladze, I. Lee, D. Newman, J. Hwang, K. Boorer, A. Pushkin, I. Kurtz, Molecular cloning, chromosomal localization, tissue distribution, and functional expression of the human pancreatic sodium bicarbonate cotransporter. *J. Biol. Chem.* **273**, 17689-17695 (1998).
57. I. Choi, M. F. Romero, N. Khandoudi, A. Bril, W. F. Boron, Cloning and characterization of a human electrogenic Na^+-HCO_3^- cotransporter isoform (hhNBC). *Am. J. Physiol.* **276**, C576-584 (1999).
58. M. O. Bevensee, B. M. Schmitt, I. Choi, M. F. Romero, W. F. Boron, An electrogenic Na^+-HCO_3^- cotransporter (NBC) with a novel COOH-terminus, cloned from rat brain. *Am. J. Physiol.* **278**, C1200-C1211 (2000).
59. X. C. Sun, J. A. Bonanno, Identification and cloning of the Na^+/HCO_3^- cotransporter (NBC) in human corneal endothelium. *Exp Eye Res* **77**, 287-295 (2003).
60. A. Pushkin, N. Abuladze, D. Newman, I. Lee, G. Xu, I. Kurtz, Cloning, characterization and chromosomal assignment of NBC4, a new member of the sodium bicarbonate cotransporter family. *Biochim Biophys Acta* **1493**, 215-218. (2000).
61. P. Sassani, A. Pushkin, E. Gross, A. Gomer, N. Abuladze, R. Dukkipati, G. Carpenito, I. Kurtz, Functional characterization of NBC4: a new electrogenic sodium-bicarbonate cotransporter. *Am J Physiol Cell Physiol* **282**, C408-416 (2002).
62. L. V. Virkki, D. A. Wilson, R. D. Vaughan-Jones, W. F. Boron, Functional characterization of human NBC4 as an electrogenic Na^+-HCO_3^-

cotransporter (NBCe2). *Am J Physiol Cell Physiol* **282**, C1278-1289 (2002).
63. J. Xu, Z. Wang, S. Barone, M. Petrovic, H. Amlal, L. Conforti, S. Petrovic, M. Soleimani, Expression of the Na^+-HCO_3^- cotransporter NBC4 in rat kidney and characterization of a novel NBC4 variant. *Am J Physiol Renal Physiol* **284**, F41-50 (2003).
64. C. W. Schweinfest, D. D. Spyropoulos, K. W. Henderson, J. H. Kim, J. M. Chapman, S. Barone, R. T. Worrell, Z. Wang, M. Soleimani, slc26a3 (dra)-deficient mice display chloride-losing diarrhea, enhanced colonic proliferation, and distinct up-regulation of ion transporters in the colon. *J Biol Chem* **281**, 37962-37971 (2006).
65. J. E. Melvin, K. Park, L. Richardson, P. J. Schultheis, G. E. Shull, Mouse down-regulated in adenoma (DRA) is an intestinal Cl^-/HCO_3^- exchanger and is up-regulated in colon of mice lacking the NHE3 Na^+/H^+ exchanger. *J. Biol. Chem.* **274**, 22855-22861 (1999).
66. C. Barmeyer, J. H. Ye, S. Sidani, J. Geibel, H. J. Binder, V. M. Rajendran, Characteristics of rat downregulated in adenoma (rDRA) expressed in HEK 293 cells. *Pflugers Arch* **454**, 441-450 (2007).
67. N. Shcheynikov, D. Yang, Y. Wang, W. Zeng, L. P. Karniski, I. So, S. M. Wall, S. Muallem, The Slc26a4 transporter functions as an electroneutral $Cl^-/I^-/HCO_3^-$ exchanger: role of Slc26a4 and Slc26a6 in I^- and HCO_3^- secretion and in regulation of CFTR in the parotid duct. *J Physiol* **586**, 3813-3824 (2008).
68. D. A. Scott, R. Wang, T. M. Kreman, V. C. Sheffield, L. P. Karnishki, The Pendred syndrome gene encodes a chloride-iodide transport protein. *Nat Genet* **21**, 440-443 (1999).
69. M. Soleimani, T. Greeley, S. Petrovic, Z. Wang, H. Amlal, P. Kopp, C. E. Burnham, Pendrin: an apical $Cl^-/OH^-/HCO_3^-$ exchanger in the kidney cortex. *Am J Physiol Renal Physiol* **280**, F356-364. (2001).
70. S. Waldegger, I. Moschen, A. Ramirez, R. J. Smith, H. Ayadi, F. Lang, C. Kubisch, Cloning and characterization of SLC26A6, a novel member of the solute carrier 26 gene family. *Genomics* **72**, 43-50 (2001).
71. Z. Wang, S. Petrovic, E. Mann, M. Soleimani, Identification of an apical Cl^-/HCO_3^- exchanger in the small intestine. *Am J Physiol Gastrointest Liver Physiol* **282**, G573-579 (2002).
72. Q. Xie, R. Welch, A. Mercado, M. F. Romero, D. B. Mount, Molecular characterization of the murine Slc26a6 anion exchanger: functional comparison with Slc26a1. *Am J Physiol Renal Physiol* **283**, F826-838 (2002).
73. S. Petrovic, X. Ju, S. Barone, U. Seidler, S. L. Alper, H. Lohi, J. Kere, M. Soleimani, Identification of a basolateral Cl^-/HCO_3^- exchanger specific to gastric parietal cells. *Am J Physiol Gastrointest Liver Physiol* **284**, G1093-1103 (2003).
74. J. B. Vincourt, D. Jullien, S. Kossida, F. Amalric, J. P. Girard, Molecular Cloning of SLC26A7, a Novel Member of the SLC26 Sulfate/Anion

Transporter Family, from High Endothelial Venules and Kidney. *Genomics* **79**, 249-256 (2002).
75. K. H. Kim, N. Shcheynikov, Y. Wang, S. Muallem, SLC26A7 is a Cl- channel regulated by intracellular pH. *J Biol Chem* **280**, 6463-6470 (2005).
76. J. Xu, J. Henriksnas, S. Barone, D. Witte, G. E. Shull, J. G. Forte, L. Holm, M. Soleimani, SLC26A9 is expressed in gastric surface epithelial cells, mediates Cl^-/HCO_3^- exchange, and is inhibited by NH_4^+. *Am J Physiol Cell Physiol* **289**, C493-505 (2005).
77. M. R. Dorwart, N. Shcheynikov, Y. Wang, S. Stippec, S. Muallem, SLC26A9 is a Cl^- channel regulated by the WNK kinases. *J Physiol* **584**, 333-345 (2007).
78. C. Loriol, S. Dulong, M. Avella, N. Gabillat, K. Boulukos, F. Borgese, J. Ehrenfeld, Characterization of SLC26A9, facilitation of Cl^- transport by bicarbonate. *Cell Physiol Biochem* **22**, 15-30 (2008).
79. J. B. Vincourt, D. Jullien, F. Amalric, J. P. Girard, Molecular and functional characterization of SLC26A11, a sodium-independent sulfate transporter from high endothelial venules. *Faseb J* **5**, 5 (2003).
80. J. Xu, S. Barone, H. Li, S. Holiday, K. Zahedi, M. Soleimani, Slc26a11, a chloride transporter, localizes with the vacuolar H(+)-ATPase of A-intercalated cells of the kidney. *Kidney Int* **80**, 926-937 (2011).
81. A. L. Obaid, T. F. Leininger, E. D. Crandall, Exchange of HCO_3^- for monovalent anions across the human erythrocyte membrane. *J Membr Biol* **52**, 173-179 (1980).
82. S. L. Alper, Molecular physiology of SLC4 anion exchangers. *Exp Physiol* **91**, 153-161. (2006).
83. A. Lambert, A. G. Lowe, Chloride/bicarbonate exchange in human erythrocytes. *J Physiol* **275**, 51-63 (1978).
84. H. Passow, Molecular aspects of Band 3-mediated anion transport across the red blood cell membrane. *Rev. Physiol. Biochem. Pharmacol.* **103**, 61-223 (1986).
85. P. A. Knauf, Erythrocyte Anion Exchange and the Band 3 Protein: Transport Kinetics and Molecular Structure. *Current Topics in Membranes and Transport* **12**, 249-363 (1979).
86. J. M. Salhany, *Erythrocyte Band 3 Protein*. (CRC Press, Boca Raton, Florida, 1990), pp. 213.
87. S. E. Lux, K. M. John, R. R. Kopito, H. F. Lodish, Cloning and characterization of Band 3, the human erythrocyte anion-exchange protein. *Proc. Natl. Acad. Sci.* **86**, 9089-9093 (1989).
88. A. Kollert-Jons, S. Wagner, S. Hubner, H. Appelhans, D. Drenckhahn, Anion exchanger 1 in human kidney and oncocytoma differs from erythroid AE1 in its NH2 terminus. *Am J Physiol* **265**, F813-821. (1993).
89. P. S. Low, Structure and function of the cytoplasmic domain of Band 3: center of erythrocyte membrane-peripheral protein interactions. *Biochim. Biophys. Acta* **864**, 145-167 (1986).

90. T. L. Steck, G. Fairbanks, D. F. Wallach, Disposition of the major proteins in the isolated erythrocyte membrane. Proteolytic dissection. *Biochemistry* **10**, 2617-2624 (1971).
91. J. O. Wieth, O. S. Andersen, J. Brahm, P. J. Bjerrum, C. L. Borders, Jr., Chloride--bicarbonate exchange in red blood cells: physiology of transport and chemical modification of binding sites. *Philos Trans R Soc Lond B Biol Sci* **299**, 383-399 (1982).
92. H. L. McMurtrie, H. J. Cleary, B. V. Alvarez, F. B. Loiselle, D. Sterling, P. E. Morgan, D. E. Johnson, J. R. Casey, The bicarbonate transport metabolon. *J Enzyme Inhib Med Chem* **19**, 231-236 (2004).
93. J. W. Vince, R. A. F. Reithmeier, Carbonic anhydrase II binds to the carboxyl-terminus of human band 3, the erythrocyte Cl^-/HCO_3^- exchanger. *J. Biol. Chem* **273**, 28430-28437 (1998).
94. D. Sterling, R. A. Reithmeier, J. R. Casey, A Transport Metabolon. Functional Interaction of Carbonic Anhydrase II and Chloride/Bicarbonate Exchangers. *J Biol Chem* **276**, 47886-47894 (2001).
95. B. V. Alvarez, D. M. Kieller, A. L. Quon, M. Robertson, J. R. Casey, Cardiac hypertrophy in anion exchanger 1-null mutant mice with severe hemolytic anemia. *Am J Physiol Heart Circ Physiol* **292**, H1301-1312. (2007).
96. S. H. Chang, P. S. Low, Identification of a critical ankyrin-binding loop on the cytoplasmic domain of erythrocyte membrane band 3 by crystal structure analysis and site-directed mutagenesis. *J Biol Chem* **278**, 6879-6884 (2003).
97. J. R. Casey, R. A. F. Reithmeier, Analysis of the oligomeric state of Band 3, the anion transport protein of the human erythrocyte membrane, by size exclusion high performance liquid chromatography: oligomeric stability and origin of heterogeneity. *J. Biol. Chem.* **266**, 15726-15737 (1991).
98. P. S. Low, P. Rathinavelu, M. L. Harrison, Regulation of glycolysis via reversible enzyme binding to the membrane protein, band 3. *J Biol Chem* **268**, 14627-14631 (1993).
99. F. Turrini, P. Arese, J. Yuan, P. S. Low, Clustering of integral membrane proteins of the human erythrocyte membrane stimulates autologous IgG binding, complement deposition, and phagocytosis. *J Biol Chem* **266**, 23611-23617 (1991).
100. S. L. Alper, J. Natale, S. Gluck, H. F. Lodish, D. Brown, Subtypes of intercalated cells in rat kidney collecting duct defined by antibodies against erythroid band 3 and renal vacuolar H^+-ATPase. *Proc Natl Acad Sci U S A* **86**, 5429-5433 (1989).
101. L. R. Carraro-Lacroix, G. Malnic, Acid-base transport by the renal distal nephron. *J Nephrol* **23 Suppl 16**, S19-27 (2010).
102. F. Wu, M. A. Saleem, N. B. Kampik, T. J. Satchwell, R. C. Williamson, S. M. Blattner, L. Ni, T. Toth, G. White, M. T. Young, M. D. Parker, S. L.

Alper, C. A. Wagner, A. M. Toye, Anion exchanger 1 interacts with nephrin in podocytes. *J Am Soc Nephrol* **21**, 1456-1467 (2010).
103. T. Keskanokwong, H. J. Shandro, G. L. Vilas, S. Kittanakom, R. A. F. Reithmeier, A. Varaporn, P. Yenchitsomanus, C. J.R., Interaction of Integrin-linked Kinase with kAE1 Cl^-/HCO_3^- Exchanger. *J. Biol. Chem.* **282**, 23205-23218 (2007).
104. F. Wu, T. J. Satchwell, A. M. Toye, Anion exchanger 1 in red blood cells and kidney: Band 3's in a pod. *Biochem Cell Biol* **89**, 106-114 (2011).
105. S. Eber, S. E. Lux, Hereditary spherocytosis--defects in proteins that connect the membrane skeleton to the lipid bilayer. *Semin Hematol* **41**, 118-141 (2004).
106. J. A. Quilty, R. A. Reithmeier, Trafficking and folding defects in hereditary spherocytosis mutants of the human red cell anion exchanger. *Traffic* **1**, 987-998 (2000).
107. L. J. Bruce, H. C. Robinson, H. Guizouarn, F. Borgese, P. Harrison, M. J. King, J. S. Goede, S. E. Coles, D. M. Gore, H. U. Lutz, R. Ficarella, D. M. Layton, A. Iolascon, J. C. Ellory, G. W. Stewart, Monovalent cation leaks in human red cells caused by single amino-acid substitutions in the transport domain of the band 3 chloride-bicarbonate exchanger, AE1. *Nat Genet* **37**, 1258-1263 (2005).
108. J. Delaunay, The molecular basis of hereditary red cell membrane disorders. *Blood Rev* **21**, 1-20 (2007).
109. S.-C. Liu, S. Zhai, J. Palek, D. E. Golan, D. Amato, K. Hassan, G. T. Nurse, D. Babano, T. Coetzer, P. Jarolim, M. Zaik, S. Borwein, Molecular defect of the Band 3 protein in southeast Asian ovalocytosis. *New Engl. J. Med.* **323**, 1530-1538 (1990).
110. A. E. Schofield, D. M. Reardon, M. J. A. Tanner, Defective anion transport activity of the abnormal Band 3 in hereditary ovalocytic blood cells. *Nature* **355**, 836-838 (1992).
111. N. K. Dahl, L. Jiang, M. N. Chernova, A. K. Stuart-Tilley, B. E. Shmukler, S. L. Alper, Deficient HCO_3^- transport in an AE1 mutant with normal Cl^- transport can be rescued by carbonic anhydrase II presented on an adjacent AE1 protomer. *J Biol Chem* **21**, 21 (2003).
112. T. Kanki, M. T. Young, N. Hamasaki, M. J. Tanner, The N-terminal region of the transmembrane domain of human erythrocyte band 3: Residues critical for membrane insertion and transport activity. *J Biol Chem* **12**, 12 (2002).
113. H. Kuma, Y. Abe, D. Askin, L. J. Bruce, T. Hamasaki, M. J. Tanner, N. Hamasaki, Molecular basis and functional consequences of the dominant effects of the mutant band 3 on the structure of normal band 3 in southeast asian ovalocytosis. *Biochemistry* **41**, 3311-3320 (2002).
114. S. J. Allen, A. O'Donnell, N. D. Alexander, C. S. Mgone, T. E. Peto, J. B. Clegg, M. P. Alpers, D. J. Weatherall, Prevention of cerebral malaria in children in Papua New Guinea by southeast Asian ovalocytosis band 3. *Am J Trop Med Hyg* **60**, 1056-1060 (1999).

115. T. N. Williams, Red blood cell defects and malaria. *Mol Biochem Parasitol* **149**, 121-127 (2006).
116. N. Rasti, M. Wahlgren, Q. Chen, Molecular aspects of malaria pathogenesis. *FEMS Immunol Med Microbiol* **41**, 9-26 (2004).
117. S. K. Patnaik, W. Helmberg, O. O. Blumenfeld, BGMUT: NCBI dbRBC database of allelic variations of genes encoding antigens of blood group systems. *Nucleic Acids Res* **40**, D1023-1029 (2012).
118. S. L. Alper, Familial renal tubular acidosis. *J Nephrol* **23 Suppl 16**, S57-76 (2010).
119. E. Y. Almomani, C. Y. Chu, E. Cordat, Mis-trafficking of bicarbonate transporters: implications to human diseases. *Biochem Cell Biol* **89**, 157-177 (2011).
120. S. Walsh, F. Borgese, N. Gabillat, R. Unwin, H. Guizouarn, Cation transport activity of anion exchanger 1 mutations found in inherited distal renal tubular acidosis. *Am J Physiol Renal Physiol* **295**, F343-350 (2008).
121. C. D. Southgate, A. H. Chishti, B. Mitchell, S. J. Yi, J. Palek, Targeted disruption of the murine erythroid band 3 gene results in spherocytosis and severe haemolytic anaemia despite a normal membrane skeleton. *Nat. Genet.* **14**, 227-230 (1996).
122. L. L. Peters, R. A. Shivdasani, S. C. Liu, M. Hanspal, K. M. John, J. M. Gonzalez, C. Brugnara, B. Gwynn, N. Mohandas, S. L. Alper, S. H. Orkin, S. E. Lux, Anion exchanger 1 (band 3) is required to prevent erythrocyte membrane surface loss but not to form the membrane skeleton. *Cell* **86**, 917-927 (1996).
123. P. A. Stehberger, B. E. Shmukler, A. K. Stuart-Tilley, L. L. Peters, S. L. Alper, C. A. Wagner, Distal renal tubular acidosis in mice lacking the AE1 (band3) Cl-/HCO3- exchanger (slc4a1). *J Am Soc Nephrol* **18**, 1408-1418 (2007).
124. M. L. Jennings, J. Whitlock, A. Shinde, Pre-steady state transport by erythrocyte band 3 protein: uphill countertransport induced by the impermeant inhibitor H_2DIDS. *Biochem Cell Biol* **76**, 807-813. (1998).
125. K. Oikawa, D. M. Lieberman, R. A. F. Reithmeier, Conformation and stability of the anion transport protein of human erythrocyte membranes. *Biochem.* **24**, 2843-2848 (1985).
126. K. Okubo, D. Kang, N. Hamasaki, M. L. Jennings, Red blood cell band 3. Lysine 539 and lysine 851 react with the same H_2DIDS (4,4'-diisothiocyanodihydrostilbene-2,2'-disulfonic acid) molecule. *J. Biol. Chem.* **269**, 1918-1926 (1994).
127. C. Landolt-Marticorena, J. R. Casey, R. A. F. Reithmeier, Transmembrane helix-helix interactions and accessibility of H_2DIDS on labelled Band 3, the erythrocyte anion exchange protein. *Mol. Mem. Biol.* **12**, 173-182 (1995).
128. X. B. Tang, J. R. Casey, Trapping of inhibitor-induced conformational changes in the erythrocyte membrane anion exchanger AE1. *Biochemistry* **38**, 14565-14572 (1999).

129. S. L. Alper, M. N. Chernova, J. Williams, M. Zasloff, F. Y. Law, P. A. Knauf, Differential inhibition of AE1 and AE2 anion exchangers by oxonol dyes and by novel polyaminosterol analogs of the shark antibiotic squalamine. *Biochem Cell Biol* **76**, 799-806. (1998).
130. M. L. Jennings, J. S. Smith, Anion-proton cotransport through the human red blood cell band 3 protein. Role of glutamate 681. *J. Biol. Chem.* **267**, 13964-13971 (1992).
131. H. Guizouarn, S. Martial, N. Gabillat, F. Borgese, Point mutations involved in red cell stomatocytosis convert the electroneutral anion exchanger 1 to a non-selective cation conductance. *Blood* **110**, 2158-2165 (2007).
132. J. C. Ellory, H. Guizouarn, F. Borgese, L. J. Bruce, R. J. Wilkins, G. W. Stewart, Review. Leaky Cl^--HCO_3^- exchangers: cation fluxes via modified AE1. *Philos Trans R Soc Lond B Biol Sci* **364**, 189-194 (2009).
133. A. K. Stewart, P. S. Kedar, B. E. Shmukler, D. H. Vandorpe, A. Hsu, B. Glader, A. Rivera, C. Brugnara, S. L. Alper, Functional characterization and modified rescue of novel AE1 mutation R730C associated with overhydrated cation leak stomatocytosis. *Am J Physiol Cell Physiol* **300**, C1034-1046 (2011).
134. D. Barneaud-Rocca, F. Borgese, H. Guizouarn, Dual transport properties of anion exchanger 1: the same transmembrane segment is involved in anion exchange and in a cation leak. *J Biol Chem* **286**, 8909-8916 (2011).
135. M. N. Chernova, A. K. Stewart, P. N. Barry, M. L. Jennings, S. L. Alper, Mouse Ae1 E699Q mediates SO_4^{2-}i/anion-o exchange with [SO_4^{2-}]i-dependent reversal of wild-type pHo sensitivity. *Am J Physiol Cell Physiol* **295**, C302-312 (2008).
136. X.-B. Tang, M. Kovacs, D. Sterling, J. R. Casey, Identification of Residues Lining the Translocation Pore of Human AE1, Plasma Membrane Anion Exchange Protein. *J. Biol. Chem.* **274**, 3557-3564 (1999).
137. Q. Zhu, J. R. Casey, The substrate anion selectivity filter in the human erythrocyte Cl^-/HCO_3^- exchange protein, AE1. *J. Biol. Chem.* **279**, 23565-23573 (2004).
138. S. Takazaki, Y. Abe, T. Yamaguchi, M. Yagi, T. Ueda, D. Kang, N. Hamasaki, Mutation of His 834 in human anion exchanger 1 affects substrate binding. *Biochim Biophys Acta* **1798**, 903-908 (2010).
139. X. R. Jin, Y. Abe, C. Y. Li, N. Hamasaki, Histidine-834 of Human Erythrocyte Band 3 Has an Essential Role in the Conformational Changes That Occur during the Band 3-Mediated Anion Exchange. *Biochemistry* **42**, 12927-12932 (2003).
140. S. Müller-Berger, D. Karbach, J. Konig, S. Lepke, P. G. Wood, H. Appelhans, H. Passow, Inhibition of mouse erythroid band 3-mediated chloride transport by site-directed mutagenesis of histidine residues and its reversal by second site mutation of Lys 558, the locus of covalent H_2DIDS binding. *Biochemistry* **34**, 9315-9324 (1995).

141. V. Ramakrishnan, D. D. Busath, An Inverting Basket Model for AE1 Transport. *J Theor Biol* **215**, 215-226 (2002).
142. S. Grinstein, S. Ship, A. Rothstein, Anion transport in relation to proteolytic dissection of Band 3 protein. *Biochim. Biophys. Acta* **507**, 294-304 (1978).
143. R. R. Kopito, B. S. Lee, D. M. Simmons, A. E. Lindsey, C. W. Morgans, K. Schneider, Regulation of intracellular pH by a neuronal homolog of the erythrocyte anion exchanger. *Cell* **59**, 927-937 (1989).
144. Q. Zhu, D. W. Lee, J. R. Casey, Novel topology in C-terminal region of the human plasma membrane anion exchanger, AE1. *J Biol Chem* **278**, 3112-3120 (2003).
145. D. Zhang, A. Kiyatkin, J. T. Bolin, P. S. Low, Crystallographic structure and functional interpretation of the cytoplasmic domain of erythrocyte membrane band 3. *Blood* **96**, 2925-2933 (2000).
146. J. L. Grey, G. C. Kodippili, K. Simon, P. S. Low, Identification of contact sites between ankyrin and band 3 in the human erythrocyte membrane. *Biochemistry* **51**, 6838-6846 (2012).
147. J. R. Casey, D. M. Lieberman, R. A. F. Reithmeier, Purification and characterization of Band 3 protein. *Methods Enzymol.* **173**, 494-512 (1989).
148. R. A. F. Reithmeier, S. L. Chan, M. Popov, in *Transport Processes in Eukaryotic and Prokaryotic Organisms,* W. N. Konings, H. R. Kaback, J. S. Lolkema, Eds. (Elsevier Science, 1996), vol. 2, pp. 281-309.
149. X. B. Tang, J. Fujinaga, R. Kopito, J. R. Casey, Topology of the region surrounding Glu681 of human AE1 protein, the erythrocyte anion exchanger. *J Biol Chem* **273**, 22545-22553 (1998).
150. J. Fujinaga, X. B. Tang, J. R. Casey, Topology of the membrane domain of human erythrocyte anion exchange protein, AE1. *J Biol Chem* **274**, 6626-6633 (1999).
151. D. Kang, K. Okubo, N. Hamasaki, N. Kuroda, H. Shiraki, A structural study of the membrane domain of band 3 by tryptic digestion. Conformational change of band 3 in situ induced by alkali treatment. *J Biol Chem* **267**, 19211-19217 (1992).
152. P. Jarolim, H. L. Rubin, D. Zakova, J. Storry, M. E. Reid, Characterization of seven low incidence blood group antigens carried by erythrocyte band 3 protein. *Blood* **92**, 4836-4843 (1998).
153. P. Pal, D. Lebedev, S. Salim, P. A. Knauf, Substrates induce conformational changes in human anion exchanger 1 (hAE1) as observed by fluorescence resonance energy transfer. *Biochemistry* **45**, 6279-6295 (2006).
154. A. Rao, R. A. F. Reithmeier, Reactive sulfhydryl groups of the Band 3 polypeptide from human erythrocyte membranes: Location in the primary structure. *J. Biol. Chem.* **254**, 6144-6150 (1979).
155. M. Popov, L. Y. Tam, J. Li, R. A. F. Reithmeier, Mapping the ends of transmembrane segments in a polytopic membrane protein. Scanning

N-glycosylation mutagenesis of extracytosolic loops in the anion exchanger, band 3. *J. Biol. Chem.* **272**, 18325-18332 (1997).
156. M. Popov, J. Li, R. A. Reithmeier, Transmembrane folding of the human erythrocyte anion exchanger (AE1, Band 3) determined by scanning and insertional N-glycosylation mutagenesis. *Biochem. J.* **339**, 269-279 (1999).
157. L. J. Bruce, D. J. Anstee, F. A. Spring, M. J. Tanner, Band 3 Memphis variant II. Altered stilbene disulfonate binding and the Diego (Dia) blood group antigen are associated with the human erythrocyte band 3 mutation Pro854-->Leu. *J Biol Chem* **269**, 16155-16158 (1994).
158. J. R. Casey, C. A. Pirraglia, R. A. F. Reithmeier, Enzymatic deglycosylation of human Band 3, the anion transport protein of the erythrocyte membrane: effect on protein structure and transport properties. *J. Biol. Chem.* **267**, 11940-11948 (1992).
159. J. Li, J. Quilty, M. Popov, R. A. Reithmeier, Processing of N-linked oligosaccharide depends on its location in the anion exchanger, AE1, membrane glycoprotein. *Biochem. J.* **349**, 51-57 (2000).
160. J. C. Cheung, J. Li, R. A. Reithmeier, Topology of transmembrane segments 1-4 in the human chloride/bicarbonate anion exchanger 1 (AE1) by scanning N-glycosylation mutagenesis. *Biochem J* **390**, 137-144 (2005).
161. J. C. Cheung, J. Li, R. A. Reithmeier, Topology of transmembrane segments 1-4 in the human chloride/bicarbonate anion exchanger 1 (AE1) by scanning N-glycosylation mutagenesis. *Biochem J* **390**, 137-144. (2005).
162. J. R. Casey, Y. Ding, R. R. Kopito, The role of cysteine residues in the erythrocyte plasma membrane anion exchange protein, AE1. *J. Biol. Chem.* **270**, 8521-8527 (1995).
163. T. Hirai, N. Hamasaki, T. Yamaguchi, Y. Ikeda, Topology models of anion exchanger 1 that incorporate the anti-parallel V-shaped motifs found in the EM structure. *Biochem Cell Biol* **89**, 148-156 (2011).
164. T. Yamaguchi, Y. Ikeda, Y. Abe, H. Kuma, D. Kang, N. Hamasaki, T. Hirai, Structure of the Membrane Domain of Human Erythrocyte Anion Exchanger 1 Revealed by Electron Crystallography. *J Mol Biol* **397**, 179-189 (2010).
165. T. L. Steck, Cross-linking the major proteins of the isolated erythrocyte membrane. *J. Mol. Biol.* **66**, 295-305 (1972).
166. A. M. Taylor, Q. Zhu, J. R. Casey, Cysteine-directed cross-linking localizes regions of the human erythrocyte anion exchange protein (AE1) relative to the dimeric interface. *Biochem. J.* **359**, 661-668 (2001).
167. A. Basu, S. Mazor, J. R. Casey, Distance measurements within a concatamer of the plasma membrane Cl^-/HCO_3^- exchanger, AE1. *Biochemistry* **49**, 9226-9240 (2010).

168. J. D. Groves, M. J. Tanner, Structural model for the organization of the transmembrane spans of the human red-cell anion exchanger (band 3; AE1). *Biochem J* **344 Pt 3**, 699-711. (1999).
169. J. D. Groves, L. Wang, M. J. Tanner, Functional reassembly of the anion transport domain of human red cell band 3 (AE1) from multiple and non-complementary fragments. *FEBS Lett* **433**, 223-227 (1998).
170. J. D. Groves, M. J. Tanner, Co-expressed complementary fragments of the human red cell anion exchanger (band 3, AE1) generate stilbene disulfonate-sensitive anion transport. *J. Biol. Chem.* **270**, 9097-9105 (1995).
171. L. Wang, J. D. Groves, W. J. Mawby, M. J. Tanner, Complementation studies with co-expressed fragments of the human red cell anion transporter (Band 3; AE1). The role of some exofacial loops in anion transport. *J. Biol. Chem.* **272**, 10631-10638 (1997).
172. M. D. Parker, M. T. Young, C. M. Daly, R. W. Meech, W. F. Boron, M. J. Tanner, A Conductive Pathway Generated From Fragments Of The Human Red Cell Anion Exchanger, AE1. *J. Physiol.*, (2007).
173. G. D. Bennett, M. M. B. Kay, Homeostatic removal of senescent murine erythrocytes by splenic macrophages. *Exp. Hematol.* **9**, 297-307 (1981).
174. J. R. Casey, R. A. F. Reithmeier, Detergent interaction with Band 3, a model polytopic membrane protein. *Biochem.* **32**, 1172-1179 (1993).
175. M. J. Lemieux, R. A. Reithmeier, D. N. Wang, Importance of detergent and phospholipid in the crystallization of the human erythrocyte anion-exchanger membrane domain. *J Struct Biol* **137**, 322-332 (2002).
176. D. N. Wang, W. Kuhlbrandt, V. Sarabia, R. A. F. Reithmeier, Two-dimensional structure of the membrane domain of human band 3, the anion transport protein of the erythrocyte membrane. *EMBO J.* **12**, 2233-2239 (1993).
177. D. N. Wang, V. E. Sarabia, R. A. Reithmeier, W. Kuhlbrandt, Three-dimensional map of the dimeric membrane domain of the human erythrocyte anion exchanger, Band 3. *EMBO J.* **13**, 3230-3235 (1994).
178. T. Yamaguchi, T. Fujii, Y. Abe, T. Hirai, D. Kang, K. Namba, N. Hamasaki, K. Mitsuoka, Helical image reconstruction of the outward-open human erythrocyte band 3 membrane domain in tubular crystals. *J Struct Biol* **169**, 406-412 (2009).
179. J. Jiang, N. Magilnick, K. Tsirulnikov, N. Abuladze, I. Atanasov, P. Ge, M. Narla, A. Pushkin, Z. H. Zhou, I. Kurtz, Single particle electron microscopy analysis of the bovine anion exchanger 1 reveals a flexible linker connecting the cytoplasmic and membrane domains. *PLoS One* **8**, (2013).
180. I. Sekler, R. R. Kopito, J. R. Casey, High level expression, partial purification and functional reconstitution of the human AE1 anion exchange protein in *Saccharomyces cerevisiae*. *J. Biol. Chem.* **270**, 21028-21034 (1995).

181. J. D. Groves, P. Falson, M. le Maire, M. J. Tanner, Functional cell surface expression of the anion transport domain of human red cell band 3 (AE1) in the yeast *Saccharomyces cerevisiae*. *Proc Natl Acad Sci U S A* **93**, 12245-12250 (1996).
182. R. Zhao, R. A. Reithmeier, Expression and characterization of the anion transporter homologue YNL275w in *Saccharomyces cerevisiae*. *Am J Physiol Cell Physiol* **281**, C33-45. (2001).
183. N. Tokuda, K. Igarashi, T. Shimamura, T. Yurugi-Kobayashi, M. Shiroishi, K. Ito, T. Sugawara, H. Asada, T. Murata, N. Nomura, S. Iwata, T. Kobayashi, Cloning, expression and purification of the anion exchanger 1 homologue from the basidiomycete *Phanerochaete chrysosporium*. *Protein Expr Purif* **79**, 81-87 (2011).
184. M. Joanne Lemieux, R. A. Reithmeier, D. N. Wang, Importance of detergent and phospholipid in the crystallization of the human erythrocyte anion-exchanger membrane domain. *J Struct Biol* **137**, 322-332 (2002).
185. M. Dolder, T. Walz, A. Hefti, A. Engel, Human erythrocyte band 3. Solubilization and reconstitution into two-dimensional crystals. *J Mol Biol* **231**, 119-132 (1993).
186. J. Deisenhofer, O. Epp, K. Miki, R. Huber, Structure of the protein subunits in the photosynthetic reaction centre of *Rhodopseudomonas viridis* at 3 Å resolution. *Nature* **318**, 618-624 (1985).
187. D. A. Doyle, J. M. Cabral, R. A. Pfuetzner, A. Kuo, J. M. Gulbis, S. L. Cohen, B. T. Chait, R. MacKinnon, The Structure of the Potassium Channel: Molecular Basis of K^+ Conduction and Ion Selectivity. *Science* **280**, 69-77 (1998).
188. http://blanco.biomol.uci.edu/Membrane_Proteins_xtal.html. (2013).
189. R. M. Bill, P. J. Henderson, S. Iwata, E. R. Kunji, H. Michel, R. Neutze, S. Newstead, B. Poolman, C. G. Tate, H. Vogel, Overcoming barriers to membrane protein structure determination. *Nat Biotechnol* **29**, 335-340 (2011).
190. C. G. Tate, Overexpression of mammalian integral membrane proteins for structural studies. *FEBS Lett* **504**, 94-98 (2001).
191. C. R. Midgett, D. R. Madden, Breaking the bottleneck: eukaryotic membrane protein expression for high-resolution structural studies. *J Struct Biol* **160**, 265-274 (2007).
192. F. Junge, B. Schneider, S. Reckel, D. Schwarz, V. Dotsch, F. Bernhard, Large-scale production of functional membrane proteins. *Cell Mol Life Sci* **65**, 1729-1755 (2008).
193. D. Drew, S. Newstead, Y. Sonoda, H. Kim, G. von Heijne, S. Iwata, GFP-based optimization scheme for the overexpression and purification of eukaryotic membrane proteins in *Saccharomyces cerevisiae*. *Nat Protoc* **3**, 784-798 (2008).
194. S. Newstead, H. Kim, G. von Heijne, S. Iwata, D. Drew, High-throughput fluorescent-based optimization of eukaryotic membrane protein

overexpression and purification in *Saccharomyces cerevisiae*. *Proc Natl Acad Sci U S A* **104**, 13936-13941 (2007).
195. C. L. Brooks, M. Morrison, M. Joanne Lemieux, Rapid expression screening of eukaryotic membrane proteins in *Pichia pastoris*. *Protein Sci* **22**, 425-433 (2013).
196. M. C. Wiener, A pedestrian guide to membrane protein crystallization. *Methods* **34**, 364-372 (2004).
197. Z. E. Newby, J. D. O'Connell, 3rd, F. Gruswitz, F. A. Hays, W. E. Harries, I. M. Harwood, J. D. Ho, J. K. Lee, D. F. Savage, L. J. Miercke, R. M. Stroud, A general protocol for the crystallization of membrane proteins for X-ray structural investigation. *Nat Protoc* **4**, 619-637 (2009).
198. R. L. Lieberman, J. A. Culver, K. C. Entzminger, J. C. Pai, J. A. Maynard, Crystallization chaperone strategies for membrane proteins. *Methods* **55**, 293-302 (2011).
199. E. R. Kunji, M. Harding, P. J. Butler, P. Akamine, Determination of the molecular mass and dimensions of membrane proteins by size exclusion chromatography. *Methods* **46**, 62-72 (2008).
200. C. G. Tate, Practical considerations of membrane protein instability during purification and crystallisation. *Methods Mol Biol* **601**, 187-203 (2010).
201. S. G. Rasmussen, H. J. Choi, D. M. Rosenbaum, T. S. Kobilka, F. S. Thian, P. C. Edwards, M. Burghammer, V. R. Ratnala, R. Sanishvili, R. F. Fischetti, G. F. Schertler, W. I. Weis, B. K. Kobilka, Crystal structure of the human beta2 adrenergic G-protein-coupled receptor. *Nature* **450**, 383-387 (2007).
202. R. Dutzler, E. B. Campbell, R. MacKinnon, Gating the selectivity filter in ClC chloride channels. *Science* **300**, 108-112 (2003).
203. C. Hunte, J. Koepke, C. Lange, T. Rossmanith, H. Michel, Structure at 2.3 Å resolution of the cytochrome bc(1) complex from the yeast Saccharomyces cerevisiae co-crystallized with an antibody Fv fragment. *Structure* **8**, 669-684 (2000).
204. Y. Jiang, A. Lee, J. Chen, V. Ruta, M. Cadene, B. T. Chait, R. MacKinnon, X-ray structure of a voltage-dependent K^+ channel. *Nature* **423**, 33-41 (2003).
205. R. Ujwal, J. U. Bowie, Crystallizing membrane proteins using lipidic bicelles. *Methods* **55**, 337-341 (2011).
206. C. J. Law, P. C. Maloney, D. N. Wang, Ins and outs of major facilitator superfamily antiporters. *Annu Rev Microbiol* **62**, 289-305 (2008).
207. S. Radestock, L. R. Forrest, The alternating-access mechanism of MFS transporters arises from inverted-topology repeats. *J Mol Biol* **407**, 698-715 (2011).
208. J. Abramson, I. Smirnova, V. Kasho, G. Verner, H. R. Kaback, S. Iwata, Structure and mechanism of the lactose permease of *Escherichia coli*. *Science* **301**, 610-615 (2003).

209. L. Guan, O. Mirza, G. Verner, S. Iwata, H. R. Kaback, Structural determination of wild-type lactose permease. *Proc Natl Acad Sci U S A* **104**, 15294-15298 (2007).
210. Y. Huang, M. J. Lemieux, J. Song, M. Auer, D. N. Wang, Structure and mechanism of the glycerol-3-phosphate transporter from *Escherichia coli*. *Science* **301**, 616-620 (2003).
211. Y. Yin, X. He, P. Szewczyk, T. Nguyen, G. Chang, Structure of the multidrug transporter EmrD from Escherichia coli. *Science* **312**, 741-744 (2006).
212. T. Hirai, J. A. Heymann, D. Shi, R. Sarker, P. C. Maloney, S. Subramaniam, Three-dimensional structure of a bacterial oxalate transporter. *Nat Struct Biol* **9**, 597-600 (2002).
213. T. Hirai, S. Subramaniam, Structure and transport mechanism of the bacterial oxalate transporter OxlT. *Biophys J* **87**, 3600-3607 (2004).
214. J. Abramson, E. M. Wright, Structure and function of Na^+-symporters with inverted repeats. *Curr Opin Struct Biol* **19**, 425-432 (2009).
215. A. Yamashita, S. K. Singh, T. Kawate, Y. Jin, E. Gouaux, Crystal structure of a bacterial homologue of Na^+/Cl^--dependent neurotransmitter transporters. *Nature* **437**, 215-223 (2005).
216. S. Ressl, A. C. Terwisscha van Scheltinga, C. Vonrhein, V. Ott, C. Ziegler, Molecular basis of transport and regulation in the Na^+/betaine symporter BetP. *Nature* **458**, 47-52 (2009).
217. S. Faham, A. Watanabe, G. M. Besserer, D. Cascio, A. Specht, B. A. Hirayama, E. M. Wright, J. Abramson, The crystal structure of a sodium galactose transporter reveals mechanistic insights into Na^+/sugar symport. *Science* **321**, 810-814 (2008).
218. S. Weyand, T. Shimamura, S. Yajima, S. Suzuki, O. Mirza, K. Krusong, E. P. Carpenter, N. G. Rutherford, J. M. Hadden, J. O'Reilly, P. Ma, M. Saidijam, S. G. Patching, R. J. Hope, H. T. Norbertczak, P. C. Roach, S. Iwata, P. J. Henderson, A. D. Cameron, Structure and molecular mechanism of a nucleobase-cation-symport-1 family transporter. *Science* **322**, 709-713 (2008).
219. X. Gao, F. Lu, L. Zhou, S. Dang, L. Sun, X. Li, J. Wang, Y. Shi, Structure and mechanism of an amino acid antiporter. *Science* **324**, 1565-1568 (2009).
220. C. Hunte, E. Screpanti, M. Venturi, A. Rimon, E. Padan, H. Michel, Structure of a Na^+/H^+ antiporter and insights into mechanism of action and regulation by pH. *Nature* **435**, 1197-1202. (2005).
221. M. Landau, K. Herz, E. Padan, N. Ben-Tal, Model structure of the Na^+/H^+ exchanger 1 (NHE1): functional and clinical implications. *J Biol Chem* **282**, 37854-37863 (2007).
222. M. Schushan, M. Xiang, P. Bogomiakov, E. Padan, R. Rao, N. Ben-Tal, Model-guided mutagenesis drives functional studies of human NHA2, implicated in hypertension. *J Mol Biol* **396**, 1181-1196 (2010).

223. B. L. Lee, B. D. Sykes, L. Fliegel, Structural analysis of the Na^+/H^+ exchanger isoform 1 (NHE1) using the divide and conquer approach. *Biochem Cell Biol* **89**, 189-199 (2011).
224. B. L. Lee, B. D. Sykes, L. Fliegel, Structural and functional insights into the cardiac Na^+/H^+ exchanger. *J Mol Cell Cardiol*, (2012).
225. R. Dutzler, E. B. Campbell, M. Cadene, B. T. Chait, R. MacKinnon, X-ray structure of a ClC chloride channel at 3.0 Å reveals the molecular basis of anion selectivity. *Nature* **415**, 287-294 (2002).
226. E. Ohana, N. Shcheynikov, D. Yang, I. So, S. Muallem, Determinants of coupled transport and uncoupled current by the electrogenic SLC26 transporters. *J Gen Physiol* **137**, 239-251 (2011).
227. T. J. Jentsch, To the editor. CLC chloride channels and transporters: from genes to protein structure, pathology and physiology. *Crit Rev Biochem Mol Biol* **44**, 64 (2009).
228. T. J. Jentsch, M. Poet, J. C. Fuhrmann, A. A. Zdebik, Physiological functions of CLC Cl- channels gleaned from human genetic disease and mouse models. *Annu Rev Physiol* **67**, 779-807 (2005).
229. C. Miller, ClC chloride channels viewed through a transporter lens. *Nature* **440**, 484-489 (2006).
230. M. Walden, A. Accardi, F. Wu, C. Xu, C. Williams, C. Miller, Uncoupling and turnover in a Cl^-/H^+ exchange transporter. *J Gen Physiol* **129**, 317-329 (2007).
231. W. Nguitragool, C. Miller, Uncoupling of a CLC Cl^-/H^+ exchange transporter by polyatomic anions. *J Mol Biol* **362**, 682-690 (2006).
232. A. Accardi, C. Miller, Secondary active transport mediated by a prokaryotic homologue of ClC Cl^- channels. *Nature* **427**, 803-807 (2004).
233. H. Jayaram, A. Accardi, F. Wu, C. Williams, C. Miller, Ion permeation through a Cl^--selective channel designed from a CLC Cl^-/H^+ exchanger. *Proc Natl Acad Sci U S A* **105**, 11194-11199 (2008).
234. H. H. Lim, C. Miller, Intracellular proton-transfer mutants in a CLC Cl^-/H^+ exchanger. *J Gen Physiol* **133**, 131-138 (2009).
235. A. Accardi, M. Walden, W. Nguitragool, H. Jayaram, C. Williams, C. Miller, Separate ion pathways in a Cl^-/H^+ exchanger. *J Gen Physiol* **126**, 563-570 (2005).
236. S. Lobet, R. Dutzler, Ion-binding properties of the ClC chloride selectivity filter. *EMBO J* **25**, 24-33 (2006).
237. J. L. Robertson, L. Kolmakova-Partensky, C. Miller, Design, function and structure of a monomeric ClC transporter. *Nature* **468**, 844-847 (2010).
238. L. Feng, E. B. Campbell, Y. Hsiung, R. MacKinnon, Structure of a eukaryotic CLC transporter defines an intermediate state in the transport cycle. *Science* **330**, 635-641 (2010).
239. S. Markovic, R. Dutzler, The structure of the cytoplasmic domain of the chloride channel ClC-Ka reveals a conserved interaction interface. *Structure* **15**, 715-725 (2007).

240. W. M. Yau, W. C. Wimley, K. Gawrisch, S. H. White, The preference of tryptophan for membrane interfaces. *Biochemistry* **37**, 14713-14718 (1998).
241. W. Nguitragool, C. Miller, CLC Cl^-/H^+ transporters constrained by covalent cross-linking. *Proc Natl Acad Sci U S A* **104**, 20659-20665 (2007).
242. A. A. Zdebik, G. Zifarelli, E. Y. Bergsdorf, P. Soliani, O. Scheel, T. J. Jentsch, M. Pusch, Determinants of anion-proton coupling in mammalian endosomal CLC proteins. *J Biol Chem* **283**, 4219-4227 (2008).

Chapter 2: Materials and Methods

2.1 Materials

DNA oligonucleotides were purchased from Integrated DNA Technologies (Coralville, IA). Pfx DNA polymerase, ProLong Gold antifade reagent with DAPI, Dulbecco's modified Eagle's medium (DMEM), fetal bovine serum, calf serum, penicillin-streptomycin-glutamine, 2', 7'-bis-(2-carboxyethyl)-5-(and-6)carboxylfluorescein, acetoxymethyl ester (BCECF-AM) and 4,4'-diisothiocyanodihydrostilbene-2,2'-disulfonate (H_2DIDS) were purchased from Invitrogen (Carlsbad, CA). T4 DNA ligase, Mung Bean Nuclease, restriction enzymes, and PNGase F were from New England Biolabs (Ipswich, MA). QuikChange Lightning Site Directed Mutagenesis Kit was from Agilent Technologies (Mississauga, ON, Canada). Glass coverslips were from Fisher Scientific (Ottawa, ON, Canada). BCA protein assay kit, Sulfo-NHS-SS-Biotin, immobilized streptavidin resin, and dithiobis(succinimidylpropionate) (DSP) were from Pierce (Rockford, IL). ECL chemiluminescent reagent and radioactive [^{35}S]Na_2SO_4 were from Perkin Elmer Life Sciences (Waltham, MA). Immobilon-P PVDF was from Millipore (Billerica, MA). Anti-AE1 antibody IVF12 was a gift from Dr. Mike Jennings (University of Arkansas) (*1*). Anti-Pma1 antibody was a gift from Dr. Gary Eitzen (University of Alberta) (*2*). Anti-Sec61 antibody was a gift from Dr. Randy Schekman (Berkeley, University of California) (*3*). The anti-rhodopsin antibody, Rho 1D4, was purchased from the University of British Columbia's University-Industry Liaison Office (www.flintbox.com) (*4*). Donkey anti-mouse IgG conjugated to horseradish peroxidase and Glutathione Sepharose

4B were from GE Healthcare Bio-Sciences (Piscattaway, NJ). Donkey anti-rabbit IgG conjugated to horseradish peroxidase and mouse anti-glyceraldehyde-3-phosphate dehydrogenase (GAPDH) were from Santa Cruz Biotechnology (Santa Cruz, CA). Anti-rabbit Alexa 484 antibody and anti-mouse Alexa 544 antibody were from Molecular Probes (Carlsbad, CA). The 1D4 peptide (TETSQVAPA) was synthesized by GenScript (Piscataway, NJ). Fos-choline 14 (FC), n-dodecyl-β-D-maltopyranoside (DDM), and n-octyl-β-D-glycopyranoside (OG) were from Anatrace (Maumee, OH). Egg L-α-lysophosphatidylcholine (LPC) was a mixture of 16:0, 18:0, 18:1, 16:1, 18:2, 14:0, and unknown lipid from Avanti Polar Lipids (Alabaster, AL). CSM Leu- amino acids and zymolyase 100T were from MP Biomedical (Solon, OH). Sephadex G-50, Sepharose 2B, egg yolk phosphatidylcholine (EYPC), octaethylene glycol mono-n-dodecyl ether ($C_{12}E_8$), nigericin, and poly-L-lysine were from Sigma-Aldrich (Oakville, ON, Canada). Affi-gel 102 and Bio-beads SM2 were from Biorad (Hercules, CA). Complete Mini Protease Inhibitor Cocktail and collagenase A were from Roche Applied Science (Indianapolis, IN). The mMessage mMachine *in vitro* T7 RNA-polymerase kit was from Ambion (Austin, TX). Hydrogen ionophore I-cocktail A was from Fluka (Buchs, Switzerland). Outdated red cells were from University of Alberta Blood Bank.

Table 2.1 AE1 Mutagenic Primers.

The desired AE1 point mutations are listed along with the corresponding forward and reverse primers used to create each mutant.

AE1 Point Mutation	Forward Primer (5'-3')	Reverse Primer (5'-3')
G463A	tgcttgtggtcgccttctcaggacccctgc	gcaggggtcctgagaaggcgaccacaagca
F464A	tgcttgtggtcggcgcctcaggacccctgc	gcaggggtcctgaggcgccgaccacaagca
S465A	gtggtcggcttcgcaggacccctgc	gcaggggtcctgcgaagccgaccac
S465D	gcttgtggtcggcttcgatggacccctgctggtgt	acaccagcaggggtccatcgaagccgaccacaagc
S465T	tgtggtcggcttcacgggacccctgctgg	ccagcaggggtcccgtgaagccgaccaca
S465N	gcttgtggtcggcttcaatggacccctgctggtgt	acaccagcaggggtccattgaagccgaccacaagc
G466A	gtcggcttctcagcacccctgctggtg	caccagcaggggtgctgagaagccgac
P467A	tcggcttctcaggagccctgctggtg	caccagcagggctcctgagaagccga
F507A	gtgttggtggtggccgccgagggtagcttcct	aggaagctaccctcggcggccaccaccaacac
E508A	gtggtggccttcgcgggtagcttcctg	caggaagctacccgcgaaggccaccac
E508D	ggtggtggccttcgatggtagcttcctg	caggaagctaccatcgaaggccaccacc
E508S	gttggtggtggccttctcgggtagcttcctggtc	gaccaggaagctacccgagaaggccaccaccaac
E508Q	ggtggtggccttccagggtagcttcct	aggaagctaccctggaaggccaccacc
E508K	tggtggtggccttcaagggtagcttcctg	caggaagctacccttgaaggccaccacca
G509A	gtggccttcgaggctagcttcctggtc	gaccaggaagctagcctcgaaggccac
S510A	ggccttcgagggtgccttcctggtccgc	gcggaccaggaaggcaccctcgaaggcc
F584A	ggccggtaccttcttcgctgccatgatgctgcgc	gcgcagcatcatggcagcgaagaaggtaccggcc
M586A	cggtaccttcttctttgccgcgatgctgcgcaagttcaag	cttgaacttgcgcagcatcgcggcaaagaagaaggtaccg
M587A	cttcttctttgccatggcgctgcgcaagttcaagaacagc	gctgttcttgaacttgcgcagcgccatggcaaagaagaag
L588A	cttcttctttgccatgatggcgcgcaagttcaagaacagc	gctgttcttgaacttgcgcgccatcatggcaaagaagaag
I605A	gctgcgtcgggtcgccggggacttcggg	cccgaagtccccggcgacccgacgcagc

G606A	gggtcatcgcggacttcggggtccc	gggaccccgaagtccgcgatgaccc
D607A	gggtcatcggggccttcggggtccc	gggaccccgaaggccccgatgaccc
F608A	ggtcatcggggacgccggggtccccatc	gatggggaccccggcgtccccgatgac c
G609A	tcggggacttcgcggtccccatctc	gagatggggaccgcgaagtccccga
F789A	ggctgtactggctggcatcttcctctaca tgggg	ccccatgtagaggaagatgccagccag tacagcc
G790A	cctggctgtactgtttgccatcttcctcta catgg	ccatgtagaggaagatggcaaacagta cagccagg
I791A	tggctgtactgtttggcgccttcctctaca tggggg	cccccatgtagaggaaggcgccaaaca gtacagcca
I791S	gctgtactgtttggcagcttcctctacatg ggg	ccccatgtagaggaagctgccaaacag tacagc
F792A	gctgtactgtttggcatcgccctctacat gggggtcac	gtgacccccatgtagagggcgatgcca aacagtacagc
F793A	ggctgtactgtttggcatcttcgcctacat gggg	ccccatgtaggcgaagatgccaaacag tacagcc
L876A	gcgtcctgctgccggccatcttcaggaa cg	cgttcctgaagatggccggcagcagga cgc
I877A	gtcctgctgccgctcgccttcaggaacgt gga	tccacgttcctgaaggcgagcggcagc aggac
F878A	ctgctgccgctcatcgccaggaacgtgg agct	agctccacgttcctggcgatgagcggca gcag
F878L	tcctgctgccgctcatcttaaggaacgtg g	ccacgttccttaagatgagcggcagcag ga
F878T	ctgctgccgctcatcaccaggaacgtgg agct	agctccacgttcctggtgatgagcggca gcag
F878Y	cctgctgccgctcatctataggaacgtg gagc	gctccacgttcctatagatgagcggcag cagg
R879A	gctgccgctcatcttcgcgaacgtggag cttcag	ctgaagctccacgttcgcgaagatgagc ggcagc
N880A	gccgctcatcttcagggccgtggagctt cagtgt	acactgaagctccacggccctgaagat gagcggc
F582W	gctcatggccggtacctggttctttgcca tgatgct	agcatcatggcaaagaaccaggtaccg gccatgagc
F583W	catggccggtaccttctggtttgccatga tgctgcg	cgcagcatcatggcaaaccagaaggta ccggccatg
F584W	catggccggtaccttcttctgggccatga tgctgc	gcagcatcatggcccagaagaaggtac cggccatg
A585W	ggccggtaccttcttcttttggatgatgct gcgcaagttc	gaacttgcgcagcatcatccaaaagaa gaaggtaccggcc
I839W	catgcacttattcacgggctggcagatc atctgcctggcag	ctgccaggcagatgatctgccagcccgt gaataagtgcatg
Q840W	cacttattcacgggcatctggatcatctg cctggcagt	actgccaggcagatgatccagatgccc gtgaataagtg

I841W	ttattcacgggcatccagtggatctgcctggcagtgctg	cagcactgccaggcagatccactggatgcccgtgaataa
I842W	cacgggcatccagatctggtgcctggcagtgctgt	acagcactgccaggcaccagatctggatgcccgtg
A855W	tgaagtccacgccgtggtccctggccctgcc	ggcagggccagggaccacggcgtggacttca
S856W	cacgccggcctggctggccctgcc	ggcagggccagccaggccggcgtg
L857W	cacgccggcctcctgggccctgcccttc	gaagggcagggcccaggaggccggcgtg
A858W	gccggcctccctgtggctgcccttcgtcc	ggacgaagggcagccacagggaggccggc
L865W	cccttcgtcctcatctggactgtgccgctgcgg	ccgcagcggcacagtccagatgaggacgaaggg
T866W	cttcgtcctcatcctctgggtgccgctgcgg	ccgcagcggcacccagaggatgaggacgaag
V867W	cttcgtcctcatcctcacttggccgctgcgg	ccgcagcggccaagtgaggatgaggacgaag
P868W	catcctcactgtgtggctgcggcgcgtc	gacgcgccgcagccacacagtgaggatg
L869W	cctcactgtgccgtggcggcgcgtcctg	caggacgcgccgccacggcacagtgagg

2.2 Methods

2.2.1 Molecular Biology

All DNA sequences generated by PCR were confirmed by DNA sequencing to ensure no sequence errors were introduced (DNA Core Services Laboratory, Dept. of Biochemistry, University of Alberta).

2.2.1.1 S. cerevisiae Expression Constructs

The yeast expression vector YEpM (*5*) was a gift from Dr. Theodore Wensel (Baylor College of Medicine). The construct corresponds to the vector called YEpPMA1MDR1 (*5*), but with the MDR1 sequence (between the BamHI and XhoI sites) replaced by the polylinker sequence, ACTAGTGTTTAAACACGCGT, that contains a 5' Spe1 site and a 3' MluI site. The yeast expression plasmid, pPB1, which encodes for the protein AE1MD-Rho, was constructed using pJRC9 (*6*) as a PCR template for AE1 and YEpM as a vector. The forward primer (5' GGCCACTAGTTTTAATTATCAAACAATATCAATATG*TCTAGATATCCATATTATT TGTCTGATATT*ACAGATGCATTCAGCCCCCAGG 3') contains a SpeI restriction site, the upstream sequence of Pma1 needed for expression (underlined), a start codon, codon preferencing in yeast for the sequence of the first 10 amino acids of AE1MD-Rho (italics), and an annealing sequence. The reverse primer (5' GGGACGCGTTTA*CGCAGGCGCGACTTGGCTGGTCTCTGT*CACAGGCATGGCCACTT CGTCG 3') contains a MluI restriction site, a stop codon, the sequence for the nine C-terminal amino acids of rhodopsin (italics), and an annealing

sequence. The PCR product and YEpM vector were digested with SpeI and MluI, and ligated to create pPB1.

2.2.1.2 E. coli Expression Constructs

pHJC1 encodes, AE1-Ct, a glutathione S-transferase (GST) fusion protein containing the last 40 amino acids of AE1 (residues 872-911). The coding sequence for the last 40 amino acids of AE1-Ct was amplified using pJRC9 (*6*) as a PCR template, and inserted into the GST expression plasmid pGEX-6p-1 (GE Healthcare Life Sciences). The forward primer sequence is 5' CGCGGATCCGTCCTGCTGCCGCTCATCTTC 3'. The reverse primer sequence is 5' CGCGGATCCTCACACAGGCATGGCCACTTCGT 3'. The PCR product and pGEX-6p-1 vector were digested with BamHI and ligated together to create pHJC1.

2.2.1.3 HEK293 Cell Expression Constructs

pJRC9, which encodes WT-AE1 and vector (pRBG4) were constructed previously (*6, 7*). AE1 point mutants were constructed using the Agilent QuikChange Lightning Kit, primers corresponding to the mutation to be created (Table 2.1), and pJRC9 as the template DNA.

The construct pPBAE1MD346, encoding AE1MD346 (amino acids 346-911 of AE1), was created using pDEJ4 as a PCR template (*8*). The forward primer (5'-GGCCTCGAGATGCGCTATCAGTCCAGCCCTG-3') contains a XhoI site, a start codon, and an annealing sequence. The reverse primer (5'-GGAAGCTTTTACACAGGCATGGCCACTTC-3') contains an annealing sequence, stop codon, and a HindIII site. The PCR product, and vector, pcDNA3.1(-),

were digested with the restriction enzymes XhoI and HindIII, and ligated together. AE1MD346 tryptophan mutants were created using the Agilent QuikChange Lightning Kit, pPBAE1MD346 as a PCR template, and primers listed in Table 2.1.

The construct pPB3, encoding AE1-Rho (full-length erythrocyte AE1 followed by the nine C-terminal amino acids of rhodopsin), was created using the cysteineless AE1 construct, pQZ2, as a PCR template (*9*). The forward primer (5'-TCTTCTTTGCCATGATGCTGCGC-3') contains an AE1 annealing sequence. The reverse primer (5'-CCTGTGTGAGGTTACGCAGGCGCGACTTGGCTGGTCTCTGTCACAGGCATGGCCA CTTCGTCG-3') contains an EcoNI site, stop codon, the nine C-terminal amino acid of rhodopsin, and an annealing sequence. The PCR product and pQZ2 were digested with the restriction enzymes NheI and EcoNI, and ligated together. H819C-AE1, described previously (*9*), and pPB3 were digested with SphI and EcoNI and ligated together to create pPB819-Rho, which encodes H819C AE1-Rho.

2.2.1.4 X. laevis Oocyte Expression Constructs

pPBAE1-oocyte, which encodes WT-AE1 in an oocyte expression vector, was constructed by digesting pDEJ4 (*8*), with XhoI, followed by treatment with Mung Bean nuclease and HindIII. This fragment was cloned into the oocyte expression vector, pGEMHE (*10*), which was digested with SmaI and HindIII, to create pPBAE1-oocyte. Oocyte expression constructs

encoding S465A, E508A, M586A, D607A, I791A and F878A-AE1 were created using the Agilent QuikChange Lightning Kit.

The oocyte expression construct for N-terminally hemagglutinin epitope (HA)-tagged glycophorin A, pSMGPA1, was created using the mammalian expression construct pHJC2 and the pGEMHE expression vector. The pHJC2 construct was created using the human glycophorin A cDNA as a PCR template, with a forward primer that encodes an N-terminal HA tag and a 5' HindIII restriction site, and a reverse primer that encodes a 3' XhoI site. The resulting PCR product and the pcDNA3.1(-) vector were digested and ligated to create pHJC2. pHJC2 was digested with HindIII, treated with Mung Bean nuclease, further digested with XbaI, and then cloned into the SmaI/XbaI cut oocyte expression vector pGEMHE.

2.2.2 Purification of AE1-Ct

AE1-Ct transformed BL21 codon plus *E. coli* cells were used to inoculate LB medium containing 0.1 mg/ml ampicillin and grown at 37 °C until an A_{600} of 0.6-0.8 was reached. Protein expression was induced by the addition of isopropyl β-D-1-thiogalactopyranoside (IPTG) to 1 mM to the culture and incubation for 3 h at 37 °C. Cells were harvested by centrifugation at 7 500 x g for 10 min at 4 °C. Cell pellets were resuspended in 4 ºC PBS (140 mM NaCl, 3 mM KCl, 6.5 mM Na_2HPO_4, 1.5 mM KH_2PO_4, pH 7.4), containing Complete Mini Protease Inhibitor Cocktail. Cells were disrupted by sonication (four times for 60 s) using a W185 probe sonifier (Heat systems-Ultrasonic Inc., Plainview, N.Y.), and stirred slowly for 30 min,

following the addition of Triton X-100 (1% v/v). Disrupted cells were centrifuged at 2 000 x g for 10 min at 4 °C. The supernatant was collected and incubated with 1.2 ml GSH-Sepharose 4B at room temperature with rotation for 1-2 h. The resin was washed six times with PBS and AE1-Ct was eluted from the GSH-Sepharose 4B three times with 100 µl glutathione elution buffer (10 mM reduced glutathione, 50 mM Tris-HCl, pH 8.0). Total protein concentration was determined by a Bradford protein assay (*11*) and protein purity was assessed by SDS-PAGE.

2.2.3 Yeast Strains and Media

The protease deficient *S. cerevisiae* strain, BJ5457 (MATalpha ura3-52 trp1 lys2-801 leu2-delta1 his3-delta200 pep4::HIS3 prb1-delta1.6R can1 GAL), was purchased from the American Type Culture Collection (Manassas, VA). Untransformed yeast cultures were grown in YPD media (1% (w/v) Bacto-yeast extract, 2% (w/v) peptone, and 2% (w/v) glucose). Yeast cultures were chemically transformed with a plasmid containing the Leu2 gene using the lithium acetate and polyethylene glycol protocol described previously (*12-14*). Transformed yeast were grown in complete synthetic media lacking leucine (0.17% (w/v) yeast nitrogen base, 2% (w/v) glucose, 0.5% (w/v) ammonium sulfate, 0.07% (w/v) Leu^- amino acids, and 0.0037% (w/v) adenine hemisulfate, pH 6.0).

2.2.4 Isolation of Yeast Membranes

Yeast cultures were grown to an A_{600} 1.0-1.5 and harvested by centrifugation at 6 500 x g for 10 min at 4 °C. The yeast pellet was

resuspended in lysis buffer (1 mM EDTA, 10% (v/v) glycerol, 25 mM Tris, pH 7.5) to a concentration of 0.5 g yeast/ml resuspension. Yeast cells were disrupted by passage through an EmulsiFlex-C3 (Avestin, Ottawa, Canada) seven times with pressures of 20 000-25 000 psi at 4 °C. Cell debris was removed by centrifugation at 6 500 x g for 10 min at 4 °C and the supernatant was recovered. Supernatant was centrifuged at 100 000 x g for 30 min at 4 °C to sediment the membranes. Membranes were resuspended in resuspension buffer (200 mM NaCl, 10% (v/v) glycerol, 25 mM Tris, pH 7.5) to 0.5 ml membranes/ml total resuspension.

2.2.5 Yeast Immunofluorescence Studies

Yeast were prepared for immunofluorescence microscopy essentially as described previously (*15*). Yeast, transformed with the plasmid pPB1, were grown in leucine auxotrophic media at 30 °C. Yeast cells were formaldehyde-fixed, washed twice with PBS, and twice with solution B (1.2 M sorbitol, 19 mM KH_2PO_4, 80 mM K_2HPO_4, pH 7.5). Yeast were spheroplasted in solution B, containing 3 µl of β-mercaptoethanol and 40 µl of zymolyase solution (5 mg/ml zymolyase 100T made up in 10% glucose) for 20-60 min at 30 °C. Yeast cells were washed twice in solution B and spotted on Poly-L-lysine treated glass slides. Slides were dried, immersed in 4 °C methanol for 6 min and in 4 °C acetone for 30 s. Air-dried slides were washed twice with PBS, containing 0.75% (w/v) glycine for 5 min. Slides were blocked twice with PBG (PBS containing 0.5% (w/v) BSA and 0.5% (v/v) fish gelatin) for 15 min. Primary antibodies (rabbit anti-Pma1 and mouse anti-AE1 antibody,

IVF12) were added simultaneously at a 1:250 dilution and incubated overnight at 4 °C. Slides were washed six times in PBG for 5 min. Secondary antibodies (anti-mouse Alexa 544 and anti-rabbit Alexa 484) were added simultaneously at a 1:250 dilution and incubated 1 h at room temperature. Slides were washed six times in PBG and three times in PBS, before ProLong® Gold antifade reagent with DAPI was added. Images were collected with a Zeiss LSM 510 laser scanning confocal microscope using a 40 X oil immersion objective. Non-fluorescent images of yeast were collected using differential interference contrast microscopy.

2.2.6 Sucrose Gradient Ultracentrifugation

Resuspended yeast membranes (1 ml) were layered onto a 12 ml 20% to 53% linear sucrose gradient. Gradients were centrifuged at 100 000 x g at 4 °C for 5 h in a Beckman SW41 rotor. Fractions (0.5 ml) were collected from the top of the gradient, separated by SDS-PAGE and analyzed by immunoblotting.

2.2.7 Deglycosylation

Protein samples (5 µg) were denatured in 1X Glycoprotein Denaturing Buffer (0.5% SDS, 40 mM dithiothreitol) at 65 °C for 5 min. Samples were then incubated in 1X G7 reaction buffer (50 mM sodium phosphate, pH 7.5), 1% NP40 and 250 U of PNGase F, at 37 °C for 1 h. Samples were separated by SDS-PAGE and analyzed by immunoblotting.

2.2.8 Detergent Selection

Resuspended membranes (200 µl) were diluted five-fold in resuspension buffer, containing 1% (w/v) detergent. Membranes were incubated for 30 min at 4 °C and centrifuged for 30 min at 100 000 x g, to remove any insoluble material. A control sample was treated with buffer containing no detergent. Samples were separated by SDS-PAGE and analyzed by immunoblotting.

2.2.9 Preparation of 1D4 Antibody Affinity Resin

Sepharose 2B was washed three times with H_20, resuspended in an equal volume of water and the pH was adjusted to 10-11 with NaOH. In a fumehood, Sepharose 2B was activated by the addition of cyanogen bromide (19 mg/ml resin), and incubated at room temperature for 30 min while maintaining the pH between 10-11 with 0.2 M NaOH. Caution must be exercised here as failure to maintain alkaline pH can result in HCN release. Borate buffer (20 mM boric acid, pH 8.4) at 4 °C was added to stop the reaction. Cyanogen bromide was removed from the activated Sepharose 2B by washing three times with 4 °C borate buffer. Activated Sepharose 2B was resuspended in an equal volume of borate buffer and incubated 5 min at 4 °C. The 1D4 antibody (0.25 mg of antibody/ml of resin) was diluted to 2 mg/ml in borate buffer and incubated with the activated Sepharose 2B at 4 °C for 4 h. The reaction was stopped by washing the resin twice in TBS (0.15 M NaCl, 50 mM Tris, pH 7.5), containing 0.05 M glycine. 1D4 immunoaffinity resin was stored at 4 °C as a 50% slurry with TBS and 0.01% NaN_3.

2.2.10 Purification of AE1MD-Rho

Resuspended yeast membranes were diluted five-fold and solubilized at 4 °C in 1% (w/v) Fos-choline 14 for 30 min. Insoluble debris was sedimented by centrifugation at 100 000 x g for 30 min at 4 °C and the supernatant was collected. The supernatant was incubated with the 1D4 resin for 1 h at 4 °C, and was removed by vacuum filtration on a sintered glass filter, while carefully ensuring that the resin never became dry. The 1D4 resin was washed with 1D4 wash buffer (200 mM NaCl, 10% (v/v) glycerol, 0.1% $C_{12}E_8$ (w/v), 25 mM Tris, pH 7.5) three times with a total of twenty times the resin volume. Washes were removed by vacuum filtration on a sintered glass filter, as above. AE1MD-Rho was eluted from the 1D4 resin by three consecutive incubations with an equal volume of 1D4 wash buffer, containing 1 mg/ml 1D4 peptide for 10 min at 4 °C and removal of the supernatant by centrifugation. For samples prepared for reconstitutions, reconstitution buffer, containing 0.1% (w/v) $C_{12}E_8$ was used instead of the 1D4 wash buffer.

2.2.11 Purification of Erythrocyte AE1

Purified human erythrocyte AE1 was prepared from outdated red cells (University of Alberta Blood Bank) as described previously (*16*). Red cells were lysed by diluting ten times in cold 5P8 buffer (5 mM Na_2HPO_4, pH 8.0) and incubated for 20 min at 4 °C. Red cell ghosts were isolated by centrifugation at 30 000 x g for 20 min at 4 °C. Following lysis, ghosts were washed by resuspension in ice cold 5P8 buffer and centrifugation at 30 000 x

g for 20 min at 4 °C approximately six times until the membranes appeared white. Ghost membranes were then stripped of peripheral membrane proteins by diluting ten times in cold 2 mM EDTA, pH 12.0 followed by centrifugation at 30 000 x g for 20 min at 4 °C. Stripped membranes were washed three times in 5P8 buffer and solubilized by the addition of 1% (w/v) $C_{12}E_8$. Solubilized membranes were loaded onto an 18 ml amino-ethyl sepharose column pre-equilibrated with 5P8 buffer containing 0.1% (w/v) $C_{12}E_8$. After washing with 20 ml of 5P8 buffer containing 0.1% (w/v) $C_{12}E_8$, erythrocyte AE1 was eluted from the column by a linear 0-500 mM NaCl gradient at 1 ml/min. Fractions (1 ml) were collected and assayed for protein content by UV absorption at 280 nm. The amount and purity of erythrocyte AE1 was assessed by SDS-PAGE.

2.2.12 Reconstitution and Radioactive Sulfate Efflux Assay

Protocol was modified from previous reports (*17, 18*). Egg yolk phosphatidylcholine (10 mg, EYPC) dissolved in chloroform was dried under a stream of nitrogen and left in a vacuum desiccator overnight. Dried EYPC was resuspended in 500 µl of reconstitution buffer (40 mM Na_2SO_4, 4 mM $MgSO_4$, 20 mM MES, 20 mM Tris, pH 6.0). Equi-molar amounts of eAE1 and AE1MD-Rho (1 mg and 0.5 mg, respectively) were added to resuspended lipids and the reconstitution mixture was made to 12 ml with reconstitution buffer, containing 1% (w/v) $C_{12}E_8$. The reconstitution mixture was incubated for 30 min at 4 °C before the addition of 0.73 g of Bio-beads SM2 and 1 mM dithiothreitol (DTT). The reconstitution mixture was sealed under a stream

of nitrogen and incubated at 4 °C for 8-12 h. Another addition of 0.73 g Bio-beads SM2 was made as described above, followed by two more additions of 1.27 g Biobeads SM2. The reconstitution mixture was separated from the Bio-beads SM2 and vesicles were isolated by centrifugation at 100 000 x g for 30 min at 4 °C. The vesicle pellet was resuspended in 1 ml of reconstitution buffer and incubated with 50 µCi of $[^{35}S]SO_4^{2-}$ overnight at room temperature. Prior to initiating transport assays, reconstituted samples were divided in two and one half was made to 200 µM H_2DIDS and 50 µM flufenamic acid. All vesicles were incubated at 4 °C for at least 1 h prior to transport. Samples (treated and un-treated with inhibitors) were centrifuged at 4 °C on 10 ml semi-dried Sephadex G-50 column, equilibrated with reconstitution buffer in the presence (treated samples) or absence (un-treated samples) of 200 µM H_2DIDS and 50 µM flufenamic acid. Before the initiation of transport assay, quadruplicate aliquots of 50 µl of vesicles were removed for the 0 min time point. Aliquots were transferred to 1 ml of stop solution (40 mM Na_2SO_4, 4 mM $MgSO_4$, 200 µM H_2DIDS, 50 µM flufenamic acid, 20 mM MES, 20 mM Tris, pH 8.0) at 4 °C, filtered on 0.22 µm nitrocellulose membranes, and washed once with reconstitution buffer at pH 8.0. Nitrocellulose membranes were collected and dissolved in scintillation fluid (ScintiSafe Econo 2 Cocktail, Fisher) overnight. To initiate transport assays $[^{35}S]SO_4^{2-}$ and SO_4^{2-} exchange samples were transferred to a 30 °C water bath. Quadruplicate aliquots (50 µl) were removed and processed as

described above at time points of 5, 10, 20, 40 and 80 min. [^{35}S] was detected in dissolved filters with a Beckman LS 6500 scintillation counter.

2.2.13 Modeling

A sequence alignment of the human AE1 membrane domain (amino acids 388-911) and *E. coli* ClC was created using a published alignment (*19*), with minor adjustments. This alignment was used to generate a homology model of AE1, using the *E. coli* ClC structure (*20*) (PDB ID 1OTS) as a template, with the program Modeller v9.7 (*21*).

2.2.14 HEK293 Cell Culture and Transfection

HEK293 cells were grown at 37 ˚C in an air:CO_2 (19:1) environment in DMEM medium, supplemented with 5% (v/v) fetal bovine serum, 5% (v/v) calf serum and 1% (v/v) penicillin-streptomycin-glutamine. cDNA encoding WT-AE1, AE1 point mutants or vector (pRBG4) were transiently transfected in HEK293 cells by the calcium phosphate transfection method (*22*). All experiments were carried out 48 h post-transfection.

2.2.15 Expression in *X. laevis* Oocytes

Plasmid cDNA was linearized using NheI and transcribed with mMessage mMachine *in vitro* T7 RNA-polymerase kit to produce capped RNA transcripts. cRNA was purified and stored at -80 °C in diethyl pyrocarbonate treated water.

X. laevis females were purchased from *Xenopus* Express, Vernassal, France. Oocytes were surgically removed under sterile conditions from anesthetized frogs and singularized by collagenase treatment in Ca^{2+}-free

oocyte Ringer's solution (82.5 mM NaCl, 2.5 mM KCl, 1 mM $MgCl_2$, 1 mM Na_2HPO_4, 5 mM Hepes, pH 7.8) at 28 °C for 1.5 h. Singularized oocytes were left to recover for approximately 16 h in HCO_3^--free oocyte Ringer's solution (Ca^{2+}-free oocyte Ringer's solution, containing 1 mM $CaCl_2$, pH 7.8). Oocytes at stage V or VI were selected and injected with 15 ng of AE1 (WT or mutant) cRNA and 1.5 ng of glycophorin A cRNA, using glass micropipettes and a microinjection device (Nanoliter 2000, World Precision Instruments, Berlin, Germany). Non-injected native oocytes were used as a control.

2.2.16 Cl^-/HCO_3^- Exchange Assays in HEK293 Cells

Anion exchange activity of transfected HEK293 cells was monitored, using a previously described assay (*23*). Briefly, HEK293 cells were grown and transfected on poly-L-lysine treated 11 X 7.5 mm glass coverslips. Cells were rinsed in serum-free DMEM medium and incubated in 2 ml of serum-free DMEM medium, containing 2 μM BCECF-AM at 37 °C for 15 min. Coverslips were mounted in a fluorescence cuvette and perfused at 3.5 ml/min alternately with Ringer's buffer (5 mM glucose, 5 mM potassium gluconate, 1 mM calcium gluconate, 10 mM HEPES, 1 mM $MgSO_4$, 2.5 mM NaH_2PO_4, 25 mM $NaHCO_3$, pH 7.4), containing 140 mM NaCl (chloride-containing) or 140 mM sodium gluconate (chloride-free). Both Ringer's buffers were bubbled continuously with air, containing 5% CO_2. Fluorescence was monitored using a Photon Technologies International RCR/Delta Scan spectrofluorimeter at excitation wavelengths 440 nm and 502.5 nm and emission wavelength 528.7 nm. Fluorescence measurements

were converted to intracellular pH by the nigericin-high potassium method (*24*) with reference pH values approximately 6.5, 7.0 and 7.5. Anion exchange activity was calculated by linear regression of the initial change (30 s) in intracellular pH upon switching from a chloride-containing to a chloride-free Ringer's buffer.

2.2.17 Intracellular pH and Membrane Current Recordings in *X. laevis* Oocytes

Intracellular pH and membrane potential were measured, using double-barreled microelectrodes, which have been described previously (*25*). Electrodes were calibrated with bicarbonate-free oocyte Ringer's solution with a pH of 7.0 and 7.4. The recording arrangement was described previously (*25, 26*). Central and reference barrels of the electrodes were connected with chloride-treated silver wires to the head-stages of an Axoclamp 2B amplifier (Axon Instruments, USA). In the experimental chamber electrodes detected changes in pH faster in saline pH than the fastest reaction expected to occur in the cytoplasm of the oocyte. As described previously, optimal intracellular oocyte pH measurements were detected when the electrode was located near the intracellular surface of the plasma membrane (*27*), which was achieved by carefully rotating the oocyte with the impaled electrode. Experiments were performed at 20 °C with oocytes voltage clamped at -40 mV, using two-electrode voltage clamp as described previously (*28*). Oocytes were successively perfused with bicarbonate-free oocyte Ringer's solution (pH 7.4), high Cl^- oocyte Ringer's

solution (57.5 mM NaCl, 2.5 mM KCl, 1 mM Na_2HPO_4, 1 mM $MgCl_2$, 1 mM $CaCl_2$, 5 mM Hepes, 24 mM $NaHCO_3$, pH 7.4), low Cl^- oocyte Ringer's solution (57.5 mM sodium gluconate, 2.5 mM KCl, 1 mM Na_2HPO_4, 1 mM $MgCl_2$, 1 mM $CaCl_2$, 5 mM Hepes, 24 mM $NaHCO_3$, pH 7.4), high Cl^- oocyte Ringer's solution and bicarbonate-free oocyte Ringer's solution (pH 7.4). High and low Cl^- oocyte Ringer's solutions were bubbled continuously with 5% CO_2/95% O_2. Changes in membrane potential were monitored, during 20 mV voltage steps from -100 mV to +20 mV in each solution, to obtain current/voltage (I/V) curves.

2.2.18 Assays of Cell Surface Processing

Assays of cell surface processing were described previously (*29*). HEK293 cells were transiently transfected with cDNA encoding WT-AE1, an AE1 point mutant or vector alone, as described above. Cells were rinsed with 4 °C PBS, followed by 4 °C borate buffer (154 mM NaCl, 7.2 mM KCl, 1.8 mM $CaCl_2$, 10 mM boric acid, pH 9.0). Cells were then incubated at 4 °C for 30 min in borate buffer, containing 0.5 mg/ml Sulfo-NHS-SS-Biotin. Cells were washed three times with quenching buffer (192 mM glycine, 25 mM Tris, pH 8.3) and solubilized for 20 min at 4 °C with 500 µl IPB buffer (1% NP40, 5 mM EDTA, 0.15 M NaCl, 0.5% deoxycholate, 10 mM Tris, pH 7.4), containing Complete Mini Protease Inhibitor Cocktail. Cell lysates were centrifuged for 20 min at 16 000 x g and the supernatant was collected. Half of each sample was removed for later immunoblot analysis (total protein, T). The remaining half of each sample was incubated with immobilized streptavidin resin (100

µl of a 50% slurry in PBS) for 16 h at 4 °C with gentle rotation. Samples were centrifuged for 2 min at 8 000 x g and the supernatant was collected (unbound protein, U). Equal amounts of the T and U fractions were separated by SDS-PAGE and analyzed by immunoblotting as described above. Values obtained from densitometric analysis were used to calculate the % of protein at the cell surface with the formula (T-U)/T X 100%.

2.2.19 Alternate HEK293 Cell Growth Conditions

HEK293 cells were transiently transfected as described previously. Immediately following transfection, HEK293 cells were grown at 37 °C or 30 °C in medium with or with the addition of 1% (v/v) DMSO.

2.2.20 Chemical Crosslinking of AE1

Chemical crosslinking of AE1 was done as described previously (*30*). AE1MD346 and AE1MD346 tryptophan mutants were expressed in HEK293 cells by transient transfection. Approximately 48 h post-transfection, cells were washed with 4 °C PBS. Cells were then incubated with 0-2 mM DSP in PBS at 4 °C for 2 h. The crosslinker, DSP, was removed by gentle aspiration, and quenched with 20 mM Tris, pH 7.5 for 15 min at 4 °C. Cells were lysed in IPB buffer, containing Complete mini protease inhibitor cocktail. Prior to electrophoresis analysis, lysates were divided in half and incubated with or without 50 mM DTT for 30 min at 37 °C. Samples were prepared in 2X sample buffer, without β-mercaptoethanol, for SDS-PAGE analysis. The percentage of AE1 dimer was calculated by densitometry of immunoblots, using the formula $AE1_{dimer}/(AE1_{dimer} + AE1_{monomer})* 100\%$.

2.2.21 SDS-PAGE and Immunoblotting

Samples were prepared in 2X sample buffer (10% (v/v) glycerol, 2% (w/v) SDS, 0.5% (w/v) bromophenol blue, 1% (v/v) β-mercaptoethanol, 75 mM Tris, pH 6.8), containing Complete Mini Protease Inhibitor Cocktail. Prior to electrophoresis samples were incubated for 4.5 min at 65 °C and insoluble material was removed by centrifugation at 16 000 x g for 10 min. Samples were resolved on 7.5 or 10% (w/v) SDS-PAGE gels (*31*) and transferred to Immobilon-P PVDF membranes at 400 mA for 1 h. Membranes were subsequently blocked with TBS-TM (TBS-T (0.15 M NaCl, 50 mM Tris, 0.1% (v/v) Tween-20, pH 7.5), containing 5% (w/v) skim milk powder) for 1 h at 20 °C. After blocking membranes were incubated for 16 h at 4 °C in TBS-TM, containing mouse anti-AE1 antibody (IVF12), rabbit anti-Pma1, rabbit anti-Sec61, and/or mouse anti-GAPDH antibody at 1:3000, 1:3000, 1:1000, 1:2500 and 1:2000 dilutions, respectively. Membranes were washed three times in TBS-T, incubated with donkey anti-mouse IgG or donkey anti-rabbit IgG conjugated to horseradish peroxidase at a 1:5000 dilution for 1 h at 20 °C, and washed three times in TBS-T. Blots were imaged using ECL chemiluminescent reagent and visualized using a Kodak Image Station 440CF (Kodak, NY). Quantitative densitometric analysis was performed, using the Kodak Molecular Imaging Software v4.0.3 (Kodak, NY).

2.2.22 Statistical Analysis

Analysis was preformed, using Prism software. Values are represented as the mean ± standard error. Groups were compared with one-

way ANOVA, paired t-test, and un-paired t-test with $P<0.05$ considered significant.

2.2.23 References

1. M. L. Jennings, M. P. Anderson, R. Monaghan, Monoclonal antibodies against human erythrocyte Band 3 protein: localization of proteolytic cleavage sites and stilbenedisulfonate-binding lysine residues. *J. Biol. Chem.* **261**, 9002-9010 (1986).
2. Q. Wang, A. Chang, Sphingoid base synthesis is required for oligomerization and cell surface stability of the yeast plasma membrane ATPase, Pma1. *Proc Natl Acad Sci U S A* **99**, 12853-12858 (2002).
3. C. J. Stirling, J. Rothblatt, M. Hosobuchi, R. Deshaies, R. Schekman, Protein translocation mutants defective in the insertion of integral membrane proteins into the endoplasmic reticulum. *Mol Biol Cell* **3**, 129-142 (1992).
4. R. S. Molday, D. MacKenzie, Monoclonal antibodies to rhodopsin: characterization, cross-reactivity, and application as structural probes. *Biochemistry* **22**, 653-660 (1983).
5. R. A. Figler, H. Omote, R. K. Nakamoto, M. K. Al-Shawi, Use of chemical chaperones in the yeast *Saccharomyces cerevisiae* to enhance heterologous membrane protein expression: high-yield expression and purification of human P-glycoprotein. *Arch Biochem Biophys* **376**, 34-46 (2000).
6. J. R. Casey, Y. Ding, R. R. Kopito, The role of cysteine residues in the erythrocyte plasma membrane anion exchange protein, AE1. *J. Biol. Chem.* **270**, 8521-8527 (1995).
7. B. S. Lee, R. B. Gunn, R. R. Kopito, Functional differences among nonerythroid anion exchangers expressed in a transfected human cell line. *J. Biol. Chem.* **266**, 11448-11454 (1991).
8. D. E. Johnson, J. R. Casey, Cytosolic H^+ microdomain developed around AE1 during AE1-mediated Cl^-/HCO_3^- exchange. *J Physiol* **589**, 1551-1569 (2011).
9. Q. Zhu, D. W. Lee, J. R. Casey, Novel topology in C-terminal region of the human plasma membrane anion exchanger, AE1. *J Biol Chem* **278**, 3112-3120 (2003).
10. E. R. Liman, J. Tytgat, P. Hess, Subunit stoichiometry of a mammalian K^+ channel determined by construction of multimeric cDNAs. *Neuron* **9**, 861-871 (1992).
11. M. M. Bradford, A rapid and sensitive method for the quantitation of microgram quantities of protein utilizing the principle of protein-dye binding. *Anal Biochem* **72**, 248-254 (1976).
12. R. Eble, A simple and efficeint procedure for transformation of yeasts. *Biotechniques* **13**, 18-20 (1992).
13. R. H. Gietz, A. S. Jean, R. A. Woods, R. H. Schiestl, Improved method for high efficiency transformation of yeast cells. *Nucl. Acids Res.* **20**, 1425 (1992).

14. R. H. Schiestl, D. Gietz, About yeast transformations. *Current Genetics* **16**, 339-346 (1989).
15. J. R. Pringle, A. E. Adams, D. G. Drubin, B. K. Haarer, Immunofluorescence methods for yeast. *Methods Enzymol* **194**, 565-602 (1991).
16. J. R. Casey, D. M. Lieberman, R. A. F. Reithmeier, Purification and characterization of Band 3 protein. *Methods Enzymol.* **173**, 494-512 (1989).
17. U. Scheuring, K. Kollewe, W. Haase, D. Schubert, A new method for the reconstitution of the anion transport system of the human erythrocyte membrane. *J. Membrane Biol.* **90**, 123-135 (1986).
18. J. M. Wolosin, A procedure for membrane-protein reconstitution and the functional reconstitution of the anion transport system of the human-erythrocyte membrane. *Biochem. J.* **189**, 35-44 (1980).
19. T. Hirai, N. Hamasaki, T. Yamaguchi, Y. Ikeda, Topology models of anion exchanger 1 that incorporate the anti-parallel V-shaped motifs found in the EM structure. *Biochem Cell Biol* **89**, 148-156 (2011).
20. R. Dutzler, E. B. Campbell, M. Cadene, B. T. Chait, R. MacKinnon, X-ray structure of a ClC chloride channel at 3.0 Å reveals the molecular basis of anion selectivity. *Nature* **415**, 287-294 (2002).
21. A. Sali, T. L. Blundell, Comparative protein modelling by satisfaction of spatial restraints. *J Mol Biol* **234**, 779-815 (1993).
22. S. Ruetz, A. E. Lindsey, R. R. Kopito, Function and biosynthesis of erythroid and nonerythroid anion exchangers. *Society of General Physiologists Series* **48**, 193-200 (1993).
23. F. B. Loiselle, J. R. Casey, Measurement of Cell pH. *Methods Mol Biol.* **227**, 259-280 (2003).
24. J. A. Thomas, R. N. Buchsbaum, A. Zimniak, E. Racker, Intracellular pH measurements in Ehrlich ascites tumor cells utilizing spectroscopic probes generated in situ. *Biochemistry* **18**, 2210-2218 (1979).
25. J. W. Deitmer, Electrogenic sodium-dependent bicarbonate secretion by glial cells of the leech central nervous system. *J Gen Physiol* **98**, 637-655 (1991).
26. T. Munsch, J. W. Deitmer, Sodium-bicarbonate cotransport current in identified leech glial cells. *J Physiol* **474**, 43-53 (1994).
27. S. Broer, H. P. Schneider, A. Broer, B. Rahman, B. Hamprecht, J. W. Deitmer, Characterization of the monocarboxylate transporter 1 expressed in *Xenopus laevis* oocytes by changes in cytosolic pH. *Biochem J* **333 (Pt 1)**, 167-174 (1998).
28. H. M. Becker, J. W. Deitmer, Carbonic anhydrase II increases the activity of the human electrogenic Na^+/HCO_3^- cotransporter. *J Biol Chem* **282**, 13508-13521 (2007).
29. G. L. Vilas, P. E. Morgan, S. K. Loganathan, A. Quon, J. R. Casey, A biochemical framework for SLC4A11, the plasma membrane protein defective in corneal dystrophies. *Biochemistry* **50**, 2157-2169 (2011).

30. G. L. Vilas, S. K. Loganathan, A. Quon, P. Sundaresan, E. N. Vithana, J. Casey, Oligomerization of SLC4A11 protein and the severity of FECD and CHED2 corneal dystrophies caused by SLC4A11 mutations. *Hum Mutat* **33**, 419-428 (2012).
31. U. K. Laemmli, Cleavage of structural proteins during assembly of the head of bacteriophage T4. *Nature* **227**, 680-685 (1970).

Chapter 3: Purification of Functional Human Cl^-/HCO_3^- Exchanger, AE1, Over-expressed in *Saccharomyces cerevisiae*

A version of this chapter has been published as P. Bonar, J.R. Casey, Purification of functional human Cl^-/HCO_3^- exchanger, AE1, over-expressed in *Saccharomyces cerevisiae*. *Protein Expr Purif*. **74,** 106-115 (2010). (Reproduced with permission).

3.1 Introduction

Most of the structural information known about the anion exchanger family arose from studies conducted on AE1 (*1*)(*2*)(*3*)(*4, 5*). The crystal structure of the N-terminal cytoplasmic domain of eAE1 (residues 1-379) has been solved to a resolution of 2.6 Å (*6*). Three-dimensional crystals grown from the membrane domain of AE1 isolated from erythrocytes have diffracted X-rays to 14 Å, but a corresponding crystal structure was not determined (*7*). Two-dimensional crystals of the eAE1 membrane domain have yielded structures at 20 Å, 18 Å, and 7.5-16 Å resolution (*8-11*). Still, none of these structures is of sufficient resolution to determine the helical packing of the entire AE1 membrane domain, the location of amino acid residues, or provides insight into its mechanism of action.

Attempts to obtain a high resolution structure of the membrane domain of AE1 purified from erythrocytes have been unsuccessful, possibly arising from heterogeneity of the protein caused by various degrees of glycosylation, proteolysis, and other modifications (*7*). AE1 has been expressed and partially purified from yeast, using a six histidine purification tag and immobilized metal affinity chromatography (IMAC) (*12, 13*). The maximum protein purity achieved (35%) was possibly limited by the presence of metal-binding proteins, endogenous to yeast, that co-purified with AE1 during IMAC. To obtain the pure population of AE1 needed for crystallization we have prepared an expression construct corresponding to amino acids 388-911 of AE1 (AE1MD, the membrane domain) with a C-

terminal purification tag, corresponding to the nine C-terminal residues of rhodopsin. The fusion protein, called AE1MD-Rho, binds the 1D4 monoclonal antibody that can be immobilized to resin to form an affinity purification matrix. AE1MD-Rho is eluted with a peptide, corresponding to the nine C-terminal residues of rhodopsin. In this report, we have successfully used this purification strategy to produce a highly pure source of AE1MD-Rho, which is structurally and functionally indistinguishable from erythrocyte AE1.

3.2 Results

3.2.1 Expression of Human AE1

The coding sequence of the human AE1 membrane domain (amino acid residues 388-911), followed by the nine C-terminal amino acids of rhodopsin (Rho epitope), were cloned into the yeast expression vector, YEpM. The resulting expression plasmid (pPB1) (Fig. 3.1 A) contains the transcriptional promoter and terminator for the yeast Pma1 gene (encoding the plasma membrane H^+-ATPase). Use of these elements from a highly abundant yeast plasma membrane protein may help to drive high-level expression of membrane proteins. To drive a high level of protein expression, codon optimization for yeast was executed for the first ten amino acids of the encoded protein, called AE1MD-Rho (Fig. 3.1 B). AE1MD-Rho lacks the N-terminal cytoplasmic domain, which is not required for the transport activity of AE1 (*14*).

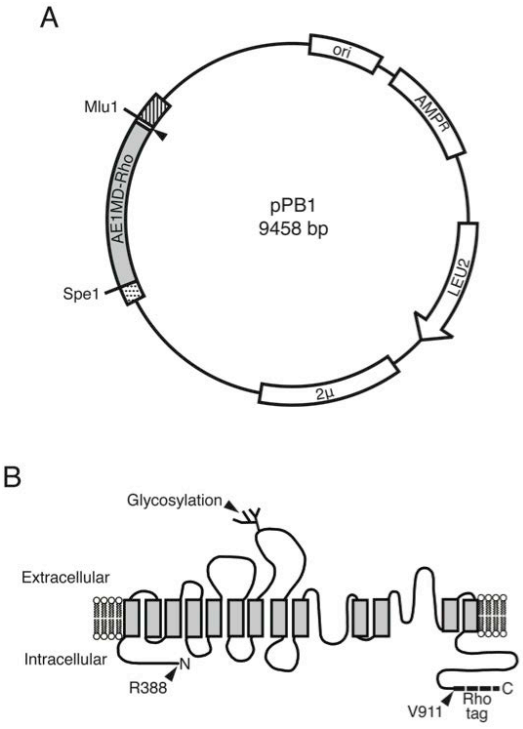

Figure 3.1 Expression Construct for AE1MD-Rho.

(A) Map of the expression plasmid, pPB1. The sequences for AE1MD-Rho, amino acids 388-911 of AE1 (gray) and the nine C-terminal amino acids of rhodopsin (arrow), were inserted into the YEpM plasmid. The promoter for plasma membrane ATPase, Pma1 (dotted), and the Pma1 terminator (striped) are shown. AMP^R indicates the ampicillin resistance gene, and ori indicates the bacterial origin of replication. The yeast origin of replication is represented by 2μ. The Leu2 gene is a selective marker that allows for growth in the Leu^- selective growth media. (B) Topology model of the recombinant protein AE1MD-Rho shown to scale. The amino (N) and carboxyl (C) termini of AE1MD-Rho are marked, and amino acids corresponding to erythrocyte AE1 residues 388 and 911 are indicated. The branched structure on the fourth extracellular loop represents the glycosylation site of AE1. The purification tag corresponding to the nine C-terminal amino acids of rhodopsin, Rho tag, is shown as a dashed line.

AE1MD-Rho was expressed in the protease deficient yeast strain BJ5457 (Fig. 3.2). Selection of yeast transformed with the pPB1 plasmid was accomplished by growth in complete synthetic medium, lacking leucine, since BJ5457 are a leucine auxotrophic strain and the YEpM expression vector carries the Leu2 gene required for growth of BJ5457 in the absence of leucine. The Pma1 promoter is constitutive, so induction of AE1MD-Rho was not required.

AE1MD-Rho expression was assayed in lysates from yeast transformed with pPB1 or YEpM (empty vector) (Fig. 3.3). An immunoreactive band was identified in lysates from yeast transformed with the AE1MD-Rho expression construct, pPB1, by both the IVF12 anti-AE1 antibody and the 1D4 anti-rhodopsin antibody. This indicates that addition of the rhodopsin epitope tag does not alter immunoreactivity toward IVF12 antibody. The 48 kDa (n=7) band observed for AE1MD-Rho is consistent with the reported electrophoretic mobility of AE1 membrane domain from erythrocytes (55 kDa) (*15*), since the membrane domain isolated by tryptic cleavage yields a protein that is 5 kDa larger (*15*). Lysates from yeast transformed with YEpM vector alone had no immunoreactivity to either antibody (Fig. 3.3). The lack of endogenous antigens recognized by the 1D4 antibody in BJ5457 lysates suggests that purification of AE1MD-Rho on a 1D4 antibody column should be specific.

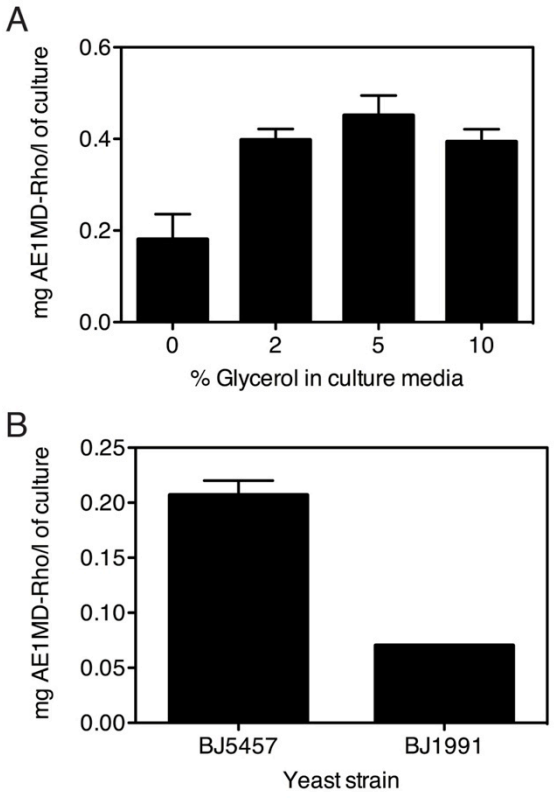

Figure 3.2 Optimization of AE1MD-Rho Expression.

(A) Cultures of yeast strain BJ5457 (5 ml), transformed with pPB1 (encoding AE1MD-Rho), were grown in complete synthetic media lacking leucine, containing 0-10% glycerol. (B) 5 ml cultures of yeast strain BJ5457 or BJ1991 (described in methods), transformed with pPB1, were grown in complete synthetic media lacking leucine, containing 5% glycerol. Lysates corresponding to 1 ml of culture were subjected to SDS-PAGE and transblotted to PVDF membranes. AE1-Ct (40 ng) was used as a reference standard. Immunoblots were probed with anti-AE1 antibody, IVF12, and quantified by densitometry to calculate mg AE1MD-Rho/l of culture. Error bars represent SE (n=3-4).

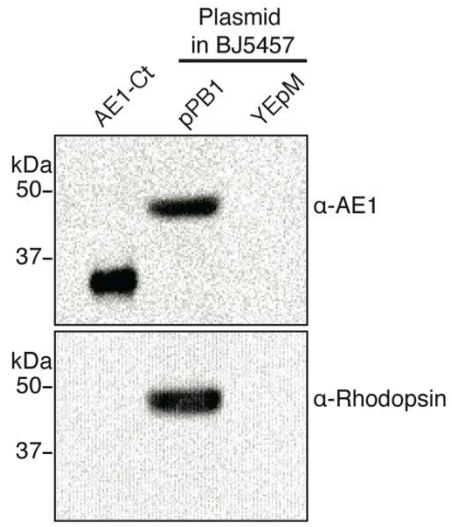

Figure 3.3 Expression of AE1MD-Rho in Yeast Strain BJ5457.

Cultures of yeast strain BJ5457 (5 ml), transformed with either pPB1 (encoding AE1MD-Rho) or YEpM (empty vector), were grown in complete synthetic media lacking leucine. Lysates corresponding to 1 ml of culture were subjected to SDS-PAGE and transblotted to PVDF membranes. AE1-Ct (40 ng) was used as a reference standard. Immunoblots were probed with anti-AE1 antibody, IVF12 (top) or anti-rhodopsin antibody, 1D4 (bottom).

The level of AE1MD-Rho expression in yeast cultures was estimated on immunoblots. To optimize the expression level of AE1MD-Rho we varied glycerol in culture medium over 0-10%, and found that 5% was optimal (Fig. 3.2 A). Purified AE1-Ct, composed of glutathione-S-transferase fused to the amino acids 872-911 of human AE1 was used as a quantification standard. The band intensity of AE1-Ct was quantified by densitometry and compared to AE1MD-Rho in yeast lysates (Fig. 3.3). Maximal expression of AE1MD-Rho was found to be 0.3 mg/l of culture, which is sufficient to produce the milligram quantities of AE1MD-Rho needed for crystallization trials in culture volumes on the order of 10 l. The expression of AE1MD-Rho in another protease deficient yeast strain, BJ1991, transformed with pPB1 was 0.1 mg/l of culture (Fig. 3.2 B). Since the expression level of AE1MD-Rho was lower in the BJ1991 yeast strain, we used the BJ5457 yeast strain for AE1MD-Rho expression.

3.2.2 Subcellular Localization and Glycosylation State of AE1MD-Rho

Confocal immunofluorescence microscopy of spheroplasted and permeabilized yeast transformed with pPB1 was used to investigate the subcellular localization of AE1MD-Rho (Fig. 3.4 A). The plasma membrane H^+-ATPase (Pma1) localized to the periphery of the cell, consistent with plasma membrane. In contrast, AE1MD-Rho localized with a diffuse distribution inside the cell. Merged images of a cell probed with anti-Pma1

and anti-Rho reveal that AE1MD-Rho does not localize to the plasma membrane, but is retained in an intracellular membrane compartment.

The subcellular localization of AE1MD-Rho was further examined by separating membranes of yeast transformed with pPB1 by ultracentrifugation on a continuous 20 – 53% sucrose gradient. Sucrose gradient fractions were analyzed on immunoblots probed for the Rho tag, the plasma membrane marker Pma1, and the endoplasmic reticulum marker Sec61 (Fig. 3.4 B). Pma1 and Sec61 immunoreactivity were separated on the gradient into two well defined regions at fraction 2 and fraction 10, respectively (Fig. 3.4 C). AE1MD-Rho did not resolve on the gradient into a well defined peak, but rather accumulated in fractions 8-21 (Fig. 3.4 C). The localization of AE1MD-Rho on the gradient did not correspond with the peak fraction of Pma1, which indicates that AE1MD-Rho is not at the plasma membrane. A portion of AE1MD-Rho did, however, co-localize with the peak fraction of Sec61, which suggests that a fraction of AE1MD-Rho localizes to the endoplasmic reticulum. AE1MD-Rho also resolved in a membrane population that did not correspond with either the plasma membrane or endoplasmic reticulum marker. The membrane population containing AE1MD-Rho may therefore represent Golgi or vacuole membranes, which were not further investigated. The present data are consistent with a previous attempt at overexpression of AE1 in yeast, which found that AE1 localized in membranes other than the plasma membrane (*12*).

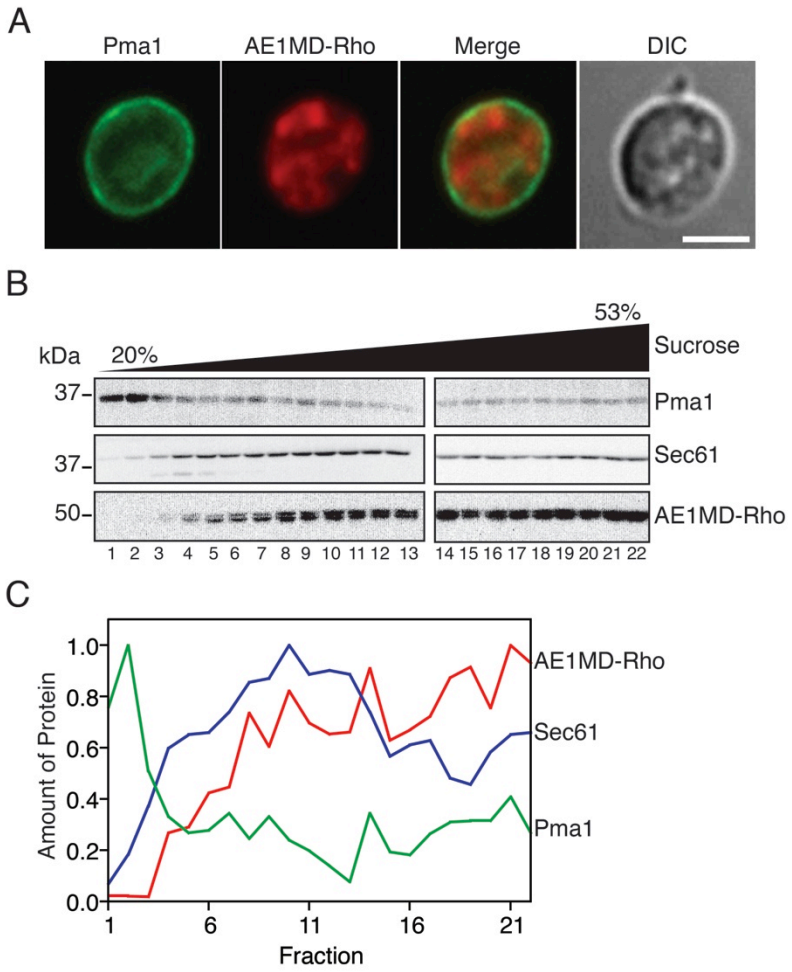

Figure 3.4 Intracellular Localization of AE1MD-Rho.

(A) Confocal immunofluorescence microscopy image of *S. cerevisiae* strain BJ5457 transformed with pPB1. Plasma membrane marker, Pma1, was detected using rabbit polyclonal anti-Pma1 antibody and anti-rabbit Alexa 484 antibody (green). AE1MD-Rho was detected using the mouse monoclonal anti-AE1 antibody, IVF12, and anti-mouse Alexa 544 antibody (red). The merged image is shown in the third panel and differential interference contrast microscopy (DIC) is indicated. Scale bar represents 5 µm. (B) Total membranes were isolated from yeast strain BJ5457 transformed with pPB1, and separated by ultracentrifugation on a 20-53% sucrose gradient. Fractions were collected from the top of the gradient and

analyzed on SDS-PAGE gels. Immunoblots were probed with either anti-Pma1 antibody, to detect the plasma membrane marker Pma1; anti-Sec61, to detect the endoplasmic reticulum marker Sec61; or anti-AE1 antibody, to detect AE1MD-Rho. (C) The amount of Pma1 (green), Sec61 (blue) and AE1MD-Rho (red) in each fraction was quantified by densitometry of immunoblots. For every protein the intensity of each fraction was normalized to the fraction with the highest intensity and plotted with fractions of increasing density.

Erythrocyte AE1 is heterogeneously glycosylated on Asn642 with 3-8 kDa of carbohydrate (*16*), but the carbohydrate chain at this site does not affect the transport activity of AE1 (*17*). Since heterogeneous glycosylation on AE1MD-Rho could interfere with subsequent crystallization efforts, the glycosylation state of AE1MD-Rho was examined. AE1MD-Rho and purified erythrocyte AE1 were subjected to deglycosylation with PNGase F. Un-treated eAE1 was detected as a broad band at approximately 100 kDa, which shifted to a sharp band with lower molecular weight upon treatment with PNGase F (Fig. 3.5). As stated previously, this indicates that PNGase F cleaved the entire N-linked oligosaccharide from eAE1 at the asparagine linkage, causing a shift in the electrophoretic mobiity of eAE1 (*17, 18*). Additional immunoreactive bands, likely corresponding to proteolytic cleavage products of eAE1, were detected at approximately 70 kDa in the eAE1 samples. Samples of purified AE1MD-Rho, whether treated or un-treated with PNGase F, were detected as sharp bands (Fig. 3.5). As a side note, the presence of a light band just below 100 kDa in lanes containing AE1MD-Rho is consistent with incomplete disruption of the dimer by SDS, as seen previously for AE1MD from erythrocytes (*19*). We conclude that AE1MD-Rho is not N-glycosylated.

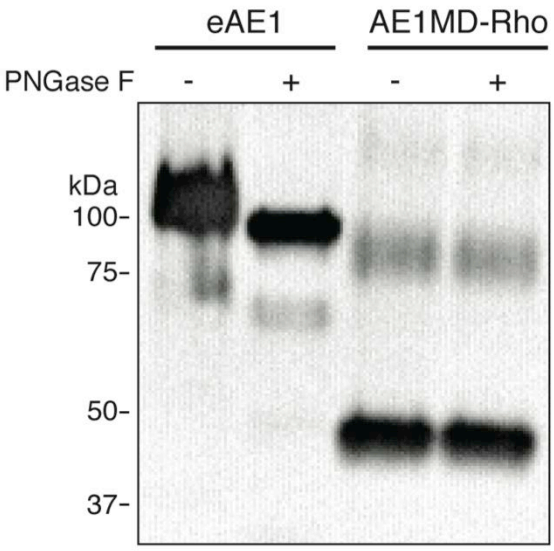

Figure 3.5 The Glycosylation State of AE1MD-Rho Assessed by Endoglycosidase F Treatment.

Purified eAE1 and purified AE1MD-Rho were denatured at 65 °C for 5 minutes then incubated at 37 °C for 1 hour in the presence (+) or absence (-) of PNGase F. The proteins were resolved on SDS-PAGE gels and immunoblots were probed with the anti-AE1 antibody, IVF12.

3.2.3 Detergent Selection and Purification of AE1MD-Rho

To maximize detergent solubilization of AE1MD-Rho from yeast membranes, a panel of six detergents were tested (Fig. 3.6). In erythrocytes, AE1 is nearly completely solubilized and has been characterized extensively in the detergents $C_{12}E_8$ and dodecyl maltoside (DDM) (*20*). However, only a small fraction of AE1MD-Rho was solubilized from yeast membranes by $C_{12}E_8$ (8%) and DDM (30%), when compared to the amount of protein solubilized by SDS (Fig. 3.6). This data agrees with a previous study, which found that AE1 expressed in yeast was minimally solubilized by $C_{12}E_8$ (*12*). AE1MD-Rho was maximally solubilized by Fos-choline 14 (FC, 90%) and lysophosphatidyl choline (LPC, 79%) (Fig. 3.6). Previous data also showed that AE1 was maximally solubilized in yeast by LPC, while still retaining its functional and structural integrity (*12*). FC and LPC are both zwitterionic lipid-like detergents, considered to be non-denaturing. Since the highest level of AE1MD-Rho solubilization was obtained with FC, this detergent was used to solubilize AE1MD-Rho from yeast membranes in all purification trials.

To purify AE1MD-Rho, yeast membranes were solubilized with 1% FC and lysates were incubated with 1D4 immunoaffinity resin. AE1MD-Rho protein was eluted from washed resin by incubation with 1 mg/ml 1D4 peptide. Densitometric analysis of the Coomassie blue stained SDS-PAGE gel reveals that a protein consistent with the molecular weight of AE1MD-Rho is the most abundant protein eluted by the 1D4 peptide (Fig. 3.7 A). An immunoblot of eluted fractions probed with the anti-AE1 antibody, IVF12,

confirmed the identity of the major band seen in the Coomassie blue stained SDS-PAGE gel as AE1MD-Rho (Fig. 3.7 B). To assess the identity and purity of the predominant band eluted by 1D4 peptide the Coomassie blue-stained band was subjected to in gel tryptic digestion and mass spectrometry. The band contained seven unique peptides corresponding to AE1 and no peptides corresponding to any other protein, reconfirming the identity of the major band as AE1MD-Rho. Densitometry of the Coomassie blue stained gel revealed that the maximal purity of AE1MD-Rho achieved by a single purification trial was 93% (Table 3.1). Thus far we have been able to purify 2.5 mg of AE1MD-Rho from 18 l of culture.

The monodispersity of purified AE1MD-Rho was assessed by size exclusion chromatography (Fig. 3.8). The major peak observed had a Stokes radius of approximately 61 Å, which is consistent with previous results obtained for erythrocyte AE1 membrane domain (*19*). Other minor peaks observed at the void and total volume of the column likely correspond to aggregated protein and peptide used to elute AE1MD-Rho, respectively (Fig. 3.8). We conclude that the expression and purification system described here provides AE1MD of sufficient amount and purity to enable crystallization trials.

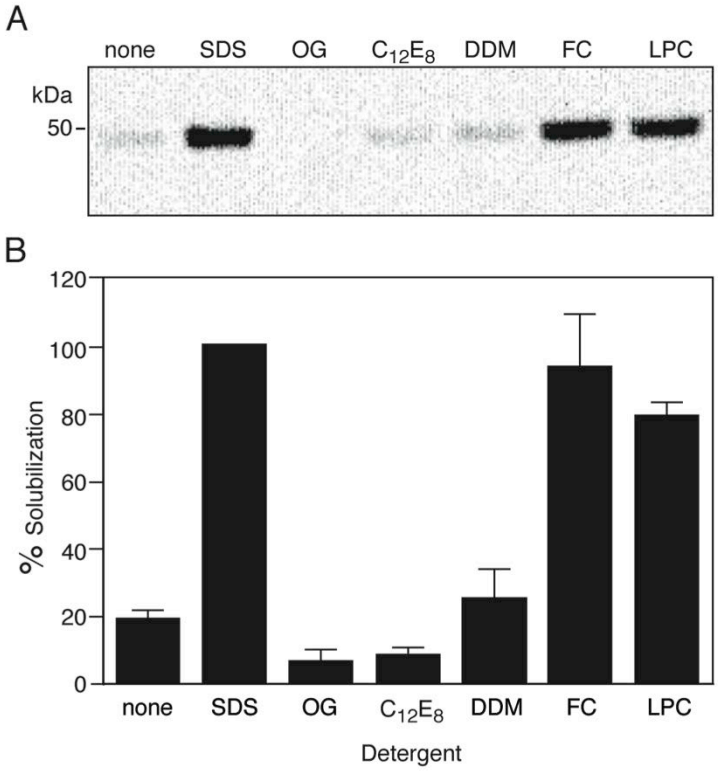

Figure 3.6 Detergent Solubilization of AE1MD-Rho from *S. cerevisiae* Strain BJ5457 Membranes.

Isolated yeast membranes were solubilized with no detergent (none) or sodium dodecyl sulfate (SDS), octyl glucoside (OG), octaethyleneglycol mono dodecyl ether ($C_{12}E_8$), dodecyl maltoside (DDM), Fos-choline 14 (FC), or lysophophatidyl choline (LPC) at a concentration of 1%. (A) Equal amounts (30 µl) of detergent solubilizations were analyzed on immunoblots probed with the anti-AE1 antibody, IVF12. (B) The amount of AE1MD-Rho solubilized by each detergent was quantified by densitometry of immunoblots. AE1MD-Rho solubilization in 1% SDS was set to 100% and solubilization of AE1MD-Rho in all other detergents was calculated as a percentage of solubilization in 1% SDS. Error bars represent SE (*n*=3).

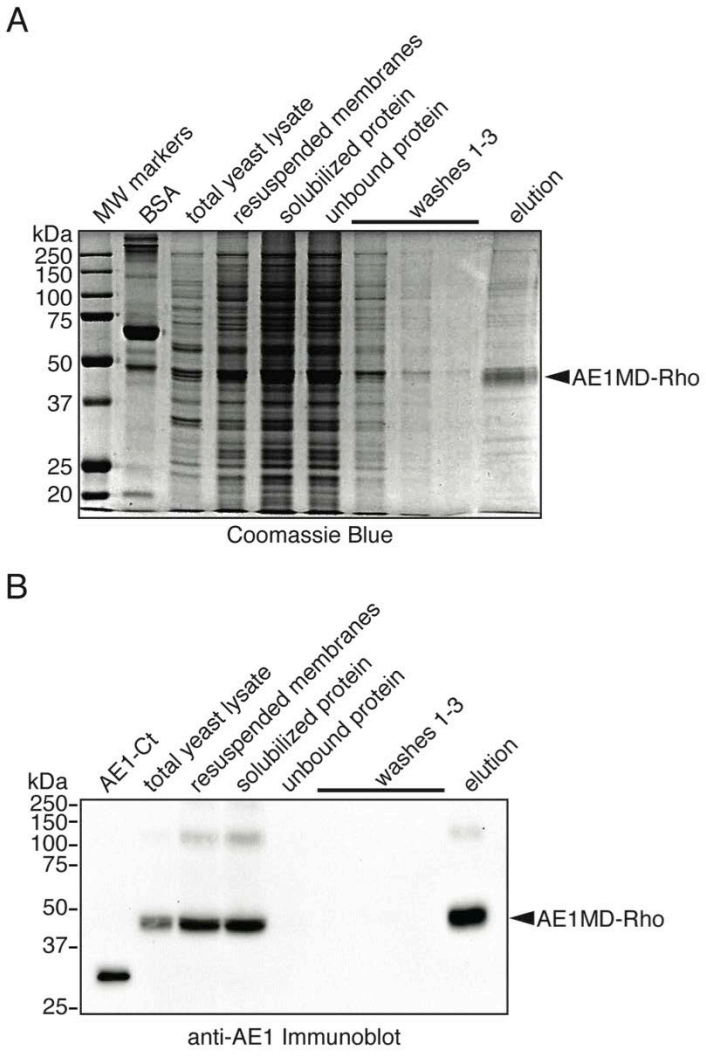

Figure 3.7 Purification of AE1MD-Rho from Yeast Membranes.

A sample of yeast transformed with the AE1MD-Rho expression vector, pPB1, was mechanically disrupted (total yeast lysate). Yeast membranes were isolated (resuspended membranes), solubilized in 1% Fos-choline 14, centrifuged and the supernatant was collected (solubilized protein). The supernatant was incubated with the 1D4 immunoaffinity resin, subsequently removed from the 1D4 immunoaffinity resin (unbound protein), and washed three times with 1D4 wash buffer (washes 1-3). AE1MD-Rho was eluted from the resin with 1D4 wash buffer containing 1 mg/ml 1D4 peptide (elution). (A) Proteins were resolved on a SDS-PAGE gel and stained with Coomassie blue. Molecular weight markers and the quantification standard,

BSA (5 μg) are indicated. The percentage of the total volume of each sample loaded onto the gel, relative to the total volume of the sample is: 0.0001% for total yeast lysate; 0.003% for resuspended membranes, solubilized protein, unbound protein and washes 1-3; and 0.06% for elution. (B) Immunoblot probed with anti-AE1 antibody, IVF12. The quantification standard AE1-Ct (20 ng) is indicated. The percentage of the total volume of each sample loaded onto the gel, relative to the total volume of the sample is: 0.0008% for total yeast lysate; 0.02% for resuspended membranes, solubilized protein, unbound protein and washes 1-3; and 0.004% for elution.

Table 3.1 Summary of the purification of AE1MD-Rho from *S. cerevisiae.*

Values were obtained from a single purification trial using 18 l of culture.

Fraction	Total Protein (mg)	AE1MD-Rho (mg)	AE1MD-Rho Purity (%)	Yield (%)
Total yeast lysate	-	5.4	-	100
Resuspended membranes	500	5.6	1	104
Solubilized protein	570	5.2	1	96
Purified AE1MD-Rho	2.7	2.5	93	46

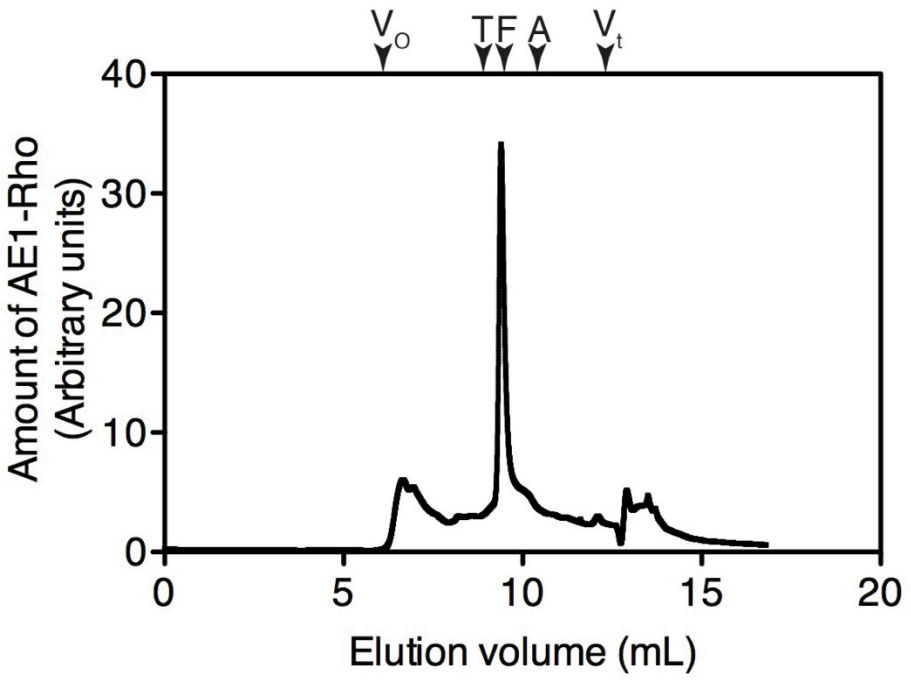

Figure 3.8 Size Exclusion Chromatography of AE1MD-Rho.

Purified AE1MD-Rho was analyzed by size exclusion chromatography using a TSK G4000SWXL 7.8 mm X 30 cm column. AE1MD-Rho eluted from the column was monitor by absorbance at 210 nm. The column was calibrated with thyroglobulin (T), ferritin (F) and aldolase (A), which had Stokes radii of 85, 61 and 48 Å, respectively. The void volume (V_O) and total volume (V_t) of the column are indicated, and were determined by the elution volumes of blue dextran (2000 kDa) and β-mercaptoethanol, respectively.

3.2.4 Anion Transport Activity of AE1MD-Rho

To assess AE1 functionality, we assayed the ability of AE1 to carry out sulfate transport. Although AE1 under physiological conditions facilitates the exchange of Cl^- for HCO_3^-, it is also able to facilitate the exchange of $[^{35}S]SO_4^{2-}$ for SO_4^{2-} at a slower, more readily measurable rate. Equimolar amounts of purified AE1MD-Rho and purified eAE1 were reconstituted into egg yolk phosphatidyl choline and anion transport activity was assessed by a $[^{35}S]SO_4^{2-}$ efflux assay. Vesicles were loaded with $[^{35}S]SO_4^{2-}$ by incubation for 12 h at 20 °C. Samples were then either treated with the anion exchange inhibitors, flufenamic acid and H_2DIDS, or were untreated. Extravesicular $[^{35}S]SO_4^{2-}$ was removed by gel filtration at 4 °C and transport assays were initiated by warming to 30 °C. Over a time course aliquots of the vesicle preparation were removed and intravesicular $[^{35}S]SO_4^{2-}$ was separated from non-occluded radioactivity by rapid filtration on 0.22 μm filters. The transport kinetics of reconstituted erythrocyte AE1 are well established, so we expected to observe a time-dependent loss of radioactivity from the vesicles as AE1 exchanged intravesicular $[^{35}S]SO_4^{2-}$ for extravesicular non-radioactive sulfate. Further, we expected that the two inhibitors would block sulfate exchange activity so little or no loss of vesicular radioactivity would occur in inhibited samples. Nonetheless some days we saw efflux of radioactivity in the presence of the inhibitors, or no radioactive efflux in the absence of inhibitors for vesicles containing native eAE1. Our interpretation was that either the vesicles were not intact, or that the incorporation of AE1

into the vesicles did not occur. When either of these events occurred for vesicles containing eAE1, the entire day's data-set was excluded from analysis.

Analysis of transport assays revealed that vesicles containing eAE1 and AE1MD-Rho both mediated sulfate efflux (Fig. 3.9 A). Moreover, the AE1 inhibitors suppressed most of the sulfate transport activity in both populations of vesicles (Fig. 3.9 A). The half time of $[^{35}S]SO_4^{2-}$ efflux was 8 ± 4 min for AE1MD-Rho vesicles and 15 ± 5 min for eAE1 vesicles (Fig. 3.9 B). While AE1MD-Rho mediated slightly faster sulfate efflux than eAE1, the difference is not statistically significant. The data presented here shows that purified AE1MD-Rho has the same anion exchange activity as purified eAE1.

3.3 Discussion

The greatest barrier to obtaining a high-resolution crystal structure of AE1 has been the ability to purify a homogeneous population of AE1. Previous efforts to overexpress and purify AE1 from yeast reported preparations that were only 35% pure, which is insufficient for crystallization trials (*12*, *13*). In this study, we expressed the membrane domain of AE1 in *S. cerevisiae*. Characterization of AE1MD-Rho here revealed that the protein was retained in an intracellular membrane fraction and was non-glycosylated. AE1MD-Rho was purified to 93% homogeneity in a single step, immunoaffinity chromatography. AE1MD-Rho reconstituted into vesicles facilitated sulfate transport indistinguishably from purified erythrocyte AE1. Retention of native functionality indicates that AE1MD-Rho

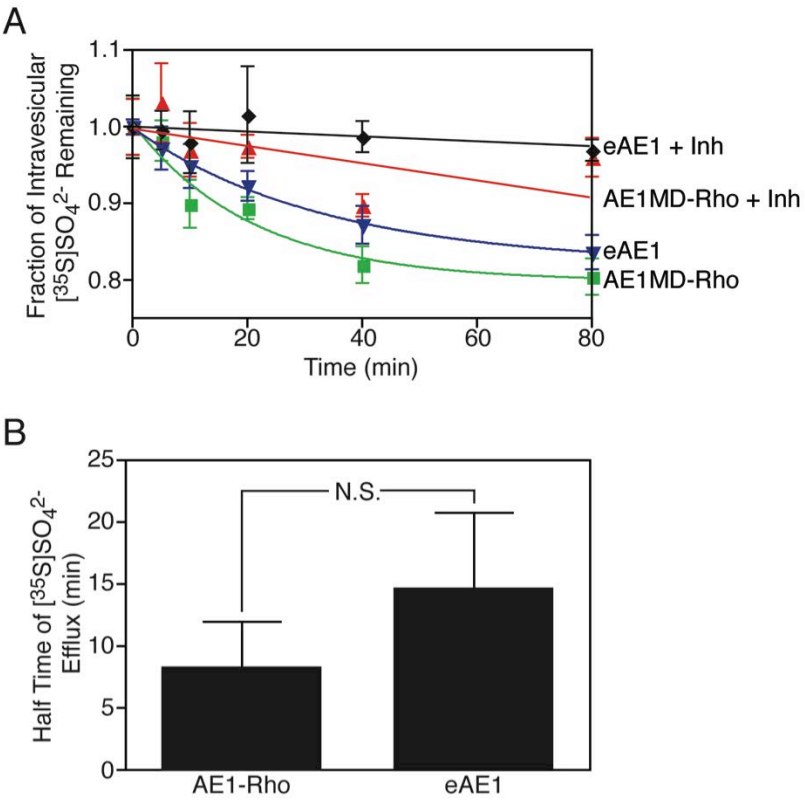

Figure 3.9 Sulfate Efflux Activity of Purified AE1.

Equi-molar amounts of purified eAE1 and purified AE1MD-Rho were reconstituted into egg yolk phosphatidylcholine. Vesicles were loaded with $[^{35}S]SO_4^{2-}$ and incubated in the presence or absence of the AE1 inhibitors H_2DIDS and flufenamic acid (Inh). (A) Transport kinetics were measured for vesicles containing AE1MD-Rho (green), AE1MD-Rho with inhibitors (red), eAE1 (blue), and eAE1 inhibitors (black) by the $[^{35}S]SO_4^{2-}$ remaining inside the vesicle. All values were normalized to the initial $[^{35}S]$ counts for a given transport kinetic. Error bars represent SE (n=4), for this representative assay. (B) Quantification of the transport activity for AE1MD-Rho and eAE1. Error bars represent SE (n=3). t-Test revealed no significant difference (N.S.) in the transport activity of AE1MD-Rho and AE1 from erythrocytes (P = 0.75).

retains a similar structure to AE1 from erythrocytes. Purified AE1MD-Rho is structurally and functionally similar to native AE1 purified from erythrocytes, and we have purified sufficient AE1MD-Rho to provide a suitable source for crystallization trials.

While AE1 is abundant in erythrocytes, purified AE1 from erythrocytes is not ideal for high-resolution crystallization studies as a result of heterogeneity. Erythrocyte AE1 is heterogeneously glycosylated (*16*), and in order to produce crystals using erythrocyte AE1 this carbohydrate must be quantitatively removed by PNGase F treatment (*7, 9-11*). Glycosylation patterns of mammalian membrane proteins in yeast have been shown to be altered (*21*). Consistent with previous reports for AE1 (*12, 13*), we found that AE1MD-Rho expressed in *S. cerevisiae* is not glycosylated. The linker (residues 361-403) connecting the N-terminal cytoplasmic domain and membrane domain of AE1 is flexible and sensitive to proteolysis (*15*). The flexibility of the linker would likely impede crystal formation, so the usual response would be to cleave it with trypsin. However, multiple tryptic sites exist in this region (Arg344, Arg345, and Arg346), which would result in "ragged" ends and protein heterogeneity (*7*). AE1MD-Rho, which spans AE1 residues 388-911, lacks the flexible linker, thus avoiding the need for heterogeneous cleavage. Previous studies of AE1MD constructs starting at residues AE1MD constructs starting at residues 361, 371, 376, and 381 were capable of radioactive chloride uptake in oocytes (*22*). In contrast, AE1MD constructs starting at 386, 391, and 396 were incapable of radioactive

chloride uptake, as a result of intracellular retention. AE1MD-Rho, which starts at residue 388, was found to be as functional as native erythrocyte AE1, possibly because our assay was independent of cell surface processing. Differences observed between these AE1MD constructs may be attributed to differences in the expression systems and transport assays. Recombinant expression systems, such as the one used in this study, are advantageous as alterations in the cDNA allow for the control of flexible or heterogeneous amino acid sequences.

Other heterologous expression systems for membrane proteins include mammalian cells, baculovirus infected insect cells, and yeast. Mammalian cells require the generation of stable transformants or large-scale transient transfections, and insect cells require the generation of recombinant baculoviruses, making these systems technically challenging (*21*). Expression of AE1 in transiently transfected human embryonic kidney 293 cells and AE2 in baculovirus infected Sf9 insect cells has resulted in low expression levels (*12, 23*), which are impractical to obtain the multi-milligram quantities of AE1 needed for protein crystallization.

We used a yeast expression system since yeast are easy to manipulate genetically and easy to culture (*24*). The two most popular yeast species for protein expression are *S. cerevisiae* and *P. pastoris*. While there are currently more high-resolution membrane protein structures from protein expressed in *P. pastoris* compared to *S. cerevisiae*, there is a larger variety of expression plasmids and yeast strains available for protein overexpression in *S.*

cerevisiae (*24*). In addition, the purification of membrane proteins from *P. pastoris* can be difficult, as the expressed protein usually represents a small fraction of the total protein when compared to *S. cerevisiae* (*24*). Here, the protease-deficient, leucine auxotrophic BJ5457 *S. cerevisiae* strain produced 0.3 mg/l of culture of functionally active AE1MD-Rho protein. The BJ5457 yeast strain was chosen because it had the highest AE1MD-Rho expression among the yeast strains tested. While AE1MD-Rho expression is not as high as other reports for AE1 expression in yeast (0.7 mg/l culture) (*12, 13*), the expression level of AE1MD-Rho is sufficient for crystallization studies since we were able to purify up to 2.5 mg in a single preparation. This data is in agreement with high-throughput expression studies in yeast, where membrane protein expression level could reach 1 mg/l of culture (*25, 26*). While examining the expression of AE1MD-Rho in yeast, we found that AE1MD-Rho was not targeted to the plasma membrane. Retention of plasma membrane proteins in intracellular organelles can be a sign of improper folding resulting in non-functional protein, however, AE1MD-Rho was fully functional in sulfate transport assays. In addition, there are other examples of plasma membrane proteins being mis-targeted to vacuoles in yeast (*26*).

Choice of detergent is a major factor in the success of membrane protein crystallization (*7, 27*). AE1 was solubilized in Fos-choline 14. The behaviour of AE1 is well known in a variety of detergents, and crystals have been obtained in several detergents including DDM, $C_{12}E_8$ and Cymal-6 (*7, 20*), but there is little information about the behaviour of AE1 in Fos-choline

14. To our knowledge the only high-resolution structure of a membrane protein purified and crystallized in Fos-choline 14, is the *E. coli* mechanosensitive channel MscS (*28*). There are, however, several reports of membrane proteins crystallized in the presence of Fos-choline 12 (*29-32*). While Fos-choline 14 may be a suitable detergent for protein crystallization, the strong interaction between the purification tag on AE1MD-Rho and the 1D4 immuno-affinity resin will allow for efficient detergent exchange into a variety of detergents that can be tested in crystallization trials.

Despite high expression levels, there have been few high-resolution membrane protein structures from proteins expressed in *S. cerevisiae* (*32-35*). This may arise from the low purity levels achieved by traditional protein purification techniques. For example, membrane protein purifications using a His tag in yeast have been unsuccessful at achieving high purity levels (*12, 36*), because of naturally occurring metal binding proteins that exist in *S. cerevisiae*. The antibody affinity purification strategy described here results in high purity levels suitable for protein crystallization. We purified 2.5 mg of 93% pure AE1MD-Rho from 18 l of culture, which is similar to the purification of the TRPV1 channel tagged with the Rho epitope (1.5 mg from 15 l of culture) (*37*). In addition, several other groups have used the Rho epitope tag to achieve high purity levels of membrane protein (*37-42*), and this has resulted in a high-resolution crystal structure of the K^+ channel Kir2.2 (*41*). Since the membrane protein expression and purification strategy described here is simple, rapid and requires only a single-step to

achieve near-homogeneity, it is amenable to high throughput screens to identify candidate proteins for crystallography.

3.3.1 Conclusions

In conclusion, we describe an expression and purification system that allows for rapid purification of milligram quantities of pure AE1MD that is structurally and functionally similar to native erythrocyte AE1. The rapid, single-step purification procedure used affords the possibility to prepare protein crystals of the AE1 membrane domain. The availability of pure, recombinant AE1 could be useful in biophysical experiments to examine the mechanism of the AE1 transport cycle. In addition, the expression and purification method described here, as well as a previous report (*37*), could be easily adapted for high-throughput expression and purification studies for a variety of eukaryotic membrane proteins.

3.4 References

1. J. R. Casey, D. M. Lieberman, R. A. F. Reithmeier, Purification and characterization of Band 3 protein. *Methods Enzymol.* **173**, 494-512 (1989).
2. Q. Zhu, D. W. K. Lee, J. R. Casey, Novel Topology in C-terminal Region of the Human Plasma membrane anion exchanger, AE1. *J. Biol. Chem.* **278**, 3112-3120 (2003).
3. A. M. Taylor, Q. Zhu, J. R. Casey, Cysteine-directed cross-linking localizes regions of the human erythrocyte anion exchange protein (AE1) relative to the dimeric interface. *Biochem. J.* **359**, 661-668 (2001).
4. X.-B. Tang, M. Kovacs, D. Sterling, J. R. Casey, Identification of Residues Lining the Translocation Pore of Human AE1, Plasma Membrane Anion Exchange Protein. *J. Biol. Chem.* **274**, 3557-3564 (1999).
5. Q. Zhu, J. R. Casey, The substrate anion selectivity filter in the human erythrocyte Cl^-/HCO_3^- exchange protein, AE1. *J. Biol. Chem.* **279**, 23565-23573 (2004).
6. D. Zhang, A. Kiyatkin, J. T. Bolin, P. S. Low, Crystallographic structure and functional interpretation of the cytoplasmic domain of erythrocyte membrane band 3. *Blood* **96**, 2925-2933 (2000).
7. M. J. Lemieux, R. A. Reithmeier, D. N. Wang, Importance of detergent and phospholipid in the crystallization of the human erythrocyte anion-exchanger membrane domain. *J Struct Biol* **137**, 322-332 (2002).
8. D. N. Wang, W. Kuhlbrandt, V. Sarabia, R. A. F. Reithmeier, Two-dimensional structure of the membrane domain of human band 3, the anion transport protein of the erythrocyte membrane. *EMBO J.* **12**, 2233-2239 (1993).
9. D. N. Wang, V. E. Sarabia, R. A. Reithmeier, W. Kuhlbrandt, Three-dimensional map of the dimeric membrane domain of the human erythrocyte anion exchanger, Band 3. *EMBO J.* **13**, 3230-3235 (1994).
10. T. Yamaguchi, T. Fujii, Y. Abe, T. Hirai, D. Kang, K. Namba, N. Hamasaki, K. Mitsuoka, Helical image reconstruction of the outward-open human erythrocyte band 3 membrane domain in tubular crystals. *J Struct Biol* **169**, 406-412 (2009).
11. T. Yamaguchi, Y. Ikeda, Y. Abe, H. Kuma, D. Kang, N. Hamasaki, T. Hirai, Structure of the Membrane Domain of Human Erythrocyte Anion Exchanger 1 Revealed by Electron Crystallography. *J Mol Biol* **397**, 179-189 (2010).
12. I. Sekler, R. R. Kopito, J. R. Casey, High level expression, partial purification and functional reconstitution of the human AE1 anion exchange protein in *Saccharomyces cerevisiae*. *J. Biol. Chem.* **270**, 21028-21034 (1995).

13. J. D. Groves, P. Falson, M. le Maire, M. J. Tanner, Functional cell surface expression of the anion transport domain of human red cell band 3 (AE1) in the yeast *Saccharomyces cerevisiae*. *Proc Natl Acad Sci U S A* **93**, 12245-12250 (1996).
14. S. Grinstein, S. Ship, A. Rothstein, Anion transport in relation to proteolytic dissection of Band 3 protein. *Biochim. Biophys. Acta* **507**, 294-304 (1978).
15. D. N. Wang, Band 3 protein: structure, flexibility and function. *FEBS Lett* **346**, 26-31 (1994).
16. M. Fukuda, A. Dell, J. E. Oates, M. N. Fukuda, Structure of the branched lactosaminoglycan, the carbohydrate moiety of Band 3 isolated from adult human erythrocytes. *J. Biol. Chem.* **259**, 8260-8273 (1984).
17. J. R. Casey, C. A. Pirraglia, R. A. F. Reithmeier, Enzymatic deglycosylation of human Band 3, the anion transport protein of the erythrocyte membrane: effect on protein structure and transport properties. *J. Biol. Chem.* **267**, 11940-11948 (1992).
18. M. Joanne Lemieux, R. A. Reithmeier, D. N. Wang, Importance of detergent and phospholipid in the crystallization of the human erythrocyte anion-exchanger membrane domain. *J Struct Biol* **137**, 322-332 (2002).
19. J. R. Casey, R. A. F. Reithmeier, Analysis of the oligomeric state of Band 3, the anion transport protein of the human erythrocyte membrane, by size exclusion high performance liquid chromatography: oligomeric stability and origin of heterogeneity. *J. Biol. Chem.* **266**, 15726-15737 (1991).
20. J. R. Casey, R. A. F. Reithmeier, Detergent interaction with Band 3, a model polytopic membrane protein. *Biochem.* **32**, 1172-1179 (1993).
21. F. Junge, B. Schneider, S. Reckel, D. Schwarz, V. Dotsch, F. Bernhard, Large-scale production of functional membrane proteins. *Cell Mol Life Sci* **65**, 1729-1755 (2008).
22. T. Kanki, M. T. Young, N. Hamasaki, M. J. Tanner, The N-terminal region of the transmembrane domain of human erythrocyte band 3: Residues critical for membrane insertion and transport activity. *J Biol Chem* **12**, 12 (2002).
23. X. He, X. Wu, P. A. Knauf, L. A. Tabak, J. E. Melvin, Functional expression of the rat anion exchanger AE2 in insect cells by a recombinant baculovirus. *Am. J. Physiol.* **264**, C1075-1079 (1993).
24. M. Freigassner, H. Pichler, A. Glieder, Tuning microbial hosts for membrane protein production. *Microb Cell Fact* **8**, 69 (2009).
25. M. Li, F. A. Hays, Z. Roe-Zurz, L. Vuong, L. Kelly, C. M. Ho, R. M. Robbins, U. Pieper, J. D. O'Connell, 3rd, L. J. Miercke, K. M. Giacomini, A. Sali, R. M. Stroud, Selecting optimum eukaryotic integral membrane proteins for structure determination by rapid expression and solubilization screening. *J Mol Biol* **385**, 820-830 (2009).
26. S. Newstead, H. Kim, G. von Heijne, S. Iwata, D. Drew, High-throughput fluorescent-based optimization of eukaryotic membrane protein

overexpression and purification in *Saccharomyces cerevisiae*. *Proc Natl Acad Sci U S A* **104**, 13936-13941 (2007).
27. Z. E. Newby, J. D. O'Connell, 3rd, F. Gruswitz, F. A. Hays, W. E. Harries, I. M. Harwood, J. D. Ho, J. K. Lee, D. F. Savage, L. J. Miercke, R. M. Stroud, A general protocol for the crystallization of membrane proteins for X-ray structural investigation. *Nat Protoc* **4**, 619-637 (2009).
28. R. B. Bass, P. Strop, M. Barclay, D. C. Rees, Crystal structure of *Escherichia coli* MscS, a voltage-modulated and mechanosensitive channel. *Science* **298**, 1582-1587 (2002).
29. Y. Chao, D. Fu, Thermodynamic studies of the mechanism of metal binding to the *Escherichia coli* zinc transporter YiiP. *J Biol Chem* **279**, 17173-17180 (2004).
30. G. Kefala, C. Ahn, M. Krupa, L. Esquivies, I. Maslennikov, W. Kwiatkowski, S. Choe, Structures of the OmpF porin crystallized in the presence of foscholine-12. *Protein Sci* **19**, 1117-1125 (2010).
31. M. Lu, D. Fu, Structure of the zinc transporter YiiP. *Science* **317**, 1746-1748 (2007).
32. J. Ma, M. Yoshimura, E. Yamashita, A. Nakagawa, A. Ito, T. Tsukihara, Structure of rat monoamine oxidase A and its specific recognitions for substrates and inhibitors. *J Mol Biol* **338**, 103-114 (2004).
33. M. Jidenko, R. C. Nielsen, T. L. Sorensen, J. V. Moller, M. le Maire, P. Nissen, C. Jaxel, Crystallization of a mammalian membrane protein overexpressed in *Saccharomyces cerevisiae*. *Proc Natl Acad Sci U S A* **102**, 11687-11691 (2005).
34. A. Marchand, A. M. Winther, P. J. Holm, C. Olesen, C. Montigny, B. Arnou, P. Champeil, J. D. Clausen, B. Vilsen, J. P. Andersen, P. Nissen, C. Jaxel, J. V. Moller, M. le Maire, Crystal structure of D351A and P312A mutant forms of the mammalian sarcoplasmic reticulum Ca^{2+} -ATPase reveals key events in phosphorylation and Ca^{2+} release. *J Biol Chem* **283**, 14867-14882 (2008).
35. B. P. Pedersen, M. J. Buch-Pedersen, J. P. Morth, M. G. Palmgren, P. Nissen, Crystal structure of the plasma membrane proton pump. *Nature* **450**, 1111-1114 (2007).
36. K. Moncoq, G. Kemp, X. Li, L. Fliegel, H. S. Young, Dimeric structure of human Na^+/H^+ exchanger isoform 1 overproduced in *Saccharomyces cerevisiae*. *J Biol Chem* **283**, 4145-4154 (2008).
37. V. Y. Moiseenkova-Bell, L. A. Stanciu, Serysheva, II, B. J. Tobe, T. G. Wensel, Structure of TRPV1 channel revealed by electron cryomicroscopy. *Proc Natl Acad Sci U S A* **105**, 7451-7455 (2008).
38. D. L. Farrens, T. D. Dunham, J. F. Fay, I. C. Dews, J. Caldwell, B. Nauert, Design, expression, and characterization of a synthetic human cannabinoid receptor and cannabinoid receptor/ G-protein fusion protein. *J Pept Res* **60**, 336-347 (2002).
39. S. Y. Lee, J. A. Letts, R. MacKinnon, Functional reconstitution of purified human Hv1 H^+ channels. *J Mol Biol* **387**, 1055-1060 (2009).

40. M. Shimada, X. Chen, T. Cvrk, H. Hilfiker, M. Parfenova, G. V. Segre, Purification and characterization of a receptor for human parathyroid hormone and parathyroid hormone-related peptide. *J Biol Chem* **277**, 31774-31780 (2002).
41. X. Tao, J. L. Avalos, J. Chen, R. MacKinnon, Crystal structure of the eukaryotic strong inward-rectifier K^+ channel Kir2.2 at 3.1 Å resolution. *Science* **326**, 1668-1674 (2009).
42. J. Wong, E. Reboul, R. Molday, J. Kast, A carboxy-terminal affinity tag for the purification and mass spectrometric characterization of integral membrane proteins. *J Proteome Res* **8**, 2388–2396 (2009).

Chapter 4: Three-Dimensional Model for the Human Cl^-/HCO_3^- Exchanger, AE1, by Homology to the *E. coli* ClC Protein

A version of this chapter has been accepted as P.T. Bonar, H.P. Scheinder, H.M. Becker, J.W. Deitmer, and J.R. Casey, Three-Dimensional Model for the Human Cl^-/HCO_3^- exchanger, AE1, by Homology to the *E. coli* ClC Protein. *Journal of Molecular Biology*. (2013). (Reproduced with permission).

4.1 Introduction

AE1, also known as Band 3 or SLC4A1, is a member of the SLC4 family of bicarbonate transporters (*1*). More specifically, AE1 belongs to a sub-family of 1:1 electroneutral chloride/bicarbonate exchangers, which includes AE2 and AE3 (*1*). In erythrocytes AE1, which comprises 50% of membrane protein, is essential to maintain the biconcave disc structure and to maximize the HCO_3^- carrying capacity of the blood (*2*). In the renal collecting duct, AE1 functions in bicarbonate reabsorption to prevent systemic acidosis (*1*). Mutations in AE1 cause blood and renal diseases, including hereditary spherocytosis and distal renal tubular acidosis (dRTA), respectively (*1*).

AE1 is comprised of two domains, a 43 kDa N-terminal cytoplasmic domain and a 55 kDa integral membrane domain with 12-14 transmembrane segments (*3*). The AE1 cytoplasmic domain forms numerous protein-protein interactions that anchor the erythrocyte cytoskeleton to the plasma membrane (*2*), while the membrane domain alone is responsible for AE1 transport activity (*4*). Although there is a 2.6 Å resolution structure of the AE1 cytoplasmic domain (*5*), structural information on the membrane domain is far more limited. Many studies have investigated the topology (*3, 6-15*), oligomerization (*16*), helical packing (*17, 18*), and overall three-dimensional structure of human AE1 (*19-23*), as a result of its abundance and ease of purification from erythrocytes (*24*). Structural studies of human erythrocyte AE1 membrane domain yielded several low-resolution structures of AE1 (*19, 21-23*). Thus far, the highest resolution structure (7.5-

16 Å) was obtained by two-dimensional crystallization and electron microscopy (*19*). This resolution does not allow determination of helical packing of the entire membrane domain and the placement of individual amino acids. Still, structural similarity between short regions of AE1 and ClC led to the proposal that AE1 has the same fold as the ClC family of chloride transporters (*19*).

The ClC family of chloride transporters comprises nine isoforms in humans that divide into three sub-families: vesicular $2Cl^-/H^+$ exchangers, plasma membrane Cl^- channels and ambiguous ClC transporters (*25*). Structures of prokaryotic and eukaryotic ClC proteins led to a model for the transport mechanism of ClCs (*26-28*). Much of the structural and functional data available is from the *E. coli* ClC protein, which is thus the focus of the current study. Three Cl^- binding sites were identified in ClC structures (*26-28*). At the external Cl^- binding site an extracellular glutamate gate (E148) is required for the transport activity (*26*). Protonation of this site is proposed to open or close the gate, allowing movement of Cl^- through the transporter (*27*). In the central Cl^- binding site of *E. coli* ClC the side chains of S107 and Y445 and the main chain amide groups of I356 and F357 together coordinate the Cl^- ion (*26*). An intracellular glutamate gate, E203 of *E. coli* ClC, is involved only in the coupling of H^+ exchange to Cl^- transport (*29*). This gate is distant from the intracellular Cl^- translocation pathway, and the mechanism of H^+ transport to this site is not known.

While AE1 and ClC proteins do not have a high sequence similarity, which is often considered a requirement for homology modeling, the proteins share many other similarities. ClCs proteins and AE1 both form dimers whose monomers function independently (*16, 30, 31*). *E. coli* ClC performs $2Cl^-/H^+$ exchange at a rate of 2.1 x 10^3 ions/s (*32*), which is much faster than classical membrane transporters; AE1 has a transport rate of 5 x 10^4 ions/s (*33*), and is even faster than *E. coli* ClC, but still slower than an ion channel flux. The proposed ClC transport mechanism is amenable to a fast transport rate, as it only requires subtle movements of residue side chains and not whole helices. ClC and AE1 are also involved in Cl^- transport coupled to the exchange of a H^+ equivalent, H^+ for ClCs and HCO_3^- for AE1. Interestingly, two other bicarbonate transporters, SLC26A3 and SLC26A6 have been modeled on the structure of the *E. coli* ClC (*34*). The SLC26 proteins, however, arose from a different evolutionary lineage than SLC4 proteins and thus do not share sequence homology with SLC4 proteins (*1*).

On the basis of an AE1 topology model, created using an *E. coli* ClC structure as a template (*35*), we constructed a three-dimensional AE1 homology. This model agrees well with existing biochemical constraints, and residues corresponding to ClC transport mechanism residues were in large part similar. When these potential transport mechanism residues were mutated in AE1, there was a significant effect on AE1 transport activity. We propose that AE1 has a similar protein fold and transport mechanism as ClC chloride channels.

4.2 Results

4.2.1 Creation of an AE1 Model Structure

We set out to develop a three-dimensional homology model of the human AE1 membrane domain. The GenTHREADER program (www.psipred.com), predicts that the *E. coli* ClC structure is a candidate for AE1 homology modeling (Table 4.1). Other candidate proteins were either from the importin/exportin family of nuclear transport proteins or integral transmembrane transport proteins (Table 4.1). The importin/exportin protein family was excluded since they are soluble proteins, which bind to macromolecules (such as RNA) and are transported through the nuclear pore complex. The remaining candidate structures were used to create crude sequence alignments and homology models. Even with manual adjustments the AE1 homology models created, using these structures as templates, did not satisfy basic biochemical constraints for AE1. All of these models had incorrect orientations of the N terminus, C terminus, or glycosylation site relative to the lipid bilayer. In the list of candidates generated by GenTHREADER only *E. coli* ClC acted as a template producing a satisfactory model. This provides the first evidence that ClC proteins provide a suitable structural model for AE1.

Table 4.1 Candidate Structurally Homologous Proteins Identified by GenTHREADER.

Results from the GenTHREADER program (www.psipred.com). Candidate protein structures for AE1 homology modeling, the candidate protein PDB ID, sequence identity between human AE1 membrane domain and the candidate protein, and p-values, are indicated.

Protein structure	PDB ID	Sequence identity (%)	p-value
Exportin	3a6p	11.1	7×10^{-6}
ApcT	3gia	11.5	1×10^{-5}
Importin	2bpt	10.7	2×10^{-5}
Exportin	1wa5	11.5	5×10^{-5}
ClC	1ots	13.3	6×10^{-5}
sGLT	3dh4	12.5	2×10^{-4}
AdiC	3l1l	11.6	4×10^{-4}
Transportin	2z5k	4.2	7×10^{-4}
Exportin	3ibv	8.4	7×10^{-4}

Further evidence for structural similarities between AE1 and ClC were provided by a recent 7.5-16 Å structure of AE1 suggested that AE1 has the same fold as ClC chloride channels (*19*). A subsequent paper elaborated on an alignment between AE1 and *E. coli* ClC (*35*). Here this alignment was modified to create a sequence alignment between *E. coli* ClC residues and the human AE1 membrane domain (amino acids 388-911, Fig. 4.1). Sequence alignment gaps between AE1 E480-S525 and T728-G838, corresponding to ClC V122-D171 and G316-A404, respectively, were minimized to increase the amount of sequence similarity. In addition, minimization of sequence alignment gaps in AE1 E480-S525 allowed for AE1 E508 to directly correspond with the ClC extracellular glutamate gate (Fig. 4.1). Alterations to sequence alignment gaps in AE1 T728-G838 also increased the agreement between the AE1 homology model and data from AE1 cysteine-scanning mutagenesis studies (*3, 7*). This alignment method was used instead of traditional sequence alignment algorithms, since the sequence similarity between human AE1 and *E. coli* ClC is too low (9.8% identical and 18.4% similar). As a result traditional sequence alignments had large gaps in transmembrane spanning helices and the models generated using these sequence alignments did not satisfy basic AE1 biochemical constraints.

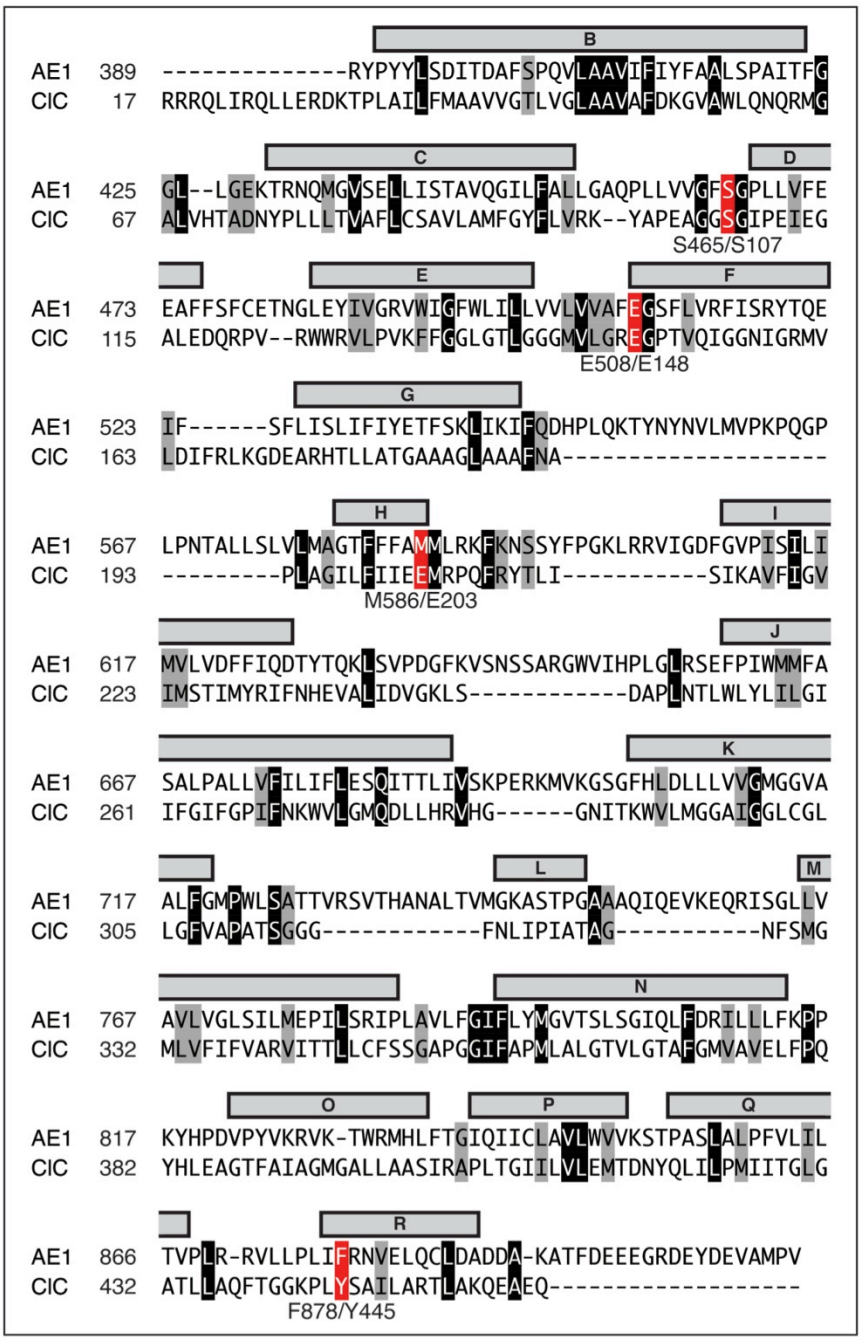

Figure 4.1 AE1 and ClC Amino Acid Sequence Alignment.

The sequences of the human AE1 membrane domain (amino acids 388-911) and *E. coli* ClC were aligned on the basis of a published structural alignment (*35*), with minor manual adjustments. Identical residues in the sequence alignment are black and similar residues are grey. Residues involved in the

ClC transport mechanism and the corresponding AE1 residues are red, with the corresponding residue numbers indicated beneath (AE1/ClC). Transmembrane spanning segments, following the assignment in the original ClC crystal structure (*26*), are indicated and labeled from B-R.

The amino acid sequence alignment (Fig. 4.1) was used to generate a homology model of AE1, on the basis of the *E. coli* ClC structure (*26*). The AE1 homology model, created using the program Modeler v9.7 (*36*), is shown with the template *E. coli* ClC structure overlaid (Fig. 4.2 and 4.3). The root-mean squared deviation between the entire AE1 homology model (amino acids 388-911) and the template ClC structure is 0.8 Å as determined by the pairwise structural alignment function on the dali server (*37*).

4.2.2 Evaluation of the AE1 Homology Model by Comparison to Substituted Cysteine Accessibility Data and Blood Group Antigens

AE1 cysteine-scanning mutagenesis studies measured residue accessibility to biotin maleimide (Table 4.2) (*3, 6, 7, 17*). To assess the agreement of the AE1 homology model with these biochemical spatial constraints, the biotinylation levels of cysteine mutants were plotted on the AE1 homology model (Fig. 4.4). The degree of biotinylation by biotin maleimide correlates with aqueous accessibility of the residue. All AE1 cysteine-scanning mutagenic studies were normalized to the amount of Y555C-AE1 biotinylation, a site that is highly aqueous accessible (*3, 6, 7, 17*). In the AE1 homology model the majority of cysteine mutants with <10% biotinylation are located within the plane of the lipid bilayer as expected. In contrast, the majority of cysteine mutants with >50% biotinylation are located in extracellular or intracellular accessible regions of the AE1 homology model. Cysteine mutants with low levels of biotinylation (10-30%)

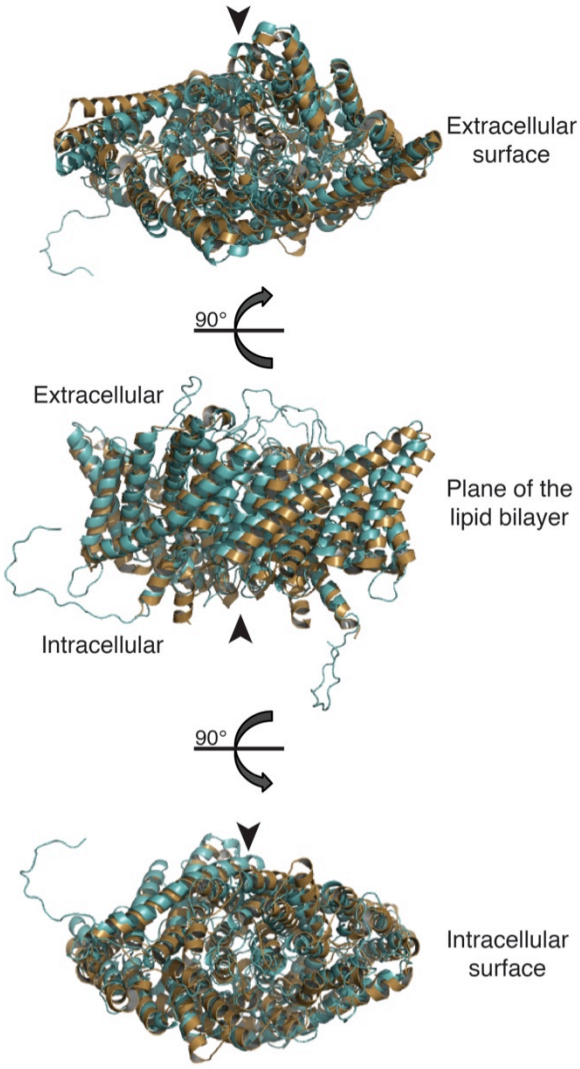

Figure 4.2 Homology Model of the AE1 Membrane Domain, using the *E. coli* ClC Structure.

A homology model of the human AE1 integral membrane domain (residues 388-911) was created using Modeller v9.7. The AE1 homology model is shown as a dimer in teal and the template ClC structure is shown in beige. Three views of the structure are shown, looking parallel to the lipid bilayer, to the extracellular side and the intracellular side. Arrowheads represent the position of the dimer interface.

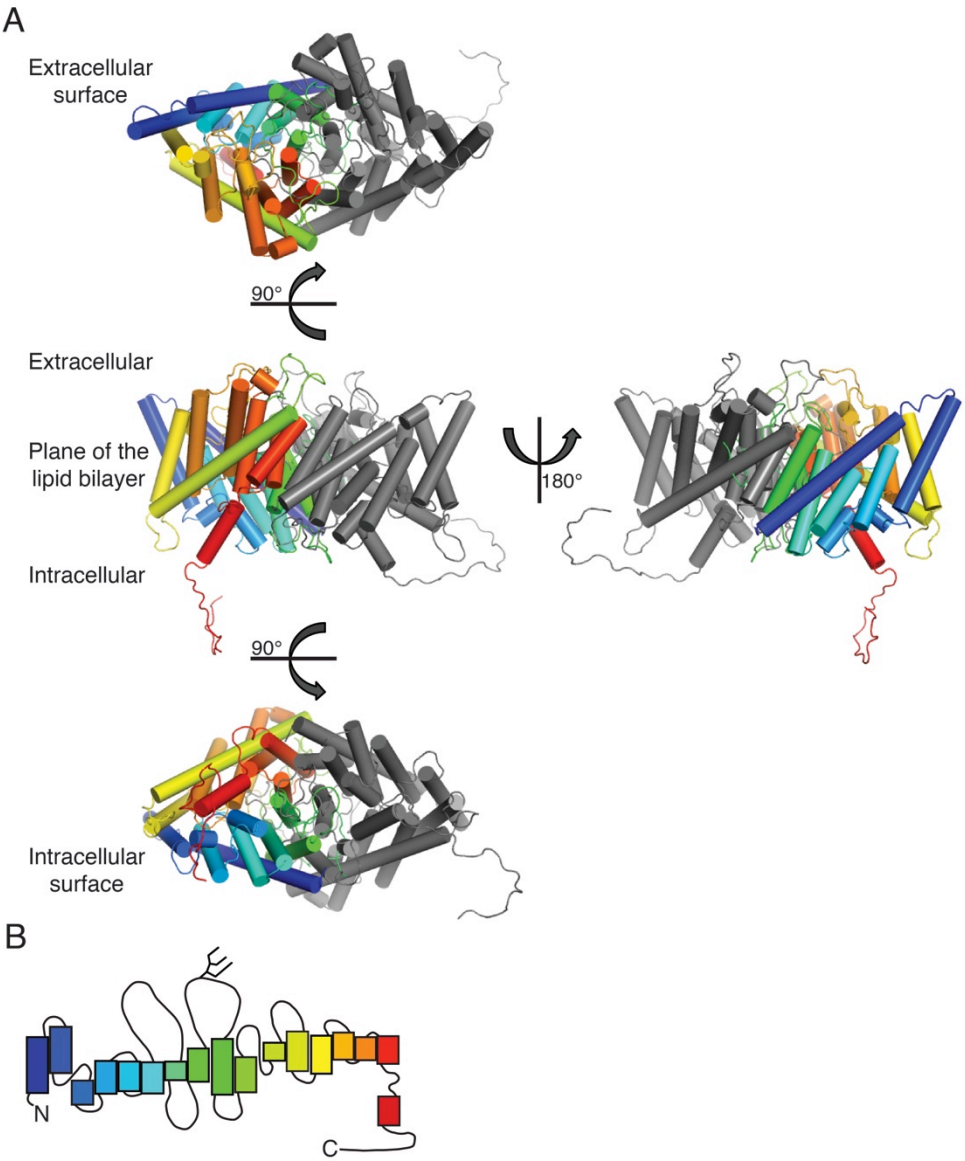

Figure 4.3 AE1 Homology Model.

(A) The AE1 homology model is shown as a dimer with one monomer colored gray and the other monomer has each transmembrane helix in a different color. Four views of the structure are shown, two views are looking parallel to the lipid bilayer, one view to the extracellular side and one view to the intracellular side. (B) A topology of AE1 colored according to the homology model (in panel A).

Table 4.2 Biochemical Spatial Constraints for AE1.

Previously published studies with the respective technique implemented and AE1 residues investigated in each publication. Biochemical constraints inconsistent with the AE1 homology model are highlighted in grey.

AE1 Residues	Type of Data	Reference
L426, F478, E485, R514, F537, L540, K551, L558, K562, K592, R603, K631, K639, R646, R656, K698, R730, K743, R760, K817, Y824, K826, W831, A855	Proteolytic cleavage	(*8, 9*)
E429, R432, Y555, P561, G565, N569, R656, P854	Blood group antigens	(*10, 15*)
K430	Amine labeling	(*11*)
K539, K851	Covalently reacts with H_2DIDS	(*8*)
H547, H734, H834	Modified with DEPC	(*13*)
Y555	Cysteine-scanning mutagenesis	(*3, 6, 7, 17*)
A402, T431, A456, Y486, G565, S595, R656, M663, I684, S690, S731, A751, D821, A855, C885	Cysteine-scanning mutagenesis	(*17*)
S574, S595, S643-I661, M664-Q683, I684-S690,	Cysteine-scanning mutagenesis	(*6*)
G428, L484, S633, G637-W648, Q754, P854	N-linked glycosylation insertion	(*14*)
N642	Glycosylation site	(*38*)
L708, G714, S725, S731, G742, S745, A751, S762, A767, L775, S781, G790, S801, F806, K814, D821, T830, G838, C843, S852, A858, T866, R871, R879, C885, K892	Cysteine-scanning mutagenesis	(*7*)
F806-C885	Cysteine-scanning mutagenesis	(*3*)
L886-V911	C-terminal cytoplasmic tail and CAII bind site	(*39*)
Q434	Distance measurements by FRET	(*40*)
T431-G456, G456-Y486, G565-S595	Cysteine crosslinking	(*17*)

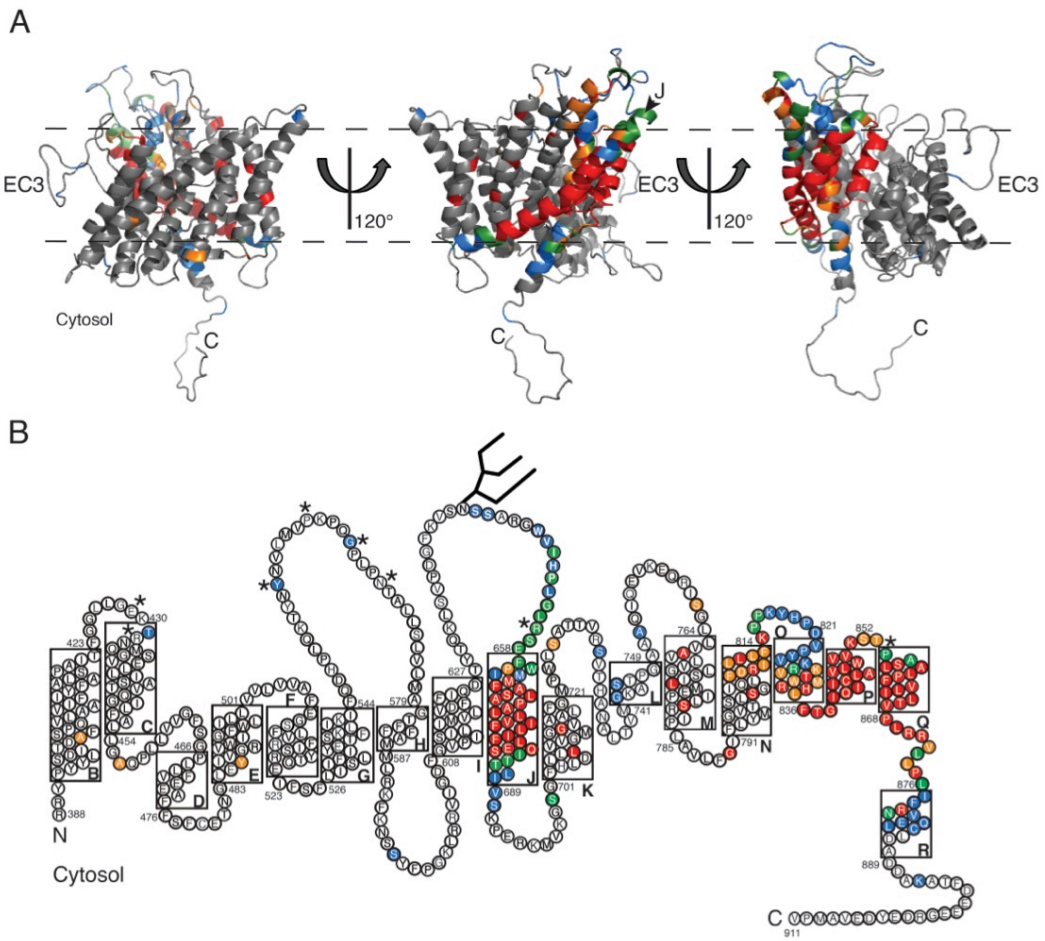

Figure 4.4 Evaluation of the AE1 Homology Model, using Existing Biochemical Constraints.

AE1 spatial constraints from published cysteine-scanning mutagenesis studies were used to examine the validity of the AE1 homology model. Mutagenized amino acids in AE1 were colored according to the level of biotin maleimide incorporation (corresponding to aqueous accessibility) (*3*, *6*, *7*, *17*). Cysteine mutants with <10% biotinylation are red, 10-30% biotinylation are orange, 30-50% biotinylation are green and >50% biotinylation are blue. Grey (A) or white (B) indicates no data available. (A) An AE1 homology model monomer, with three different orientations parallel to the lipid bilayer. C marks the cytosolic C-terminus of AE1 and dashed lines represent the approximate boundaries of the lipid bilayer. EC3 marks AE1 extracellular loop 3. In the middle panel the N-terminus of transmembrane helix J is

indicated with an arrow head. The dimer interface of the AE1 homology model faces the reader in the right panel. (B) Topology model of AE1, based on the three-dimensional homology model. Transmembrane spanning segments are indicated and labeled from B-R. The N-linked glycosylation site is indicated by a large branched structure and sites of blood group antigens (Table 4.2) are indicated by *. The N-terminus and C-terminus are indicated by N and C, respectively.

or moderate levels of biotinylation (30-50%) clustered in regions near the interface between the plane of the lipid bilayer and extra/intra-cellular surfaces of the AE1 homology model.

In addition, all eight blood group antigens attributed to an AE1 sequence (Table 4.2) and the N-linked glycosylation site (N642) were appropriately located on the extracellular surface of the AE1 homology model (Fig. 4.4 B) (*10, 15, 38*). Thus, the AE1 homology model is fundamentally consistent with previously published biochemical data gathered from cysteine-scanning mutagenesis and blood group antigen mapping.

4.2.3 Identification of Residues Possibly Involved in the AE1 Transport Mechanism

Interestingly, although the amino acid sequence alignment shows low sequence similarity, all of the residues involved in the ClC transport mechanism are identical or similar to the corresponding residues in the AE1 homology model (Fig. 4.5). The sole exception is the intracellular glutamate gate (E203) in ClC, located 13 Å away from the central Cl^- binding site, which corresponds to M586 in AE1 (Fig. 4.5). Since this residue is not similar to the intracellular glutamate gate of ClC, we considered two other candidate residues that could fulfill this role. The closest acidic residue in the AE1 primary sequence is D607, which is located 27 Å away from the central Cl^- binding site in the homology model (Fig. 4.5 C). In addition, AE1 E681 has a key role in AE1 transport activity (*41-43*), and is 14 Å away from the central

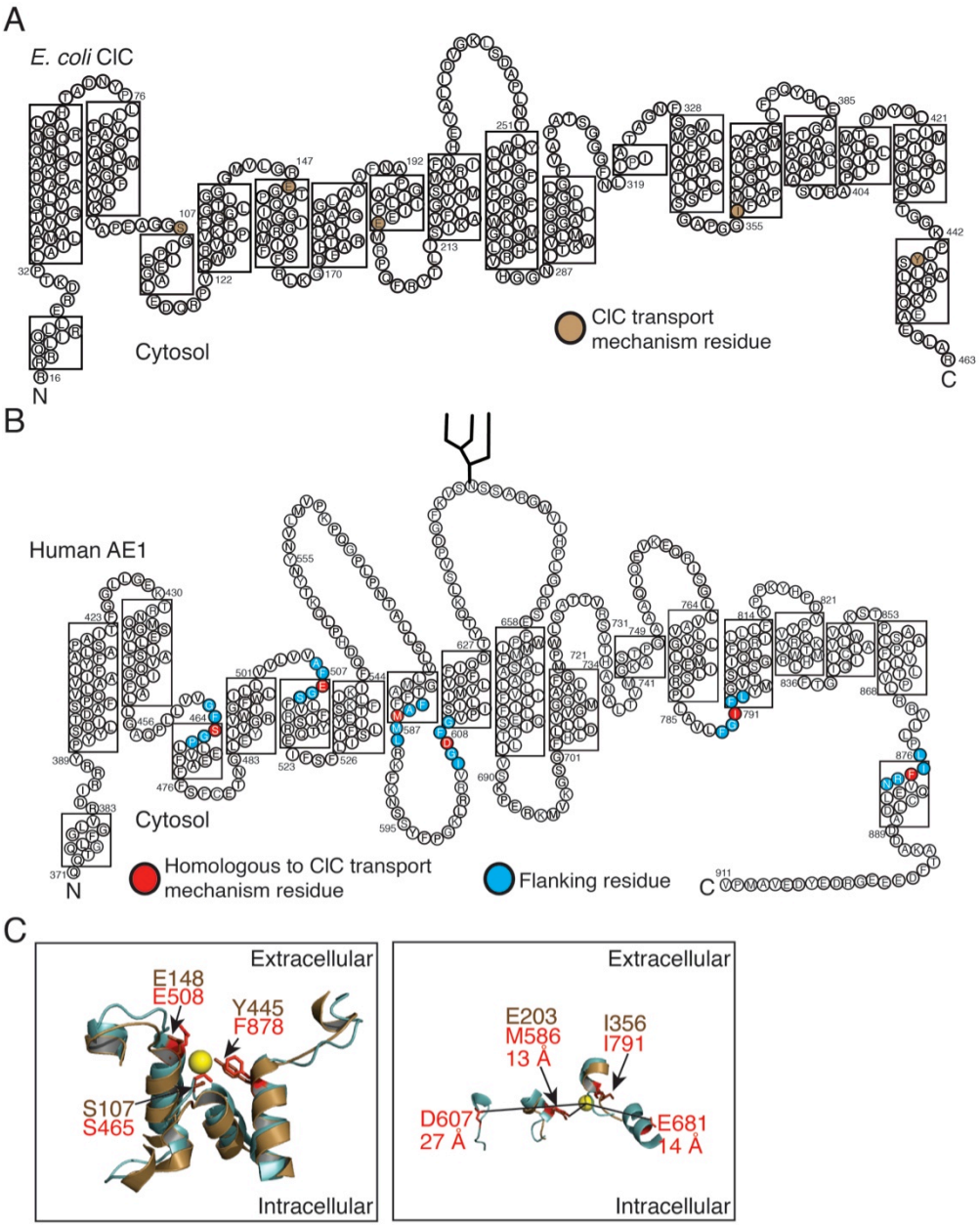

Figure 4.5 Identification of Possible Transport Mechanism Residues.

(A) In the *E. coli* ClC topology model residues involved in the transport mechanism of ClC are colored beige. (B) In the AE1 topology model candidate transport mechanism residues are colored red and flanking residues are colored blue. The N-terminus and C-terminus are indicated by N and C, respectively. (C) Three-dimensional structure of the central Cl^- coordination site, with two different views (left and right panels). The ClC

structure is shown in beige and the residues involved in the transport mechanism are indicated in brown. The AE1 homology model is shown with residues corresponding to residues in ClC involved in the transport mechanism indicated in red and flanking residues indicated in teal. A yellow sphere represents a Cl^- in the central Cl^- coordination site. In the right panel distances between AE1 residues and Cl^- are marked by black lines and indicated in red below the corresponding AE1 residue.

Cl^- binding site (Fig. 4.5 C). The extracellular glutamate gate of ClC is E148, and the residue corresponding in the AE1 homology model is E508. S107 and Y445 form the central Cl^--binding site of ClC through their side chain moieties, and the corresponding residues in the AE1 homology model are S465 and F878 (Fig. 4.5).

4.2.4 Transport Activity of AE1 Point Mutants Assessed in HEK293 Cells

To test the validity of the AE1 homology model we mutated all of the identified candidate AE1 transport mechanism residues to alanine. As well, D607 was mutated, since it is an AE1 intracellular glutamate gate candidate. We chose not to investigate AE1 E681, although it is also an AE1 intracellular glutamate gate candidate, since the role of E681 in AE1 transport activity is established (*41, 43*). To examine whether the effects on AE1 transport activity were directly attributed to a functional role of the single point mutation, or if the point mutation was located in a region sensitive to mutagenesis, we also mutated the four residues flanking each candidate transport mechanism site (Fig. 4.5).

Transport activity of AE1 mutants was assessed by Cl^-/HCO_3^- exchange activity assays (Fig. 4.6). HEK293 cells grown on glass coverslips were transiently transfected with cDNA encoding WT-AE1, an AE1 point mutant, or vector. Cells were subsequently loaded with the pH sensitive dye, BCECF-AM (2', 7'-bis-(2-carboxyethyl)-5-(and-6)carboxylfluorescein, acetoxymethyl ester), and cells were alternately perfused with CO_2-bubbled

Cl^--containing and Cl^--free Ringer's buffer. In AE1 transfected cells, switching from a Cl^--containing to a Cl^--free Ringer's buffer induced cytosolic alkalinization due to AE1 mediated Cl^- efflux and HCO_3^- influx (Fig. 4.6 A). In comparison, vector-transfected cells had a low background rate of alkalinization, following the switch from Cl^--containing to Cl^--free Ringer's buffer (Fig. 4.6 B). Bicarbonate transport rates were calculated by linear regression of the initial rate of cytosolic alkalinization upon switching to Cl^--free Ringer's buffer. Bicarbonate transport rates were subsequently corrected for background in vector-transfected HEK293 cells, and normalized for the amount of protein expressed at the cell surface (Fig. 4.7 and 4.8). Several AE1 mutants (G463A, S465A, E508A, E508D, E508S, E508K, M587A and L793A) accumulated to less than 50% of WT-AE1 total protein expression (Fig. 4.7). In contrast, the percentage of AE1 processed to the plasma membrane was not significantly different between WT-AE1 and AE1 mutants (Fig. 4.8).

The Cl^- coordinating residue, S107, of ClC corresponds to AE1 S465. Thus, we investigated G463A, F464A, S465A, G466A, and P467A-AE1 (Fig. 4.6 C). S465A had a significantly reduced Cl^-/HCO_3^- exchange activity (14±3% compared to WT-AE1). In comparison, flanking mutants F464A, G466A and P467A had transport activities not significantly different from WT-AE1.

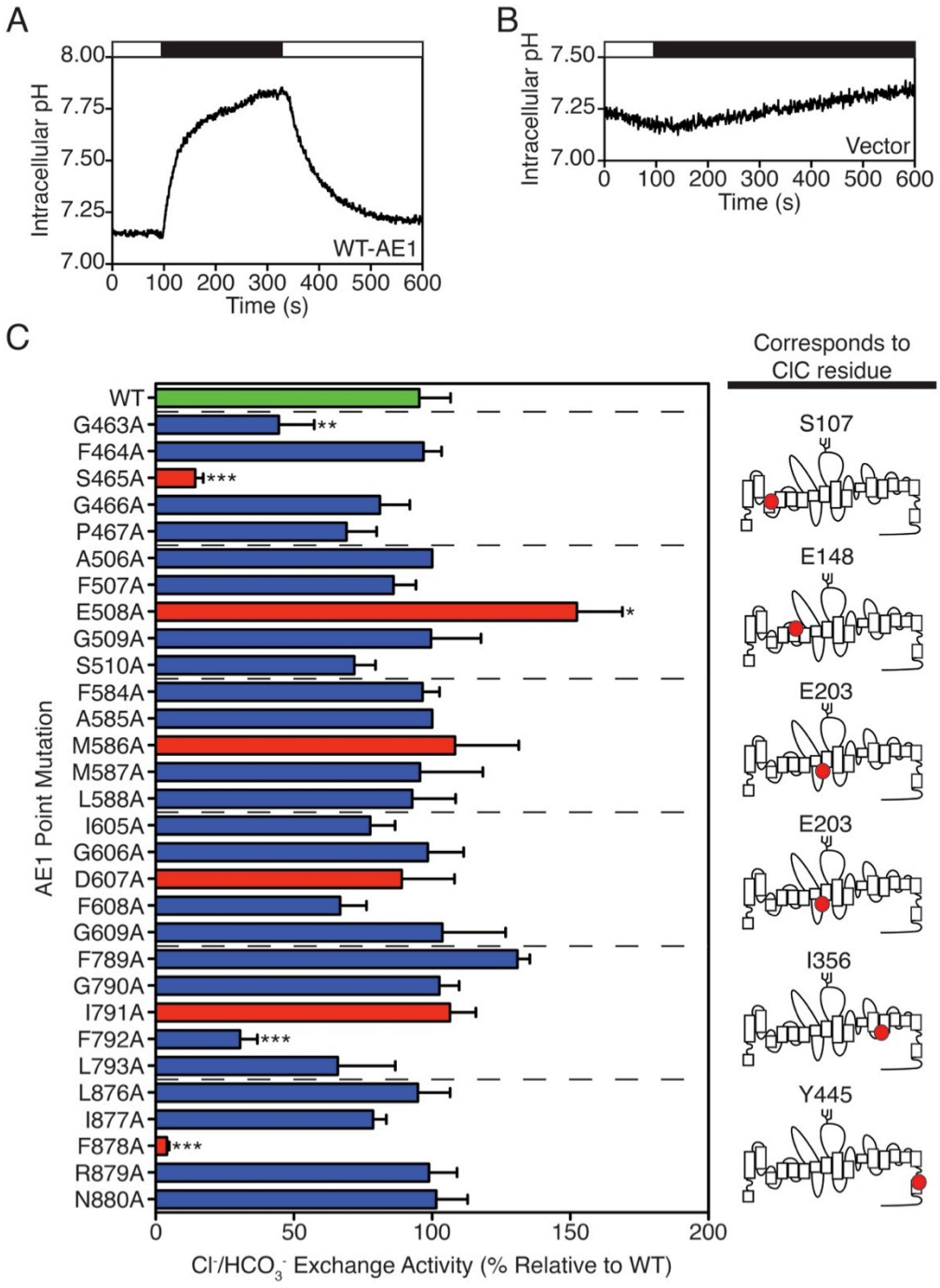

Figure 4.6 Transport Activity of AE1 Alanine Point Mutants.

HEK293 cells were grown on glass coverslips and transiently transfected with cDNA encoding WT-type AE1 (A), an AE1 alanine point mutant, or vector (B). Cells were loaded with the pH sensitive dye, BCECF-AM, and fluorescence was monitored as cells were alternately perfused with Ringer's

buffer containing sodium chloride (open bar), or chloride-free Ringer's buffer (black bar). Transport rates were monitored by the rate of alkalinization induced upon switching to chloride-free medium. (C) Anion exchange activity was measured for WT-AE1 and alanine point mutants, with the corresponding ClC transport mechanism residues indicated in the topology models. The bar graph shows transport rates corrected for background, and normalized to protein expression and cell surface processing as described in methods. Anion exchange activity was measured and plotted relative to WT (0.76 dpH_i/dt). Error bars represent SE (n=3-6), while *, ** and *** indicates a significance difference from WT ($p<0.05$, $p<0.01$ and $p<0.001$, respectively).

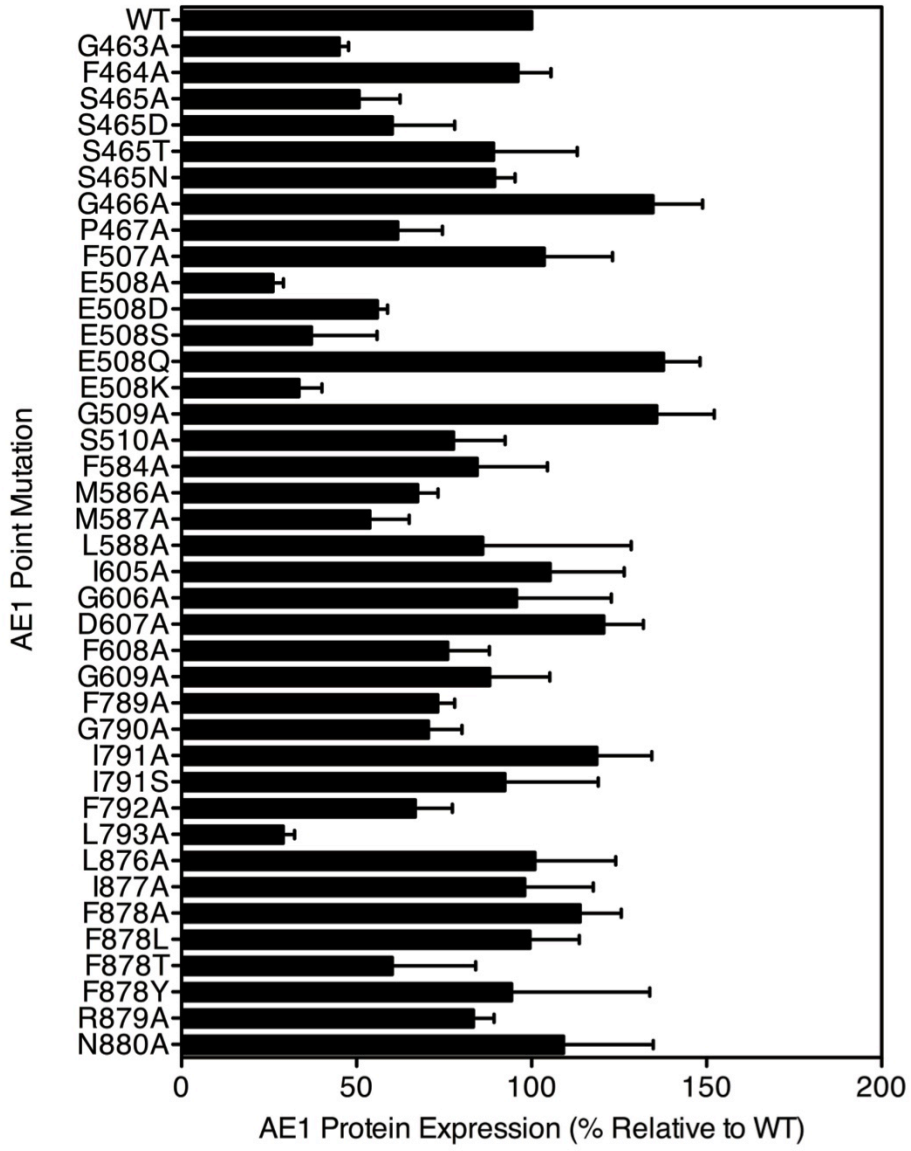

Figure 4.7 Expression of AE1 Point Mutations.

HEK293 cells were transiently transfected with cDNA encoding either WT-AE1 or an AE1 point mutant. Cell lysates were harvested and samples were resolved by SDS-PAGE. Immunoblots were quantified by densitometry and values were expressed as a percentage of WT-AE1 expression. Error bars represent SE (n=3-6).

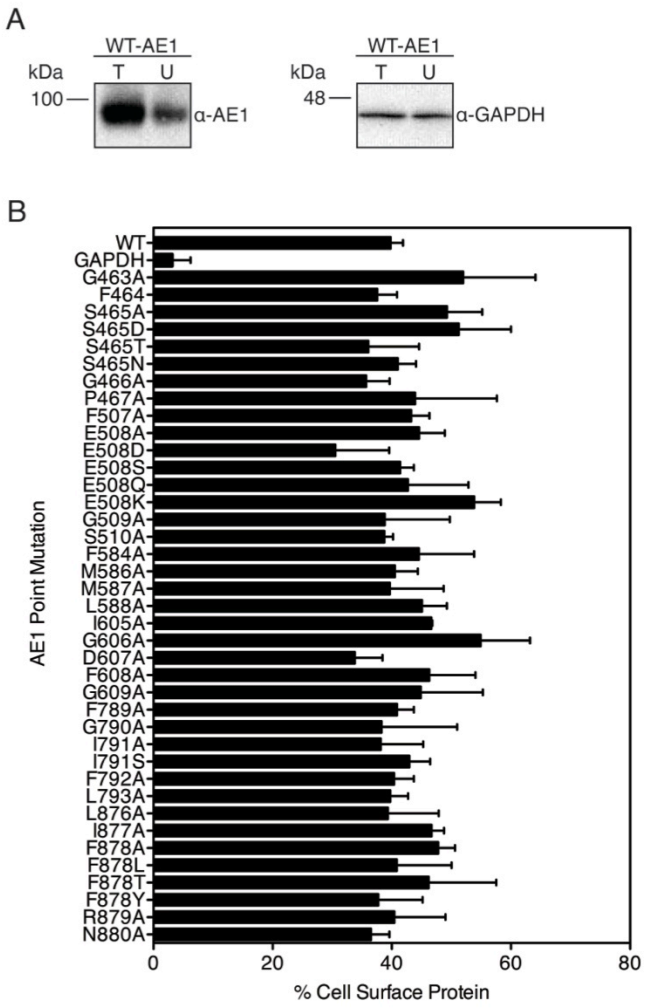

Figure 4.8 Cell Surface Processing of AE1 Point Mutations.

(A) HEK293 cells were transiently transfected with cDNA encoding either WT-AE1 or an AE1 point mutant. Cells were treated with the biotinylation reagent and cell lysates were harvested. Half of the cell lysate was kept as the total fraction (T). The remaining lysate was incubated with immobilized streptavidin to bind biotinylated cell surface protein, and the unbound fraction was collected (U). Samples were resolved by SDS-PAGE and immunoblots were probed with antibodies against AE1 and the cytosolic protein GAPDH. (B) The percent of cell surface protein was calculated as (T-U)/T*100%. Error bars represent SE (n=3-4).

G463A had a transport activity of 44±13%, which was significantly different from WT-AE1. S465N and S465D had significantly reduced transport activity, 6±6% and 5±5% relative to WT-AE1, respectively (Fig. 4.9). Transport activity of S465T (43±5% relative to WT-AE1), however, was significantly faster than S465-AE1 transport activity (Fig. 4.9).

The ClC extracellular glutamate gate (E148) corresponds to E508 in the AE1 homology model. None of the flanking mutants had transport rates significantly different from WT-AE1 (Fig. 4.6 C). In contrast, E508A has a significantly increased transport rate (152±16% compared to WT-AE1), which is remarkable as the transport rate of WT-AE1 is unusually fast for a transporter (5×10^4 ions/s) so it is exceptional to create an AE1 mutant with a higher transport rate than WT-AE1. Similar to E508A-AE1, E508D, E508S and E508K-AE1 had significantly faster transport activities (186±35%, 210±26% and 211±55%, respectively) compared to WT-AE1 (Fig. 4.9). Interestingly, E508Q-AE1 had a transport activity of 75±5%, which was not significantly different from WT-AE1 (Fig. 4.9).

The AE1 residue corresponding to the intracellular glutamate gate of ClC (E203) is M586. Alanine mutants at AE1 M586, D607 and flanking these sites had transport activities not significantly different from WT-AE1 (Fig. 4.6 C), which suggests that M586 and D607 are not the functional equivalent of the ClC intracellular glutamate gate, E203.

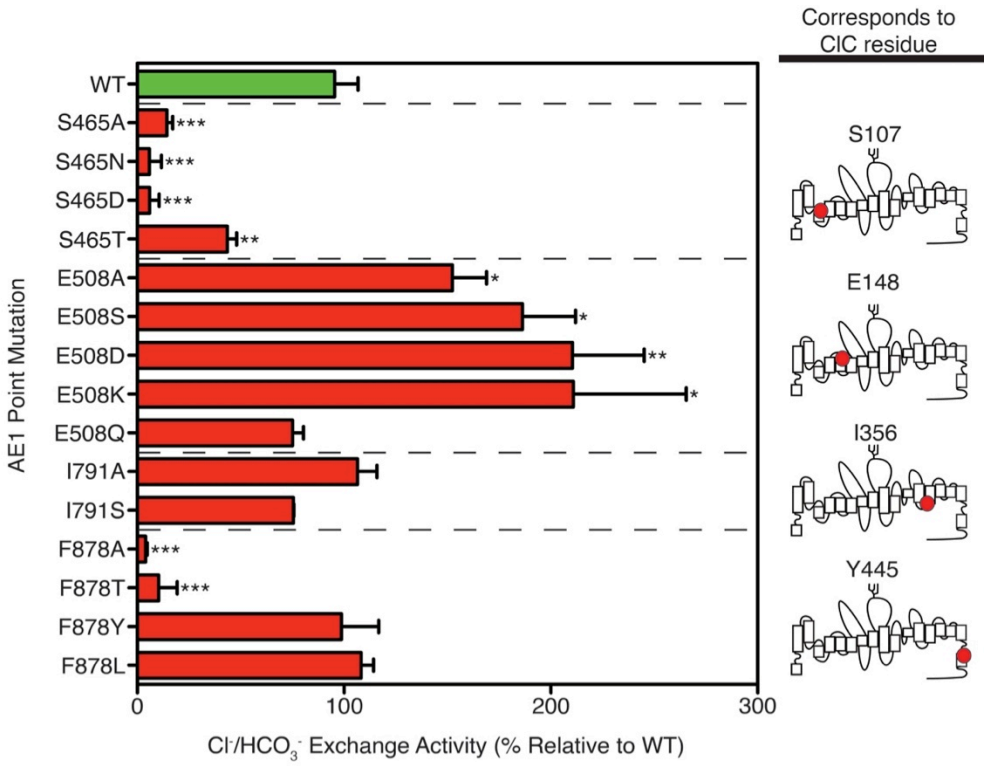

Figure 4.9 Functional Characterization of AE1 Point Mutations.

Chloride bicarbonate exchange activity of WT (0.76 dpH_i/dt) and AE1 point mutants was measured in transfected HEK293 cells. Topology models indicate the corresponding ClC transport mechanism residues. The bar graph shows transport rates corrected for background, protein expression and cell surface processing. Error bars represent SE (n=3-6), while *, ** and *** indicate a significant difference relative WT ($p<0.05$, $p<0.01$ and $p<0.001$, respectively).

We investigated the functional role of AE1 I791 and F792, since these residues correspond to ClC I356 and F357, which are involved in Cl^- coordination through their backbone amides. F789A, G790A, I791A and L793A-AE1 all had transport rates not significantly different from WT-AE1 (Fig. 4.6 C). F792A-AE1 had a significantly reduced transport activity (31±6%, compared to WT-AE1). This indicates that either the side-chain of F792 is involved in AE1 transport activity, or that mutation of F792 causes structural changes in AE1 that alter the transport activity. Since I791A-AE1 is a conservative mutation, we assessed I791S-AE1, which was not significantly different from WT-AE1 (Fig. 4.9). This confirms that the side chain of I791 is not involved in the AE1 transport mechanism.

ClC Y445 coordinates Cl^- through interactions with the tyrosine hydroxyl. The corresponding residue in AE1 is F878. Mutants flanking AE1 F878 had no significant difference in transport activity relative to WT-AE1 (Fig. 4.6 C). F878A-AE1 had a significantly reduced transport activity (4±1%) compared to WT-AE1 (Fig. 4.5 C). A major reduction in transport activity of F878T-AE1 (10±9% relative to WT-AE1) was also observed (Fig. 4.9). In contrast, the more conservative F878Y and F878L-AE1 mutants had transport activities not significantly different from WT-AE1 (Fig. 4.9). Thus, it appears that mutation of AE1 F878 to large hydrophobic or aromatic amino acids has no effect on transport activity, but mutation of AE1 F878 to small hydrophobic or small polar amino acids abolishes transport activity almost completely.

In summary, AE1 residues corresponding to the ClC transport mechanism residues had significant changes in transport activity when mutated. The only exception was AE1 M586, corresponding to the ClC intracellular glutamate gate (E203). In the ClC transport mechanism this residue is only involved in transport of H^+ coupled to Cl^- transport, and is located distant from the central Cl^- coordination site. We hypothesize that E681 of AE1 may fulfill a similar role to the E203 residue of ClC, as this residue in the AE1 homology model is also located on the intracellular side of the lipid bilayer approximately 14 Å away from the central Cl^- binding site, and affects AE1 transport activity (*41, 43, 44*).

4.2.5 Transport Activity of AE1 Point Mutants in *Xenopus laevis* Oocytes

To investigate the electrogenicity and transport stoichiometry of AE1 alanine point mutations at positions corresponding to ClC transport mechanism residues, *X. laevis* oocytes were co-injected with cRNA encoding WT or mutant AE1 and glycophorin A, or remained non-injected (native) as a control. Previous studies revealed that optimal cell surface expression of AE1 in oocytes was achieved only when glycophorin A was co-expressed (*45*). Cytosolic pH and membrane potential were monitored, using double-barreled microelectrodes inserted just beneath the intracellular surface of the oocyte (Fig. 4.10). Upon switching from HCO_3^--free oocyte Ringer's solution to high Cl^- oocyte Ringer's solution a larger acidification was observed in native oocytes, than in those expressing WT-AE1 (Fig. 4.10 A and

B). This acidification arose from diffusion of the acid, CO_2, into the oocyte. In AE1 expressing oocytes, acidification was minimized by AE1 mediated exchange of extracellular HCO_3^- for intracellular Cl^-.

Similar transport activity data were observed in *X. laevis* oocytes as in HEK293 cells. In *X. laevis* oocytes, M586A, D607A and I791A-AE1 had transport rates similar to WT-AE1 (Fig. 4.10 D), consistent with results obtained in HEK293 cells. These residues correspond to the intracellular glutamate gate (E203) and the residue (I356) that coordinates Cl^- through its backbone amide in ClC. E508A, S465A and F878A-AE1, which correspond to the extracellular glutamate gate and Cl^- coordinating residues, all had transport rates significantly different from WT-AE1 (34±5%, 56±16% and 23±5%, respectively, Fig. 4.10 C). While S465A and F878A-AE1 had reduced transport activity when expressed in both HEK293 cells and *X. laevis* oocytes, the reduction in transport activity was smaller in *X. laevis* oocytes than in HEK293 cells. Interestingly, the behavior of E508A-AE1 differs in the two expression systems. In HEK293 cells, E508A has a significantly faster transport rate compared to WT-AE1, but has a significantly slower transport rate in *X. laevis* oocytes.

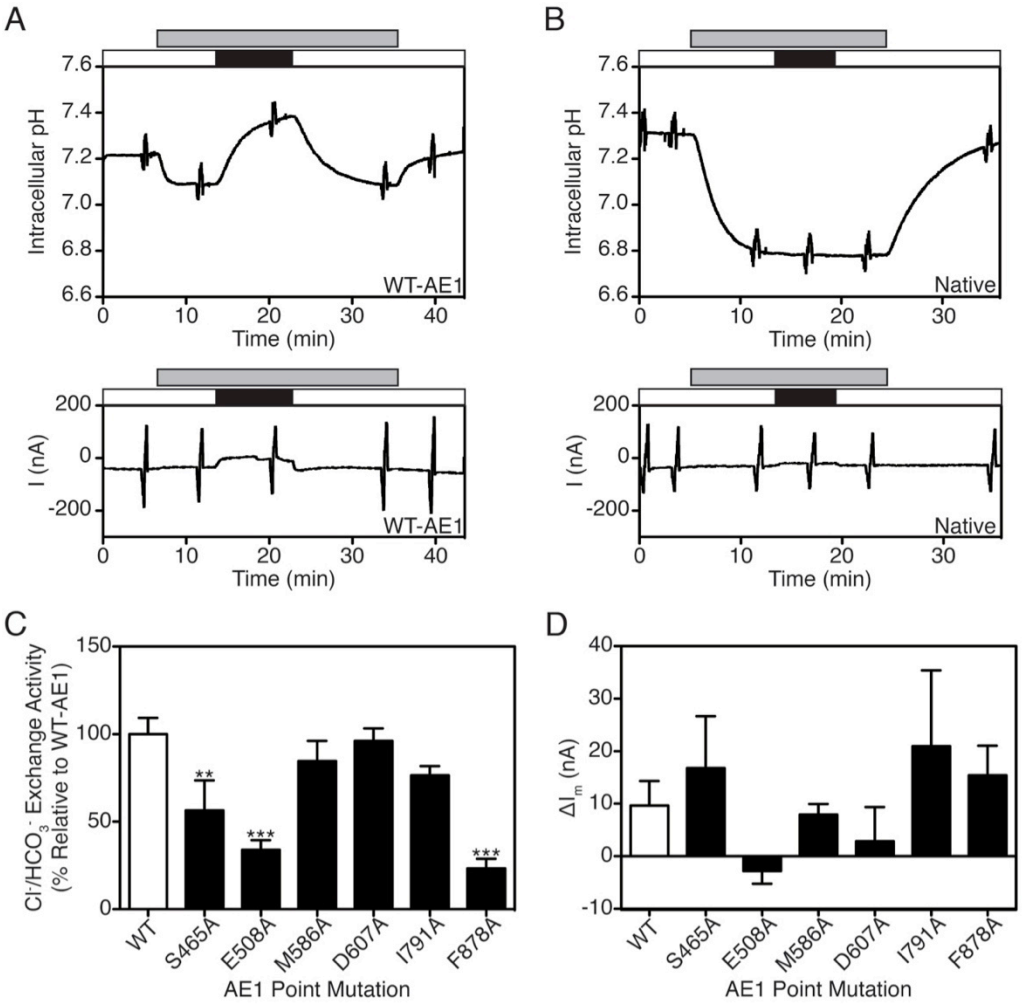

Figure 4.10 Characterization of AE1 Point Mutants in *X. laevis* Oocytes.

(A) Oocytes were co-injected with cRNA encoding WT-AE1 and glycophorin A. (B) Non-injected oocytes were used as a control (native). Current and pH were simultaneously measured using a double-barreled microelectrode combined with two-electrode voltage clamp. Oocytes were perfused with high Cl^- (white bar) and low Cl^- (black bar) solution. The application of CO_2/HCO_3^- is indicated (grey bar). Changes in current were monitored during 20 mV voltage steps from -100 mV to +20 mV in each solution. (C) The transport rate was monitored by the rate of alkalinization upon switching from high Cl^- to low Cl^- oocyte Ringer's solution. The bar graph shows transport rates corrected for background activity in native oocytes

and plotted relative to WT. (D) AE1 mediated membrane current, induced by switching from high Cl^- to low Cl^- oocyte Ringer's solution, is shown for oocytes expressing WT-AE1 and AE1 mutants. All values were corrected for the difference in current observed in native oocytes. Error bars represent SE (n=5-13), while ** and *** indicate a significant difference from WT ($p<0.01$ and $p<0.001$, respectively).

Application of CO_2/HCO_3^- and reduction of extracellular Cl^- concentration, respectively, did not induce appreciable membrane currents in native oocytes or oocytes expressing WT or mutant AE1. Small changes in current observed upon reduction of extracellular Cl^- concentration were due to artifacts observed by the microelectrode when placed in a low Cl^- solution. AE1 mediated membrane currents (calculated by subtraction of the current measured in native oocytes from the current measured in AE1 expressing oocytes), induced upon switching from high to low Cl^- oocyte Ringer's solution were not significantly different from zero (Fig. 4.10 D). Also, there was no significant difference in membrane current between WT-AE1 and AE1 mutants (Fig. 4.10 D). Furthermore, no significant differences in oocyte membrane conductance were observed in WT-AE1, AE1 mutants, or native oocytes (Fig. 4.11 A and B). For all transporters expressed, G_m was around 2 μS and was not significantly different from the G_m determined in native oocytes. As for the conductance, no changes in the reversal potential could be detected by expression of WT-AE1 or AE1 mutant, even when compared to native oocytes (Fig. 11 C). Thus, none of the AE1 mutations resulted in a shift of transport stoichiometry, which would create an electrogenic AE1 transporter.

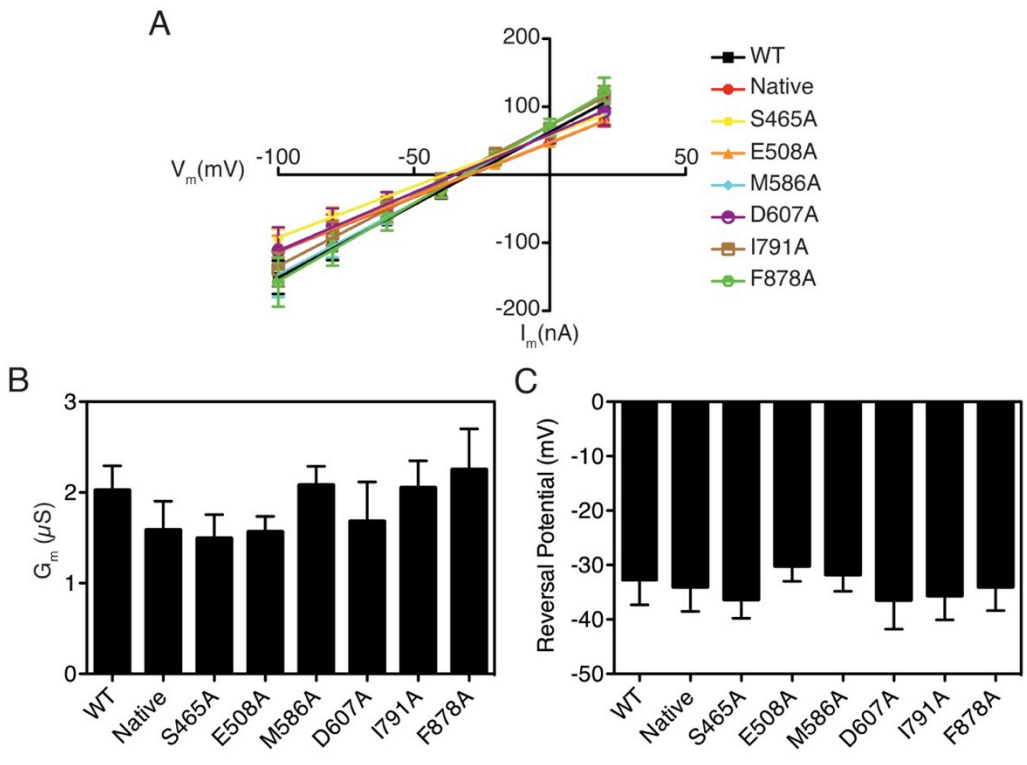

Figure 4.11 Current Voltage Relationships of AE1 Point Mutations.

Oocytes were co-injected with cRNA encoding WT-AE1 or an AE1 point mutant and glycophorin A. Non-injected oocytes were used as a control (native). Membrane current was monitored during 20 mV voltage steps. (A) Current voltage relationships are shown for oocytes in low Cl^- oocyte Ringer's solution. The membrane conductance (B), calculated by measuring the slope of each I/V curve, and the reversal potential (C) from the corresponding I/V curves are shown. Error bars represent SE (n=5-13).

4.3 Discussion

We developed a three-dimensional AE1 membrane domain homology model, on the basis of the *E. coli* ClC X-ray crystal structure (*26*). Leading us to develop this model, was the recalcitrance of AE1 to be crystallized because of protein micro-heterogeneity arising from proteolysis and post-translational modifications (*20*). The most recent low-resolution structure of the AE1 membrane domain led to the proposal that the AE1 membrane domain shares the same protein fold as ClC chloride channels (*19, 35*). We tested the validity of the AE1 homology model by comparison to published biochemical data, measurements of transport activity and electrical activity of AE1 mutants assessed in HEK293 cells and *X. laevis* oocytes. Together the data suggest that AE1 has a fold similar to ClC proteins, as well as a similar transport mechanism.

4.3.1 Structural Features of the AE1 Homology Model

The AE1 homology model agrees well with cysteine-scanning mutagenesis data, and blood group antigen data (*3, 6, 7, 10, 15, 17*). The position of residues relative to the lipid bilayer is similar between a previously published AE1 topology (*3*) and the ClC based AE1 topology model (*35*) (Fig. 4.12). Differences between the two AE1 topology models were discussed previously (*35*).

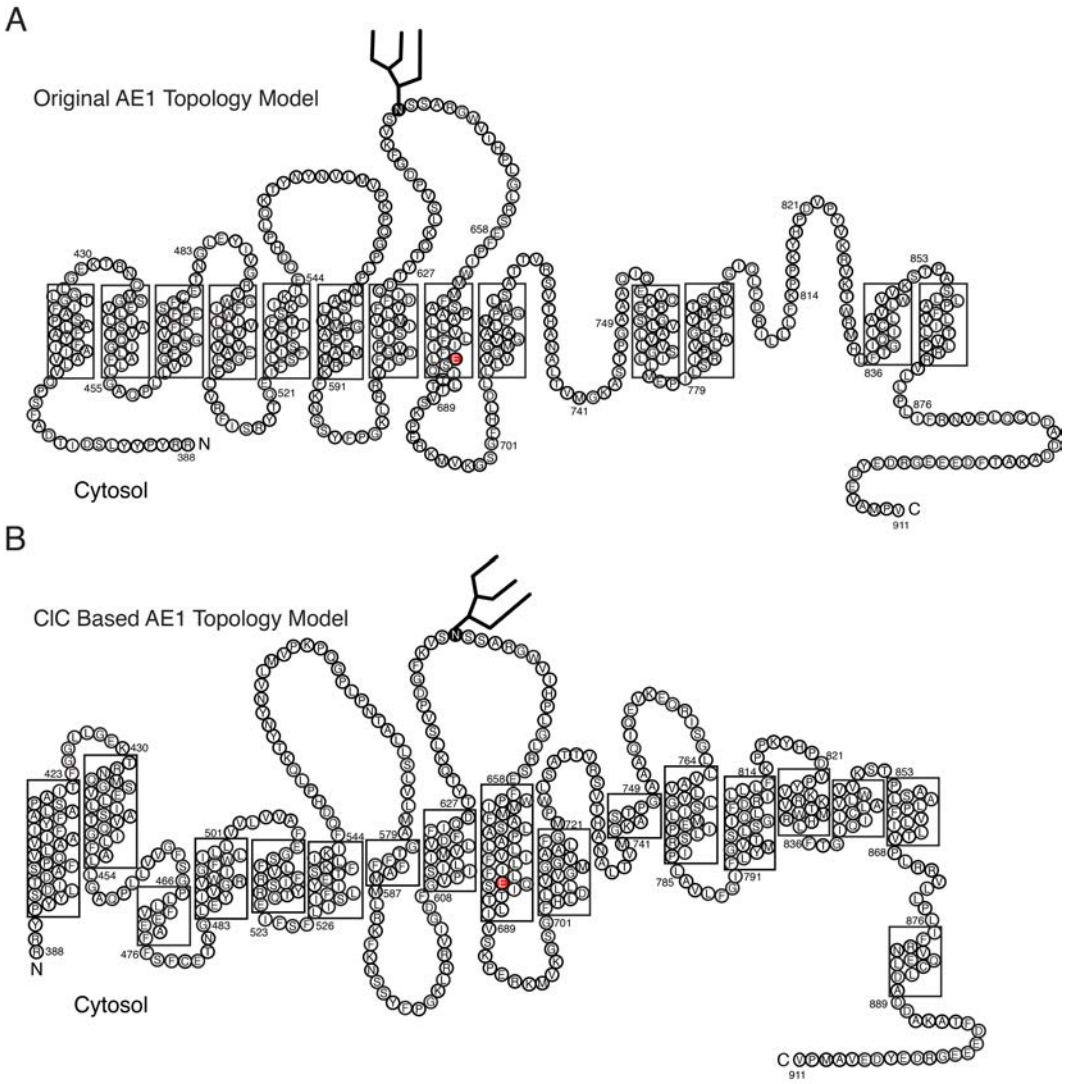

Figure 4.12 Comparison of Human AE1 Topology Models.

The original AE1 topology model (*3*) (A) and the ClC based AE1 topology model (B) are shown. Residue E681, involved in the permeability barrier and anion translocation pathway, is shown in red. AE1 has a single N-linked glycosylation site, N642, which is marked by a large branched structure. N and C indicate N and C-termini, respectively.

Greater discrepancies arise in comparing biochemical evidence for structure of lactose permease and the corresponding crystal structure (*46*). The "fit" of AE1 biochemical data may reflect the relatively small conformational changes expected in a high turnover transporter like AE1. Large conformational changes, evident in the inward and outward states of major facilitator superfamily proteins like lactose permease (*47*), would give rise to biochemical data reflecting a range of conformational states.

In the AE1 homology model the large third extracellular loop (between transmembrane helices G and H) extends into the lipid bilayer (Fig. 4.4). When creating the AE1 sequence alignment during homology modeling (Fig. 4.1), a large gap in the corresponding ClC third extracellular loop was added to accommodate the large AE1 third extracellular loop. Thus, the modeling program (Modeller) could not confidently assign a structure to this region of AE1. While the model shows the region in the bilayer plane, the location of this loop is likely to extend into the extracellular space. Consistent with this notion several blood group antigen sites are present in EC3 (*10, 15*), and must be extracellularly accessible.

Previous cysteine-scanning mutagenesis predicted M663-S690 to be an unusually long helix extending past the intracellular surface of the lipid bilayer (*44, 48*). Consistent with this, the corresponding region in the homology model is transmembrane helix J, which spans the lipid bilayer at an angle, making it longer than average transmembrane helices (Fig. 4.4 A).

Proteolytic cleavage data also provide insight into the AE1 homology model (Table 4.2). Several reported AE1 proteolytic cleavage sites (*8, 9*) are located in aqueous accessible extra-/intra-cellular regions in the AE1 homology model (Fig. 4.4). The cleavage site K743 has been reported as both extracellularly (*7*) and intracellularly (*49*) located, and the AE1 homology model localizes K743 to the extracellular surface of AE1. The remaining sites (R514, F537, L540, and W831) (*8, 9*) are located in the homology model transmembrane helices (Fig. 4.4). Much of the proteolytic cleavage data was obtained upon alkaline treatment of AE1, which denatures AE1 making certain cleavage sites more accessible (*8, 9*). It is likely that the proteolytic cleavage sites within the homology model transmembrane helices are only accessible upon alkaline treatment of AE1, but the studies do not state which cleavage sites are affected by alkaline treatment (*8, 9*). We do note that chymotryptic cleavage site AE1 W831 (located in transmembrane helix O), is predicted to be in the plane of the lipid bilayer on the basis of lack of biotinylation when mutated to cysteine (*3*), strongly suggesting that the proteolysis data is somewhat unreliable in predicting topology.

Additional biochemical data provides insights into the validity of the AE1 model (Table 4.2). Fluorescein maleimide labels AE1 K430 from the extracellular surface (*11*), consistent with the AE1 homology model, where AE1 K430 is in the first extracellular loop. AE1 histidine residues (H547, H734 and H834), accessible to the small hydrophilic probe diethylpyrocarbonate (*13*), localize to extracellular loops (H547 and H734)

or pore lining (H834) in the homology model. Mutagenesis to introduce N-glycosylation acceptor sites at AE1 G428, S633, G637-W648, Q754 and P854 resulted in glycosylation (*14*), indicating extracellular localization. In the AE1 homology model these residues are all located in extracellular loops, consistent with the data. The AE1 inhibitor, H_2DIDS, crosslinks residues K539 and K851 (*8, 50*). In the AE1 homology model both residues are located close to the extracellular surface and the distance between these residues overlaps with the central Cl^- binding site. H_2DIDS is 20 Å long, and in our AE1 model residues K539-K851 are 22 Å apart. Thus, our model is in good agreement with the ability of H_2DIDS to act as an AE1 inhibitor and crosslink K539-K851 of AE1. The AE1 homology model also has a large cytoplasmic C-terminal domain and the carbonic anhydrase II (CAII) binding site (L886-D890) is aqueous accessible (Fig. 4.4) (*39*). Taken together we conclude that the AE1 homology model agrees substantially with biochemical data.

Interestingly, the dimer interface of the AE1 homology model, transmembrane helices H, I, P and Q, (Fig. 4.4) has structural features consistent with the dimer interface of *E. coli* ClC. The dimer interface of ClC is formed by the hydrophobic interactions of small alkyl residues found in transmembrane helices H, I, P and Q (*30*). Mutation of ClC small alkyl residues in the dimer interface (I201, L406, I422 and L434) to bulky tryptophan residues converted ClC to monomers (*30*). While the corresponding residues in the AE1 homology model (F584, Q840, S856 and

P868) are not small alkyl residues, there are several flanking small alkyl residues in the corresponding helices, which may form a hydrophobic AE1 dimer interface (discussed further in Chapter 5).

4.3.2 *E. coli* ClC and AE1 Transport Mechanisms

In the AE1 homology model E508 corresponds to the extracellular glutamate gate of ClC (E148). E508A-AE1 had an increased transport activity compared to WT-AE1 when expressed in HEK293 cells. In contrast, E508A-AE1 had a significantly reduced transport activity when expressed in *X. laevis* oocytes. Differences in the two expression systems, such as changes in plasma membrane lipid composition, membrane protein trafficking and experimental set-up, may account for the difference in E508A-AE1 transport activity. Four mutations at AE1 E508 increased AE1 transport activity. Interestingly, only E508Q had activity similar to WT-AE1, likely due to similarity in size of glutamine and glutamic acid moieties. Thus, the acidic nature of the glutamic acid side chain is not required to maintain normal AE1 transport activity, but the site is very sensitive to changes in the size and shape of the side chain. In contrast, E148Q-ClC, which removes the glutamate carboxylate group, has H^+ uncoupled Cl^- transport (*51*). In both AE1 and ClC mutation of the residue corresponding to the extracellular glutamate results in significant changes in transport activity, however, the type of changes in transport activity observed and mutations that elicit these changes differ between AE1 and ClC. Interestingly, changes in transport activity of the

mutants were not associated with changes in AE1 stoichiometry, which would make the mutants electrogenic transporters (Fig. 4.10).

In the AE1 homology model M586 corresponds to the ClC intracellular glutamate gate. This Met residue is not conserved amongst chicken AE1, human AE2 or human AE3 (Fig. 4.13). Mutation of M586 and the flanking AE1 residues had no effect on the transport activity, nor did mutation of the closest acidic residue in the AE1 amino acid sequence (D607). While the intracellular glutamate gate in ClC is located approximately 15 Å from the central Cl^- binding site, the distance of D607 from this site in the AE1 homology model is almost double (27 Å). For these reasons, D607 of AE1 is unlikely to be involved in the transport mechanism of AE1.

This led us to AE1 E681 as the most likely candidate to fulfill the role of the intracellular glutamate gate. E681 is located 14 Å away from the central Cl^- binding site in the AE1 homology model, which is similar to the distance between the central Cl^- binding site and intracellular glutamate gate of ClC. Modification or mutation of AE1 E681 alters transport activity by inhibiting monovalent anion exchange, increasing divalent anion transport and eliminating H^+ co-transport during Cl^-/SO_4^{2-} exchange (*41, 43, 44*). Mutational studies of E203 in ClC (the intracellular glutamate gate) demonstrated that an ionizable side chain is essential for H^+ coupled Cl^- transport by ClC, but is not required for independent Cl^- transport (*52*).

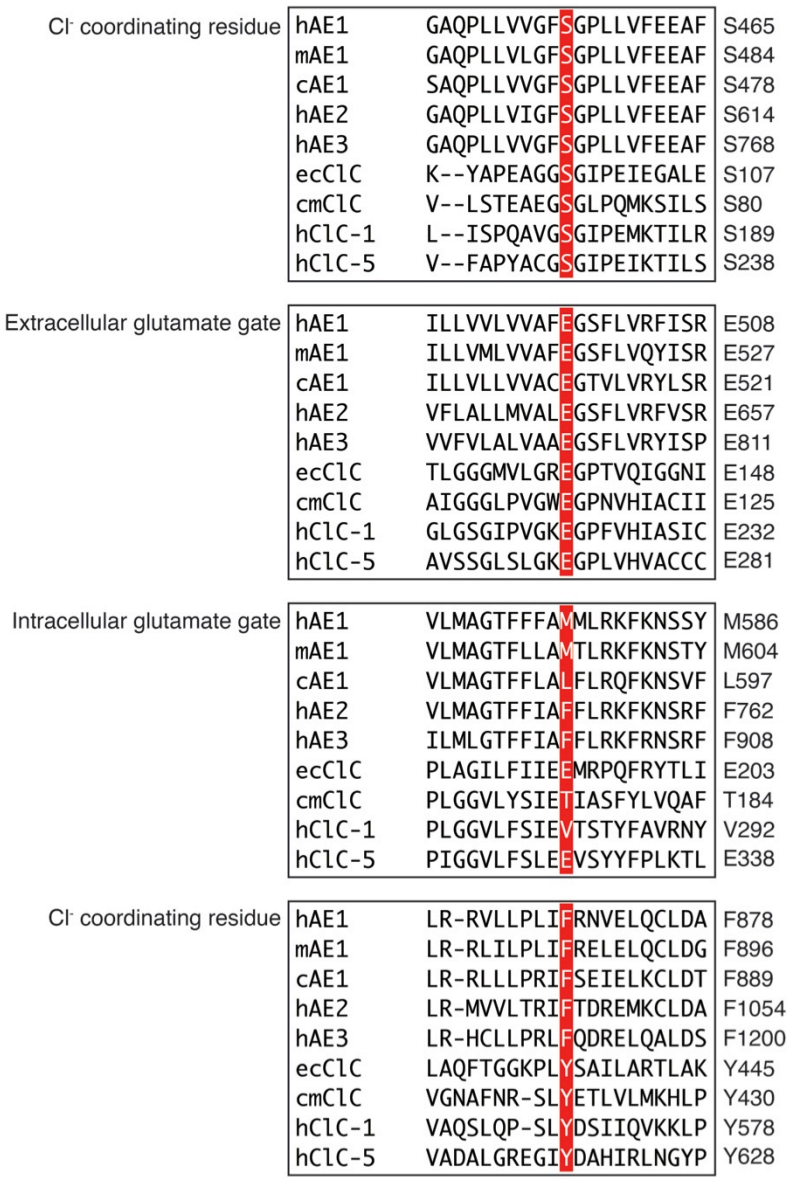

Figure 4.13 Multiple Sequence Alignment of Electroneutral Anion Exchangers and ClC Proteins.

Amino acid sequences of human, mouse and chicken AE1 (hAE1, mAE1, and cAE1, respectively), as well as human AE2 (hAE2) and AE3 (hAE3) were aligned on the basis of sequence similarity, using Clustal W software. The sequences of *E. coli* ClC (ecClC), *C. merolae* ClC (cmClC), human ClC-1 (hClC-1), and human ClC-5 (hClC-5) were aligned with the anion exchanger sequences, on the basis of a published structural alignment (*35*), with minor

manual adjustments. Regions surrounding the four identified key residues in the ClC transport mechanism are indicated. These are: two Cl^- coordinating residues, extracellular glutamate gate and intracellular glutamate gate. Residues involved in the ClC transport mechanism and the corresponding anion exchanger residues are boxed in red, and their residue numbers are indicated on the right.

Interestingly, the intracellular glutamate gate of the ClC family is only conserved amongst $2Cl^-/H^+$ exchanger-type ClC proteins, and is a valine residue in channel-like ClC proteins. Thus, another possibility is that Cl^-/HCO_3^- exchange in AE1 may not require an intracellular glutamate gate similar to channel-like ClC proteins.

S465 in the AE1 homology model corresponds to the ClC Cl^--coordinating residue, S107. AE1 transport activity is highly sensitive to S465 mutagenesis, but alanine substitutions in flanking residues of S465 had no effect on transport activity of AE1, with the exception of the G463A mutation, which may reduce helix flexibility. Mutation of ClC S107, an important chloride-coordinating residue, however, gives rise to Cl^- transport uncoupled from H^+ transport (*53*). No mutagenic studies have been conducted on the residues flanking *E. coli* ClC S107. Taken together the data suggest that AE1 S465 may be an anion coordinating site.

In the AE1 homology model, F878 corresponds to the ClC Cl^- coordinating Y445. Mutagenesis of AE1 F878 to a large alkyl or aromatic side chain had no effect on transport activity, but mutagenesis to a small alkyl or hydroxyl side chain abolished transport activity. A similar pattern of effects was observed for ClC residue Y445 (*29*); mutation of ClC Y445 to a large aromatic residue did not disrupt ClC transport activity, but mutation to a large alkyl residue moderately disrupted H^+ coupled Cl^- transport and mutation to small alkyl, hydroxyl or charged residues severely disrupted of

H^+ coupled Cl^- transport. Thus, the data suggest that AE1 F878 has a similar role as ClC Y445 in the central Cl^- coordination site.

I791 and F792 in the AE1 homology model correspond to ClC I356 and F357, which contribute to the formation of the central Cl^- binding site through their backbone amides. I791A-AE1 had a transport activity similar to WT-AE1. F792A, which is not a conservative AE1 mutation, had a reduced transport activity. Mutations of ClC I356 and F357 might be expected to have no effect on function, but these sites have not been mutated in ClC. Together these data are consistent with a role of I791 and F792 in Cl^- coordination through backbone groups, rather than side chain moieties.

In our analysis of identified candidate transport mechanism residues, all mutations altered AE1 transport activity, but transport stoichiometry was unchanged on the basis of lack of changes in electrical activity. In contrast, mutation of residues critical to the ClC transport mechanism disrupted H^+ coupled Cl^- transport, thus altering the transport stoichiometry. Interestingly, variations of transport stoichiometry and substrate specificity are observed amongst different members of the ClC family. As discussed above, only $2Cl^-/H^+$ ClC exchangers possess an intracellular glutamate gate, which is replaced by a valine residue in Cl^- channels, such as human ClC-1 (Fig. 4.13) (*26*). Interestingly, the $2Cl^-/H^+$ exchanger, *Cyanidioschyzon merolae* ClC (cmClC), has a threonine at the position corresponding to the intracellular glutamate gate (Fig. 4.13) (*27*), possibly suggesting that some ion exchangers (like AE1 and cmClC) either dispense with this gate, or (as

suggested (*27*)) have a gate located elsewhere. In addition, some plant ClC proteins function as NO_3^-/H^+ exchangers, which possess a proline residue at the position of the serine residue involved in Cl^- coordination (*54*).

The AE1 homology model allowed us to identify several residues important in AE1 transport mechanism. Consistent with a role in transport mechanism these residues (human AE1 S465, E508, and Y878) were conserved amongst human, mouse and chicken AE1, as well as the two other human electroneutral Cl^-/HCO_3^- exchangers, AE2 and AE3 (Fig. 4.13). Ideally these residues could be rationalized to provide a transport mechanism for AE1. Unfortunately, the AE1 homology model provides insufficient information on the orientation of amino acid side chains. The role of the key residues identified here will be clarified upon determination of high-resolution structures of AE1 in multiple conformations.

4.3.3 AE1 Functional Studies in the Context of the Homology Model

AE1 cysteine-scanning mutagenesis studies have been valuable in identifying AE1 pore-lining residues (*44, 55*). AE1 E681 was proposed to be located in a transmembrane helix near the intracellular side of the lipid bilayer. Residues on the same helical face as E681 were reactive to sulfhydryl reagents, which altered transport activity (*44*). The AE1 homology model proposes that E681 forms an intracellular glutamate gate, thus residues surrounding E681 are pore lining. Closer to the C-terminus, AE1 F806-C885 contained several pore-lining residues (*55*). Interestingly, F878C-

AE1 had a low transport activity compared to WT-AE1 activity of flanking mutants (*55*), which is consistent with our analysis of AE1 F878 and the surrounding region. Other residues that affect transport activity by mutagenesis or reaction with sulfhydryl reagents (*55*), are located in regions of the AE1 homology model that are extracellular to F878 and line the pore.

Modification of human AE1 H834 (or murine H852) with diethylpyrocarbonate or mutagenesis caused a change in anion transport activity (*56, 57*). Interestingly, the effects of murine H852Q-AE1 on transport activity were reversed upon mutation of K558N, which corresponds to human AE1 K539 (*57*). In the AE1 homology model H834 is located close to the central Cl^- binding site (Fig. 4.5 and 4.12), and K539 is located opposite to this histidine residue in the pore, which is consistent with the observed functional data in human and murine AE1.

Mutations in AE1 can induce a cation leak (*58-61*). L687P-AE1, which has a cation leak (*59*), localizes to the intracellular end of extended helix J and faces into the pore (Fig. 4.4). Alterations at the nearby intracellular gate, E681, could explain induced cation leak. D705Y-AE1 also has an associated cation leak (*59*) and is located in the plane of the lipid bilayer, but is not a pore forming residue in the AE1 homology model. Cation leak inducing S731P, R730C and H734R-AE1 (*59, 62*) are located in the flexible region at the extracellular end of transmembrane helix L (Fig. 4.4). Similarly, R760Q-AE1 (Band 3 Prague II) (*58*) is in the extracellular loop before helix M (Fig. 4.4). Interestingly, cation leak inducing R589H, G609R (which also mis-

targets AE1 to the apical membrane instead of the basolateral membrane), S613F, G701D (*61, 63*) are at the intracellular ends of transmembrane regions H, I and K (Fig. 4.4). Location of cation leak forming residues, in extracellular loops and at helix ends, suggest a possible role of these regions in charge selection of substrates.

Another naturally occurring AE1 mutant, Band 3 HT (P868L), is remarkable for its increased AE1 transport activity (*64*). In the AE1 homology model this residue is located near the flexible region prior to transport mechanism residue F878, where mutations could change the structure of the central Cl^- binding site. Consistent with this possibility, we found mutation of E508 in the central Cl^- binding site increases the transport activity of AE1.

Individuals lacking expression of GPA in their erythrocytes provide insight into the role of GPA in the function of AE1. Lack of GPA in their erythrocytes decreased the transport activity of AE1 by 60% for both monovalent anions (Cl^- and I^-) and SO_4^{2-} (*65*). While the substrate affinity of I^- remains unchanged in erythrocytes lacking GPA, the substrate affinity of SO_4^{2-} increases (*65*). The flexibility of the eosin-5-malemide AE1 binding site was also increased in erythrocytes lacking GPA, without an associated decrease in H_2DIDS binding (*65*). Together this indicates that AE1 adopts a high transport activity structure and low transport activity structure in the presence or absence of GPA, respectively. The Wright blood group antigen is formed by AE1 E658 and GPA residues 58-70 (*66*). In the AE1 homology

model E658 is located at the protein-lipid boundary near the AE1 dimer interface. The position is consistent with a AE1 and GPA interaction site, which may be required to maintain the high transport activity structure of AE1.

4.3.4 AE1 Homology Model in Relation to Other SLC4 Proteins

Analysis of other SLC4 proteins is relevant to the AE1 homology model. The AE1 transport mechanism residues, whose mutations affected transport activity, are conserved across human AE1, AE2 and AE3, suggesting a common transport mechanism across the SLC4 anion exchangers. Several histidine residues in AE2 are critical to maintain transport activity and pH sensitivity (*67*). H1060A-AE2 decreases transport activity, but H1060E-AE2 has a WT level of function (*67*). The homologous residue, AE1 H734, is located in the extracellular flexible region at the N-terminal end of transmembrane helix L in the AE1 homology model (Fig. 4.4 and 4.5). Close inspection of the homology model places this site at the mouth of the ion translocation pore where steric or charge effects could influence transport. Mutation of AE2 H1144 and H1145, homologous to AE1 Y818 and H819, changed extracellular pH sensitivity (*67*). Interestingly, AE2 H1145 mutation also had an increased inhibition by acidic intracellular pH (*67*). In the AE1 homology model these residues are located in the extracellular loop between transmembrane helices N and O, which is consistent with extracellular pH sensing, but inconsistent with AE2 H1145 intracellular pH sensing. Murine AE2 residues involved in intracellular pH activation (R921, R1107) and

residues involved in extracellular pH activation (E888, K889, E981, K982, D1075) (*68*) correspond to sites in intracellular and extracellular loops of the AE1 homology model, respectively.

NBCe1 (SLC4A4), a sodium coupled bicarbonate transporter, and AE1 share 50% sequence similarity in their membrane domains. Cysteine-scanning mutagenesis of NBCe1 Q424-G448 suggested that this region forms part of the transmembrane ion conduction pore (*69*), but the corresponding region of the AE1 homology model (Q404-G428) is not pore lining. Consistent with the AE1 homology model (F423-G428), NBCe1 F443-G448 was predicted to form an extracellular loop (*69*). Interestingly, the region surrounding NBCe1 D764, corresponding to AE1 E681, is pore lining (*70*), which is consistent with AE1 biochemical data and the AE1 homology model. Biochemical data from cysteine-scanning mutagenesis of NBCe1 A800-K967 (*71*) has several differences from the corresponding study of AE1 T727-A891 (*3*), suggesting that NBCe1 has a different C-terminal fold than AE1.

4.3.5 Conclusion

Mutagenic analysis of AE1 presented here supports the AE1 homology model created, using *E. coli* ClC as a structural template. With the exception of the intracellular glutamate gate, transport mechanism residues predicted by the homology model were conserved. Mutation of these residues resulted in drastic changes of the AE1 transport activity. In addition, the AE1 homology model satisfies the majority of the existing biochemical constraints for the AE1 topology. The role of functionally important residues identified

here will be clarified by future high-resolution AE1 structures. Until a high-resolution structure of AE1 is available, the homology model of AE1 developed here will serve as a guide for future functional and structural studies.

4.4 References

1. E. Cordat, J. R. Casey, Bicarbonate transport in cell physiology and disease. *Biochem J* **417**, 423-439 (2009).
2. P. S. Low, Structure and function of the cytoplasmic domain of Band 3: center of erythrocyte membrane-peripheral protein interactions. *Biochim. Biophys. Acta* **864**, 145-167 (1986).
3. Q. Zhu, D. W. Lee, J. R. Casey, Novel topology in C-terminal region of the human plasma membrane anion exchanger, AE1. *J Biol Chem* **278**, 3112-3120 (2003).
4. S. Grinstein, S. Ship, A. Rothstein, Anion transport in relation to proteolytic dissection of Band 3 protein. *Biochim. Biophys. Acta* **507**, 294-304 (1978).
5. D. Zhang, A. Kiyatkin, J. T. Bolin, P. S. Low, Crystallographic structure and functional interpretation of the cytoplasmic domain of erythrocyte membrane band 3. *Blood* **96**, 2925-2933 (2000).
6. X. B. Tang, J. Fujinaga, R. Kopito, J. R. Casey, Topology of the region surrounding Glu681 of human AE1 protein, the erythrocyte anion exchanger. *J Biol Chem* **273**, 22545-22553 (1998).
7. J. Fujinaga, X. B. Tang, J. R. Casey, Topology of the membrane domain of human erythrocyte anion exchange protein, AE1. *J Biol Chem* **274**, 6626-6633 (1999).
8. K. Okubo, D. Kang, N. Hamasaki, M. L. Jennings, Red blood cell band 3. Lysine 539 and lysine 851 react with the same H_2DIDS (4,4'-diisothiocyanodihydrostilbene-2,2'-disulfonic acid) molecule. *J. Biol. Chem.* **269**, 1918-1926 (1994).
9. D. Kang, K. Okubo, N. Hamasaki, N. Kuroda, H. Shiraki, A structural study of the membrane domain of band 3 by tryptic digestion. Conformational change of band 3 in situ induced by alkali treatment. *J Biol Chem* **267**, 19211-19217 (1992).
10. P. Jarolim, H. L. Rubin, D. Zakova, J. Storry, M. E. Reid, Characterization of seven low incidence blood group antigens carried by erythrocyte band 3 protein. *Blood* **92**, 4836-4843 (1998).
11. P. Pal, D. Lebedev, S. Salim, P. A. Knauf, Substrates induce conformational changes in human anion exchanger 1 (hAE1) as observed by fluorescence resonance energy transfer. *Biochemistry* **45**, 6279-6295 (2006).
12. A. Rao, R. A. F. Reithmeier, Reactive sulfhydryl groups of the Band 3 polypeptide from human erythrocyte membranes: Location in the primary structure. *J. Biol. Chem.* **254**, 6144-6150 (1979).
13. X. R. Jin, Y. Abe, C. Y. Li, N. Hamasaki, Histidine-834 of Human Erythrocyte Band 3 Has an Essential Role in the Conformational Changes That Occur during the Band 3-Mediated Anion Exchange. *Biochemistry* **42**, 12927-12932 (2003).

14. M. Popov, J. Li, R. A. Reithmeier, Transmembrane folding of the human erythrocyte anion exchanger (AE1, Band 3) determined by scanning and insertional N-glycosylation mutagenesis. *Biochem. J.* **339**, 269-279 (1999).
15. L. J. Bruce, D. J. Anstee, F. A. Spring, M. J. Tanner, Band 3 Memphis variant II. Altered stilbene disulfonate binding and the Diego (Dia) blood group antigen are associated with the human erythrocyte band 3 mutation Pro854-->Leu. *J Biol Chem* **269**, 16155-16158 (1994).
16. J. R. Casey, R. A. F. Reithmeier, Analysis of the oligomeric state of Band 3, the anion transport protein of the human erythrocyte membrane, by size exclusion high performance liquid chromatography: oligomeric stability and origin of heterogeneity. *J. Biol. Chem.* **266**, 15726-15737 (1991).
17. A. M. Taylor, Q. Zhu, J. R. Casey, Cysteine-directed cross-linking localizes regions of the human erythrocyte anion exchange protein (AE1) relative to the dimeric interface. *Biochem. J.* **359**, 661-668 (2001).
18. J. D. Groves, M. J. Tanner, Structural model for the organization of the transmembrane spans of the human red-cell anion exchanger (band 3; AE1). *Biochem J* **344 Pt 3**, 699-711. (1999).
19. T. Yamaguchi, Y. Ikeda, Y. Abe, H. Kuma, D. Kang, N. Hamasaki, T. Hirai, Structure of the Membrane Domain of Human Erythrocyte Anion Exchanger 1 Revealed by Electron Crystallography. *J Mol Biol* **397**, 179-189 (2010).
20. M. Joanne Lemieux, R. A. Reithmeier, D. N. Wang, Importance of detergent and phospholipid in the crystallization of the human erythrocyte anion-exchanger membrane domain. *J Struct Biol* **137**, 322-332 (2002).
21. D. N. Wang, V. E. Sarabia, R. A. Reithmeier, W. Kuhlbrandt, Three-dimensional map of the dimeric membrane domain of the human erythrocyte anion exchanger, Band 3. *EMBO J.* **13**, 3230-3235 (1994).
22. D. N. Wang, W. Kuhlbrandt, V. Sarabia, R. A. F. Reithmeier, Two-dimensional structure of the membrane domain of human band 3, the anion transport protein of the erythrocyte membrane. *EMBO J.* **12**, 2233-2239 (1993).
23. J. Jiang, N. Magilnick, K. Tsirulnikov, N. Abuladze, I. Atanasov, P. Ge, M. Narla, A. Pushkin, Z. H. Zhou, I. Kurtz, Single particle electron microscopy analysis of the bovine anion exchanger 1 reveals a flexible linker connecting the cytoplasmic and membrane domains. *PLoS One* **8**, e55408 (2013).
24. J. R. Casey, D. M. Lieberman, R. A. F. Reithmeier, Purification and characterization of Band 3 protein. *Methods Enzymol.* **173**, 494-512 (1989).

25. T. J. Jentsch, V. Stein, F. Weinreich, A. A. Zdebik, Molecular structure and physiological function of chloride channels. *Physiol Rev* **82**, 503-568 (2002).
26. R. Dutzler, E. B. Campbell, M. Cadene, B. T. Chait, R. MacKinnon, X-ray structure of a ClC chloride channel at 3.0 Å reveals the molecular basis of anion selectivity. *Nature* **415**, 287-294 (2002).
27. L. Feng, E. B. Campbell, Y. Hsiung, R. MacKinnon, Structure of a eukaryotic CLC transporter defines an intermediate state in the transport cycle. *Science* **330**, 635-641 (2010).
28. R. Dutzler, E. B. Campbell, R. MacKinnon, Gating the selectivity filter in ClC chloride channels. *Science* **300**, 108-112 (2003).
29. M. Walden, A. Accardi, F. Wu, C. Xu, C. Williams, C. Miller, Uncoupling and turnover in a Cl^-/H^+ exchange transporter. *J Gen Physiol* **129**, 317-329 (2007).
30. J. L. Robertson, L. Kolmakova-Partensky, C. Miller, Design, function and structure of a monomeric ClC transporter. *Nature* **468**, 844-847 (2010).
31. M. L. Jennings, H. Passow, Anion transport across the erythrocyte membrane *in situ* proteoysis of Band 3 protein, and cross-linking of proteolytic fragments by 4,4'-diisothiocyano dihydrostilbene-2,2'-disulfonate. *Biochim. Biophys. Acta* **554**, 498-519 (1979).
32. A. Accardi, A. Picollo, CLC channels and transporters: proteins with borderline personalities. *Biochim Biophys Acta* **1798**, 1457-1464 (2010).
33. M. L. Jennings, Structure and function of the red blood cell anion transport protein. *Annu. Rev. Biophys. Biophys. Chem.* **18**, 397-430 (1989).
34. E. Ohana, N. Shcheynikov, D. Yang, I. So, S. Muallem, Determinants of coupled transport and uncoupled current by the electrogenic SLC26 transporters. *J Gen Physiol* **137**, 239-251 (2011).
35. T. Hirai, N. Hamasaki, T. Yamaguchi, Y. Ikeda, Topology models of anion exchanger 1 that incorporate the anti-parallel V-shaped motifs found in the EM structure. *Biochem Cell Biol* **89**, 148-156 (2011).
36. A. Sali, T. L. Blundell, Comparative protein modelling by satisfaction of spatial restraints. *J Mol Biol* **234**, 779-815 (1993).
37. http://ekhidna.biocenter.helsinki.fi/dali_server/. (2013).
38. R. R. Kopito, H. F. Lodish, Primary structure and transmembrane orientation of the murine anion exchange protein. *Nature* **316**, 234-238 (1985).
39. J. W. Vince, R. A. Reithmeier, Identification of the Carbonic Anhydrase II Binding Site in the Cl^-/HCO_3^- Anion Exchanger AE1. *Biochemistry* **39**, 5527-5533 (2000).
40. A. Basu, S. Mazor, J. R. Casey, Distance measurements within a concatamer of the plasma membrane Cl^-/HCO_3^- exchanger, AE1. *Biochemistry* **49**, 9226-9240 (2010).

41. M. N. Chernova, L. Jiang, M. Crest, M. Hand, D. H. Vandorpe, K. Strange, S. L. Alper, Electrogenic sulfate/chloride exchange in *Xenopus* oocytes mediated by murine AE1 E699Q. *J Gen Physiol* **109**, 345-360 (1997).
42. M. L. Jennings, Evidence for a second binding/transport site for chloride in erythrocyte anion transporter AE1 modified at glutamate 681. *Biophys J* **88**, 2681-2691 (2005).
43. M. L. Jennings, J. S. Smith, Anion-proton cotransport through the human red blood cell band 3 protein. Role of glutamate 681. *J. Biol. Chem.* **267**, 13964-13971 (1992).
44. X.-B. Tang, M. Kovacs, D. Sterling, J. R. Casey, Identification of Residues Lining the Translocation Pore of Human AE1, Plasma Membrane Anion Exchange Protein. *J. Biol. Chem.* **274**, 3557-3564 (1999).
45. J. D. Groves, M. J. Tanner, Glycophorin A facilitates the expression of human Band 3-mediated anion transport in *Xenopus* oocytes. *J. Biol. Chem.* **267**, 22163-22170 (1992).
46. J. Abramson, I. Smirnova, V. Kasho, G. Verner, H. R. Kaback, S. Iwata, Structure and mechanism of the lactose permease of *Escherichia coli*. *Science* **301**, 610-615 (2003).
47. I. Smirnova, V. Kasho, J. Y. Choe, C. Altenbach, W. L. Hubbell, H. R. Kaback, Sugar binding induces an outward facing conformation of LacY. *Proc Natl Acad Sci U S A* **104**, 16504-16509 (2007).
48. X. B. Tang, J. Fujinaga, R. Kopito, J. R. Casey, Topology of the region surrounding Glu681 of human AE1 protein, the erythrocyte anion exchanger. *J. Biol. Chem.* **273**, 22545-22553 (1998).
49. H. Kuma, A. A. Shinde, T. R. Howren, M. L. Jennings, Topology of the anion exchange protein AE1: the controversial sidedness of lysine 743. *Biochemistry* **41**, 3380-3388 (2002).
50. D. Bartel, H. Hans, H. Passow, Identification by site-directed mutagenesis of lys-558 as the covalent attachment site of H_2DIDS in the mouse erythroid Band 3 protein. *Biochim. Biophys. Acta* **985**, 355-358 (1989).
51. A. Accardi, C. Miller, Secondary active transport mediated by a prokaryotic homologue of ClC Cl^- channels. *Nature* **427**, 803-807 (2004).
52. H. H. Lim, C. Miller, Intracellular proton-transfer mutants in a CLC Cl^-/H^+ exchanger. *J Gen Physiol* **133**, 131-138 (2009).
53. H. Jayaram, A. Accardi, F. Wu, C. Williams, C. Miller, Ion permeation through a Cl^--selective channel designed from a CLC Cl^-/H^+ exchanger. *Proc Natl Acad Sci U S A* **105**, 11194-11199 (2008).
54. A. De Angeli, D. Monachello, G. Ephritikhine, J. M. Frachisse, S. Thomine, F. Gambale, H. Barbier-Brygoo, The nitrate/proton antiporter AtCLCa mediates nitrate accumulation in plant vacuoles. *Nature* **442**, 939-942 (2006).
55. Q. Zhu, J. R. Casey, The substrate anion selectivity filter in the human erythrocyte Cl^-/HCO_3^- exchange protein, AE1. *J. Biol. Chem.* **279**, 23565-23573 (2004).

56. S. Takazaki, Y. Abe, T. Yamaguchi, M. Yagi, T. Ueda, D. Kang, N. Hamasaki, Mutation of His 834 in human anion exchanger 1 affects substrate binding. *Biochim Biophys Acta* **1798**, 903-908 (2010).
57. S. Müller-Berger, D. Karbach, J. Konig, S. Lepke, P. G. Wood, H. Appelhans, H. Passow, Inhibition of mouse erythroid band 3-mediated chloride transport by site-directed mutagenesis of histidine residues and its reversal by second site mutation of Lys 558, the locus of covalent H_2DIDS binding. *Biochemistry* **34**, 9315-9324 (1995).
58. L. J. Bruce, H. C. Robinson, H. Guizouarn, F. Borgese, P. Harrison, M. J. King, J. S. Goede, S. E. Coles, D. M. Gore, H. U. Lutz, R. Ficarella, D. M. Layton, A. Iolascon, J. C. Ellory, G. W. Stewart, Monovalent cation leaks in human red cells caused by single amino-acid substitutions in the transport domain of the band 3 chloride-bicarbonate exchanger, AE1. *Nat Genet* **37**, 1258-1263 (2005).
59. H. Guizouarn, S. Martial, N. Gabillat, F. Borgese, Point mutations involved in red cell stomatocytosis convert the electroneutral anion exchanger 1 to a non-selective cation conductance. *Blood* **110**, 2158-2165 (2007).
60. J. C. Ellory, H. Guizouarn, F. Borgese, L. J. Bruce, R. J. Wilkins, G. W. Stewart, Review. Leaky Cl^--HCO_3^- exchangers: cation fluxes via modified AE1. *Philos Trans R Soc Lond B Biol Sci* **364**, 189-194 (2009).
61. S. Walsh, F. Borgese, N. Gabillat, R. Unwin, H. Guizouarn, Cation transport activity of anion exchanger 1 mutations found in inherited distal renal tubular acidosis. *Am J Physiol Renal Physiol* **295**, F343-350 (2008).
62. A. K. Stewart, P. S. Kedar, B. E. Shmukler, D. H. Vandorpe, A. Hsu, B. Glader, A. Rivera, C. Brugnara, S. L. Alper, Functional characterization and modified rescue of novel AE1 mutation R730C associated with overhydrated cation leak stomatocytosis. *Am J Physiol Cell Physiol* **300**, C1034-1046 (2011).
63. N. Rungroj, M. A. Devonald, A. W. Cuthbert, F. Reimann, V. Akkarapatumwong, P. T. Yenchitsomanus, W. M. Bennett, F. E. Karet, A novel missense mutation in AE1 causing autosomal dominant distal renal tubular acidosis retains normal transport function but is mistargeted in polarized epithelial cells. *J Biol Chem* **279**, 13833-13838 (2004).
64. L. J. Bruce, M. M. B. Kay, C. Lawrence, M. J. A. Tanner, Band 3 HT, a human red cell variant associated with acanthocytosis and increased anion transport, carries the mutation Pro-868-->Leu in the membrane domain of band 3. *Biochem. J.* **293**, 317-320 (1993).
65. L. J. Bruce, R. J. Pan, D. L. Cope, M. Uchikawa, R. B. Gunn, R. J. Cherry, M. J. Tanner, Altered structure and anion transport properties of band 3 (AE1, SLC4A1) in human red cells lacking glycophorin A. *J Biol Chem* **279**, 2414-2420 (2004).
66. L. J. Bruce, M. J. Tanner, Structure-function relationships of band 3 variants. *Cell Mol Biol (Noisy-le-grand)* **42**, 953-973 (1996).

67. A. K. Stewart, C. E. Kurschat, D. Burns, N. Banger, R. D. Vaughan-Jones, S. L. Alper, Transmembrane domain histidines contribute to regulation of AE2-mediated anion exchange by pH. *Am J Physiol Cell Physiol* **292**, C909-918 (2007).
68. A. K. Stewart, C. E. Kurschat, S. L. Alper, Role of nonconserved charged residues of the AE2 transmembrane domain in regulation of anion exchange by pH. *Pflugers Arch* **454**, 373-384 (2007).
69. Q. Zhu, R. Azimov, L. Kao, D. Newman, W. Liu, N. Abuladze, A. Pushkin, I. Kurtz, NBCe1-A Transmembrane Segment 1 Lines the Ion Translocation Pathway. *J Biol Chem* **284**, 8918-8929 (2009).
70. S. D. McAlear, M. O. Bevensee, A cysteine-scanning mutagenesis study of transmembrane domain 8 of the electrogenic sodium/bicarbonate cotransporter NBCe1. *J Biol Chem* **281**, 32417-32427 (2006).
71. Q. Zhu, L. Kao, R. Azimov, N. Abuladze, D. Newman, A. Pushkin, W. Liu, C. Chang, I. Kurtz, Structural and functional characterization of the C-terminal transmembrane region of NBCe1-A. *J Biol Chem* **285**, 37178-37187 (2010).

Chapter 5: Identification of AE1 Residues Involved in the Dimer Interface

5.1 Introduction

AE1 is an electroneutral Cl^-/HCO_3^- exchanger expressed as two different transcript variants (*1*). The full-length erythrocyte AE1 variant maximizes the CO_2 carrying capacity of the blood and maintains the signature biconcave shape of the erythrocyte (*1, 2*). The N-terminally truncated kidney AE1 variant, expressed basolaterally in type-A intercalated cells, prevents systemic acidosis by reabsorbing bicarbonate from urine back into the bloodstream (*1*). AE1 is composed of two distinct domains, the 43 kDa N-terminal cytoplasmic domain and the 52 kDa membrane domain, containing 12-14 transmembrane spanning segments (*3*). A recent AE1 EM structure suggested that the membrane domain shares a common protein fold with ClC chloride channels (*4*). Thus, a homology model of AE1 was created, using *E. coli* ClC as a structural template (Fig. 4.2 and 4.3).

All published AE1 EM structures are dimeric, however, AE1 exists in erythrocytes as a mixture of dimers and tetramers (*5*). Interestingly, erythrocyte AE1 tetramers only form under conditions where AE1 is bound to ankyrin and forms a multimeric protein complex (*6, 7*). Size exclusion chromatography of purified erythrocyte AE1, in the detergent $C_{12}E_8$, reveals that 70% of the protein is dimeric, and the remaining 30% of the protein is tetrameric or aggregated (*8*). The AE1 dimer is very stable, as monomeric AE1 only exists under protein denaturing conditions (*8*).

Both the N-terminal cytoplasmic domain and membrane domain of AE1 form dimers independently (*8, 9*). The N-terminal cytoplasmic

dimerization domain consists of a dimerization arm (residues 314-344), which forms backbone hydrogen bonds between two monomers (*9*). A hydrophobic leucine core further stabilizes the AE1 cytoplasmic dimerization domain (*9*). In contrast to full-length AE1, which forms dimers and tetramers, the membrane domain exclusively forms dimers (*8*). This suggests that formation of AE1 tetramers is driven by N-terminal cytoplasmic domain interactions, not the membrane domain (*8*).

Studies investigating the helical packing of the AE1 membrane domain suggested certain AE1 regions to be located at or near the dimer interface (*10, 11*). A helical packing model of AE1, created using data collected from co-expression of AE1 fragments, suggested that residues G361-Y553 and M696-Y824 form the core of the AE1 membrane domain structure, which also includes the dimer interface (*10*). Also, AE1 transmembrane spanning regions T431-G456, G456-Y486 and G565-S595 were found to be at most one helix away from the dimer interface, using chemical crosslinking of AE1 introduced cysteine mutants (*11*).

Similar to the AE1 membrane domain, *E. coli* ClC also forms stable dimers (*12*). The dimer interface of *E. coli* ClC is formed by four transmembrane helices (residues P193-E203, S214-N233, P405-T416, and I422-F438), which all have one helical face that is comprised of small hydrophobic residues and orientated to face the dimer interface (*12*). These helices create a large flat hydrophobic surface, which is 1,200 $Å^2$ in size, that drives ClC dimerization (*12*). A study investigating *E. coli* ClC dimerization

found that tryptophan point mutations of several hydrophobic residues in the dimeric interface helices disrupted the integrity of ClC dimers, by introducing unfavorable steric interactions in the dimer interface (*13*). The double *E. coli* ClC point mutant, I201W/I422W, was exclusively monomeric and able to preform $2Cl^-/H^+$ exchange (*13*). In addition, the monomeric ClC mutant structure was essentially the same as wild-type (WT) ClC with the exception of the altered orientation of the N-terminal cytoplasmic helix (*13*). While this method successfully disrupted the ClC dimer interface, the thermodynamics of the disruption are still not understood (*13*).

Here, the dimer interface of AE1 was examined, using a similar strategy as the monomeric ClC mutant study, in order to disrupt the dimer interface and create monomeric AE1. The AE1 homology model, created using *E. coli* ClC as a template, guided tryptophan mutation of AE1 residues proposed to form the dimer interface. In order to nullify oligomerization effects of the AE1 N-terminal cytoplasmic domain, an AE1 membrane domain construct was created as a background to introduce tryptophan mutations. AE1 tryptophan mutants were monitored for expression under a variety of growth conditions and oligomeric state using chemical crosslinking.

5.2 Results

5.2.1 Expression and Functional Activity of AE1MD346

The AE1 N-terminal cytoplasmic domain itself is capable of dimerization (*9*). Since the goal of this study is to assess the role of membrane domain residues in AE1 dimerization, we designed a N-terminally

truncated AE1 construct. The AE1 cytoplasmic domain crystal structure reveals a dimerization arm, consisting of amino acids 314-344, that forms AE1's N-terminal cytoplasmic dimerization region (*9*). Thus, an AE1 membrane domain construct starting at residue R346 (AE1MD346) was created, since this residue is C-terminal to the dimerization arm of the N-terminal cytoplasmic domain. In addition, AE1MD346 had a higher protein accumulation than an AE1 membrane domain construct starting at residue R388 (Fig. 5.1), which was the site previously used in overexpression and purification of AE1 from *S. cerevisiae* (*14*).

To determine whether AE1MD346 would be a suitable background to test the oligomeric state of different AE1 mutants, its transport activity was measured and compared to full-length WT-AE1 (Fig. 5.2). HEK293 cells were transiently transfected with cDNA encoding AE1MD346 or WT-AE1. Cells were loaded with the pH sensitive fluorescent dye, BCECF-AM, and alternately perfused with Cl^--containing and Cl^--free Ringer's buffer. Transport activity was calculated by the slope of the initial alkalinization observed upon switching to Cl^--free Ringer's buffer, and values were expressed relative to WT-AE1 activity. The transport activity of AE1MD346 was significantly reduced (72±5%) compared to WT-AE1 (Fig. 5.2). Transport activity was not corrected for protein expression or cell surface processing, however, and the difference observed may arise because of these factors. The inset immunoblot also shows that AE1MD346 migrates at a molecular weight corresponding to 50 kDa and accumulates to levels similar

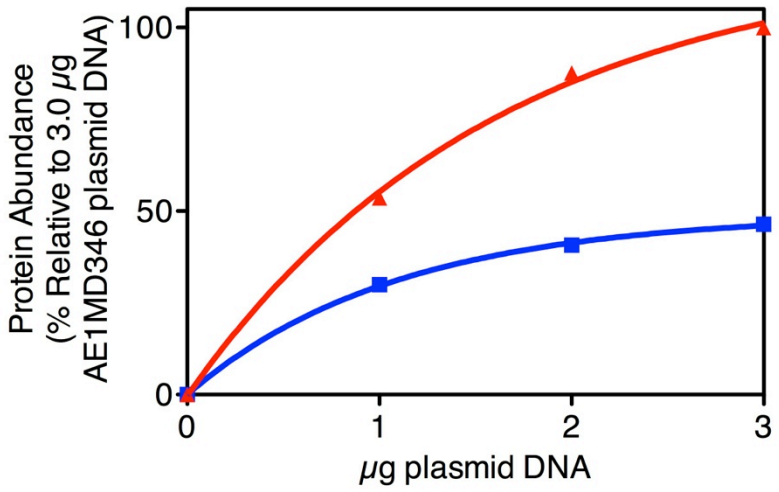

Figure 5.1 Protein Abundance of AE1MD346 and AE1MD388.

HEK293 cells were transiently transfected with varying amounts of cDNA encoding AE1MD346 (red) or AE1MD388 (blue). Cell lysates were harvested and samples were resolved by SDS-PAGE. Immunoblots were quantified by densitometry and values were expressed as a percentage of AE1MD346 abundance when HEK293 cells were transfected with 3.0 μg of corresponding cDNA (n=1).

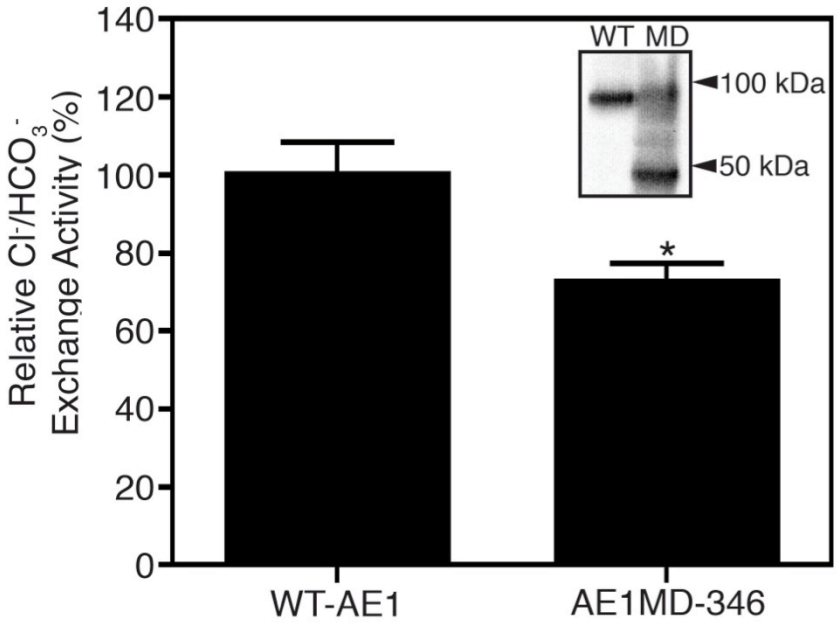

Figure 5.2 Transport Activity of AE1MD346.

HEK293 cells, grown on glass coverslips, were transiently transfected with cDNA encoding WT-AE1 or AE1MD346. Cells were loaded with the pH sensitive dye, BCECF-AM, and fluorescence was monitored. Transport rates were calculated by the rate of alkalinization induced upon switching from chloride-containing to chloride-free Ringer's buffer. The bar graph shows transport rates plotted relative to WT (0.74 dpH_i/dt). Inset a representative immunoblot, using an anti-AE1 antibody (IVF12), indicates WT-AE1 (WT) and AE1MD346 (MD) and the positions of molecular weight markers. Error bars represent SE (n=4-6), and * indicates a significance difference from WT ($p<0.05$).

to WT-AE1 (Fig. 5.2). AE1MD346 is thus not grossly altered in its expression or functional activity. Therefore, AE1MD346 is a suitable background for the expression of AE1 mutants and monitoring their oligomeric state.

5.2.2 Identification of Possible AE1 Residues Involved in the Dimeric Interface

The AE1 homology model, created using *E. coli* ClC as a structural template, was used as a guide for mutagenic analysis (Chapter 4). In the AE1 homology model helices H, I, P and Q correspond to the helices in ClC that form the dimer interface (Fig. 5.3). I201W, L406W, I422W, and L434W-ClC all disrupted the dimer interface of ClC to varying degrees, as revealed by the monomeric state of these ClC mutants (*13*). Using the AE1 homology model, AE1 F584, Q840, S856, and P868 correspond to the residues in ClC that were identified as critical to maintain a stable dimeric state (Fig. 5.3). None of these AE1 residues, however, have small hydrophobic side chain moieties, which are the driving force for ClC dimerization, suggesting that these residues are not involved in dimerization. Small changes in the register of the AE1/ClC amino acid sequence alignment would cause rotation of transmembrane helices, resulting in a shift in the position of residues in the model. Thus, we included in our analysis not only the AE1 residues corresponding to ClC dimer interface residues, but also flanking residues (Fig. 5.3). The majority of AE1 flanking residues have small hydrophobic side chain moieties, similar to ClC dimer interface residues. Using the same strategy as the ClC dimer interface mutagenic study, AE1 residues,

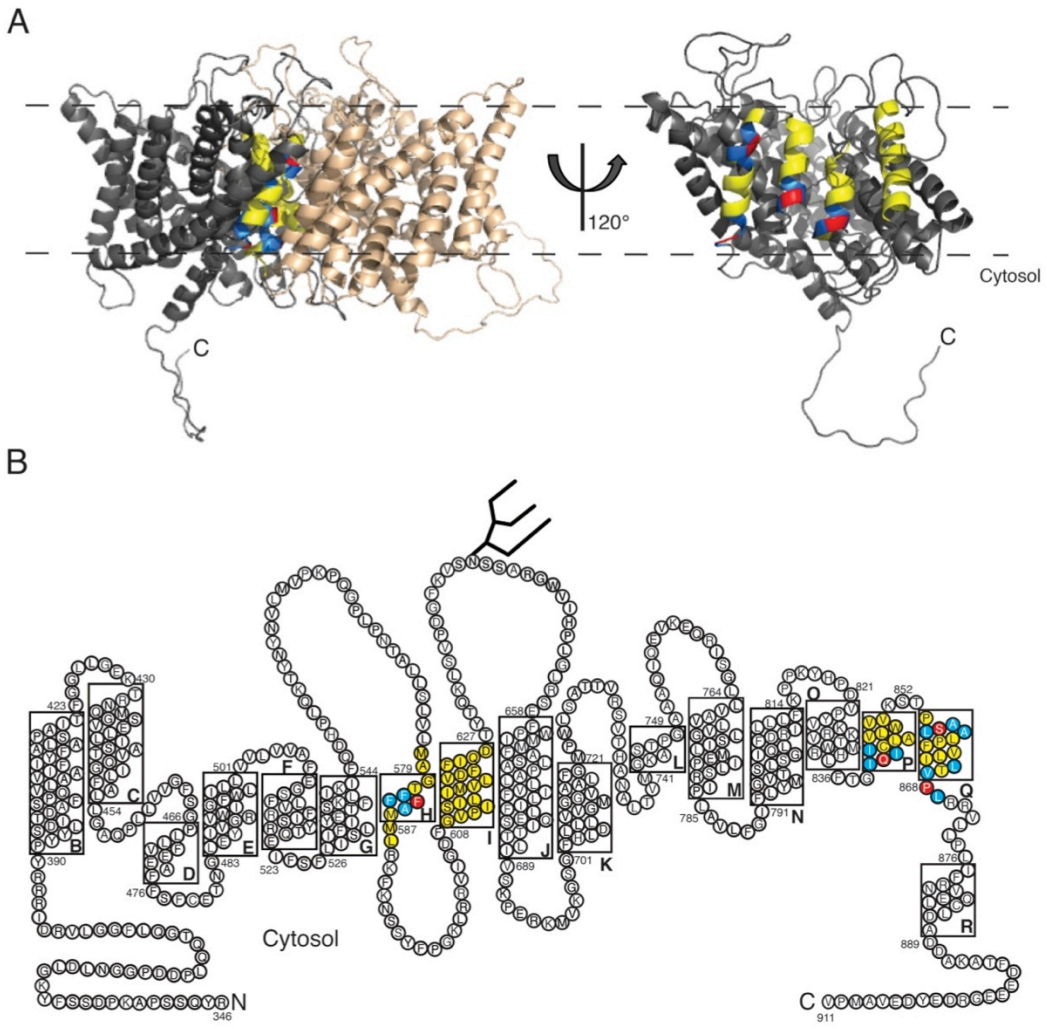

Figure 5.3 Identification of Possible Dimer Interface Residues in AE1.

Helices of the AE1 homology model (residues M578-L588, G609-D626, I839-V850, and P854-L869), corresponding to helices involved in the dimer interface of ClC, are colored yellow. AE1 residues, corresponding to positions of ClC tryptophan mutants that disrupted the dimer interface, are colored red and flanking residues are colored blue. (A) An AE1 homology model dimer (left) and monomer (right) are shown. The AE1 monomer is shown in grey, and the second monomer of the AE1 dimer is shown in beige. Dashed lines indicate the approximate boundaries of the lipid bilayer, and C indicates the C-terminus. The dimer interface of the AE1 monomer (right) faces the reader. (B) A topology model of AE1MD346, which is based on the three-

dimensional AE1 homology model, is labeled with transmembrane spanning helices labeled from B-R. The N-linked glycosylation site is represented by a large branched structure and N and C indicate the N- and C-termini, respectively.

corresponding to ClC dimer interface residues, and flanking AE1 residues were mutated to tryptophan residues to assess their role in dimerization.

5.2.3 Abundance of AE1 Introduced Tryptophan Mutants

AE1MD346 introduced tryptophan mutants were expressed in HEK293 cell by transient transfection. Cell lysates were prepared and analyzed by immunoblots. Densitometry of immunoblots revealed varying levels of AE1MD346 introduced tryptophan mutant abundance (Fig. 5.4). AE1 mutants, corresponding to the regions surrounding ClC I201 and L406, all accumulated to significantly reduced levels compared to AE1MD346. F583W, F584W, I839W, I841W, and I842W had moderate abundance levels relative to AE1MD346 of 40±20%, 61±9%, 40±10%, 48±3%, and 61±9% respectively. In contrast, F582W, A585W, and Q840W had minimal abundance levels relative to AE1MD346 of 13±5%, 2±1% and 8±2%, respectively. All AE1 mutants, corresponding to the region surrounding ClC I422, had abundance levels similar to AE1MD346. AE1 mutants, corresponding to the region surrounding ClC L434, had protein abundance values that were not significantly different from AE1MD346 (L865W) and significantly reduced (V867W, P868W and L869W at 18±9%, 60±6% and 30±10%, respectively).

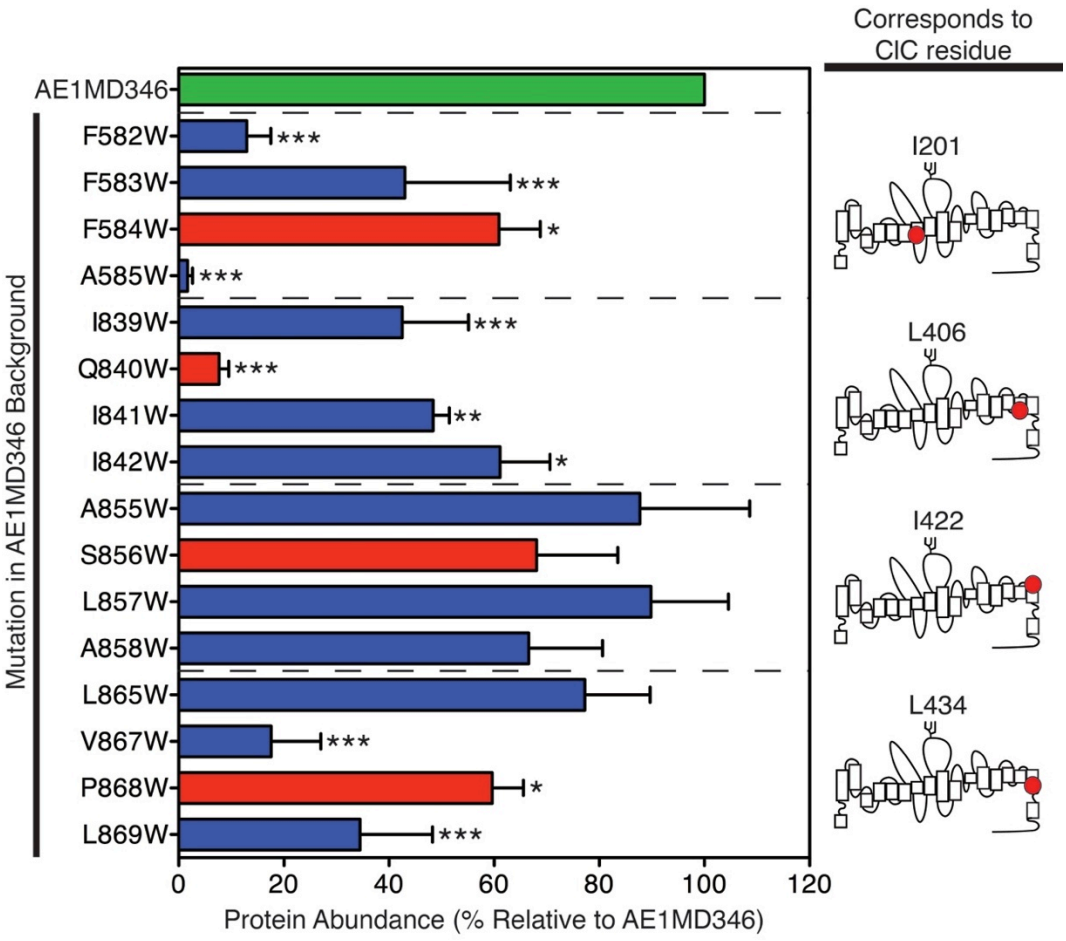

Figure 5.4 Abundance of AE1MD346 Introduced Tryptophan Point Mutants.

HEK293 cells were transiently transfected with cDNA encoding either AE1MD346 or an AE1MD346 introduced tryptophan mutant. Cell lysates were harvested and samples were resolved by SDS-PAGE. Immunoblots were quantified by densitometry and values were expressed as a percentage of AE1MD346 (green) expression. AE1 introduced tryptophan mutants, corresponding to ClC residues critical to dimer interface interactions, are colored red, and flanking AE1 introduced tryptophan mutants are colored blue. Error bars represent SE (n=3-4) and *, ** and *** indicates a significant difference from AE1MD346 ($p<0.05$, $p<0.01$ and $p<0.001$, respectively).

Attempts were made to increase the steady-state level of expression of AE1 introduced tryptophan mutants, since the majority of the mutants had significantly reduced protein abundance (Fig. 5.4). In some cases growth at low temperature allows mis-folded membrane proteins to accumulate (*15*). In addition, several small molecule chemical chaperones, such as dimethyl sulfoxide (DMSO), have a similar effect on increasing the accumulation of membrane proteins (*16*). These approaches have been used with some success for various AE1 mutants (*17*). Thus, different incubation conditions for HEK293 cells, transiently transfected with WT or mutant AE1MD346, were investigated.

Total AE1 protein abundance was measured in transfected HEK293 cells grown at 37 °C or 30 °C in medium with or without 1% DMSO (Fig. 5.5). Protein abundance of AE1 variants was corrected for total protein abundance (effectively normalizing for amount of protein per cell), using the cytosolic control protein, GAPDH, and expressed as a percentage of AE1 abundance at 37 °C (in growth medium without 1% DMSO). These results are preliminary, since some of the AE1 introduced tryptophan mutants have not been investigated (I842W and L869W) and the remaining mutants only have one or two replicates completed thus far.

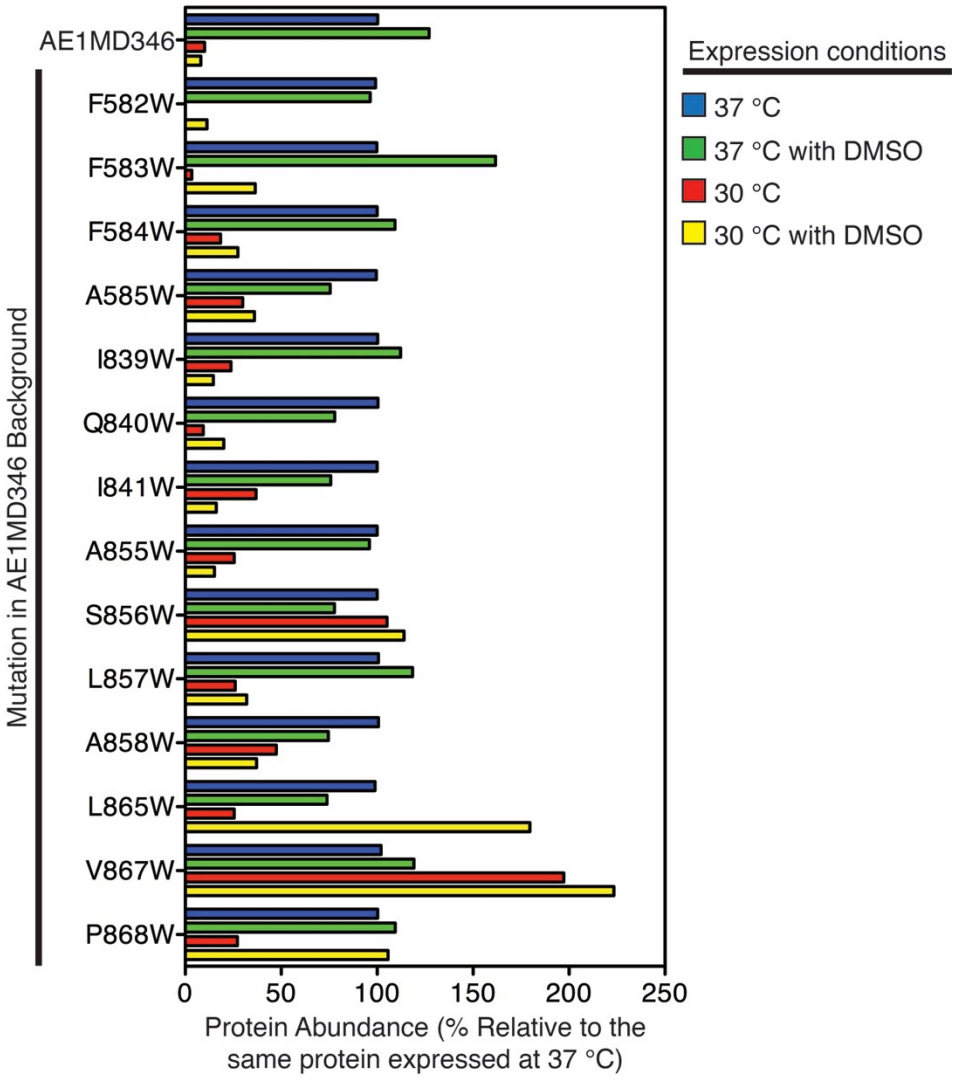

Figure 5.5 Effect of Growth Conditions on AE1MD346 Introduced Tryptophan Mutant Abundance Level.

HEK293 cells were transiently transfected with cDNA encoding either AE1MD346 or an AE1MD346 introduced tryptophan mutant. Cells were incubated for 48 h at 37 °C with (blue) and without (green) DMSO, and at 30 °C with (red) and without (yellow) DMSO. Cell lysates were harvested and samples were resolved by SDS-PAGE. Immunoblots were quantified by densitometry and values were expressed as a percentage of 37 °C (without DMSO) abundance relative to each protein (n=1-2).

In general HEK293 cells, expressing WT or mutant AE1MD346, grown at 30 °C had a dramatic decrease (0-60%) in overall AE1 protein abundance compared to cells grown at 37 °C (Fig. 5.5). The only exceptions were S856W and V867W-AE1MD346, which had overall AE1 protein abundance levels of 105% and 197% when HEK293 cells were grown at 30 °C compared to 37 °C. The addition of 1% DMSO to HEK293 cell growth medium (at 30 °C or 37 °C) had little effect on the total abundance of WT or mutant AE1MD346 (Fig. 5.5). F583W-AE1MD346 was the only mutant to have a substantial increase in AE1 abundance (162%) upon the addition of 1% DMSO, when HEK293 cells were grown at 37 °C (Fig. 5.5). In addition, there were only two AE1 mutants (L865W and P868W) which had an increase in AE1 abundance (180% and 106%, respectively) with DMSO at 30 °C. P868W-AE1MD346 abundance, at 30 °C with DMSO, did not have an increase in AE1 expression when compared to expression in HEK293 cells grown at 37 °C (with or without DMSO). Taken together, the preliminary results do not provide strong support to alter standard HEK293 cell growth conditions (37 °C in medium without DMSO) to increase expression of the AE1MD346 introduced tryptophan mutants.

5.2.4 Assessing Oligomeric State of AE1 Introduced Tryptophan Mutants

The oligomeric state of AE1MD346 introduced tryptophan mutants was assessed by chemical crosslinking, using DSP. DSP is a membrane permeant crosslinker, which reacts with primary amines and contains a

reducing agent cleavable disulfide bond. Multiple DSP concentrations (0-2 mM) were tested to determine the amount of DSP needed to fully crosslink dimeric WT-AE1MD346 (Fig. 5.6). The amount of DSP crosslinked AE1 dimers was assessed by densitometry of immunoblots (Fig. 5.6 A). AE1MD346 monomer is approximately 50 kDa and AE1MD346 dimer is approximately 100 kDa. The percentage of AE1 dimer was calculated by dividing the amount of dimer by the total amount of AE1 (dimer and monomer). Samples left untreated (-, green) after DSP crosslinking represent the oligomeric state of AE1 (Fig. 5.6). Samples treated with DTT (+, red), which cleaves the disulfide bond in DSP, were used as a control to ensure higher molecular weight AE1 oligomers formed as a result of DSP crosslinking (Fig. 5.6). Increasing concentrations of DSP crosslinker did not affect the percentage of AE1MD346 dimer observed (approximately 25%) in samples treated with DTT (Fig. 5.6 B). In contrast, the percentage of AE1MD346 dimer in untreated samples increased with higher concentrations of DSP crosslinker (Fig. 5.6 B). The maximal amount of AE1MD346 dimer observed upon DSP crosslinking, approximately 80%, was attained at 1-2 mM DSP. Thus, 1 mM DSP was used to assess the oligomeric state of AE1MD346 introduced tryptophan mutants.

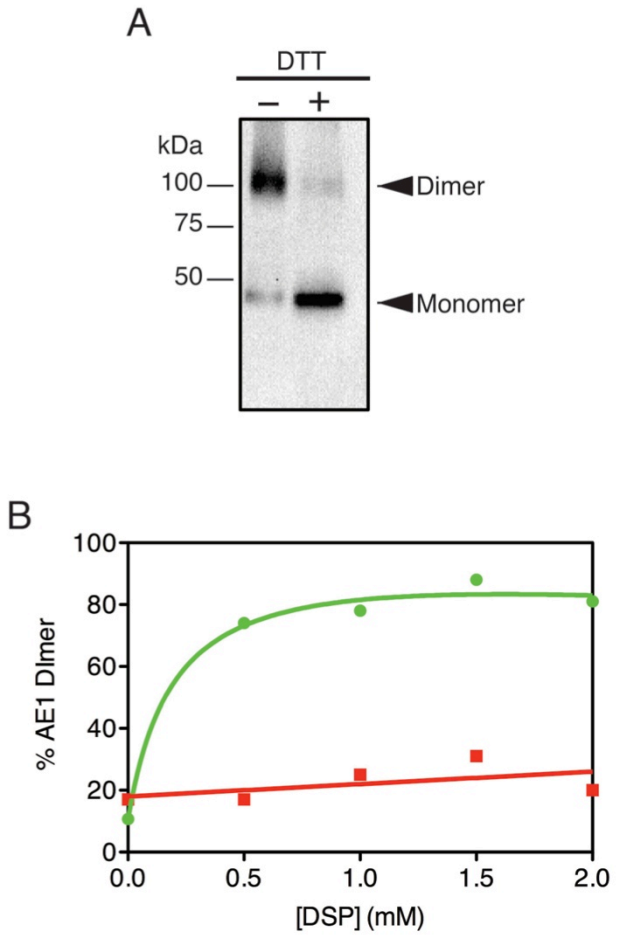

Figure 5.6 Chemical Crosslinking of AE1MD346.

HEK293 cells, transiently transfected with cDNA encoding AE1MD346, were incubated with 0-2 mM DSP crosslinker. Cell lysates were harvested and incubated with (red) or without (green) 50 mM DTT, prior to separation by SDS-PAGE. (A) A representative immunoblot shows AE1MD346 crosslinked with 1 mM DSP. AE1 dimers and monomers are indicated. (B) Immunoblots were quantified by densitometry and percent of AE1 dimer was calculated as $AE1_{dimer}/(AE1_{dimer} + AE1_{monomer})*100\%$. The percent of AE1 dimer was plotted against the concentration of DSP crosslinker (n=1).

Crosslinking of WT-AE1MD346 with 1 mM DSP gave 82±3% AE1 dimer (Fig. 5.7). All AE1MD346 introduced tryptophan mutants crosslinked with 1 mM DSP had AE1 dimer percentage values that were not significantly different from WT-AE1MD346 (Fig. 5.7), which indicates that none of the mutations disrupted the AE1 dimer interface to create AE1 monomers. All DSP crosslinked samples treated with DTT were still composed of 30±2% AE1 dimer (Fig. 5.7). Together, this indicates that the stable dimer interface is intact in AE1MD346 and all of the introduced tryptophan mutants.

5.3 Discussion

In this study an AE1 membrane domain construct, which is suitable for AE1 membrane domain dimer interface investigations, was successfully created and characterized. Several AE1 residues, possibly involved in dimer formation, were identified using the AE1 homology constructed previously (Fig. 4.2 and 4.3). To assess the role of these residues in AE1 dimerization, tryptophan mutations were introduced at these sites. Expression and oligomeric state of the AE1 tryptophan mutants was investigated. Unfortunately, the data was not able to conclusively identify AE1 residues involved in the dimer interface.

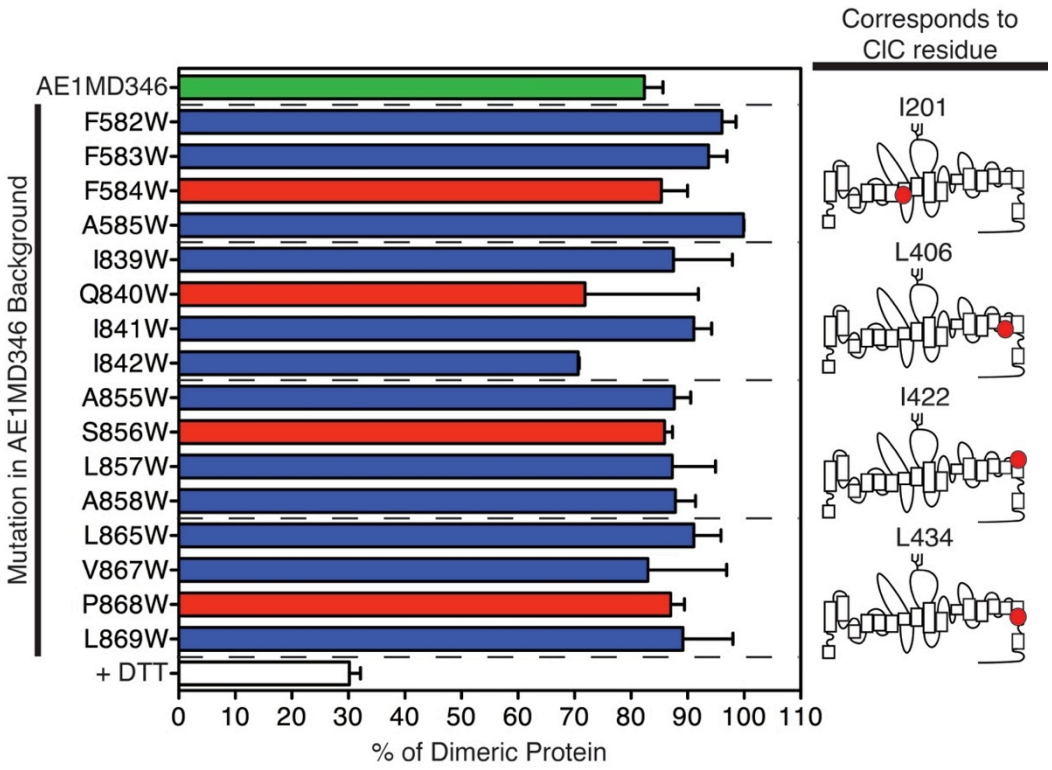

Figure 5.7 Chemical Crosslinking of AE1MD346 Introduced Tryptophan Mutants.

HEK293 cells were transiently transfected with cDNA encoding AE1MD346 or an AE1MD346 introduced tryptophan mutant. Cells were treated with 1 mM DSP and lysates were recovered. Samples were incubated with or without 50 mM DTT, and resolved by SDS-PAGE. Immunoblots were quantified by densitometry and percent of AE1 dimer was calculated as $AE1_{dimer}/(AE1_{dimer} + AE1_{monomer})*100\%$. AE1MD346 is colored green. The data from all samples treated with DTT were pooled, termed +DTT, and colored white. AE1 introduced tryptophan mutants, corresponding to ClC residues critical to dimer interface interactions, are colored red, and flanking AE1 introduced tryptophan mutants are colored blue. Error bars represent SE (n=3-13).

5.3.1 Comparison of AE1MD346 with Other AE1 Membrane Domain Variants

The AE1 membrane domain construct, AE1MD346, had a significantly reduced transport activity compared to WT-AE1. Interestingly, other AE1 membrane domain variants, created by mutagenesis or proteolysis, have similar transport activities as full length WT-AE1 (*14, 18, 19*). Thus, the reduction in AE1MD346 transport activity is likely due to differences in AE1 protein accumulation and cell surface processing, which were not accounted for here. While AE1MD346 is an appropriate background to study the dimer interface, different AE1 membrane domain constructs with alternate N-terminal truncation sites may accumulate to higher levels, enabling future AE1 dimer interface studies.

5.3.2 The AE1 Homology Model Dimer Interface

Using the AE1 homology model as a guide (Fig. 4.2 and 4.3), transmembrane helix residues M578-L588, G609-D626, I839-V850, and P854-L869 were predicted to form the dimer interface. An AE1 cysteine crosslinking study identified AE1 transmembrane helices between residues T431-G456, G456-Y486 and G565-S595 as being at most one helix away from the dimer interface (*11*). The region G565-S595 found to be at most one helix away from the dimer interface, by chemical crosslinking (*11*), overlaps with the region M578-L588, which is a dimer interface forming transmembrane helix in the AE1 homology model (Fig. 4.2 and 4.3).

In contrast, the regions T431-G456 and G456-Y486 are located approximately 30-40 Å away from the AE1 dimer interface in the AE1 homology model (Fig. 4.2 and 4.3), which is greater than one helix away from dimer interface, as predicted by chemical crosslinking (*11*). Interestingly, these residues are located near the protein lipid bilayer interface in the AE1 homology model.

Residues in the AE1 homology model dimer interface that correspond to *E. coli* ClC tryptophan mutation sites, which disrupt the ClC dimer interface (*13*), were identified. These AE1 residues were not similar to the small hydrophobic residues found in ClC dimeric interface. AE1 residues flanking these sites, however, were mostly small hydrophobic residues, which is consistent with the ClC dimer interface. Three possibilities may explain the discrepancy: 1. Inaccuracy of the AE1 homology model at the dimer interface. 2. Non-hydrophobic interactions, such as hydrogen bonds, may form the dimer interface. 3. Errors in helix register at the dimer interface. Only slight alterations of the AE1 homology model would be necessary to re-orientate flanking residues to face the dimer interface in order to create a flat non-polar surface similar to the dimer interface of ClC. Inclusion of flanking residues may identify residues in the dimer interface of AE1 and improve the accuracy of the AE1 homology model.

5.3.3 Reduced Abundance of AE1 Introduced Tryptophan Mutants

Several of the AE1 introduced tryptophan mutants had a reduced protein accumulation compared to AE1MD346. This could arise due to mis-folding of the AE1 mutants. Mis-folded membrane proteins are routinely recognized by quality control mechanisms in the endoplasmic reticulum, causing these proteins to be retained in the endoplasmic reticulum and targeted for degradation. Many diseases caused by mutated membrane proteins are the result of point mutations, which result in protein mis-folding and subsequent ER retention and degradation (*20-22*). In many instances the point mutation does not cause gross mis-folding of the membrane protein, and the protein remains functional (*20, 21*). Rescue of these membrane protein mutants to the plasma membrane can in some cases relieve the effects of the disease (*23*).

An alternative argument for the observed reduction in AE1 introduced tryptophan mutant abundance is that indeed AE1 monomers are formed, but the monomers are recognized as mis-folded by the ER quality control machinery and degraded. Unlike the *E. coli* ClC dimer interface study, which used a prokaryotic expression system (*13*), here a eukaryotic expression system was utilized. A eukaryotic expression system contains ER stringent quality control mechanisms, not present in prokaryotes. Our study focuses on human AE1, and as a result a prokaryotic expression system is not suitable, because higher eukaryotic membrane proteins do not express well

in prokaryotic organisms. Since AE1 evolved to be expressed as a dimer, the ER quality control machinery may recognize monomeric AE1 as mis-folded. Indeed, the exposed dimer interface surface of AE1 monomers is foreign to the ER quality control machinery. In addition, the exposed dimer interface surface of AE1 monomers could form non-specific interactions with other membrane proteins in the ER, if the dimer interface is indeed a large hydrophobic surface similar to *E. coli* ClC. This may result in protein aggregation in the ER and degradation of AE1 monomers, consistent with reduced accumulation of AE1 mutants that induce monomerization.

Interestingly, some Dent's disease causing point mutations in human ClC-5 cluster to the protein's dimer interface (*24*). These ClC-5 mutations can be classified into three groups: class one mutants are retained in the ER and targeted for degradation, class two mutants have a reduced plasma membrane stability, and class three mutants have an altered transport activity (*24*). Many of the class one ClC-5 mutations are located at the dimer interface, and it is hypothesized that these mutations disrupt ClC-5 dimer formation, which results in ER-associated protein degradation (*24*). The low protein accumulation of ClC-5 class one mutations, located at the dimer interface, is similar to the low protein accumulation of AE1 tryptophan mutants, possibly located at the dimer interface.

Several AE1 distal renal tubular acidosis (dRTA) mutations (R589H/C/S, R602H, G609R, S613F, ΔV850 and A858D) also cluster to the dimer interface of the AE1 homology model (*25*). Some of these AE1 mutants

are retained intracellularly, while others are expressed normally at plasma membrane and have an associated cation leak (*25, 26*). The incomplete dRTA causing mutation, A858D, which maps to the dimer interface in the AE1 homology model, has a similar protein accumulation and a decrease in cell surface processing compared to WT-AE1, which indicates that the protein is slightly mis-folded (*27*). Here, A858W-AE1 was found to have a similar expression as WT-AE1, consistent with the A858D dRTA mutation, yet it remains to be determined whether A858W has a decrease in cell surface processing compared to WT-AE1.

Attempts to increase the expression of AE1 introduced tryptophan mutants, by decreasing incubation temperatures and adding DMSO, were generally unsuccessful. Only a few mutants (F583W, L865W, and V867W) had increased protein expression upon growth in different conditions. The data, however, are inconclusive since more replicates must be completed to determine the statistical significance of these changes. Also, additional analysis of the efficiency of cell surface processing must be completed to definitively determine optimal conditions to maximize AE1 abundance at the cell surface, as decreased incubation temperatures and addition of DMSO often only increase cell surface protein abundance and not total protein abundance (*15-17*).

5.3.4 Alternate Strategies to Monitor the Oligomeric State of AE1 Mutants

Chemical crosslinking did not detect changes in the level of AE1 introduced tryptophan mutant dimerization. While chemical cross-linking is a rapid method to investigate membrane protein oligomeric state (*13, 22*), there are several disadvantages to using this method here. DSP is a membrane permeant chemical cross-linker, and thus cross-links protein in the ER as well as at the plasma membrane. The ER contains folded as well as mis-folded or aggregated proteins, which can misrepresent the true oligomeric state of AE1 tryptophan mutants. Thus, isolation of plasma membranes, by differential or sucrose gradient centrifugation, or crosslinking with a membrane-impermeant crosslinker, such as DTSSP, could be useful alternatives. In addition, if only a small fraction of AE1 exists as monomers, chemical crosslinking may not detect these changes in AE1 oligomeric state. Chemical crosslinking was also performed while AE1 mutants were embedded in a lipid bilayer. Detergent solubilized membrane proteins are less stable, and mildly denaturing conditions (such as low levels of SDS) could potentially differentiate strong and weak dimer interface interactions.

Analytical size exclusion is able to sensitively detect small amounts of detergent solubilized membrane proteins in denaturing conditions ranging from mild to strong. The most common method of monitoring proteins during size exclusion chromatography is to measure the absorbance at 280

nm of purified proteins. In order to avoid purification of numerous AE1 introduced tryptophan mutants for size exclusion chromatography, fusion of AE1 mutants to fluorescent proteins could serve as an alternative. In this manner the fluorescence of whole cell lysates can be used to rapidly monitor the oligomeric state of AE1 introduced tryptophan mutants. This strategy has been successfully used in high-throughput screens of membrane protein expression and solubilization conditions for purification and crystallization trials (*28-30*). Implementing these other strategies to monitor AE1 introduced tryptophan mutant oligomerization could allow detection of subtle disruptions in the AE1 dimer interface.

5.3.5 Conclusion

Several AE1 residues were identified as candidates to form the AE1 dimer interface. N-terminally truncated AE1, AE1MD346, was created to allow assessment of membrane domain dimerization without influence of the cytoplasmic domain. AE1 tryptophan mutations were introduced at sites corresponding to sites in *E. coli* ClC that disrupted the dimer interface. The majority of AE1 introduced tryptophan mutations decreased protein abundance, and it is unclear whether this arises from ER associated degradation of mis-folded protein or AE1 monomers, which are foreign to the ER. The effects of the mutations on cell surface AE1 accumulation remains to be determined. There were no detectable changes in the oligomeric state of AE1 introduced tryptophan mutants observed by chemical crosslinking. Alternative techniques to monitor AE1 oligomerization will be valuable to

determine if small disruptions in the AE1 dimer interface, not detected by chemical crosslinking, occurred upon introduced tryptophan mutagenesis. Multiple introduced tryptophan mutations may need to be combined in a single AE1 mutant in order to disrupt the dimer interface, as was necessary to completely disrupt the ClC dimer interface (*13*). The alternate strategies discussed here may succeed in monitoring the disruption of the AE1 dimer interface, which was not accomplished by chemical crosslinking methods used in this study.

5.4 References

1. E. Cordat, J. R. Casey, Bicarbonate transport in cell physiology and disease. *Biochem J* **417**, 423-439 (2009).
2. P. S. Low, Structure and function of the cytoplasmic domain of Band 3: center of erythrocyte membrane-peripheral protein interactions. *Biochim. Biophys. Acta* **864**, 145-167 (1986).
3. Q. Zhu, D. W. Lee, J. R. Casey, Novel topology in C-terminal region of the human plasma membrane anion exchanger, AE1. *J Biol Chem* **278**, 3112-3120 (2003).
4. T. Yamaguchi, Y. Ikeda, Y. Abe, H. Kuma, D. Kang, N. Hamasaki, T. Hirai, Structure of the Membrane Domain of Human Erythrocyte Anion Exchanger 1 Revealed by Electron Crystallography. *J Mol Biol* **397**, 179-189 (2010).
5. M. L. Jennings, Oligomeric structure and the anion transport function of human erythrocyte Band 3 protein. *J. Membrane Biol.* **80**, 105-117 (1984).
6. B. J. Thevenin, P. S. Low, Kinetics and regulation of the ankyrin-band 3 interaction of the human red blood cell membrane. *J Biol Chem* **265**, 16166-16172 (1990).
7. K. Mulzer, L. Kampmann, P. Petrasch, D. Schubert, Complex associations between membrane proteins analyzed by analytical ultracentrifugation: studies on the erythrocyte membrane proteins Band 3 and ankyrin. *Colloid and Polym. Sci.* **268**, 60-64 (1990).
8. J. R. Casey, R. A. F. Reithmeier, Analysis of the oligomeric state of Band 3, the anion transport protein of the human erythrocyte membrane, by size exclusion high performance liquid chromatography: oligomeric stability and origin of heterogeneity. *J. Biol. Chem.* **266**, 15726-15737 (1991).
9. D. Zhang, A. Kiyatkin, J. T. Bolin, P. S. Low, Crystallographic structure and functional interpretation of the cytoplasmic domain of erythrocyte membrane band 3. *Blood* **96**, 2925-2933 (2000).
10. J. D. Groves, M. J. Tanner, Structural model for the organization of the transmembrane spans of the human red-cell anion exchanger (band 3; AE1). *Biochem J* **344 Pt 3**, 699-711. (1999).
11. A. M. Taylor, Q. Zhu, J. R. Casey, Cysteine-directed cross-linking localizes regions of the human erythrocyte anion exchange protein (AE1) relative to the dimeric interface. *Biochem. J.* **359**, 661-668 (2001).
12. R. Dutzler, E. B. Campbell, M. Cadene, B. T. Chait, R. MacKinnon, X-ray structure of a ClC chloride channel at 3.0 Å reveals the molecular basis of anion selectivity. *Nature* **415**, 287-294 (2002).
13. J. L. Robertson, L. Kolmakova-Partensky, C. Miller, Design, function and structure of a monomeric ClC transporter. *Nature* **468**, 844-847 (2010).

14. P. Bonar, J. R. Casey, Purification of functional human Cl^-/HCO_3^- exchanger, AE1, over-expressed in *Saccharomyces cerevisiae*. *Protein Expr Purif* **74**, 106-115 (2010).
15. G. M. Denning, M. P. Anderson, J. F. Amara, J. Marshall, A. E. Smith, M. J. Welsh, Processing of mutant cystic fibrosis transmembrane conductance regulator is temperature-sensitive. *Nature* **358**, 761-764 (1992).
16. C. R. Brown, L. Q. Hong-Brown, J. Biwersi, A. S. Verkman, W. J. Welch, Chemical chaperones correct the mutant phenotype of the delta F508 cystic fibrosis transmembrane conductance regulator protein. *Cell Stress Chaperones* **1**, 117-125 (1996).
17. C. Y. Chu, J. C. King, M. Berrini, R. T. Alexander, E. Cordat, Functional rescue of a kidney anion exchanger 1 trafficking mutant in renal epithelial cells. *PLoS One* **8**, e57062 (2013).
18. I. Sekler, R. R. Kopito, J. R. Casey, High level expression, partial purification and functional reconstitution of the human AE1 anion exchange protein in *Saccharomyces cerevisiae*. *J. Biol. Chem.* **270**, 21028-21034 (1995).
19. S. Grinstein, S. Ship, A. Rothstein, Anion transport in relation to proteolytic dissection of Band 3 protein. *Biochim. Biophys. Acta* **507**, 294-304 (1978).
20. L. J. Bruce, D. L. Cope, G. K. Jones, A. E. Schofield, M. Burley, S. Povey, R. J. Unwin, O. Wrong, M. J. Tanner, Familial distal renal tubular acidosis is associated with mutations in the red cell anion exchanger (Band 3, AE1) gene. *J Clin Invest* **100**, 1693-1707 (1997).
21. T. Okiyoneda, H. Barriere, M. Bagdany, W. M. Rabeh, K. Du, J. Hohfeld, J. C. Young, G. L. Lukacs, Peripheral protein quality control removes unfolded CFTR from the plasma membrane. *Science* **329**, 805-810 (2010).
22. G. L. Vilas, S. K. Loganathan, A. Quon, P. Sundaresan, E. N. Vithana, J. Casey, Oligomerization of SLC4A11 protein and the severity of FECD and CHED2 corneal dystrophies caused by SLC4A11 mutations. *Hum Mutat* **33**, 419-428 (2012).
23. F. Van Goor, S. Hadida, P. D. Grootenhuis, B. Burton, J. H. Stack, K. S. Straley, C. J. Decker, M. Miller, J. McCartney, E. R. Olson, J. J. Wine, R. A. Frizzell, M. Ashlock, P. A. Negulescu, Correction of the F508del-CFTR protein processing defect in vitro by the investigational drug VX-809. *Proc Natl Acad Sci U S A* **108**, 18843-18848 (2011).
24. S. Lourdel, T. Grand, J. Burgos, W. Gonzalez, F. V. Sepulveda, J. Teulon, ClC-5 mutations associated with Dent's disease: a major role of the dimer interface. *Pflugers Arch* **463**, 247-256 (2012).
25. E. Cordat, Unraveling trafficking of the kidney anion exchanger 1 in polarized MDCK epithelial cells. *Biochem Cell Biol* **84**, 949-959. (2006).
26. S. Walsh, F. Borgese, N. Gabillat, R. Unwin, H. Guizouarn, Cation transport activity of anion exchanger 1 mutations found in inherited

distal renal tubular acidosis. *Am J Physiol Renal Physiol* **295**, F343-350 (2008).
27. D. Ungsupravate, N. Sawasdee, S. Khositseth, W. Udomchaiprasertkul, S. Khoprasert, J. Li, R. A. Reithmeier, P. T. Yenchitsomanus, Impaired trafficking and intracellular retention of mutant kidney anion exchanger 1 proteins (G701D and A858D) associated with distal renal tubular acidosis. *Mol Membr Biol* **27**, 92-103 (2010).
28. D. Drew, S. Newstead, Y. Sonoda, H. Kim, G. von Heijne, S. Iwata, GFP-based optimization scheme for the overexpression and purification of eukaryotic membrane proteins in *Saccharomyces cerevisiae*. *Nat Protoc* **3**, 784-798 (2008).
29. S. Newstead, H. Kim, G. von Heijne, S. Iwata, D. Drew, High-throughput fluorescent-based optimization of eukaryotic membrane protein overexpression and purification in *Saccharomyces cerevisiae*. *Proc Natl Acad Sci U S A* **104**, 13936-13941 (2007).
30. C. L. Brooks, M. Morrison, M. Joanne Lemieux, Rapid expression screening of eukaryotic membrane proteins in *Pichia pastoris*. *Protein Sci* **22**, 425-433 (2013).

Chapter 6: Summary and Future Directions

6.1 Summary

The objective of this thesis was to develop a structural model for the AE1 membrane domain. An AE1 membrane domain construct, AE1MD-Rho was created, expressed in *S. cerevisiae*, and purified using an immuno-affinity chromatography. AE1MD-Rho has a transport activity similar to erythrocyte AE1, and thus is a suitable target for crystallization trials. A parallel strategy, to obtain a three-dimensional structure of the AE1 membrane domain, was to create an AE1 homology modeling using the *E. coli* ClC Cl^- channel structure as a template. The AE1 homology model was validated by comparison to AE1 biochemical spatial constraints and functional assays of AE1 point mutants at sites that corresponded to ClC transport mechanism residues. The AE1 homology model was further used to identify possible residues in the AE1 dimer interface. While introduced tryptophan mutations at these sites in AE1 did not disrupt the dimer interface to a measurable degree, as similar mutations had done in *E. coli* ClC, there were reductions in the steady-state accumulation of these AE1 mutants. Further analysis will be necessary to make convincing conclusions about the AE1 dimer interface. While a high-resolution crystal structure of the AE1 membrane domain was not obtained in this thesis, an AE1 homology model and several advancements in the understanding of AE1 structure and function were made. Together the data presented here will be useful in validating any future AE1 crystal structures.

6.2 Future Directions

While a three-dimensional AE1 homology model was developed (Fig. 4.2), there is still no high-resolution structure of the AE1 membrane domain. Future structural efforts for AE1 should focus on optimization of the AE1MD-Rho expression and purification strategy to maximize the chances of obtaining AE1 crystals that diffract to a high-resolution to determine a three-dimensional AE1 structure.

Alternatively, the AE1 homology model may be useful to guide the selection of single or multiple AE1 transmembrane spanning helices suitable for expression, purification, and structural determination, using nuclear magnetic resonance (NMR) techniques. This strategy has proven successful for studies of several NHE1 transmembrane spanning segment, which used the Nhe1 homology model based on the *E. coli* NhaA structure as a guide (*1*). In this manner the validity of the AE1 homology model could be tested.

Further assessment of the AE1 homology model could be accomplished by single molecule fluorescence resonance energy transfer (smFRET), which is a powerful technique used to measure distances and conformational changes (*2*-*5*). Data from smFRET would produce experimentally obtained distance measurements between different AE1 residues. Distances obtained by smFRET could then be compared to distances between AE1 residues observed in the AE1 homology model.

Finally, alternative strategies will need to be implemented to investigate the dimer interface of AE1. The results in Chapter 5, thus far, are incomplete and

inconclusive. Several strategies, with their own advantages and disadvantages, have been used to determine the oligomeric state of other membrane proteins. For the purposes of determining the oligomeric state of AE1 dimer interface mutants, a GFP-based size exclusion chromatography method will likely produce the most convincing data.

Together these additional experiments could provide useful insights into AE1 structure. Further validation of the AE1 homology model could also benefit from these studies. The goal is to eventually obtain a high-resolution structure of the AE1 membrane domain, in several conformations during the transport cycle, in order to explain mechanistic and structural features of the protein.

6.2.1 Optimization of AE1MD-Rho Expression

Additional optimization of AE1MD-Rho expression could be extremely valuable in future crystallization trials, by increasing the purification efficiency. Several protease deficient *S. cerevisiae* strains and expression vectors with different constitutive or inducible promoters exist (*6*), and could easily be tested for AE1MD-Rho expression. Much success in membrane protein expression has also been observed using *Pichia pastoris* yeast as an expression system, although typically observed increases in expression compared to *S. cerevisiae* are relative to the culture volume and not the number of cells (*6*). Other membrane protein expression systems, such as mammalian cell lines, insect cells, and cell free extracts would likely not be included in future AE1MD-Rho expression screens, as there have been few

reports of high levels of membrane protein expression suitable for crystallization trials in these systems (*7, 8*).

Alternatively alterations to AE1MD-Rho itself may increase protein expression. Codon preference optimization for yeast was only completed for the first 20 amino acids of AE1MD-Rho. Today, synthetic production of the entire codon preference optimized AE1MD-Rho coding region is a financially realistic option to increase protein expression. In addition, alternate N-terminal cytosolic domain truncation sites for AE1MD-Rho could be investigated. These sites would include D183 and R346, which have successfully been used to express AE1 membrane domain in *S. cerevisiae* (*9*) and HEK293 cells (Fig. 5.1), respectively. While increasing the number of cytoplasmic residues included in AE1MD-Rho may increase expression, it may also increase the flexibility of AE1MD-Rho and impede the formation of highly diffracting AE1 crystals (*10*).

As was done for other membrane proteins, a N-terminal GFP fusion to AE1MD-Rho could be useful for rapid screening of the several combinations of expression conditions described above (*11-13*). GFP would be fused to the N-terminus of AE1MD-Rho, separated by a tobacco etch virus (TEV) protease cleavage site, to enable removal of GFP during AE1MD-Rho purification. Fusion of a large N-terminal cytoplasmic domain, like GFP, may itself promote an increase in AE1MD-Rho expression. The N-terminal GFP fusion method would be extremely advantageous as not only AE1 expression

conditions, but also AE1 monodispersity in detergent solution, could be screened in a rapid manner.

6.2.2 Crystallization of AE1MD-Rho

Crystallization of a membrane protein depends on several factors, including detergent, heterogeneity and membrane protein stability (*14, 15*). Information gathered from the crystallization conditions of other membrane proteins (*14-17*) and conditions that previously produced erythrocyte AE1 crystals (*10*) would be valuable to test conditions that have the highest probability of AE1MD-Rho crystal formation.

Detergent is a major factor in the success of crystallization of membrane proteins. In our purification scheme, AE1 is solubilized in Fos-choline 14, which is probably not the most suitable detergent for crystallization, as few membrane protein structures are reported using this detergent (*18, 19*). Thus, detergent exchange will likely be necessary to proceed with crystallization screens. Previously, it had been shown that the best crystals obtained for AE1 were found in the detergent, DDM (*10*). Other detergents that have also been successful in the crystallization of AE1 are $C_{12}E_8$ and Cymal-6 (*10*). All of these detergents should be tested at the lowest concentration that still maintains AE1MD-Rho in a monodisperse state (*20*). In addition, the amount of washing during the purification will need to be monitored to obtain the optimal amount of lipid associated with AE1, which is known to affect crystallization (*10*).

In order to obtain a high-resolution crystal structure of AE1MD-Rho, the protein will need to be highly homogeneous. The first step to achieve this is size exclusion chromatography, which allows purification of only one AE1 oligomeric state. In addition, any AE1 flexibility caused by conformational changes during the transport cycle would introduce heterogeneity and hinder the formation of crystals. To avoid this problem, AE1 can be crystallized in the presence of the covalent inhibitor H_2DIDS. If excess amounts of H_2DIDS are left for a sufficient amount of time, however, the inhibitor will react with other accessible lysine residues on AE1MD-Rho and introduce heterogeneity. Non-covalent AE1 inhibitors, which include other stilbene disulfonates (SITS, DIDS, DADS), flufenamic acid, oxonol dyes and squalamines, may be suitable alternatives to H_2DIDS (*21, 22*). As well, several AE1 mutants have a decreased transport activity compared to WT-AE1, such as S465A and F878A-AE1 (Fig. 4.5) and mutations at E681 (*23, 24*), and may be more successful crystallization targets.

Initial 3D crystallization trials of AE1MD-Rho have not generated any crystallized protein, whereas initial 2D crystallization trials have been successful in generating sheets of two-dimensional arrays of AE1MD-Rho reconstituted into dimyristolyphosphatidylcholine at a lipid:protein ratio of 1.25. Further testing of crystallization conditions, which successfully produced erythrocyte AE1 crystals (*10*), can be used for AE1MD-Rho. If these crystallization conditions are unsuccessful additional commercially available crystallization screens can be tested. Three-dimensional crystallization of

AE1MD-Rho can also be tested using bicelle and lipid cubic phase membrane protein crystallization methods (*25, 26*). These strategies may improve AE1MD-Rho stability and crystal quality, since they utilize lipid environments more similar to the native lipid bilayer environment than detergent micelles. As well, antibody Fab fragments can be generated from the monoclonal antibodies for AE1 (IVF12) and the AE1MD-Rho rhodopsin epitope purification tag (1D4). Co-crystallization of AE1MD-Rho with these Fab fragments may provide the hydrophilic surfaces needed for crystal contact formation (*14, 15, 27*).

6.2.3 NMR Structural Determination of Individual AE1 Transmembrane Spanning Segments

Alternatively, structural determination of individual AE1 transmembrane spanning helices may be accomplished by NMR analysis, similar to the studies of NHE1 and bacteriorhodopsin (*1, 28*). A proposed model for membrane protein folding suggests that transmembrane spanning helices fold independently in a lipid bilayer and then these helices interact with one another to form the membrane protein structure (*29*). Thus, the structure of individually expressed transmembrane spanning helices should have the same structure as in the full-length membrane protein. The advantages of expressing individual transmembrane spanning helices, rather than the full-length protein, are that these shorter amino acid chains that can more easily be expressed and purified from *E. coli* and studied by NMR. The advantage of using NMR is that purified proteins are analyzed while in

detergent micelles or a non-polar solution, which eliminates lengthy crystallization trials needed for X-ray crystal structure determination. Thus far, structures of NHE1 transmembrane helices IV (residues 155-177), VI (residues 226-250), VII (residues 250-275), IX (residues 338-365), and XI (residues 447-472) have been similar to corresponding transmembrane helices in the NHE1 homology model (*1, 30*).

In order to conduct NMR-based structural studies on AE1 we must identify individual or multiple transmembrane spanning helices suitable for expression and purification from *E. coli*. This could be accomplished by using the AE1 homology model (Fig. 4.3) and/or previous transmembrane fragment studies of AE1 (*31-34*). AE1 homology model transmembrane spanning helices have several unique features (Fig. 4.3), such as extended helices (B and J) and unstructured regions in the lipid bilayer (between helices C/D and K/L), which would be very interesting to assess using NMR. Structures of individual or multiple transmembrane helices could be assembled to form a structure of the AE1 membrane domain, using the AE1 homology model or to some extent with AE1 EM structures (*35, 36*)(*37-39*). If successful, structures obtained by NMR could validate the AE1 homology model and possibly highlight subtle differences between the structures of ClC and AE1, which could not be assessed by homology modeling.

6.2.4 smFRET Distance Measurements Between AE1 Residues

Further validation of the AE1 homology model could be accomplished using FRET based distance measurements, which are valid between 10-100

Å. This technique was successfully used to measure the intradimeric distance between AE1 Q434 on adjacent monomers (*40*). In this study a concatamer of AE1 was created, which fused two monomers of AE1 together to form a single polypeptide dimer of AE1 (*40*). A cysteine-less AE1 concatamer, with Q434C mutations in each monomeric unit (AE1(Q434C).AE1(Q434C)-C^-), was expressed in *X. laevis* oocytes. AE1(Q434C).AE1(Q434C)-C^- was labeled with fluorescent donor and acceptor sulfhydryl reactive probes, and the FRET efficiency was measured to calculate the intradimeric distance between AE1 Q434 on adjacent monomers. While this is a powerful technique that could be used to calculate the distances between several AE1 residues, it only reports an average distance representing all conformations of AE1.

Alternatively, several studies have been successful in developing techniques for smFRET of membrane proteins (*2*-*5*). The advantage of smFRET is the ability to monitor fluorescence signals from individual molecules, rather than multiple molecules at the same time. This allows for distance measurements of only donor and acceptor labeled proteins, not donor or acceptor labeled proteins. In addition, smFRET based distance measurements can reflect changes in the protein's conformation over time. The disadvantage of smFRET is that immobilized purified protein is required for analysis.

Preliminary work has been completed to develop a system to measure distances between AE1 residues using smFRET. Sufficient amounts of

cysteine-less AE1, with a C-terminal rhodopsin epitope purification tag (AE1-Rho), were expressed and purified from HEK293 cells for smFRET (Fig. 6.1), since smFRET only requires nanomolar amounts of protein (*3*-*5*). An AE1-Rho mutant, with a single cysteine point mutation (H819C), was also created. While AE1-Rho was immobilized on the 1D4 purification resin, the protein was labeled with varying concentrations of fluorescent Cy5-maleimide. Purified cysteine-less and H819C AE1-Rho were resolved by SDS-PAGE and visualized on an Odyssey Li-Cor Imaging System with a 700 nm filter (Fig. 6.1). The only strong bands visualized corresponded to H819C AE1-Rho labeled with Cy5-maleimide. No bands were visualized in the corresponding position of lanes containing cysteine-less AE1-Rho, which indicates that the protein is not labeled by Cy5-maleimide. The immunoblot, however, shows that there is a similar amount of cysteine-less and H819C AE1-Rho present in all samples (Fig. 6.1). Quantification of the SDS-PAGE gel revealed that maximal H819C AE1-Rho labeling was achieved at 1 μM Cy5-maleimide (Fig. 6.1). While the SDS-PAGE gel shows strong labeling of H819C AE1-Rho, there is also labeling of contaminating proteins (Fig. 6.1). Thus, additional optimization of AE1-Rho labeling or purification is required to produce samples suitable for smFRET studies. Strategies for AE1-Rho labeling optimization would include alterations to the labeling conditions (such as time, temperature and pH), the detergent used during purification, and the sulfhydryl reactive group on the fluorescent probe.

Once AE1-Rho labeling and purification are optimized, the protein can be immobilized on a glass coverslip for smFRET measurements by confocal microscopy. Previously, protocols for membrane protein immobilization for smFRET were described (*3*-*5*). The basis of these methods is to coat glass coverslips with a mixture of polyethylene glycol (PEG) and biotin conjugated PEG, and allow streptavidin to bind to the immobilized biotin (Fig 6.2). The most suitable method (*4*) for AE1-Rho immobilization requires biotinylated Protein G to bind to the immobilized streptavidin (Fig 6.2). Then AE1-Rho bound to an anti-AE1 antibody (IVF12) is immobilized by antibody interactions with Protein G (Fig. 6.2).

The fluorescence of donor and acceptor fluorescent probes on immobilized AE1-Rho can be monitored to determine FRET efficiencies and calculate distances between AE1 residues. Since AE1 is dimeric, a single introduced cysteine allows for intradimeric distance measurements between the corresponding residues on adjacent AE1 monomers. If distances between AE1 residues within a single monomer are to be measured, the AE1 concatamer can be used to avoid contaminating signals from the adjacent monomer in the AE1 dimer, which is 60 X 110 Å (*40*). Finally, distances between AE1 residues calculated, using smFRET, can be compared to distances between AE1 residues in the AE1 homology model to provide further validation of the model.

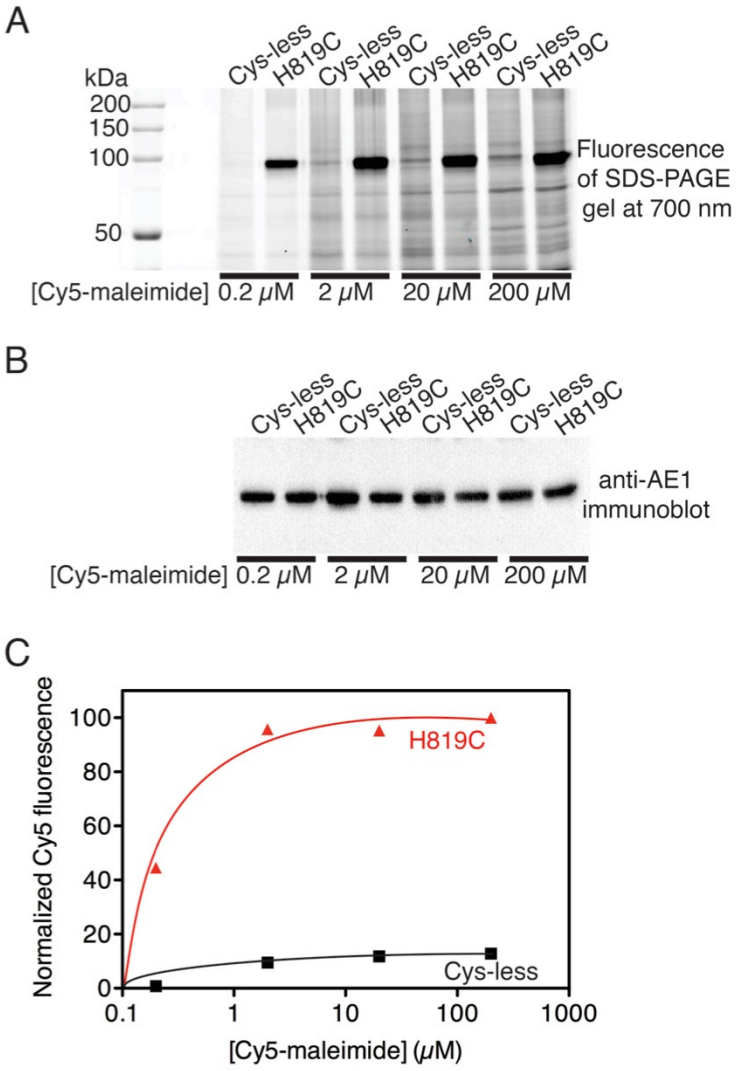

Figure 6.1 Labeling of AE1-Rho Single Cysteine Mutants with Maleimide-Conjugated Fluorescent Probes.

HEK293 cells were transiently transfected with plasmid DNA encoding either a cysteine-less AE1-Rho protein (Cys-less) or an AE1-Rho protein with a single cysteine amino acid substitution at histidine 819 (H819C). HEK293 cells were harvested and solubilized in 1% (w/v) octaethylene glycol mono-n-dodecyl ether ($C_{12}E_8$). Cell lysates were incubated with the 1D4 antibody (which recognizes the Rho epitope) conjugated to Sepharose. Unbound proteins were removed and AE1-Rho immobilized to the 1D4 antibody resin was labeled for 2 h with various concentrations of fluorescent probe, Cy5-

maleimide (0.2 - 200 μM). Unbound Cy5-maleimide was removed by washing the 1D4 resin six times with PBS, containing 1% $C_{12}E_8$. AE1-Rho was eluted from the 1D4 antibody resin with 1 mg/ml peptide (corresponding to the Rho epitope). Samples were resolved on a 7.5% SDS-PAGE gel. (A) The gel was visualized on an Odyssey Li-Cor Imaging System with a 700 nm filter. (B) Subsequently, the gel was transferred to a PVDF membrane and probed with the anti-AE1 antibody IVF12. (C) The gel was analyzed by scanning densitometry, and the normalized Cy5 fluorescence was calculated. Normalized Cy5 fluorescence of H819C is shown in orange and Cys-less is shown in black.

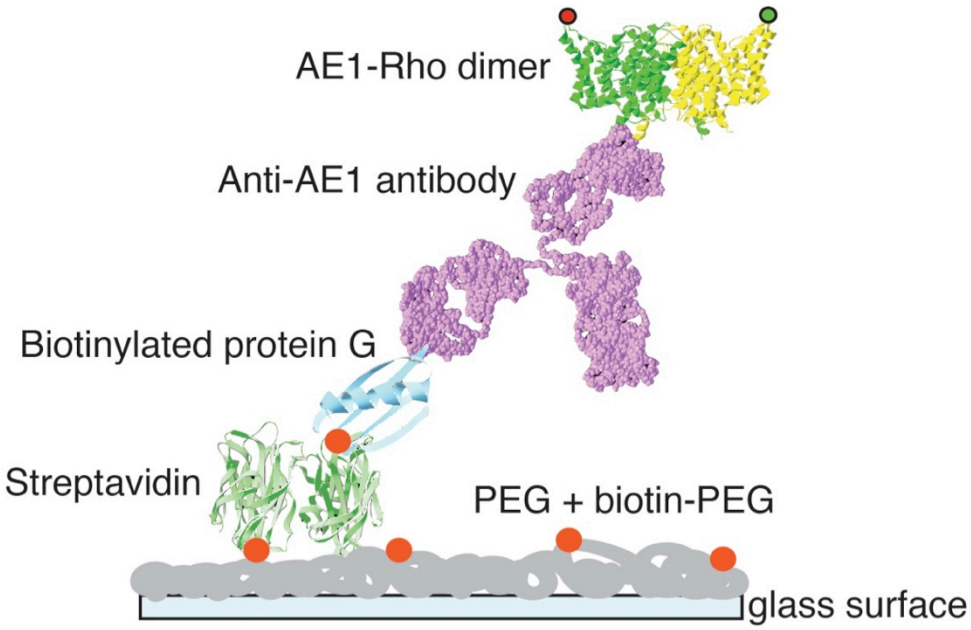

Figure 6.2 Immobilization of AE1-Rho for smFRET Studies.

Glass slides and coverslips are used to create a microfluidic chamber that is treated with aminosilane to cross-link PEG and biotin-PEG to the glass surface (*2*). Streptavidin binds to the biotin-PEG and subsequently binds biotinylated protein G. AE1-Rho dimers bind to the anti-AE1 antibody, which in turn binds protein G. Each monomer in the AE1-Rho dimer will contain a corresponding single mutated cysteine residue that is labeled with fluorescent probes conjugated to maleimides (A and D).

6.2.4 Alternate Strategies to Measure AE1 Oligomerization

Issue arose when measuring the effect of introduced tryptophan mutations in AE1 on the oligomeric state, using chemical crosslinking (Chapter 5). Several alternative methods have been used to measure the oligomeric state of membrane proteins, including size exclusion chromatography, FRET, co-immunoprecipitation, and enzyme complementation (for example split-TEV) (*41-45*). Similar issues would arise using many of these methods. FRET and enzyme complementation monitor the oligomeric state of membrane proteins in the lipid bilayer, which prohibits the use of mild denaturing conditions that could be useful to detect slight disruptions in the dimer interface. While co-immunoprecipitation, using different epitope tags on AE1 monomers, occurs in a detergent micelle solution, this method only detects changes in the amount of heterodimers formed. AE1 heterodimers would only represent a fraction of AE1 dimers, since there would also be homodimers of each epitope tagged AE1. This would not be conducive to measuring AE1 monomer formation by introduced tryptophan mutagenesis, since these mutations may only convert a small fraction of AE1 dimers to monomers. Thus, the most suitable alternative for measuring the oligomeric state of AE1 mutants, with introduced tryptophan residues, is size exclusion chromatography.

Typically, the oligomeric state of purified proteins is monitored by absorbance at 280 nm during size exclusion chromatography. While a rhodopsin epitope tagged AE1MD346 can be created, expressed and purified

from HEK293 cells, using a rhodopsin antibody epitope purification tag, this is inconvenient if many tryptophan mutants are to be studied. An alternative approach uses membrane proteins fused to GFP for rapid screening of detergent extraction conditions, by monitoring GFP fluorescence during size exclusion chromatography (*11-13*). Fusion of a fluorescent protein to AE1 would allow for whole cell lysates to be monitored during size exclusion chromatography, and eliminate the requirement of AE1 purification. GFP would not be a suitable fluorescent fusion protein, however, since it is dimeric (*46*). GFP fusion to AE1 could drive dimerization, confounding studies of AE1 dimeric interface mutants. The N-terminal fusion of a monomeric fluorescent protein, mNectarine, to AE1 has been expressed successfully in HEK293 cells (*47*). Thus, mNectarine could be fused to the N-terminus of WT-AE1MD346 and tryptophan introducing AE1MD346 mutants. In this manner, rapid screening of the oligomeric state for tryptophan introducing AE1 mutations, by mNectarine fluorescence monitoring during size exclusion chromatography, can be a reality. If successful this study would identify residues critical for AE1 dimer interface interactions, and create the first non-denatured monomeric AE1 species.

6.3 References

1. B. L. Lee, B. D. Sykes, L. Fliegel, Structural and functional insights into the cardiac Na^+/H^+ exchanger. *J Mol Cell Cardiol*, (2012).
2. R. Roy, S. Hohng, T. Ha, A practical guide to single-molecule FRET. *Nat Methods* **5**, 507-516 (2008).
3. Y. Zhao, D. Terry, L. Shi, H. Weinstein, S. C. Blanchard, J. A. Javitch, Single-molecule dynamics of gating in a neurotransmitter transporter homologue. *Nature* **465**, 188-193 (2010).
4. P. Pal, J. F. Lesoine, M. A. Lieb, L. Novotny, P. A. Knauf, A novel immobilization method for single protein spFRET studies. *Biophys J* **89**, L11-13 (2005).
5. J. F. Lesoine, B. Holmberg, P. Maloney, X. Wang, L. Novotny, P. A. Knauf, Development of an spFRET method to measure structure changes in ion exchange proteins. *Acta Physiol (Oxf)* **187**, 141-147 (2006).
6. M. Freigassner, H. Pichler, A. Glieder, Tuning microbial hosts for membrane protein production. *Microb Cell Fact* **8**, 69 (2009).
7. C. R. Midgett, D. R. Madden, Breaking the bottleneck: eukaryotic membrane protein expression for high-resolution structural studies. *J Struct Biol* **160**, 265-274 (2007).
8. F. Junge, B. Schneider, S. Reckel, D. Schwarz, V. Dotsch, F. Bernhard, Large-scale production of functional membrane proteins. *Cell Mol Life Sci* **65**, 1729-1755 (2008).
9. I. Sekler, R. R. Kopito, J. R. Casey, High level expression, partial purification and functional reconstitution of the human AE1 anion exchange protein in *Saccharomyces cerevisiae*. *J. Biol. Chem.* **270**, 21028-21034 (1995).
10. M. Joanne Lemieux, R. A. Reithmeier, D. N. Wang, Importance of detergent and phospholipid in the crystallization of the human erythrocyte anion-exchanger membrane domain. *J Struct Biol* **137**, 322-332 (2002).
11. C. L. Brooks, M. Morrison, M. Joanne Lemieux, Rapid expression screening of eukaryotic membrane proteins in *Pichia pastoris*. *Protein Sci* **22**, 425-433 (2013).
12. D. Drew, S. Newstead, Y. Sonoda, H. Kim, G. von Heijne, S. Iwata, GFP-based optimization scheme for the overexpression and purification of eukaryotic membrane proteins in *Saccharomyces cerevisiae*. *Nat Protoc* **3**, 784-798 (2008).
13. S. Newstead, H. Kim, G. von Heijne, S. Iwata, D. Drew, High-throughput fluorescent-based optimization of eukaryotic membrane protein overexpression and purification in *Saccharomyces cerevisiae*. *Proc Natl Acad Sci U S A* **104**, 13936-13941 (2007).
14. R. M. Bill, P. J. Henderson, S. Iwata, E. R. Kunji, H. Michel, R. Neutze, S. Newstead, B. Poolman, C. G. Tate, H. Vogel, Overcoming barriers to

membrane protein structure determination. *Nat Biotechnol* **29**, 335-340 (2011).
15. M. C. Wiener, A pedestrian guide to membrane protein crystallization. *Methods* **34**, 364-372 (2004).
16. M. J. Lemieux, A perspective on the structural studies of inner membrane electrochemical potential-driven transporters. *Biochim Biophys Acta* **1778**, 1805-1813 (2008).
17. Z. E. Newby, J. D. O'Connell, 3rd, F. Gruswitz, F. A. Hays, W. E. Harries, I. M. Harwood, J. D. Ho, J. K. Lee, D. F. Savage, L. J. Miercke, R. M. Stroud, A general protocol for the crystallization of membrane proteins for X-ray structural investigation. *Nat Protoc* **4**, 619-637 (2009).
18. W. Wang, S. S. Black, M. D. Edwards, S. Miller, E. L. Morrison, W. Bartlett, C. Dong, J. H. Naismith, I. R. Booth, The structure of an open form of an *E. coli* mechanosensitive channel at 3.45 Å resolution. *Science* **321**, 1179-1183 (2008).
19. R. B. Bass, P. Strop, M. Barclay, D. C. Rees, Crystal structure of *Escherichia coli* MscS, a voltage-modulated and mechanosensitive channel. *Science* **298**, 1582-1587 (2002).
20. J. R. Casey, R. A. F. Reithmeier, HPLC gel filtration analysis of oligomeric structure of Band 3, the anion exchange protein of the erythrocyte membrane. *Biophysical J.* **57**, 95a (1990).
21. H. Passow, Molecular aspects of Band 3-mediated anion transport across the red blood cell membrane. *Rev. Physiol. Biochem. Pharmacol.* **103**, 61-223 (1986).
22. S. L. Alper, M. N. Chernova, J. Williams, M. Zasloff, F. Y. Law, P. A. Knauf, Differential inhibition of AE1 and AE2 anion exchangers by oxonol dyes and by novel polyaminosterol analogs of the shark antibiotic squalamine. *Biochem Cell Biol* **76**, 799-806. (1998).
23. X.-B. Tang, M. Kovacs, D. Sterling, J. R. Casey, Identification of Residues Lining the Translocation Pore of Human AE1, Plasma Membrane Anion Exchange Protein. *J. Biol. Chem.* **274**, 3557-3564 (1999).
24. M. N. Chernova, A. K. Stewart, P. N. Barry, M. L. Jennings, S. L. Alper, Mouse Ae1 E699Q mediates SO_4^{2-}i/anion-o exchange with [SO_4^{2-}]i-dependent reversal of wild-type pHo sensitivity. *Am J Physiol Cell Physiol* **295**, C302-312 (2008).
25. R. L. Lieberman, J. A. Culver, K. C. Entzminger, J. C. Pai, J. A. Maynard, Crystallization chaperone strategies for membrane proteins. *Methods* **55**, 293-302 (2011).
26. R. Ujwal, J. U. Bowie, Crystallizing membrane proteins using lipidic bicelles. *Methods* **55**, 337-341 (2011).
27. R. Dutzler, E. B. Campbell, R. MacKinnon, Gating the selectivity filter in ClC chloride channels. *Science* **300**, 108-112 (2003).
28. M. Katragadda, J. L. Alderfer, P. L. Yeagle, Assembly of a polytopic membrane protein structure from the solution structures of overlapping peptide fragments of bacteriorhodopsin. *Biophys J* **81**, 1029-1036 (2001).

29. J. L. Popot, D. M. Engelman, Membrane protein folding and oligomerization: the two-stage model. *Biochemistry* **29**, 4031-4037 (1990).
30. M. Landau, K. Herz, E. Padan, N. Ben-Tal, Model structure of the Na^+/H^+ exchanger 1 (NHE1): functional and clinical implications. *J Biol Chem* **282**, 37854-37863 (2007).
31. J. D. Groves, M. J. Tanner, Co-expressed complementary fragments of the human red cell anion exchanger (band 3, AE1) generate stilbene disulfonate-sensitive anion transport. *J. Biol. Chem.* **270**, 9097-9105 (1995).
32. J. D. Groves, M. J. Tanner, Topology studies with biosynthetic fragments identify interacting transmembrane regions of the human red-cell anion exchanger (band 3; AE1). *Biochem J* **344 Pt 3**, 687-697 (1999).
33. G. Fu, T. Wang, B. Yang, F. Lv, C. Shi, X. Jiang, L. Tian, W. Yu, N. Hamasaki, Purification and Characterization of the Human Erythrocyte Band 3 Protein C-Terminal Domain. *Biochemistry* **43**, 1633-1638 (2004).
34. A. Mori, K. Okubo, D. Kang, N. Hamasaki, A structural study of the carboxyl terminal region of the human erythrocyte band 3 protein. *J Biochem (Tokyo)* **118**, 1192-1198 (1995).
35. T. Yamaguchi, Y. Ikeda, Y. Abe, H. Kuma, D. Kang, N. Hamasaki, T. Hirai, Structure of the Membrane Domain of Human Erythrocyte Anion Exchanger 1 Revealed by Electron Crystallography. *J Mol Biol* **397**, 179-189 (2010).
36. T. Yamaguchi, T. Fujii, Y. Abe, T. Hirai, D. Kang, K. Namba, N. Hamasaki, K. Mitsuoka, Helical image reconstruction of the outward-open human erythrocyte band 3 membrane domain in tubular crystals. *J Struct Biol* **169**, 406-412 (2009).
37. J. Jiang, N. Magilnick, K. Tsirulnikov, N. Abuladze, I. Atanasov, P. Ge, M. Narla, A. Pushkin, Z. H. Zhou, I. Kurtz, Single particle electron microscopy analysis of the bovine anion exchanger 1 reveals a flexible linker connecting the cytoplasmic and membrane domains. *PLoS One* **8**, e55408 (2013).
38. D. N. Wang, W. Kuhlbrandt, V. Sarabia, R. A. F. Reithmeier, Two-dimensional structure of the membrane domain of human band 3, the anion transport protein of the erythrocyte membrane. *EMBO J.* **12**, 2233-2239 (1993).
39. D. N. Wang, V. E. Sarabia, R. A. Reithmeier, W. Kuhlbrandt, Three-dimensional map of the dimeric membrane domain of the human erythrocyte anion exchanger, Band 3. *EMBO J.* **13**, 3230-3235 (1994).
40. A. Basu, S. Mazor, J. R. Casey, Distance measurements within a concatamer of the plasma membrane Cl^-/HCO_3^- exchanger, AE1. *Biochemistry* **49**, 9226-9240 (2010).
41. G. L. Vilas, S. K. Loganathan, A. Quon, P. Sundaresan, E. N. Vithana, J. Casey, Oligomerization of SLC4A11 protein and the severity of FECD

and CHED2 corneal dystrophies caused by SLC4A11 mutations. *Hum Mutat* **33**, 419-428 (2012).
42. J. L. Robertson, L. Kolmakova-Partensky, C. Miller, Design, function and structure of a monomeric ClC transporter. *Nature* **468**, 844-847 (2010).
43. E. Jeworutzki, T. Lopez-Hernandez, X. Capdevila-Nortes, S. Sirisi, L. Bengtsson, M. Montolio, G. Zifarelli, T. Arnedo, C. S. Muller, U. Schulte, V. Nunes, A. Martinez, T. J. Jentsch, X. Gasull, M. Pusch, R. Estevez, GlialCAM, a protein defective in a leukodystrophy, serves as a ClC-2 Cl^- channel auxiliary subunit. *Neuron* **73**, 951-961 (2012).
44. A. A. Kaczor, J. Selent, Oligomerization of G protein-coupled receptors: biochemical and biophysical methods. *Curr Med Chem* **18**, 4606-4634 (2011).
45. K. Hashimoto, H. Nishi, S. Bryant, A. R. Panchenko, Caught in self-interaction: evolutionary and functional mechanisms of protein homooligomerization. *Phys Biol* **8**, 035007 (2011).
46. F. Yang, L. G. Moss, G. N. Phillips, Jr., The molecular structure of green fluorescent protein. *Nat Biotechnol* **14**, 1246-1251 (1996).
47. D. E. Johnson, J. R. Casey, Cytosolic H^+ microdomain developed around AE1 during AE1-mediated Cl^-/HCO_3^- exchange. *J Physiol* **589**, 1551-1569 (2011).